

Improving the Foundation Layers for Concrete Pavements

TECHNICAL REPORT:

Pavement Foundation Layer Reconstruction – Michigan I-94 Field Study



January 2016

Sponsored by

Federal Highway Administration (DTFH 61-06-H-00011 (Work Plan #18))

FHWA TPF-5(183): California, Iowa (lead state), Michigan, Pennsylvania, Wisconsin

National Concrete Pavement
Technology Center



CENTER FOR

CEER

EARTHWORKS ENGINEERING
RESEARCH

IOWA STATE UNIVERSITY
Institute for Transportation

About the National CP Tech Center

The mission of the National Concrete Pavement Technology (CP Tech) Center is to unite key transportation stakeholders around the central goal of advancing concrete pavement technology through research, tech transfer, and technology implementation.

About CEER

The mission of the Center for Earthworks Engineering Research (CEER) at Iowa State University is to be the nation's premier institution for developing fundamental knowledge of earth mechanics, and creating innovative technologies, sensors, and systems to enable rapid, high quality, environmentally friendly, and economical construction of roadways, aviation runways, railroad embankments, dams, structural foundations, fortifications constructed from earth materials, and related geotechnical applications.

Disclaimer Notice

The contents of this report reflect the views of the authors, who are responsible for the facts and the accuracy of the information presented herein. The opinions, findings and conclusions expressed in this publication are those of the authors and not necessarily those of the sponsors.

The sponsors assume no liability for the contents or use of the information contained in this document. This report does not constitute a standard, specification, or regulation.

The sponsors do not endorse products or manufacturers. Trademarks or manufacturers' names appear in this report only because they are considered essential to the objective of the document.

Iowa State University Non-Discrimination Statement

Iowa State University does not discriminate on the basis of race, color, age, ethnicity, religion, national origin, pregnancy, sexual orientation, gender identity, genetic information, sex, marital status, disability, or status as a U.S. veteran. Inquiries regarding non-discrimination policies may be directed to Office of Equal Opportunity, Title IX/ADA Coordinator, and Affirmative Action Officer, 3350 Beardshear Hall, Ames, Iowa 50011, 515-294-7612, email eooffice@iastate.edu.

Iowa Department of Transportation Statements

Federal and state laws prohibit employment and/or public accommodation discrimination on the basis of age, color, creed, disability, gender identity, national origin, pregnancy, race, religion, sex, sexual orientation or veteran's status. If you believe you have been discriminated against, please contact the Iowa Civil Rights Commission at 800-457-4416 or the Iowa Department of Transportation affirmative action officer. If you need accommodations because of a disability to access the Iowa Department of Transportation's services, contact the agency's affirmative action officer at 800-262-0003.

The preparation of this report was financed in part through funds provided by the Iowa Department of Transportation through its "Second Revised Agreement for the Management of Research Conducted by Iowa State University for the Iowa Department of Transportation" and its amendments.

The opinions, findings, and conclusions expressed in this publication are those of the authors and not necessarily those of the Iowa Department of Transportation or the U.S. Department of Transportation Federal Highway Administration.

Technical Report Documentation Page

1. Report No. DTFH 61-06-H-00011 Work Plan 18		2. Government Accession No.		3. Recipient's Catalog No.	
4. Title and Subtitle Improving the Foundation Layers for Pavements: Pavement Foundation Layer Reconstruction – Michigan I-94 Field Study				5. Report Date January 2016	
				6. Performing Organization Code	
7. Author(s) David J. White, Pavana Vennapusa, Heath H. Gieselman, Alexander J. Wolfe, Samuel Douglas, Jia Li				8. Performing Organization Report No. InTrans Project 09-352	
9. Performing Organization Name and Address National Concrete Pavement Technology Center and Center for Earthworks Engineering Research (CEER) Iowa State University 2711 South Loop Drive, Suite 4700 Ames, IA 50010-8664				10. Work Unit No. (TRAIS)	
				11. Contract or Grant No.	
12. Sponsoring Organization Name and Address Federal Highway Administration U.S. Department of Transportation 1200 New Jersey Avenue SE Washington, DC 20590				13. Type of Report and Period Covered Technical Report	
				14. Sponsoring Agency Code TPF-5(183)	
15. Supplementary Notes Visit www.cptechcenter.org or www.ceer.iastate.edu for color PDF files of this and other research reports.					
16. Abstract <p>This report is one of the field project reports developed as part of the TPF-5(183) and FHWA DTFH 61-06-H-00011:WO18 studies. The project involved constructing a 280 mm thick jointed PCC pavement by undercutting the existing foundation layers to a depth of about 690 mm and placing an open-graded drainage course (OGDC) layer composed of recycled steel slag over the subgrade with a geotextile separation layer at the subgrade/OGDC layer interface. Field testing was conducted on two test sections with OGDC base layer and one test section with the existing pavement system. Point test methods including nuclear gauge, light-weight deflectometer, falling weight deflectometer, dynamic cone penetration (DCP), gas permeability testing, and plate load testing, and roller-integrated compaction monitoring with 100% coverage, were used. Point testing was conducted by spacing the test measurements about 50 to 100 m apart to capture the variability along the road alignment. Testing was also conducted in a dense grid pattern (with 0.6 to 1.5 m spacing) to capture spatial variability over a small area. Geostatistical semivariogram analysis was performed to analyze field point test data from the dense grid pattern testing to characterize and quantify spatial non-uniformity of the PCC surface and foundation layer properties. The composite modulus of subgrade reaction (k_{comp}) measured from field plate load test was about 34 kPa/mm, which was about 2.5 times lower than the design target of 84 kPa/mm (310 pci). But the k_{comp} values estimated from empirical relationships with DCP measurements and from laboratory measurements were about 1.1 to 2 times higher than the design k_{comp}. The field permeability measurements confirmed that the coefficient of drainage (C_d) values assumed in design were met in the field.</p> <p>Laboratory testing conducted to assess permanent deformation of the recycled slag indicated very low permanent strains (< 1%) after 100,000 cycles with negligible particle degradation. Comparing resilient modulus (M_r) of homogenous and layered composite test results revealed that the average M_r of composite sample is about 1.7 times lower than the average M_r of a homogenous OGDC sample at a similar density. This reduction in M_r in the layered composite sample is attributed to the weaker subgrade layer.</p>					
17. Key Words concrete pavement—pavement foundation—quality assurance—quality control— recycled base—subbase—subgrade				18. Distribution Statement No restrictions.	
19. Security Classification (of this report) Unclassified.		20. Security Classification (of this page) Unclassified.		21. No. of Pages 222	22. Price NA

**IMPROVING THE FOUNDATION LAYERS
FOR CONCRETE PAVEMENTS:
PAVEMENT FOUNDATION LAYER
RECONSTRUCTION – MICHIGAN I-94 FIELD STUDY**

Technical Report
January 2016

Research Team Members

Tom Cackler, David J. White, Jeffrey R. Roesler, Barry Christopher, Andrew Dawson,
Heath Gieselman, and Pavana Vennapusa

Report Authors

David J. White, Pavana K. R. Vennapusa,
Heath H. Gieselman, Alexander J. Wolfe, Samuel Douglas, Jia Li
Iowa State University

Sponsored by

the Federal Highway Administration (FHWA)
DTFH61-06-H-00011 Work Plan 18
FHWA Pooled Fund Study TPF-5(183): California, Iowa (lead state),
Michigan, Pennsylvania, Wisconsin

Preparation of this report was financed in part
through funds provided by the Iowa Department of Transportation
through its Research Management Agreement with the
Institute for Transportation
(InTrans Project 09-352)

**National Concrete Pavement Technology Center and
Center for Earthworks Engineering Research (CEER)**

Iowa State University
2711 South Loop Drive, Suite 4700
Ames, IA 50010-8664
Phone: 515-294-8103
www.cptechcenter.org and www.ceer.iastate.edu

TABLE OF CONTENTS

ACKNOWLEDGMENTS	xiii
LIST OF ACRONYMS AND SYMBOLS	xv
EXECUTIVE SUMMARY	xvii
CHAPTER 1. INTRODUCTION	1
CHAPTER 2. PROJECT INFORMATION	3
Project Background.....	3
Pavement Design Input Parameter Selection and Assumptions	7
Construction Details and Specifications	8
CHAPTER 3. EXPERIMENTAL TEST METHODS.....	14
Laboratory Testing Methods and Data Analysis	14
Particle Size Analysis and Index Properties	14
Resilient Modulus, Shear Strength, and Cyclic Triaxial Testing Sample Preparation	14
Resilient Modulus, Shear Strength, and Cyclic Triaxial Testing.....	20
Resilient Modulus Data Analysis.....	23
Determination of Dynamic Secant Modulus from Cyclic Stress-Strain Data	23
Laboratory Permeability Tests.....	24
Microstructural Analysis.....	24
In Situ Testing Methods.....	25
Real-Time Kinematic Global Positioning System	25
Zorn Light Weight Deflectometer	27
Kuab Falling Weight Deflectometer	27
Dynamic Cone Penetrometer	29
Nuclear Gauge	30
Rapid Gas Permeameter Test.....	30
Static Plate Load Test	31
Roller-Integrated Compaction Measurements	32
Machine Drive Power (MDP) Value	33
Compaction Meter Value (CMV)	34
Determination of <i>k</i> -values.....	34
CHAPTER 4. LABORATORY TEST RESULTS	35
Particle Size Analysis Results.....	36
Moisture-Dry Unit Weight Results.....	37
M _r and UU Test Results	40
Cyclic Triaxial and Aggregate Degradation Test Results.....	50
Laboratory Permeability Test Results.....	54
Microstructural Analysis.....	55
CHAPTER 5. IN SITU TEST RESULTS	60
Description of Test Sections	60

Geostatistical Data Analysis	61
TS1 and TS3: Newly Constructed OGDC Base and Subgrade Layers	62
Test Sections Construction and Experimental Testing	62
In Situ Point Test Results and Discussion	64
Statistical Analysis of Dense Grid Point Testing – TS1-B	73
Analysis of Roller-Integrated CMV and MDP ₄₀ Measurements – TS3b	79
Comparisons of Design Value, In situ Measurements, and Laboratory Measurements	85
TS2: Existing PCC Surface, Subbase, and Subgrade	87
Experimental Testing	87
In Situ Test Results and Discussion	91
CHAPTER 6. SUMMARY AND CONCLUSIONS	102
REFERENCES	105
APPENDIX A: MDOT OFFICE MEMORANDUM (FEBRUARY 29, 2008): PAVEMENT SELECTION	109
APPENDIX B: AASHTO 1972, AASHTO (1993), AND PCA (1984) DESIGN CHARTS	141
APPENDIX C: MDOT FIELD MOISTURE/DENSITY REPORTS, AGGREGATE INSPECTION REPORT, AND MDOT DENSITY GUIDELINES	145
APPENDIX D: STRESS-STRAIN CURVES FROM RESILIENT MODULUS TESTING	161
APPENDIX E: SEM IMAGES AND ELEMENTAL ANALYSIS RESULTS FOR OGDC BASE MATERIAL	185

LIST OF FIGURES

Figure 1. Map showing the project and test section locations	4
Figure 2. Thickness of the existing PCC pavement and existing foundation material	6
Figure 3. Cross sections of the existing (built in 1969; left) and the new (built in 2010; right) pavement layers.....	6
Figure 4. Detailed cross section of the new (2010) pavement	6
Figure 5. Four-sided impact roller used to break the existing pavement layer (top) and pavement surface after impact roller passes (bottom)	9
Figure 6. Subgrade layer after undercutting (top) and trench drain installer (bottom).....	10
Figure 8. OGDC base layer placement and compaction.....	12
Figure 9. OGDC base layer before trimming (top) and a close-up view of the OGDC base layer after trimming and compaction (bottom).....	13
Figure 10. Split mold, steel platen (4 in. diameter), and vibratory hammer for compaction of granular materials	15
Figure 12. MDOT drill rig used to obtain Shelby tube samples from subgrade.....	17
Figure 13. Aluminum spacers (4 in. diameter) used during static compaction	17
Figure 14. Photos showing static compaction procedure (left) and sample extrusion procedure (right) of a compacted cohesive soil sample.....	18
Figure 15. Elements of an idealized fabricated layered composite sample versus a homogenous sample.....	18
Figure 16. Pore water pressure display, pore water pressure transducer, and triaxial cell used in back saturation prior to M_r testing.....	19
Figure 17. Sample in a triaxial cell and pressure control wall used in back saturation prior to M_r testing	20
Figure 18. Triaxial chamber, load frame, and computer equipment for resilient modulus tests	21
Figure 19. Graphical representation of one load cycle in M_r testing	22
Figure 20. Example plot of cyclic stress-strain data from a M_r test and determination of E_s	24
Figure 21. Large scale aggregate compaction mold laboratory permeameter (Vennapusa 2004)	25
Figure 22. Trimble SPS-881 hand-held receiver, Kuab falling weight deflectometer, and Zorn light weight deflectometer (top row left to right); dynamic cone penetrometer, nuclear gauge, and gas permeameter device (middle row left to right); static plate load test (bottom row).....	26
Figure 23. FWD deflection sensor setup used for this study and an example deflection basin with SCI, BDI, and BCI calculation procedure.....	28
Figure 24. Void detection using load-deflection data from FWD test.....	29
Figure 25. E_{v1} and E_{v2} determination procedure from static PLT for subgrade and base materials	31
Figure 27. Particle size distribution curves of actual base material and modified gradation after scalp and replace procedure (for material retained on 19 mm (3/4 in.) sieve).....	36
Figure 28. Particle size distribution curves of existing sand subbase material.....	37
Figure 29. Particle size distribution curves of subgrade material	37
Figure 30. Laboratory and in situ moisture-density summary for OGDC base material.....	38

Figure 31. Laboratory and in situ moisture-density summary for existing sand subbase material	39
Figure 32. Laboratory and in situ moisture-density summary for subgrade material.....	40
Figure 33. Summary of σ_d versus M_r for Shelby tubes taken 0.4 m to 1.0 m below the ground surface.....	44
Figure 34. Summary of σ_d versus M_r for Shelby tubes taken 1.0 m to 1.7 m below the ground surface.....	45
Figure 35. Summary of σ_d versus M_r for subgrade samples (compacted in laboratory)	46
Figure 36. Summary of σ_B versus M_r for existing sand subbase samples	46
Figure 37. Summary of σ_B versus M_r for OGDC base samples	47
Figure 38. Relationships between dry unit weight, moisture content, and degree of saturation, and M_r on homogenous samples	48
Figure 39. Untrimmed base (16.65 kN/m ³ at 1.6% moisture) over subgrade (17.37 kN/m ³ at 15.0% moisture) during M_r testing	49
Figure 40. Untrimmed base (16.65 kN/m ³ at 1.6% moisture) over subgrade (17.37 kN/m ³ at 15.0% moisture) after M_r testing.....	49
Figure 41. Comparison of σ_B versus M_r for layered composite sample and OGDC base and subgrade homogenous samples.....	50
Figure 42. Comparison of homogenous and layered composite samples of base and subgrade $M_{r(T307)}$ values	50
Figure 43. Results of cyclic triaxial tests on OGDC base material	53
Figure 44. Particle size analysis test results of OGDC base material before and after cyclic triaxial tests	54
Figure 45. Color stereo microscope image of rough gray vesicular surface at 7x magnification, and SEM images at 7x, 25x, 100x, and 300x magnification	56
Figure 46. Color stereo microscope image of polished surface B at 7x magnification, and SEM images at 7x, 25x, 100x, and 300x magnification	57
Figure 47. Elemental maps of gray vesicular surface at 300x magnification.....	58
Figure 48. Elemental maps of polished surface B at 400x magnification	58
Figure 49. Elemental analysis of polished surfaces A and B at 25x magnification.....	59
Figure 50. Description of a typical experimental and spherical semivariogram and its parameters	62
Figure 51. TS1: Plan view of in situ test locations	63
Figure 52. TS1-B: Photograph showing testing on the 0.6 m x 0.6 m grid pattern.....	63
Figure 53. Plan view of in situ test locations on TS3-A (left) and photograph of TS3-A untrimmed OGDC base layer (right)	64
Figure 54. TS1-A: In situ NG and DCP test results from Sta. 804+00 to Sta. 814+00	66
Figure 55. TS1-A: In situ modulus and estimated composite stiffness measurements from Sta. 804+00 to Sta. 814+00.....	67
Figure 56. TS1-A: DCP-CBR profiles along centerline from Sta. 804+00 to Sta. 813+00	68
Figure 57. TS3-A In situ NG, DCP-CBR, and base layer thickness measurements on untrimmed OGDC base layer.....	69
Figure 58. TS3-A: In situ modulus measurements on untrimmed OGDC base layer	70
Figure 59. DCP-CBR profiles along centerline from Sta. 840+00 to Sta. 866+00 – TS3-A.....	71
Figure 60. Comparison of estimated and measured k_{comp} – TS3-A.....	72

Figure 61. Kriged spatial contour map (top), semivariogram (middle), and histogram (bottom) plots of γ_d (left) and w (right) measurements – TS1-B	75
Figure 62. Kriged spatial contour map (top), semivariogram (middle), and histogram (bottom) plots of percent fines (left) and K_{sat} (right) measurements – TS1-B	76
Figure 63. Kriged spatial contour map (top), semivariogram (middle), and histogram (bottom) plots of E_{LWD-Z3} (left) and DCP-CBR _{Base} (right) measurements – TS1-B	77
Figure 64. Kriged spatial contour map (top), semivariogram (middle), and histogram (bottom) plots of DCP-CBR _{Subgrade} measurements – TS1-B.....	78
Figure 65. Effect of fines content on K_{sat} – TS1-B.....	79
Figure 66. CMV and MDP ₄₀ maps on untrimmed OGDC base and subgrade layers – TSs 3a, 3b, and 3c	81
Figure 67. CMV histograms on untrimmed OGDC base and subgrade layers – TSs 3a, 3b, and 3c	82
Figure 68. MDP ₄₀ histograms on untrimmed OGDC base and subgrade layers – TSs 3a, 3b, and 3c.....	83
Figure 69. TS3-A, TS3-B, and TS3-C: Semivariograms of CMV (left column) and MDP40 (right column) measurements on untrimmed OGDC base and subgrade layers.....	84
Figure 71. TS2-B: Laying out the test grid (left) and Kuab FWD testing on the grid (right)	88
Figure 77. TS2-B: Plate load testing in progress	90
Figure 78. Results from FWD tests at the center of pavement panels from TS2a.....	92
Figure 79. Results from FWD tests at pavement joints from TS2a.....	93
Figure 80. Kriged spatial contour maps of FWD test results (normalized for $F = 40$ kN (9000 lbs)) on pavement surface from TS2-B	95
Figure 81. Semivariograms of FWD test results (normalized for $F = 40$ kN (9000 lbs)) on pavement surface from TS2-B	96
Figure 82. Histograms of FWD test results (normalized for $F = 40$ kN (9000 lbs)) on pavement surface from TS2-B.....	97
Figure 83. Kriged spatial contour maps of in situ point measurements on the existing subbase and subgrade layers from TS2-B.....	98
Figure 84. Semivariograms of in situ point measurements on existing subbase and subgrade layers from TS2-B.....	99
Figure 85. Histograms of in situ point measurements on existing subbase and subgrade layers from TS2-B.....	100
Figure 86. DCP-CBR profiles on the existing foundation layers from TS2-B.....	101
Figure 87. Chart to estimate modulus of subbase layer (E_{SB}) from CBR (from AASHTO 1993 based on results from Til et al. 1972)	141
Figure 88. Chart to estimate M_r of subgrade from CBR (from AASHTO 1993 Appendix FF).....	142
Figure 89. Chart for estimating composite modulus of subgrade reaction (k_{comp} -AASHTO(1993)) assuming a semi-infinite subgrade depth (from AASHTO 1993).....	143
Figure 90. Cyclic stress-strain curves from M_r test for Shelby tube A4 (0.4–1.0 m).....	161
Figure 91. Cyclic stress-strain curves from M_r test for Shelby tube C2 (0.4–1.0 m)	162
Figure 92. Cyclic stress-strain curves from M_r test for Shelby tube C2 (1.0–1.7 m)	163
Figure 93. Cyclic stress-strain curves from M_r test for Shelby tube C4 (0.4–1.0 m)	164
Figure 94. Cyclic stress-strain curves from M_r test for Shelby tube C4 (1.0–1.7 m)	165
Figure 95. Cyclic stress-strain curves from M_r test for Shelby tube E2 (0.4–1.0 m)	166

Figure 96. Cyclic stress-strain curves from M_r test for Shelby tube E2 (1.0–1.7 m)	167
Figure 97. Cyclic stress-strain curves from M_r test for Shelby tube E4 (0.4–1.0 m)	168
Figure 98. Cyclic stress-strain curves from M_r test for Shelby tube E4 (1.0–1.7 m)	169
Figure 99. Cyclic stress-strain curves from M_r test for Shelby tube G1 (0.4–1.0 m)	170
Figure 100. Cyclic stress-strain curves from M_r test for Shelby tube G1 (1.0–1.7 m)	171
Figure 101. Cyclic stress-strain curves from M_r test for Shelby tube G3 (0.4–1.0 m)	172
Figure 102. Cyclic stress-strain curves from M_r test for Shelby tube G3 (1.0–1.7 m)	173
Figure 103. Cyclic stress-strain curves from M_r test for subgrade sample 17.85 kN/m ³ @ 18.4% moisture	174
Figure 104. Cyclic stress-strain curves from M_r test for subgrade sample 18.30 kN/m ³ @ 9.3% moisture	175
Figure 105. Cyclic stress-strain curves from M_r test for subgrade sample 18.95 kN/m ³ @ 13.8% moisture	176
Figure 106. Cyclic stress-strain curves from M_r test for existing sand subbase sample 16.85 kN/m ³ @ 14.4% moisture	177
Figure 107. Cyclic stress-strain curves from M_r test for existing sand subbase sample 19.28 kN/m ³ @ 14.9% moisture	178
Figure 108. Cyclic stress-strain curves from M_r test for untrimmed base sample 13.63 kN/m ³ @ 0.9% moisture	179
Figure 109. Cyclic stress-strain curves from M_r test for untrimmed base sample 15.72 kN/m ³ @ 0.9% moisture	180
Figure 110. Cyclic stress-strain curves from M_r test for untrimmed base sample 16.45 kN/m ³ @ 1.3% moisture, scalp and replace method.....	181
Figure 111. Cyclic stress-strain curves from M_r test for untrimmed base sample 17.93 kN/m ³ @ 1.4% moisture, scalp and replace method.....	182
Figure 112. Cyclic stress-strain curves from M_r test for untrimmed base sample 16.21 kN/m ³ back saturated, scalp and replace method.....	183
Figure 113. Color stereo microscope images of polished surfaces A, B, C, and D at 2 mm magnification	185
Figure 114. Color stereo microscope images of polished surfaces E, F, G, and H at 2 mm magnification	186
Figure 115. Color stereo microscope images of polished surface I, rough black angular, rough black glassy, and rough black vesicular surfaces at 2 mm magnification	187
Figure 116. Color stereo microscope images of rough brown and gray vesicular surfaces at 2 mm magnification	188
Figure 117. SEM images of polished surface A at 25x, 100x, and 300x magnification	189
Figure 118. SEM images of polished surface B at 25x, 100x, and 300x magnification.....	190
Figure 119. SEM images of polished surface C at 25x, 100x, and 300x magnification.....	191
Figure 120. SEM images of polished surface D at 25x, 100x, 300x, and 1000x magnification	192
Figure 121. SEM images of polished surface E at 25x and 100x magnification.....	193
Figure 122. SEM images of polished surface F at 25x, 100x, 300x, and 1000x magnification	193
Figure 123. SEM images of polished surface G at 25x, 100x, and 300x magnification	194
Figure 124. SEM images of polished surface H at 25x, 100x, and 300x magnification	195
Figure 125. SEM images of polished surface I at 25x, 100x, and 300x magnification.....	196

Figure 126. SEM images of black angular surface at 25x and 100x magnification	197
Figure 127. SEM images of black glassy surface at 25x and 100x magnification	197
Figure 128. SEM image of black vesicular surface at 25x magnification	197
Figure 129. SEM image of brown vesicular surface at 25x magnification	198
Figure 130. SEM images of gray vesicular surface at 25x, 100x, and 300x magnification	198
Figure 131. Elemental maps of polished surface B at 400x magnification	199
Figure 132. Elemental maps of polished surface D at 1000x magnification	199
Figure 133. Elemental maps of polished surface F at 1000x magnification.....	200
Figure 134. Elemental maps of polished surface G at 500x magnification	200
Figure 135. Elemental maps of gray vesicular surface at 300x magnification.....	201
Figure 136. Elemental analysis of polished surfaces A and B at 25x magnification.....	201
Figure 137. Elemental analysis of polished surfaces C and G at 25x magnification.....	202
Figure 138. Elemental analysis of polished surfaces H and I at 25x magnification.....	202

LIST OF TABLES

Table 1. Pavement thickness design input parameters and assumptions	7
Table 2. Summary of bid quantities and estimated and bid costs	8
Table 3. Resilient modulus test sequences and stress values for base/subbase and subgrade materials (AASHTO T-307)	22
Table 4. Caterpillar CS683 vibratory smooth drum IC roller features	33
Table 5. Summary of material index properties.....	35
Table 6. Mr and UU test results for all samples	42
Table 7. Summary of cyclic triaxial and degradation test results on OGDC base material	52
Table 8. Summary of test sections and in situ testing.....	60
Table 9. TS1-A and TS3-A: Summary statistics of in situ test results	73
Table 10. TS3-A, TS3-B, and TS3-C: CMV and MDP ₄₀ measurements	85
Table 11. Design, in situ, and laboratory values.....	86
Table 12. TS2: Summary statistics of in situ test results	94

ACKNOWLEDGMENTS

This research was conducted under Federal Highway Administration (FHWA) DTFH61-06-H-00011 Work Plan 18 and the FHWA Pooled Fund Study TPF-5(183), involving the following state departments of transportation:

- California
- Iowa (lead state)
- Michigan
- Pennsylvania
- Wisconsin

The authors would like to express their gratitude to the National Concrete Pavement Technology (CPTech) Center, the FHWA, the Iowa Department of Transportation (DOT), and the other pooled fund state partners for their financial support and technical assistance.

Mark Grazioli, Soils and Materials Managing Engineer with the Michigan Department of Transportation (MDOT) Metro Region along with several others at MDOT, provided assistance in identifying the project, providing access to the project site, and obtaining quality assurance (QA) test results and project design information. We greatly appreciate their help.

Caterpillar, Inc. provided the CS-683 smooth drum roller used on the project that was outfitted with compaction measurement and documentation systems.

We also thank Jiake Zhang, Luke Johanson, and Stephen Quist of Iowa State University for their help with laboratory and field testing; Christianna White for comments and editing support; and the Materials Analysis and Research Laboratory staff at Iowa State University for their help with chemical analysis of the aggregate samples.

LIST OF ACRONYMS AND SYMBOLS

BCI	Base curvature index
BDI	Base damage index
CBR	California bearing ratio
CMV	Compaction meter value
COV	Coefficient of variation
DCP-CBR _{Subgrade}	CBR of subgrade determined from DCP test
DCP-CBR _{Subbase}	CBR of subbase determined from DCP test
DPI	Dynamic penetration index
D ₀	Deflection measured under the plate
D ₁ to D ₇	Deflections measured away from the plate at various set distances
D ₁₀	Grain size diameter corresponding to 10% passing by mass
D ₆₀	Grain size diameter corresponding to 60% passing by mass
E	Elastic modulus
E _s or E _{s(T307)}	Dynamic secant modulus
E _{LWD-Z3}	Elastic modulus determined from 300 mm diameter plate Zorn light weight deflectometer
F	Shape factor
G _s	Specific gravity
I	Intercept
<i>k</i>	Modulus of subgrade reaction
<i>k</i> _{AASHTO(1972)}	Modulus of subgrade reaction determined following AASHTO (1972) procedure
<i>k</i> _{AASHTO(1993)}	Modulus of subgrade reaction determined following AASHTO (1993) procedure
<i>k</i> _{comp}	Composite modulus of subgrade reaction
<i>k</i> _{comp- AASHTO(1972)}	Composite modulus of subgrade reaction determined following AASHTO (1972) procedure
<i>k</i> _{comp- AASHTO(1993)}	Composite modulus of subgrade reaction determined following AASHTO (1993) procedure
<i>k</i> _{comp- ACPA (2012)}	Composite modulus of subgrade reaction determined following ACPA (2012) online estimator
<i>k</i> _{PCA}	Modulus of subgrade reaction estimated from CBR following PCA (1984) procedure
<i>k</i> _{FWD-Dynamic}	Dynamic modulus of subgrade reaction from FWD test
<i>k</i> _{FWD-Static}	Static modulus of subgrade reaction from FWD test
k ₁ , k ₂ , k ₃	Regression coefficients in “universal” model
K _{sat}	Saturated hydraulic conductivity determined using rapid gas permeameter test device
LL	Liquid limit
LTE	Load transfer efficiency
MDP	Machine drive power
M _r	Resilient modulus
<i>n</i>	Number of measurements
<i>p</i>	Number of parameters

PI	Plasticity index
PL	Plastic limit
P_a	Atmospheric pressure
R^2	Coefficient of determination
SCI	Surface curvature index
r	Plate radius
s_u	Undrained shear strength
w	Moisture content
w_{opt}	Optimum moisture content
ε	Axial strain
ε_p	Permanent strain
ε_r	Resilient strain
γ_d	Dry unit weight
γ_{dmin}	Minimum dry unit weight
γ_{dmax}	Maximum dry unit weight
μ	Statistical mean or average
η	Poisson's ratio
σ	Statistical standard deviation
σ_B	Bulk stress
σ_d	Deviator stress
σ_0	Applied axial stress
$\sigma_1, \sigma_2, \sigma_3$	Principal stresses
τ_{oct}	Octahedral shear stress

EXECUTIVE SUMMARY

Quality foundation layers (the natural subgrade, subbase, and embankment) are essential to achieving excellent pavement performance. Unfortunately, many pavements in the United States still fail due to inadequate foundation layers. To address this problem, a research project, Improving the Foundation Layers for Pavements (FHWA DTFH 61-06-H-00011 WO #18; FHWA TPF-5(183)), was undertaken by Iowa State University to identify, and provide guidance for implementing, best practices regarding foundation layer construction methods, material selection, in situ testing and evaluation, and performance-related designs and specifications. As part of the project, field studies were conducted on several in-service concrete pavements across the country that represented either premature failures or successful long-term pavements. A key aspect of each field study was to tie performance of the foundation layers to key engineering properties and pavement performance. In situ foundation layer performance data, as well as original construction data and maintenance/rehabilitation history data, were collected and geospatially and statistically analyzed to determine the effects of site-specific foundation layer construction methods, site evaluation, materials selection, design, treatments, and maintenance procedures on the performance of the foundation layers and of the related pavements. A technical report was prepared for each field study.

This report presents results and analysis from a field study conducted on I-94 between mile posts 23.0 and 6.1 in St. Clair and Macomb Counties, Michigan. The research objectives of this project were to assess the in situ mechanistic properties of the newly constructed foundation layers and the existing foundation layers. The project involved constructing a 280 mm (11 in.) thick jointed PCC pavement by undercutting the existing foundation layers to a depth of about 690 mm (27 in.) and placing an open-graded drainage course (OGDC) layer composed of recycled steel slag over the subgrade with a geotextile separation layer at the subgrade/OGDC layer interface. Review of construction bid documents indicated that the construction cost of the foundation layers (i.e., excavation, OGDC base layer, geotextile separator) was about 50% (\$5,424,275) of the total cost of the project (\$10,918,175).

Field testing was conducted on three test sections (TS). Testing on TS1 and TS3 was conducted on the compacted OGDC base layer, and testing on TS2 was conducted on the existing pavement system. In situ testing was conducted on TS1, TS2, and TS3 by using point test methods (i.e., nuclear gauge, light-weight deflectometer, falling weight deflectometer, dynamic cone penetration, and plate load testing) and roller-integrated compaction monitoring to obtain 100% coverage over the OGDC base layer. Field point testing was conducted by spacing the test measurements about 50 to 100 m apart to capture the variability along the road alignment. Testing was also conducted in a dense grid pattern (spaced at about 0.6 to 1.5 m) to capture spatial variability over a small area. Geostatistical semivariogram analysis was performed to analyze the point test data from the dense grid pattern testing to characterize and quantify spatial non-uniformity of the PCC surface and foundation layer properties. Geostatistical analysis was also performed on spatially referenced roller-integrated compaction measurements to quantify spatial non-uniformity of the foundation layers.

Comparison of the measured properties from laboratory and in situ testing, and the design assumed values revealed the following:

- The measured E_{SB} values (either by LWD or FWD or PLT) and the estimated E_{SB} values (from DCP measurements) were on average about 1.5 to 7 times lower than the design target value. The laboratory determined E_{SB} values were, however, about 1.7 times higher than the design target value. It must be noted that the E_{SB} values obtained by LWD, FWD, and PLT represent a composite response in situ with the influence of both base layer and the underlying subgrade layer stiffness.
- M_r tests conducted on “undisturbed” in situ subgrade samples showed an average $M_r = 61$ MPa (8.8 ksi), which exceeds the design target $M_r = 21$ MPa (3 ksi). The average in situ estimated M_r value from DCP-CBR_{Subgrade} measurements was about 41 MPa (5.9 ksi), which also exceeds the design target value.
- The k_{comp} values determined in situ from PLT showed an average k_{PLT^*} of about 34 kPa/mm (124 pci), which was about 2.5 times lower than the design target $k_{comp} = 84$ kPa/mm (310 pci). The $k_{comp-AASHTO(1993)}$ values were estimated using E_{SB} based on DCP, LWD, and FWD measurements. These estimated values ranged from about 1.1 to 1.4 times the design target k_{comp} , depending on the selected E_{SB} value. The $k_{comp-AASHTO(1993)}$ determined using laboratory measurements was about 163 kPa/mm (600 pci), which is about 2 times higher than the design target k_{comp} value. These results indicate that the k_{comp} values vary significantly based on the method or procedure used.
- The C_d value assumed in design = 1.1, which represents that the quality of drainage is “good” to “excellent” according to AASHTO (1993). Based on the pavement geometry and the range of K_{sat} values obtained from field, the time for 90% of drainage ranged from 0.1 hour to 1.4 days. For an average $K_{sat} = 2.9$ cm/s, time for 90% drainage was estimated at about 1.1 hours. The average in situ $K_{sat} = 2.9$ cm/s compared well with the laboratory measured $K_{sat} = 3.1$ cm/s. These times for 90% drainage estimates indicate that the quality of the OGDC drainage layer is “good” to “excellent” according to AASHTO (1993) and therefore that it meets the design requirements.

Laboratory testing was conducted on foundation layer materials obtained from the field to determine index properties, moisture-dry unit weight relationships from compaction tests, resilient modulus, and aggregate degradation under cyclic loading. The resilient tests were conducted on homogenous samples as well as layered composite samples (i.e., OGDC base over subgrade) to assess its influence on the resilient modulus values. In addition, microstructural analysis using SEM on the OGDC base layer material samples was performed. Some key findings from laboratory testing are as follows:

- Results indicated that the M_r of OGDC base layer material increase with increasing bulk stresses, as expected for granular materials. M_r of subgrade materials decreased with increasing deviator stress, as expected for non-granular materials. Increasing moisture content decreased M_r and increasing dry unit weight increased M_r for both subbase and subgrade materials.
- Comparing M_r values obtained on OGDC base material before and after back-saturation indicated that increasing saturation decreased the average M_r value by about 1.4 times.

- Comparisons of homogenous and layered composite M_r test results revealed that the average M_r of composite sample is about 1.7 times lower than the average M_r of a homogenous OGDC sample at a similar density. This reduction in M_r in the layered composite sample is attributed to the weaker subgrade layer.
- Cyclic triaxial testing (up to 100,000 cycles) and corresponding aggregate degradation tests were conducted on OGDC base layer material samples compacted to different target dry unit weights, fines content, moisture content, and deviator/confining stress combinations. Results indicated very low permanent strains (< 0.7%) after 100,000 cycles for the recycled steel slag material used in the OGDC base layer for this project. No considerable aggregate degradation was found after 100,000 cycles on any of the OGDC base layer samples tested.

The findings from the field studies under the Improving the Foundation Layers for Pavements research project will be of significant interest to researchers, practitioners, and agencies dealing with design, construction, and maintenance of PCC pavements. The technical reports are included in Volume II (Appendices) of the *Final Report: Improving the Foundation Layers for Pavements*. Data from the field studies are used in analyses of performance parameters for pavement foundation layers in the *Mechanistic-Empirical Pavement Design Guide* (MEPDG) program. New knowledge gained from this project will be incorporated into the *Manual of Professional Practice for Design, Construction, Testing and Evaluation of Concrete Pavement Foundations* published in 2015.

CHAPTER 1. INTRODUCTION

This report presents results and analysis from a field study conducted on Interstate highway I-94 between mile posts 23.0 and 6.1 in St. Clair and Macomb Counties, Michigan. The existing interstate highway was constructed between 1963 and 1964 and consisted of a 230 mm (9 in.) thick jointed portland cement concrete (PCC) pavement underlain by about 100 mm (4 in.) of gravelly sand base, about 300 mm (12 in.) of sand subbase, and silty clay subgrade. Field studies by Michigan Department of Transportation (MDOT) indicated that the ride quality of the existing pavement was poor and that the pavement needed to be replaced. MDOT evaluated two reconstruction alternatives.

Alternative #1 was to reconstruct the roadway with a 20-year design life hot mix asphalt (HMA) pavement, and alternative #2 was to reconstruct with a 20-year design life jointed PCC pavement. Based on life cost analysis of the two alternatives, MDOT selected alternative #2, which involved construction of a 280 mm (11 in.) thick jointed PCC pavement, and undercutting the existing foundation layers to a depth of about 690 mm (27 in.) for placement of an open-graded drainage course (OGDC) layer over the subgrade with a geotextile separation layer at the subgrade/OGDC layer interface. Both alternatives were designed using *AASHTO design guide for design of pavement structures* (AASHTO 1993).

The Iowa State University (ISU) research team was present at the project site from May 27 to May 30, 2009, during the construction process to conduct a field study on the existing pavement and foundation layers and the newly constructed OGDC base layer. Field testing involved: Kuab falling weight deflectometer (FWD) to determine elastic modulus and deflection basin parameters; Zorn light weight deflectometer (LWD) to determine elastic modulus; dynamic cone penetrometer (DCP) to estimate California bearing ratio and resilient modulus values; Humboldt nuclear gauge (NG) to determine moisture and dry unit weight; rapid gas permeameter test (GPT) device to measure saturated hydraulic conductivity; static plate load test (PLT) to obtain elastic modulus and modulus of subgrade reaction; and roller-integrated compaction monitoring (RICM) measurements to obtain 100% subgrade coverage of compacted soil properties. In addition, MDOT field personnel used a drill rig to obtain “undisturbed” Shelby tube samples from the subgrade layer for laboratory testing. The spatial northing and easting of all test measurement locations were obtained using a real-time kinematic (RTK) global positioning system (GPS).

Laboratory testing was conducted on the materials collected from the field to characterize the index properties (i.e., gradation, compaction, specific gravity, soil classification). Resilient modulus (M_r) and undrained shear strength tests were conducted on the subgrade, existing subbase, and the OGDC base materials. M_r testing was also conducted on layered composite OGDC base and subgrade materials to assess the influence of the support conditions. Cyclic triaxial tests were performed on the OGDC base material for 100,000 cycles at different deviator and confining stress combinations to evaluate permanent deformation and aggregate degradation characteristics of the base material. Permeability tests were conducted on OGDC material to determine its saturated hydraulic conductivity.

Field testing was conducted on three test sections (TS). TS1 and TS3 were the newly constructed OGDC base layer, TS2 consisted of the existing PCC surface and foundation layers. The length of the test sections varied from 100 m to 2600 m. Field point testing was conducted by spacing the test locations about 50 m to 100 m apart to capture variability along the road alignment. Testing was also conducted in a dense grid pattern (spaced at about 0.6 m to 1.5 m) to capture spatial variability over a small area. Geostatistical semivariogram analysis was performed to analyze the point test data from dense grid pattern testing to characterize and quantify spatial non-uniformity of the PCC surface and foundation layer properties. Geostatistical analysis was also performed on spatially referenced RICM measurements to quantify spatial non-uniformity of the foundation layers.

This report contains six chapters. Chapter 2 provides background information about the project, including the two alternatives evaluated by MDOT; life cycle cost analysis results; selection criteria for the PCC pavement structure; AASHTO (1993) pavement design input parameters; and construction methods and specifications. Chapter 3 presents an overview of the laboratory and in situ testing methods followed in this project. Chapter 4 presents results from laboratory testing. Chapter 5 presents results from in situ testing and analysis and compares laboratory and in situ measured values with the design assumed values. Chapter 6 presents key findings and conclusions from the field study.

The findings from this report should be of significant interest to researchers, practitioners, and agencies who deal with design, construction, and maintenance aspects of PCC pavements. This project report is one of several field project reports developed as part of the TPF-5(183) and FHWA DTFH 61-06-H-00011:WO18 studies.

CHAPTER 2. PROJECT INFORMATION

This chapter presents the project background, pavement design input parameter selection and assumptions, and construction details and specifications including the selection of pavement thickness design parameters and assumptions during the design phase of the project; and the new pavement foundation layer construction details. Some of this information was obtained from field observations and some was obtained from an MDOT office memorandum dated February 29, 2008. A full copy of the memorandum is included in Appendix A.

Project Background

This project is located on I-94 in St. Clair and Macomb Counties, Michigan (Figure 1). The project involved reconstruction of pavement foundation layers of the existing interstate highway between about mile posts 23.6 and 6.1 (about Station 794+12 to 1121+70; Michigan Project No. IM0877(023) and Job Number 100701A). The existing PCC pavement was constructed between 1963 and 1964, followed by rehabilitation work comprising full-depth concrete patching and partial-depth bituminous repairs undertaken in the mid-1990s. Results from pavement coring and borings performed by MDOT at 35 locations (18 on east bound (EB) and 17 on west bound (WB) lanes) were reported in the 2008 MDOT memorandum are summarized in the following list.

- Average PCC layer thickness was about 244 mm (9.6 in.) and varied between 214 mm (8.4 in.) to 274 mm (10.8 in.) on the EB lanes and was about the same at all core locations on the WB lanes. Three core locations showed 3 in. of HMA overlay.
- Three of the WB lane core locations showed an average of about 110 mm (4.4 in.) thick aggregate base layer, while none of the cores on the EB lane showed an aggregate base layer.
- All cores showed a sand subbase. The average thickness of the subbase was about 373 mm (14.7 in.) on the EB lanes and 343 mm (13.5 in.) on the WB lanes.
- The subgrade soil varied from brown to gray, stiff to very stiff, silty clay with trace sand and gravel in 77% of the borings and brown to gray, stiff to very stiff, silty clay with trace sand and organics in the remaining 23% of the borings.
- All cores generally showed similar subgrade soil in the form of stiff, brown gray, silty clay at the anticipated new subgrade elevation, and up to depths of at about 1.5 m (5 ft) below that elevation.

Field observations and testing by the ISU research team near the east end of the project (east of the Adair rest stop on-ramp) indicated that the existing pavement was about 230 mm (9 in.) thick underlain by a 100 mm (4 in.) thick gravelly sand base; an approximately 300 mm (12 in.) thick sand subbase; and silty clay subgrade to a depth of 2 m (5 ft) (boring termination depth) below the pavement surface.

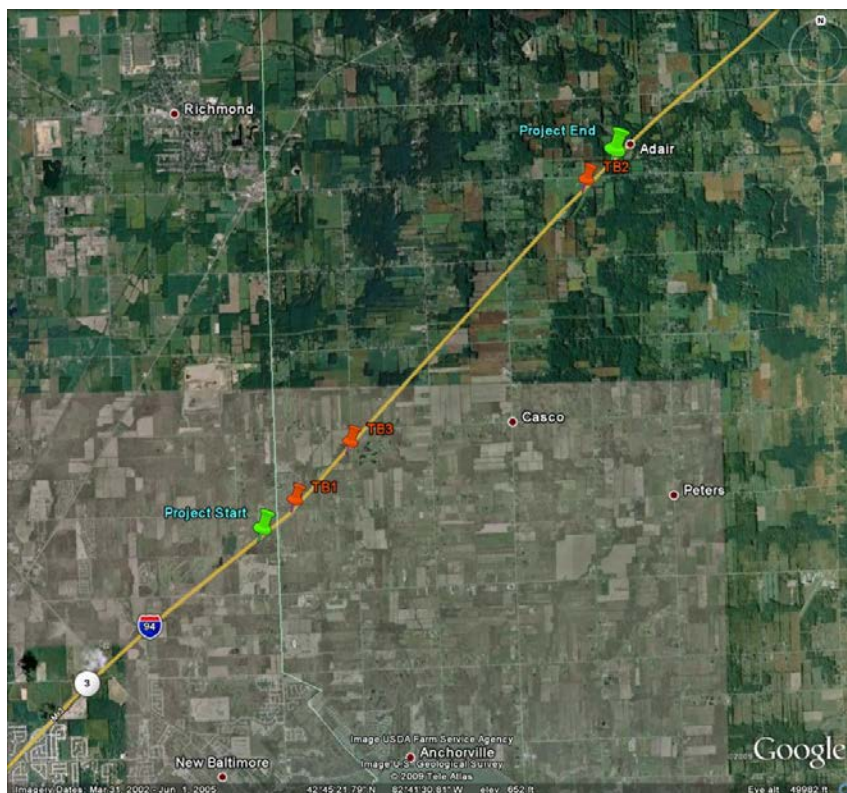


Figure 1. Map showing the project and test section locations

According to the MDOT memorandum, the ride quality index (RQI) of the existing pavement was about 73 and the average remaining service life (RSL) was about 4 on the east and west bound lanes, which indicated that the pavement quality was poor. Two new pavement reconstruction alternatives were evaluated by MDOT: alternative #1: reconstruct with HMA pavement with 20-year design life, and alternative #2: reconstruct with jointed plain concrete pavement (JPCP) with 20-year design life.

The two alternatives were evaluated using the 1993 AASHTO pavement design procedures and life cycle cost analysis using the Equivalent Uniform Annual Cost (EUAC) calculation method approved by the Engineering Operations Committee, MDOT, in June 1999 (MDOT 2005). The estimated construction costs were reportedly historical averages from similar projects, and user costs were reportedly calculated using MDOT's Construction Congestion Cost model developed by the University of Michigan.

Alternative #1 consisted of the following pavement and foundation layer structure:

- 51 mm (2.0 in.) HMA, gap-graded superpave, top course (mainline and inside shoulder)
- 64 mm (2.5 in.) HMA, 4E30, leveling course (mainline and inside shoulder)
- 152 mm (6.0 in.) HMA, 3E30, base course (mainline and inside shoulder)
- 51 mm (2.0 in.) HMA, 5E3, top course (outside shoulder)
- 64 mm (2.5 in.) HMA, 4E3, leveling course (outside shoulder)

- 152 mm (6.0 in.) HMA, 3E3, base course (outside shoulder)
- 406 mm (16.0 in.) Open-graded drainage course (OGDC) with a geotextile separator at the subgrade/OGDC interface
- 203 mm (8.0 in.) Sand subbase
- 152 mm (6.0 in.) Underdrain system (diameter)
- 876 mm (34.5 in.) Total section thickness

Life cycle analysis of alternative #1 showed the following results:

Present value initial construction cost: \$1,010,802/directional mile
 Present value initial user cost: \$499,860/directional mile
 Present value maintenance cost: \$127,428/directional mile
 Equivalent uniform annual cost (EUAC): **\$89,536/directional mile**

Alternative #2 consisted of the following pavement and foundation layer structure:

- 267 mm (10.5 in.) Non-reinforced concrete pavement with 14 ft joint spacing
- 406 mm (16.0 in.) OGDC, geotextile separator at subgrade/OGDC interface
- 152 mm (6.0 in.) Open-graded underdrain system (diameter)
- 673 mm (26.5 in.) Total section thickness

Life cycle analysis results for alternative #2 produced the following results:

Present value initial construction cost: \$819,071/directional mile
 Present value initial user cost: \$375,461/directional mile
 Present value maintenance cost: \$76,707/directional mile
 Equivalent uniform annual cost (EUAC): **\$69,484/directional mile**

Based on guidelines outlined in MDOT (2005), the alternative with lowest EUAC (i.e., alternative #2) was selected. Although the new PCC pavement design thickness was 267 mm (10.5 in.), the pavement was constructed with 280 mm (11 in.) thickness to match a previous project on the corridor (Email communication with Mark Grazioli, MDOT). The existing pavements were removed and the foundation layers were undercut to a depth of about 690 mm (27 in.) below the existing pavement surface elevation for placement of the OGDC layer with a geotextile separation layer at the interface. Cross-sections of the existing and the old pavement and foundation are shown in Figure 3, and a detailed cross-sectional view of the new pavement is provided in Figure 4.



Figure 2. Thickness of the existing PCC pavement and existing foundation material

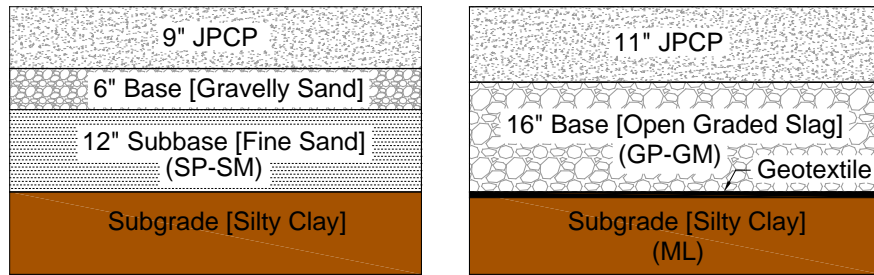


Figure 3. Cross sections of the existing (built in 1969; left) and the new (built in 2010; right) pavement layers

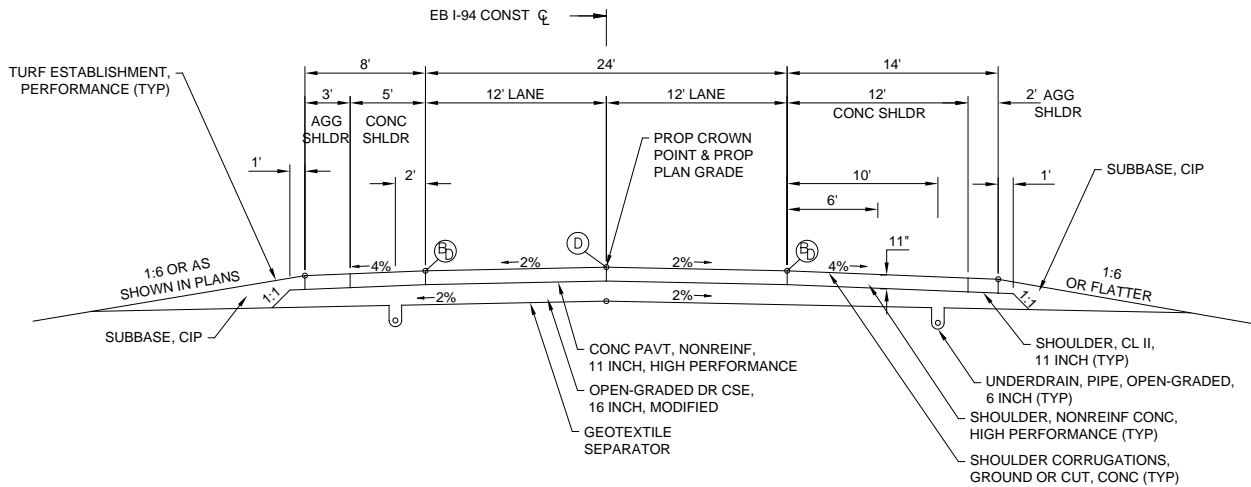


Figure 4. Detailed cross section of the new (2010) pavement

Pavement Design Input Parameter Selection and Assumptions

A summary of pavement thickness design input parameters is provided in Table 1. A composite modulus of subgrade reaction, $k_{comp} = 84$ kPa/mm (310 pci), was determined by the MDOT design engineer following the AASHTO (1993) design guidelines based on an assumed base layer elastic modulus, E_{SB} ; subgrade resilient modulus, M_r ; and target subbase layer thickness, D_{SB} , as summarized in Table 1. The design guide requires determining seasonal variations in the E_{SB} and M_r values and then an average value for analysis. The E_{SB} and M_r values provided in Table 1 are the average values. Seasonal variations in the E_{SB} and M_r values were not determined by the design engineer (Email communication with Mark Grazioli, MDOT).

Table 1. Pavement thickness design input parameters and assumptions

Parameter	Value
<i>General Assumptions</i>	
ESALs over initial performance period	22,500,000 (18-kip)
Design period	20 years
<i>Surface Layer Design Assumptions</i>	
Pavement Type	JPCP
Initial serviceability	4.5
Terminal serviceability	2.5
28-day Mean PCC modulus of rupture, S_c	4620 kPa (670 psi)
28-day Mean Modulus of Elasticity of Concrete, E_c	29,000 MPa (4,200,000 psi)
Reliability level	95%
Overall standard deviation	0.39
Load transfer coefficient, J	2.7
<i>Foundation Layer Design Assumptions</i>	
Subbase layer thickness, D_{SB}	406 mm (16 in.) (open graded drainage course)
Subbase elastic modulus, E_{SB}	165 MPa (24,000 psi)
Subgrade resilient modulus, M_r	20 MPa (3,000 psi) [stiff clay to semi-infinite depth, i.e., > 10 ft]
Composite modulus of subgrade reaction, k_{comp}	84 kPa/mm (310 pci)
Loss of support (due to erosion), LS	0.5
Effective modulus of subgrade reaction, k_{eff}	51 kPa/mm (190 psi/in.)
Overall drainage coefficient, C_d	1.1
Other	Geotextile separator between subbase and subgrade and open-graded under drains (6 in. diameter)
<i>Pavement Thickness Design</i>	
Calculated design thickness	267 mm (10.5 in.) [280 mm (11") actual built]

The effective modulus of subgrade reaction, k_{eff} , was then estimated based on an assumed potential loss of support (LS) from erosion of $LS = 0.5$. The assumed drainage coefficient $C_d = 1.1$ represents that the quality of drainage is good to excellent (varies as a function of time above a threshold base saturation level). These design assumptions are compared with actual field measurements in Chapter 6.

Construction Details and Specifications

Table 2 summarizes some key bid items, quantities, estimated costs, and bid costs. Based on the contractor's bid costs, the cost of the construction of foundation layers (i.e., subgrade, base, and geotextile separator) was about 50% of the total cost of the project.

A four-sided impact roller was used to breakdown the existing pavement layer (Figure 5). The existing foundation layers were undercut to about 690 mm (27 in.) below the top of the new pavement elevation. A longitudinal trench was excavated along the side of the road (Figure 6) and a drain tile was installed in the trench by wrapping around a non-woven geotextile and placing open-graded porous backfill material (Figure 7). Geoturf[®] W270 woven geotextile was installed on top of the silty subgrade (Figure 7) and then the 405 mm (16 in.) thick OGDC layer was placed and compacted in two lifts. The OGDC layer consisted of crushed recycled steel slag or crushed limestone. The second lift of the OGDC layer was placed, trimmed to the desired elevation, and then compacted using a smooth drum vibratory roller (Figure 8). Figure 9 shows photographs of the OGDC layer before trimming and after trimming, and compaction at a location. MDOT density guidelines indicate that the OGDC layer be compacted to a minimum of 95% relative compaction (Note: MDOT density test guidelines are somewhat unique and should be reviewed for details on the process). MDOT QA density test results are summarized later in Chapter 5.

Table 2. Summary of bid quantities and estimated and bid costs

Item	Bid Quantity	Unit	Engineer's Estimate	Contractor Bid
Earth excavation	109,700	yd ³	\$3.75	\$10.78
Sand undercut (excavation and replacement)	28,000	yd ³	\$8.00	\$1.00
Geotextile separator	531,000	yd ²	\$1.00	\$1.11
16 in. OGDC layer	387,1000	yd ²	\$11.00	\$10.00
11 in. PCC layer	174,900	yd ²	\$26.00	\$20.10
Contraction joint with load transfer	122,000	ft	\$7.75	\$8.41
Total Project Cost			\$10,213,374	\$10,918,175
Total Foundation Layer Construction Cost			\$5,671,864	\$5,425,275



Figure 5. Four-sided impact roller used to break the existing pavement layer (top) and pavement surface after impact roller passes (bottom)



Figure 6. Subgrade layer after undercutting (top) and trench drain installer (bottom)



Figure 7. Geoturf[®] W270 woven geotextile separator installed on top of the subgrade (top) and longitudinal trench drain wrapped around a non-woven geotextile and porous backfill material (bottom)



Figure 8. OGDC base layer placement and compaction



Figure 9. OGDC base layer before trimming (top) and a close-up view of the OGDC base layer after trimming and compaction (bottom)

CHAPTER 3. EXPERIMENTAL TEST METHODS

This chapter presents a summary of the laboratory and in situ testing methods used in this study.

Laboratory Testing Methods and Data Analysis

Particle Size Analysis and Index Properties

Samples from existing subbase layers, subgrade layers, and the new OGDC base layer were collected from the field and were carefully sealed and transported to the laboratory for testing. Particle-size analysis tests on the OGDC base layer samples were performed in accordance with ASTM C136-06 *Standard test method for sieve analysis of fine and coarse aggregates*. Particle-size analysis tests on the existing sand subbase and subgrade materials were conducted in accordance with ASTM D422-63 *Standard Test Method for Particle-Size Analysis of Soils*.

Atterberg limit tests (i.e., liquid limit—LL, plastic limit—PL, and plasticity index—PI) were performed in accordance with ASTM D4318-10 *Standard test methods for liquid limit, plastic limit, and plasticity index of soils using the dry preparation method*. Using the results from particle size analysis and Atterberg limits tests, the samples were classified using the unified soil classification system (USCS) in accordance with ASTM D2487-10 *Standard Practice for Classification of Soils for Engineering Purposes (Unified Soil Classification System)* and the AASHTO classification system in accordance with ASTM D3282-09 *Standard Practice for Classification of Soils and Soil-Aggregate Mixtures for Highway Construction Purposes*.

Two laboratory compaction tests were used to determine the relationship between dry density and moisture content for the soils obtained from the field. Subgrade soil compaction characteristics were determined using standard and modified Proctor compaction methods in accordance with ASTM D698-07 *Standard test methods for laboratory compaction characteristics of soil using standard effort* and ASTM D1557-07 *Standard test methods for laboratory compaction characteristics of soil using modified effort*, respectively. Maximum and minimum index density tests were performed using a vibratory table on the existing sand subbase and OGDC base materials in accordance with ASTM D4253-00 *Standard test methods for maximum index density and unit weight of soil using a vibratory table* and D4254-00 *Standard test methods for minimum index density and unit weight of soils and calculation of relative density*. Additionally, moisture-unit weight relationships for the existing subbase sand were determined by performing maximum index density tests by incrementally increasing the moisture content by approximately 1.5% for each test.

Resilient Modulus, Shear Strength, and Cyclic Triaxial Testing Sample Preparation

Two material types were tested for resilient modulus (M_r) and unconsolidated undrained (UU) shear strength generally following the AASHTO T-307 procedure—granular base/subbase and cohesive subgrade. Layered composite soil samples (i.e., those with both base and subgrade)

were also tested. In some cases, the samples were back-saturated prior to M_r and UU testing. The following sections describe the methods used to prepare the samples.

Granular Materials

Granular materials were prepared using the vibratory compaction method as described in AASHTO T-307 for preparation of granular base/subbase materials. Prior to compaction, materials were moisture-conditioned and allowed to mellow for at least 3 to 6 hours. A 101.6 mm (4 in.) diameter split mold was used to compact the sample (Figure 10) in five lifts of equal mass and thickness using an electric rotary hammer drill and a circular steel platen placed against the material (Figure 11). Calipers were used to verify consistent compaction layer thicknesses (Figure 11). AASHTO T-307 procedure requires that the maximum particle size of the material should be $1/5^{\text{th}}$ of the sample diameter, which is approximately 20.3 mm (0.8 in.) for a 101.6 mm (4 in.) diameter sample. The OGDC base material tested in this study contained a maximum particle size larger than 25.4 mm (1 in.). To meet the AASHTO T-307 specifications, the particle size distribution of the untrimmed base material was modified by scalping off particles retained on the 19.1 mm (0.75 in.) sieve and replacing them with the same percentage by weight of the material that was retained on the No. 4 sieve and passing the 19.1 mm ($3/4$ in.) sieve. For comparison purposes on the effect of different gradations on M_r , few samples were prepared and tested without the scalp and replace procedure.



Figure 10. Split mold, steel platen (4 in. diameter), and vibratory hammer for compaction of granular materials



Figure 11. Compaction of granular materials in split mold and verification of thickness of each lift using calipers

Cohesive Materials

The cohesive subgrade samples were obtained from the field in an “undisturbed” state using Shelby tube sampling methods. Disturbed bag samples of the subgrade material were also obtained for testing by compacting the material to a target moisture and density.

Undisturbed samples of subgrade materials were collected using an MDOT drill rig (Figure 12) by hydraulically pushing a 75 mm (3 in.) diameter thin-walled Shelby tube into the subgrade. Samples were obtained from various depths ranging from 0.4 to 1.7 m below the bottom of the pavement. Samples extracted from the Shelby tubes were carefully trimmed and cut to about 142 mm (5.6 in.) height for M_r and UU testing. Prior to testing, the sample dimensions were measured and the samples were weighed to determine the wet density. After testing, the entire sample was oven dried for at least 24 hours to determine the moisture content and dry density of the material.

Disturbed bag samples were used to prepare samples for testing using static compaction method as described in AASHTO T-307. Before compaction, the materials were moisture-conditioned and allowed to mellow for at least 16 hours. Static compaction involved a hydraulic press, steel mold, and six steel spacers (Figure 13) to form the soil into a 101.6 mm diameter by 203.2 mm tall (4 in. diameter by 8 in. tall) cylinder. It must be noted that AASHTO T-307 describes compaction procedure to prepare 71 mm diameter by 142 mm tall (2.8 in. diameter by 5.6 in. tall) samples. The larger samples were used in this study to compare with layered composite (base+subgrade) samples. The static compaction process is shown in Figure 14. When making the samples, the soil was compacted in five lifts of equal mass and thickness. Each lift of soil

was pressed between the steel spacers to a uniform thickness. After compaction, the soil samples were extruded (Figure 14).



Figure 12. MDOT drill rig used to obtain Shelby tube samples from subgrade



Figure 13. Aluminum spacers (4 in. diameter) used during static compaction



Figure 14. Photos showing static compaction procedure (left) and sample extrusion procedure (right) of a compacted cohesive soil sample

Composite Samples

AASHTO T-307 does not describe a procedure for fabricating layered composite samples. The sample sizes included 101.6 mm (4 in.) thick base over 101.6 mm (4 in.) thick subgrade. Figure 15 shows the difference between a layered composite sample and homogenous sample.

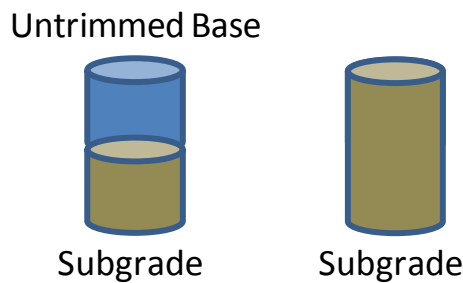


Figure 15. Elements of an idealized fabricated layered composite sample versus a homogenous sample

For the layered composite sample of base over subgrade, the bottom subgrade layer was compacted first using the static compaction technique described above, in three lifts. The first two lifts were about 40.6 mm (1.6 in.) thick, and the third lift was about 20.3 mm (0.8 in.) thick. A pre-determined amount of material was placed in each lift keeping the unit weight constant in each lift. After compaction of the subgrade, the sample was extruded and placed on the triaxial chamber base. The split mold used for granular materials was then placed around the sample, and

the base layer was compacted in three equal lifts of 33.9 mm (1.3 in.) using the vibratory compaction procedure described above.

Back-Saturation Process

Back pressure saturation was performed in accordance with the procedure described in ASTM D4767-04 “*Standard Test Method for Consolidated Undrained Triaxial Compression Test for Cohesive Soils.*” The process involved incrementally increasing both confining stresses (i.e., cell pressure) and water pressures into the bottom of a sample (i.e., back pressure) until the sample was saturated using a triaxial cell and a control panel to regulate the cell and back pressures. OGDC base samples were tested in this study to evaluate the effect of saturation on M_r and UU shear strength properties. Cell pressure was applied to the sample using water around the sample and then water was forced into the bottom of the sample at a slightly lower back pressure than the cell pressure. For the OGDC materials tested in this study, a low pressure difference worked best as the material became saturated quickly. Measurements of pore water pressure were taken after each increase in cell pressure by placing the pore water pressure transducer at the center height of the sample (Figure 16). The cell pressure was increased first; then the back pressure was increased. After the pressures were increased, pore water pressures were monitored until they were stabilized, and then the sequence was repeated. The back saturation equipment is shown in Figure 16 and Figure 17.

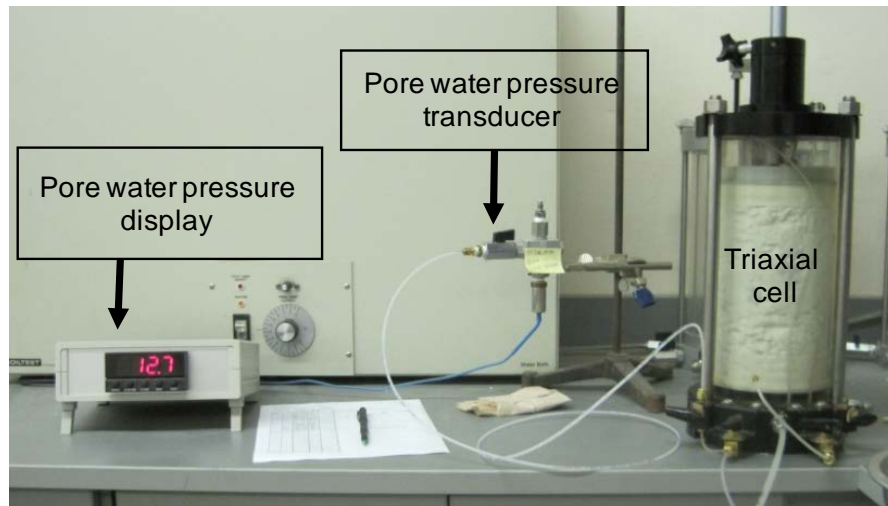


Figure 16. Pore water pressure display, pore water pressure transducer, and triaxial cell used in back saturation prior to M_r testing



Figure 17. Sample in a triaxial cell and pressure control wall used in back saturation prior to M_r testing

A sample was considered to be adequately saturated when the ratio of the difference in pore water pressures (Δu) and the difference in confining stresses ($\Delta \sigma_3$) was greater than or equal to 0.95, as shown in Equation 1:

$$\frac{\Delta u}{\Delta \sigma_3} \geq 0.95 \quad (1)$$

where, Δu is the difference in pore water pressure from the previous stress increase and $\Delta \sigma_3$ is the difference in confining stress from the previous stress increase.

After the back-saturation process was complete, the samples were allowed to drain for six minutes. During this time, all of the drains on the triaxial chamber were opened to atmospheric pressure. This draining period simulated wet pavement foundation systems that are still able to drain. Once the draining was complete, each sample was immediately tested.

Resilient Modulus, Shear Strength, and Cyclic Triaxial Testing

M_r and UU tests were performed using the Geocomp automated M_r test setup (Figure 18) in accordance with AASHTO T-307. The setup consists of a Load Trac-II load frame, electrically controlled servo valve, an external signal conditioning unit, and a computer with a network card for data acquisition. The system uses a real-time adjustment of proportional-integral-derivative (PID) controller to adjust the system control parameters as the stiffness of the sample changes to apply the target loads during the test. Figure 18 shows the triaxial test chamber used in this study. The chamber is setup to perform 71 mm (2.8 in.) or 101.6 mm (4 in.) diameter samples.

Two linear voltage displacement transducers (LVDTs) are mounted to the piston rod to measurement resilient strains in the sample during the test.



Figure 18. Triaxial chamber, load frame, and computer equipment for resilient modulus tests

For this research study, M_r tests were performed following the AASHTO T-307 conditioning and loading sequences suggested for base and subgrade materials (Table 3). Each load cycle consisted of a 0.1 second haversine-shaped load pulse followed by a 0.9 second rest period. M_r is calculated as the ratio of the applied cyclic deviator stress (σ_d) and resilient strain (ϵ_r). The σ_d and ϵ_r values from a typical stress-strain cycle during the test are shown in Figure 19. The average σ_d and ϵ_r of the last five cycles of a loading sequence are used in M_r calculations. After M_r testing, UU shear strength testing was performed on each sample by applying a confining pressure of 34.5 kPa (5 psi) to the base and subbase samples and 27.6 kPa (4 psi) to the subgrade samples.

Cyclic triaxial testing was also performed on the OGDC base material using the Geocomp setup using a confining stress of 20.7 kPa (3 psi) and a deviator stress of 41.4 kPa (6 psi) or 62.1 kPa (9 psi) for 100,000 cycles. These tests were performed to evaluate permanent deformation (ϵ_p) and aggregate degradation characteristics of the OGDC base material. During sample preparation process, the gradation of the OGDC base material was altered by controlling the amount of fines content (F_{200}), to assess the influence of F_{200} on the ϵ_p and degradation characteristics. Particle size analysis tests were conducted on the sample before and after the cyclic triaxial tests.

Table 3. Resilient modulus test sequences and stress values for base/subbase and subgrade materials (AASHTO T-307)

Base/Subbase Materials						Subgrade Materials					
Sequence No.	Confining Pressure		Max. Axial Stress		No. of cycles	Sequence No.	Confining Pressure		Max. Axial Stress		No. of cycles
	kPa	psi	kPa	psi			kPa	psi	kPa	psi	
0	103.4	15	103.4	15	500-1000	0	41.4	6	27.6	4	500-1000
1	20.7	3	20.7	3	100	1	41.4	6	13.8	2	100
2	20.7	3	41.4	6	100	2	41.4	6	27.6	4	100
3	20.7	3	62.1	9	100	3	41.4	6	41.4	6	100
4	34.5	5	34.5	5	100	4	41.4	6	55.2	8	100
5	34.5	5	68.9	10	100	5	41.4	6	68.9	10	100
6	34.5	5	103.4	15	100	6	27.6	4	13.8	2	100
7	68.9	10	68.9	10	100	7	27.6	4	27.6	4	100
8	68.9	10	137.9	20	100	8	27.6	4	41.4	6	100
9	68.9	10	206.8	30	100	9	27.6	4	55.2	8	100
10	103.4	15	68.9	10	100	10	27.6	4	68.9	10	100
11	103.4	15	103.4	15	100	11	13.8	2	13.8	2	100
12	103.4	15	206.8	30	100	12	13.8	2	27.6	4	100
13	137.9	20	103.4	15	100	13	13.8	2	41.4	6	100
14	137.9	20	137.9	20	100	14	13.8	2	55.2	8	100
15	137.9	20	275.8	40	100	15	13.8	2	68.9	10	100

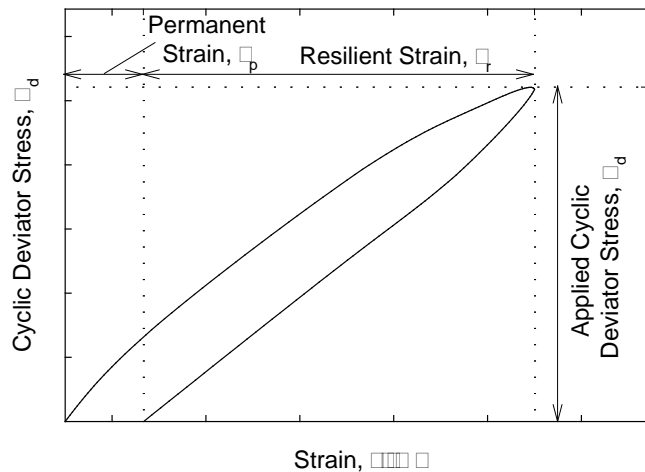


Figure 19. Graphical representation of one load cycle in M_R testing

Resilient Modulus Data Analysis

M_r values are used in pavement design as a measure of stiffness of unbound materials in the pavement structure. The M_r parameter is a highly stress-dependent parameter. Many non-linear constitutive models have been proposed that incorporate the effects of stress levels and predict M_r values. Most soils exhibit the effects of increasing stiffness with increasing bulk stress and decreasing stiffness with increasing shear stress (Andrei et al. 2004). A non-linear constitutive model (also called as “universal” model) proposed by Witczak and Uzan (1988) as shown in Equation 2 was used in this study:

$$M_r = k_1 P_a \left(\frac{\sigma_B}{P_a} \right)^{k_2} \left(\frac{\tau_{oct}}{P_a} + 1 \right)^{k_3} \quad (2)$$

where, P_a = atmospheric pressure (MPa); σ_B = bulk stress (MPa) = $\sigma_1 + \sigma_2 + \sigma_3$; τ_{oct} = octahedral shear stress (MPa) = $\frac{\sqrt{(\sigma_1 - \sigma_2)^2 + (\sigma_2 - \sigma_3)^2 + (\sigma_3 - \sigma_1)^2}}{3}$; $\sigma_1, \sigma_2, \sigma_3$ = principal stresses; and k_1, k_2, k_3 = regression coefficients.

Equation 2 combines the effects of bulk and shear stresses into a single constitutive model. Bulk stress, octahedral shear stress, and measured resilient modulus values from the last five load cycles in each loading sequence were input into the statistical analysis program, JMP, to determine the regression coefficients k_1, k_2 , and k_3 . The k_1 coefficient is proportional to M_r and therefore is always > 0 . The k_2 coefficient explains the behavior of the material with changes in the bulk stresses. Increasing bulk stresses increases the M_r value and therefore the k_2 coefficient should be ≥ 0 . The k_3 coefficient explains the behavior of the material with changes in shear stresses. Increasing shear stress softens the material and decreases the M_r value. Therefore the k_3 coefficient should be ≤ 0 .

The R^2 values determined from were adjusted for the number of regression parameters using Equation 3:

$$R^2 (\text{Adjusted}) = 1 - \left[\frac{(1 - R^2)(n - 1)}{n - p - 1} \right] \quad (3)$$

where, n = the number of data points and p = the number of regression parameters.

Determination of Dynamic Secant Modulus from Cyclic Stress-Strain Data

The cyclic stress-strain data obtained from the resilient modulus test was used to estimate dynamic secant modulus (E_s) to compare with dynamic elastic modulus measurements from field. Secant modulus was determined from the slope of the line connecting the origin to a

selected point on the stress-strain curve of a material, as illustrated in Figure 20. The difference between secant moduli and resilient moduli is the use of permanent strain instead of resilient strain in the calculations.

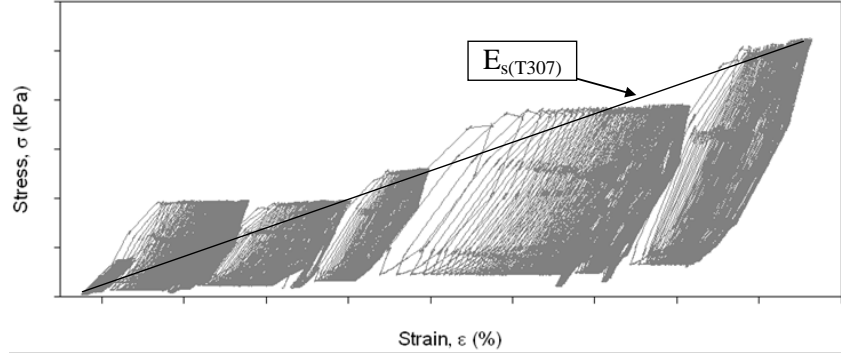


Figure 20. Example plot of cyclic stress-strain data from a M_r test and determination of E_s

Laboratory Permeability Tests

A specially fabricated 0.3 m diameter by 0.3 m high aggregate compaction mold large scale laboratory permeameter (LSLP) was used to perform falling head permeability tests (Figure 21). The LSLP test equipment is described in detail in White et al. (2004). Preparation of the test samples for the LSLP tests involved uniform mixing and compaction of the material in three lifts of equal thickness. Falling head permeability tests were conducted by recording the time taken for the water head in the reservoir to drop from H_1 to H_2 to determine K_{sat} using Equation 4:

$$K_{sat} = \left(\frac{aL}{At} \right) \ln \left(\frac{H_1}{H_2} \right) \quad (4)$$

where K_{sat} = saturated hydraulic conductivity (cm/s), a = area of the reservoir (cm²), L = length of the sample (cm), A = cross-sectional area of the sample (cm²), t = time (sec) taken for the water head to drop from H_1 to H_2 , H_1 and H_2 = water height above the exit (which is at the bottom of the sample).

Microstructural Analysis

Microstructural analysis features of the OGDC slab base material were determined from scanning electron microscopy (SEM). Elemental compositional analysis of the materials was determined from energy dispersive spectrometry (EDS) analysis using the SEM samples.

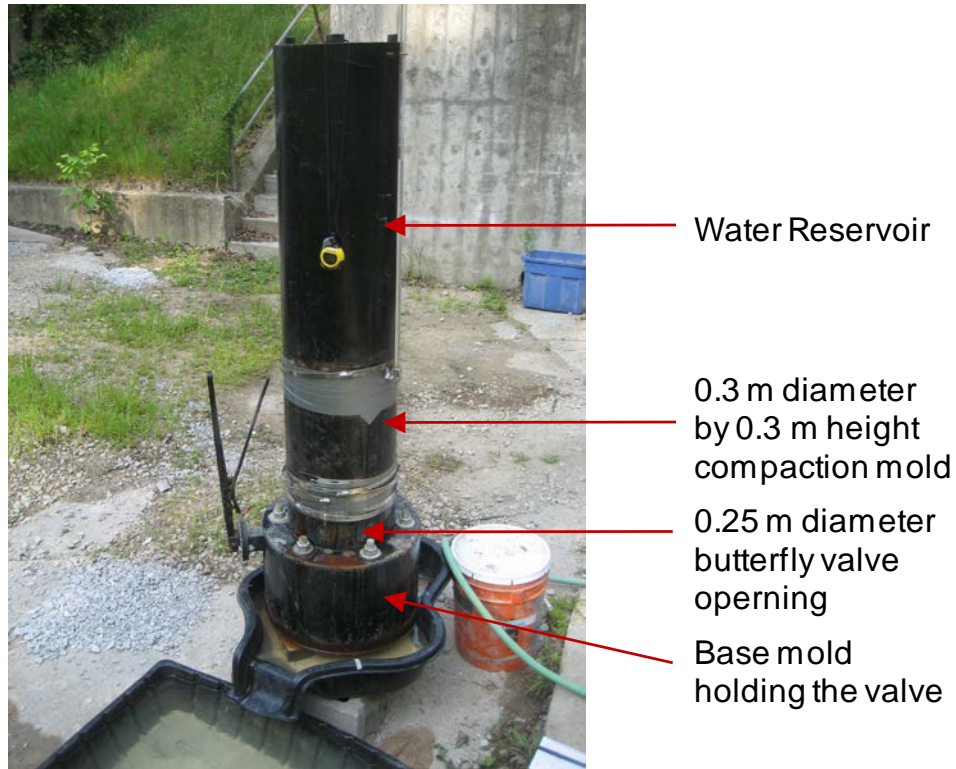


Figure 21. Large scale aggregate compaction mold laboratory permeameter (Vennapusa 2004)

In Situ Testing Methods

The following in situ testing equipment and methods were used in this study: real-time kinematic (RTK) global positioning system (GPS); Kuab FWD setup with 300 mm diameter plate; Zorn LWD setup with 300 mm diameter plate; DCP; calibrated Humboldt NG; rapid GPT device; static PLT setup with 300 mm diameter plate; and roller-integrated compaction monitoring measurements. Photographs of these devices are shown in Figure 22.

Real-Time Kinematic Global Positioning System

RTK-GPS system was used to obtain spatial coordinates (x, y, and z) of in situ test locations and tested pavement slabs. A Trimble SPS 881 receiver was used with base station correction provided from a Trimble SPS851 established on site. According to the manufacturer, this survey system is capable of horizontal accuracies of < 10 mm and vertical accuracies < 20 mm.



Figure 22. Trimble SPS-881 hand-held receiver, Kuab falling weight deflectometer, and Zorn light weight deflectometer (top row left to right); dynamic cone penetrometer, nuclear gauge, and gas permeameter device (middle row left to right); static plate load test (bottom row)

Zorn Light Weight Deflectometer

Zorn LWD tests were performed on base and subbase layers to determine elastic modulus. The LWD was setup with 300 mm diameter plate and 71 cm drop height. The tests were performed following manufacturer recommendations (Zorn 2003) and the elastic modulus values were determined using Equation 5:

$$E = \frac{(1 - \eta^2)\sigma_0 r}{D_0} \times F \quad (5)$$

where E = elastic modulus (MPa), D_0 = measured deflection under the plate (mm), η = Poisson's ratio (0.4), σ_0 = applied stress (MPa), r = radius of the plate (mm), F = shape factor depending on stress distribution (assumed as 8/3) (see Vennapusa and White 2009). The results are reported as E_{LWD-Z3} (Z represents Zorn LWD and 3 represents 300 mm diameter plate).

Kuab Falling Weight Deflectometer

Kuab FWD tests on this project were conducted on PCC surface and the OGDC base layers. FWD tests on PCC surface were conducted by applying one seating drop using a nominal force of about 27 kN (6000 lb) followed by three test drops each at a nominal force of about 27 kN (6000 lb), 40 kN (9000 lb), and 54 kN (12000 lb). The test procedure on OGDC base layers was also similar to the procedure followed on the PCC surface, but the loading drops varied from about 27 kN (6000 lb) to 45 kN (10,000 lb). The actual applied force was recorded using a load cell. Deflections were recorded using seismometers mounted on the device. The deflection sensor setup used in this study and an example deflection basin data is presented in Figure 23. A composite modulus value (E_{FWD-K3}) was calculated using the measured deflection at the center of the plate (D_0), corresponding applied contact force, and Equation 5, for tests conducted on the OGDC base layers. Shape factor $F = 2$ was assumed in the calculations assuming a uniform stress distribution (see Vennapusa and White 2009). For tests conducted on the PCC surface, the deflection basin data was used to calculate effective static modulus of subgrade reaction ($k_{FWD-Static}$) value using the Engineering and Research International (ERI) data analysis software. The $k_{FWD-Static}$ is determined using deflections obtained from D_0 , D_2 , D_4 , and D_5 , and the AREA method as described in AASHTO (1993).

Other parameters calculated using the FWD deflection basin measurements on PCC surface include: (a) surface curvature index (SCI); (b) base damage index (BDI); (c) base curvature index (BCI); and (d) area factor. These parameters were calculated using Equations 6 to 9 (D_0 , D_2 , D_4 , and D_5 are defined in Figure 23):

$$SCI \text{ (mm)} = D_0 - D_2 \quad (6)$$

$$BDI \text{ (mm)} = D_2 - D_4 \quad (7)$$

$$BCI \text{ (mm)} = D_4 - D_5 \quad (8)$$

$$\text{Area Factor (mm)} = \frac{152.4(D_0 + 2D_2 + 2D_4 + D_5)}{D_0} \quad (9)$$

The SCI parameter provides a measure of the strength/stiffness of the upper portion (base layers) of the pavement foundation layers (Horak 1987). The BDI parameter provides a measure of the strength/stiffness properties of layers between 300 mm and 600 mm depth (base and subbase layers) from the surface (Kilareski and Anani 1982). The BDI parameter provides a measure of the strength/stiffness properties of layers between 600 mm and 900 mm depth (subgrade layers) from the surface (Kilareski and Anani 1982). The area factor is primarily the normalized (with D_0) area under the basin curve up to sensor D_5 (AASHTO 1993). The area factor has been used to characterize variations in the foundation layer material properties by some researchers (e.g., Substad 2002). Comparatively, lower SCI, BDI, BCI, or area factor values indicate better support conditions (Horak 1987).

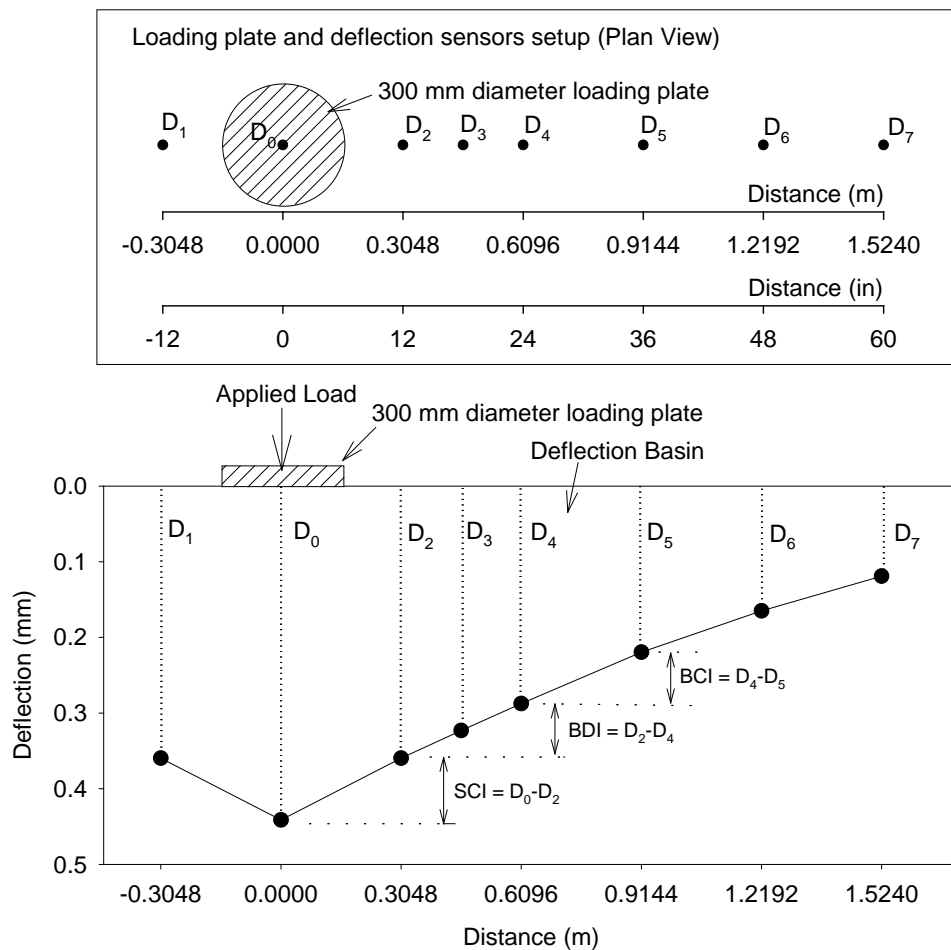


Figure 23. FWD deflection sensor setup used for this study and an example deflection basin with SCI, BDI, and BCI calculation procedure

Load transfer efficiency (LTE) at joints was determined by obtaining deflections on the loaded slab (D_0) and deflections of the unloaded slab (D_1) (Equation 10). If the entire applied load is transferred over to the adjacent slab, then the LTE would be 100%.

$$LTE(\%) = \frac{D_1}{D_0} \times 100 \quad (10)$$

Voids underneath pavement can be predicted by plotting the applied load measurements on the X-axis and the corresponding deflection measurements on the y-axis, and plotting a best fit linear regression line as illustrated in Figure 24. AASHTO (1993) recommends $I = 0.05$ mm (2 mils) as a critical value for void detection. According to Quintus and Simpson (2002), if $I = -0.01$ and $+0.01$ mm, then the response would be considered elastic. If $I > 0.01$ then the response would be considered deflection hardening, and if $I < -0.01$ then the response would be considered deflection softening.

Based on field measurements, Vandenbossche (2005) concluded that the LTEs of doweled PCC slabs are not affected by temperature gradients or slab temperature, but the intercept values are significantly affected. Large positive gradients (surface warmer than bottom) result in negative intercept values, while large negative gradients (surface cooler than bottom) result in positive intercept values (Vandenbossche 2005).

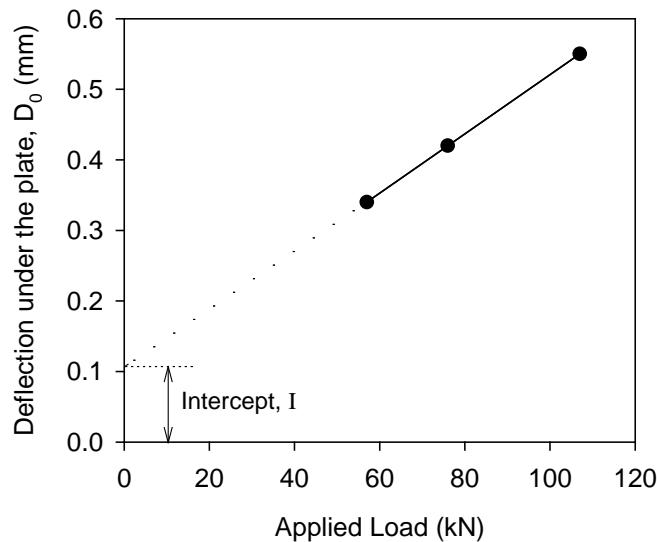


Figure 24. Void detection using load-deflection data from FWD test

Dynamic Cone Penetrometer

DCP tests were performed in accordance with ASTM D6951-03 “*Standard Test Method for Use of the Dynamic Cone Penetrometer in Shallow Pavement Applications*” to determine dynamic penetration index (DPI) and calculate California bearing ratio (CBR) using Equation 11.

$$\text{CBR} = \frac{292}{\text{DPI}^{1.12}} \quad (11)$$

The DCP test results are presented in this report as CBR with depth profiles at a test location and as point values of DCP-CBR_{Base} or DCP-CBR_{Subbase} or DCP-CBR_{Subgrade}. The point data values represent the weighted average CBR within each layer. The depths of each layer were identified using the DCP-CBR profiles.

Nuclear Gauge

A calibrated nuclear moisture-density gauge (NG) device was used to provide rapid measurements of soil dry unit weight (γ_d) and moisture content (w) in the base materials. Tests were performed following ASTM D6938-10 *Standard Test Method for In-Place Density and Water Content of Soil and Soil-Aggregate by Nuclear Methods (Shallow Depth)*. Measurements of w and γ_d were obtained at each test location and average values are reported.

Rapid Gas Permeameter Test

A rapid gas permeameter test device (GPT) was used to determine saturated hydraulic conductivity of OGDC base and the existing subbase layers. The GPT is a recently developed rapid permeability testing device that uses gas as a permeating fluid to determine the saturated hydraulic conductivity (K_{sat}) at a test location in situ (White et al. 2010a). Air was used as the permeating gas in this field study. The GPT consists of a self-contained pressurized gas system with a self-sealing base plate and a theoretical algorithm to rapidly determine the K_{sat} . The gas flow is controlled using a regulator and a precision orifice. The inlet pressure and flow rate values are recorded in the device and are used in K_{sat} calculations using Equation 12:

$$K_{\text{sat}} = \left[\frac{2\mu_{\text{gas}}QP_1}{rG_o(P_1^2 - P_2^2)} \right] \times \frac{\rho g}{\mu_{\text{water}}(1 - S_e)^2(1 - S_e^{(2+\lambda)/\lambda})} \quad (12)$$

where, K_{sat} = saturated hydraulic conductivity (cm/s); K_{gas} = gas permeability; K_{rg} = relative permeability to gas; μ_{gas} = kinematic viscosity of the gas (PaS); Q = volumetric flow rate (cm³/s); P_1 = absolute gas pressure on the soil surface (Pa) $P_{o(g)} \times 9.81 + 101325$; $P_{o(g)}$ = gauge pressure at the orifice outlet (mm of H₂O); P_2 = atmospheric pressure (Pa); r = radius at the outlet (4.45 cm); G_o = Geometric factor (constant based on geometry of the device and test area; White et al. 2007), S_e = effective water saturation [$S_e = (S - S_r)/(1 - S_r)$]; λ = Brooks-Corey pore size distribution index; S_r = residual water saturation; S = water saturation; ρ = density of water (g/sm³); g = acceleration due to gravity (cm/s²); μ_{water} = absolute viscosity of water (gm/cm-s).

More details on the test device and K_{sat} calculation procedure are provided in White et al. (2007), (2010a). The degree of saturation (S) values were obtained from in situ dry unit weight and moisture content measurements. The S_r and λ parameters can be obtained by determining the

soil-water retention properties (also known as soil water characteristic curves (SWCC) of the materials). Tests to determine the SWCC parameters can be time-consuming and require precise calibration of test equipment. As an alternative, empirical relationships from material gradation properties can be used (Zapata and Houston 2008). A summary of these relationships and the procedure to estimate S_r and λ parameters are summarized in White et al. (2010a). For the results presented in this report, $\lambda = 0.98$ and $S_r = 12\%$ were used for OGDC base material, and $\lambda = 2.0$ and $S_r = 10\%$ were used for sand subbase material.

Static Plate Load Test

Static PLTs were conducted on the OGDC layer by applying a static load on 300 mm diameter plate against a 6.2kN capacity reaction force. The applied load was measured using a 90-kN load cell and deformations were measured using three 50-mm LVDTs. The load and deformation readings were continuously recorded during the test using a data logger. The E_{V1} and E_{V2} values were determined from Equation 5 using deflection values at 0.2 and 0.4 MPa contact stresses as illustrated in Figure 25. Modulus of subgrade reaction were also determined from the PLT results using Equation 13:

$$k_{PLT} = \frac{\sigma_0}{D_0} \quad (13)$$

where k_{PLT} = modulus of subgrade reaction from 300 mm diameter plate load test (kPa/mm), D_0 = measured deflection under the plate (mm) for 200 kPa to 400 kPa applied stress range, and σ_0 = applied stress (kPa).

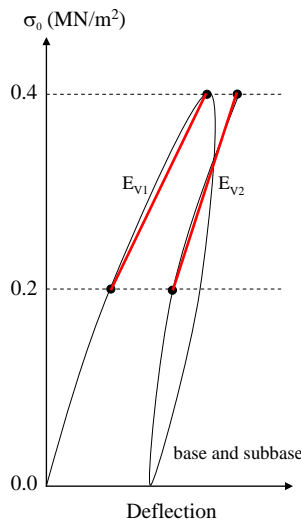


Figure 25. E_{V1} and E_{V2} determination procedure from static PLT for subgrade and base materials

The PLT was performed using a 300 mm (11.8 in.) diameter plate, but the k -value used in the pavement design guides is based on a 762 mm (30 in.) diameter plate. Therefore, the measured k_{PLT} values were corrected for plate size using a theoretical relationship (Equation 14) proposed by Terzaghi (Terzaghi and Peck 1967) for granular soils.

$$k_{PLT^*} = k_{PLT} \left[\frac{B + B_1}{2B} \right]^2 \quad (14)$$

where k_{PLT^*} = modulus of subgrade reaction using a 762 mm (30 in.) diameter plate, B_1 = 300 mm, and B = 762 mm.

Roller-Integrated Compaction Measurements

A Caterpillar CS683 vibratory smooth drum roller was used on the project (Figure 26). The device was equipped with two roller-integrated compaction monitoring measurements: (a) machine drive power (MDP), and (b) compaction meter value (CMV). Brief descriptions of these measurement values (MVs) are provided below, and some key features of the roller are summarized in Table 4.



Figure 26. Caterpillar CS683 vibratory smooth drum IC roller

Table 4. Caterpillar CS683 vibratory smooth drum IC roller features

Feature	Description
Drum Geometry	2.13 m width and 1.52 m diameter
Frequency (<i>f</i>)	30 Hz
Amplitude (<i>a</i>) Settings	Static, 0.90 mm (low amplitude), and Static, 1.80 mm (high amplitude)
Compaction Measurement Values (MVs)	MDP ₄₀ (shown as CCV in the output) and CMV
Display Software	AccuGrade
GPS coordinates	UTM Zone 15N (NAD83)
Output Documentation	Date/Time; Location (Northing/Easting/Elevation of left and right ends of the roller drum); Speed; CCV; CMV; Frequency; Amplitude; Direction (forward/backward); Vibration (On/Off)

Machine Drive Power (MDP) Value

MDP technology relates mechanical performance of the roller during compaction to the properties of the compacted soil. Detailed background information on the MDP system is provided in White et al. (2005). Controlled field studies documented by White and Thompson (2008), Thompson and White (2008), and Vennapusa et al. (2009) verified that MDP values are empirically related to soil compaction characteristics (e.g., density, stiffness, and strength). MDP is calculated using Equation 15:

$$MDP = P_g - Wv \left(\sin\alpha + \frac{A'}{g} \right) - (mv + b) \quad (15)$$

where MDP = machine drive power (kJ/s), P_g = gross power needed to move the machine (kJ/s), W = roller weight (kN), A' = machine acceleration (m/s^2), g = acceleration of gravity (m/s^2), α = slope angle (roller pitch from a sensor), v = roller velocity (m/s), and m (kJ/m) and b (kJ/s) = machine internal loss coefficients specific to a particular machine (White et al. 2005).

MDP is a relative value referencing the material properties of the calibration surface, which is generally a hard compacted surface (MDP = 0 kJ/s). Positive MDP values therefore indicate material that is less compact than the calibration surface, while negative MDP values indicate material that is more compacted than the calibration surface (i.e., less roller drum sinkage). The MDP values obtained from the machine were recalculated to range between 1 and 150 using Equation 16 (referred to as MDP₄₀).

$$MDP_{40} = 54.23 - 0.355(MDP) \quad (16)$$

In Equation 16, the calibration surface with MDP = 0 kJ/s was scaled to MDP₄₀ = 150 and a soft surface with MDP = 54.23 kJ/s (40000 lb-ft/s) was scaled to MDP₄₀ = 1.

Compaction Meter Value (CMV)

CMV is a dimensionless compaction parameter developed by Geodynamik that depends on roller dimensions, (i.e., drum diameter and weight) and roller operation parameters (e.g., frequency, amplitude, speed), and is determined using the dynamic roller response (Sandström 1994). It is calculated using Equation 19:

$$CMV = C \cdot \frac{A_{2\Omega}}{A_{\Omega}} \quad (19)$$

where, C is a constant (300), $A_{2\Omega}$ = the acceleration of the first harmonic component of the vibration, and A_{Ω} = the acceleration of the fundamental component of the vibration (Sandström and Pettersson 2004).

Correlation studies relating CMV to soil dry unit weight, strength, and stiffness are documented in the literature (e.g., Floss et al. 1983, Samaras et al. 1991, Brandl and Adam 1997, Thompson and White 2008, White and Thompson 2008).

Determination of k -values

The subgrade k values were determined from field measurements, using empirical relationships from DCP test measurements, and empirical relationships from laboratory measurements. All these values are compared in this report with reference to the design assumed value. The k values determined using different procedures and notations are listed below:

- k_{PLT^*} – determined from the static plate load test (and corrected for plate size).
- $k_{FWD-Static}$ – determined from the FWD test.
- $k_{comp-AASHTO(1993)}$ – determined using subgrade M_r determined from DCP-CBR_{Subgrade}, E_{SB} , and thickness of subbase/base layer (H_{SB}) using charts provided in AASHTO (1993) (see Appendix B). H_{SB} is determined from DCP profiles, and E_{SB} is determined using charts provided in AASHTO (1993) (see Appendix B), or directly measured from LWD or FWD tests.

CHAPTER 4. LABORATORY TEST RESULTS

Three soil samples were collected from the field and tested in the laboratory as part of this project. A summary of the material index properties (i.e., laboratory compaction test, grain-size analysis, Atterberg limits test, soil classification, and specific gravity results) is provided in Table 5.

Table 5. Summary of material index properties

Parameter	Untrimmed		
	Base (Steel Slag)	Existing Sand Subbase	Subgrade
Standard Proctor Test Results (ASTM D698-07)			
γ_{dmax} (kN/m ³)	—	—	18.58
w_{opt}	—	—	13.8
Modified Proctor Test Results (ASTM D1557-07)			
γ_{dmax} (kN/m ³)	—	—	19.84
w_{opt}	—	—	9.6
Maximum and Minimum Relative Density Test Results (ASTM D4253-00 and D4254-00)			
γ_{dmax} (kN/m ³)	16.23	19.09	—
γ_{dmin} (kN/m ³)	14.05	15.65	—
Particle-Size Analysis Results (ASTM D 422-63 & ASTM C136-06)			
Gravel Content (%) (> 4.75mm)	98	2	2
Sand Content (%) (4.75mm – 75 μ m)	0	87	47
Silt Content (%) (75 μ m – 2 μ m)	2	8	25
Clay Content (%) (< 2 μ m)	—	4	26
D ₁₀ (mm)	13.44	0.07	—
D ₃₀ (mm)	19.57	0.15	0.0037
D ₆₀ (mm)	26.18	0.24	0.17
Coefficient of Uniformity, c_u	2.0	3.5	—
Coefficient of Curvature, c_c	1.1	1.3	—
Atterberg Limits Test Results (ASTM D4318-05)			
Liquid Limit, LL (%)	Non Plastic		32
Plastic Limit, PL (%)			17
AASHTO Classification (ASTM D3282-09)	A-1-a	A-2-4(0)	A-4(0)
USCS Classification (ASTM D2487-00)	GP	SP-SM	ML
Specific Gravity, G_s (*Assumed)	2.70*	2.67	2.75*

Particle Size Analysis Results

Grain-size distribution curves from particle-size analysis tests for OGDC base, existing subbase, and subgrade materials are provided in Figure 27 through Figure 29, respectively. Figure 27 includes OGDC base layer material actual gradation and the modified gradation following the scalp and replace procedure described earlier in the laboratory test methods section to conduct M_r testing on granular materials.

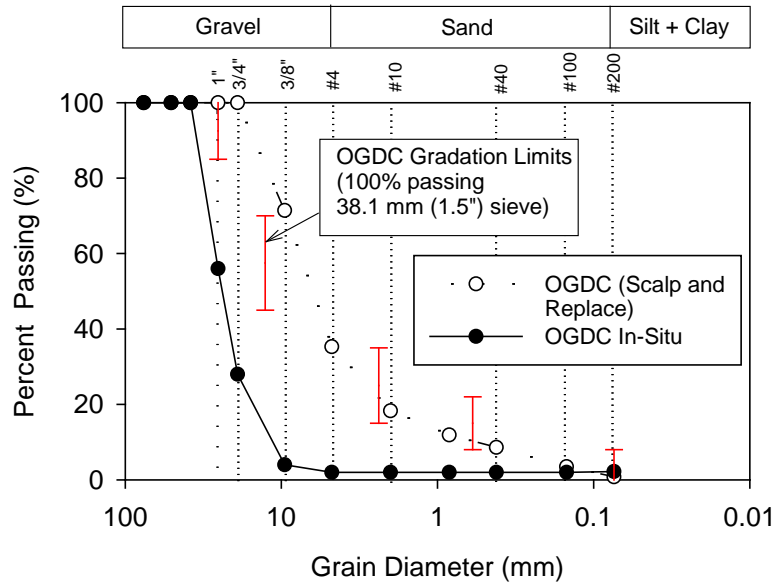


Figure 27. Particle size distribution curves of actual base material and modified gradation after scalp and replace procedure (for material retained on 19 mm (3/4 in.) sieve)

The in situ relative densities of OGDC base material ranged from 128% to 380% with an average of about 260%. The maximum relative density of the M_r and UU test samples was about 178%, which was the maximum density that could be achieved using the vibratory compaction process and scalp and replacing excess size particles (procedure described in detail in Chapter 3). It is likely that the higher densities observed in the field were due to possible segregation and variations in gradation in the material.

In situ moisture-dry unit weight measurements were not obtained for the existing subbase material. The M_r and UU tests were performed on the existing sand subbase material at two target relative densities: 36% and 106%. These tests were conducted to evaluate the effect of dry unit weight on M_r and UU properties on subbase material.

In situ dry unit of subgrade materials were obtained from “undisturbed” Shelby tube samples obtained from the project. Results indicate that in situ subgrade samples were at about 2.8 to 8.4% wet of standard Proctor w_{opt} and the dry unit weights ranged from about 89 to 93% of standard Proctor γ_{dmax} . Resilient modulus tests were conducted at three different target moisture and dry unit weights, as shown in Figure 32, to evaluate the effect of moisture and dry unit weight on resilient modulus of the subgrade material.

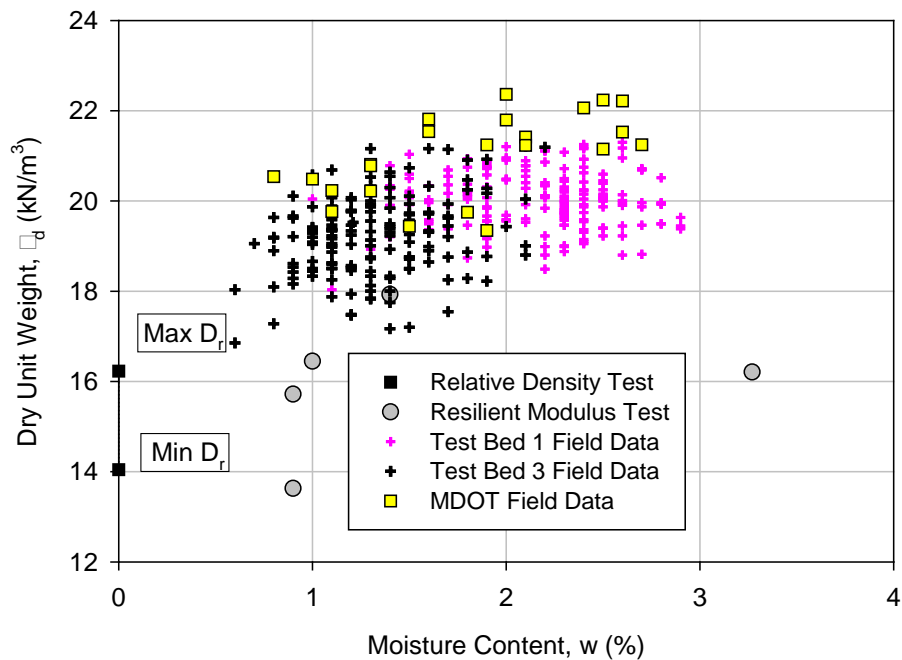


Figure 30. Laboratory and in situ moisture-density summary for OGDC base material

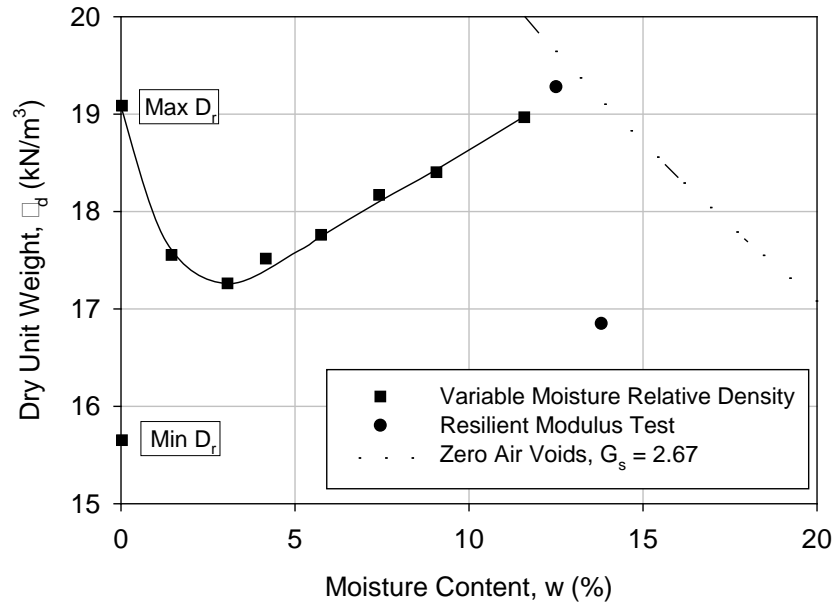


Figure 31. Laboratory and in situ moisture-density summary for existing sand subbase material

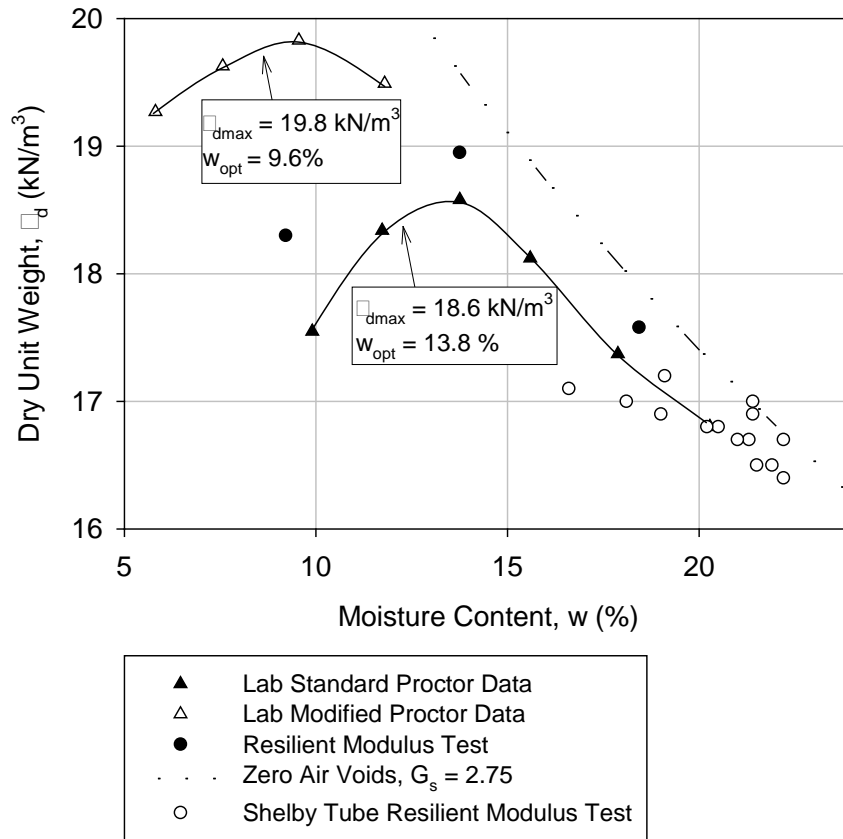


Figure 32. Laboratory and in situ moisture-density summary for subgrade material

M_r and UU Test Results

A summary of the test results for the three materials showing the γ_d , $w\%$, average M_r of the 15 AASHTO T-307 loading sequences, M_r at specific stress states, dynamic secant modulus (E_s), permanent strain (ϵ_p) at the end of the M_r test, “universal model” regression coefficients, undrained shear strength (s_u) at failure or at 5% axial strain, and s_u at 1% strain are presented in Table 6. Stress-strain curves from all resilient modulus tests are presented in Appendix D.

Stress states for granular and cohesive materials were recommended in NCHRP 1-28A report (NCHRP 2004) as $\sigma_3 = 35$ kPa (5 psi) and $\sigma_{cyclic} = 103$ kPa (15 psi) for base or subbase materials and $\sigma_3 = 14$ kPa (2 psi) and $\sigma_{cyclic} = 41$ kPa (6 psi) for subgrade materials. Equation 2 and the k_1 , k_2 , and k_3 regression coefficients were used to calculate the M_r at these stress states.

Deviator stress (σ_d) versus M_r for the Shelby tube subgrade samples obtained from field along with the “universal model” prediction curves are presented in Figure 33 and 33. σ_d versus M_r for laboratory compacted subgrade samples are presented in Figure 35. As expected for cohesive materials, these figures illustrate that the M_r generally decreases with increasing σ_d . The Shelby tube and laboratory compacted samples could not be directly compared because of the

differences in moisture and unit weight values. The laboratory samples had high dry unit weights and low moisture contents, while the Shelby tube samples had low dry unit weights and high moisture contents. Therefore, as expected, the laboratory compacted samples showed higher M_r compared to the field samples.

Bulk stress (σ_B) versus M_r for the OGDC base and existing sand subbase samples along with the corresponding “universal model” prediction curves are presented in Figure 36 and 36, respectively. Bulk stress is made up of the three orthogonal stresses. For triaxial samples, the intermediate and confining stresses are assumed to be equal ($\sigma_2 = \sigma_3$), so bulk stress is more an indicator of the confining stress applied to the sample than the deviator stress. Figure 36 and Figure 37 illustrate the confining stress dependency of granular materials (i.e., increasing confining stresses increases the M_r , as expected). Also included in Figure 37 are M_r results on samples prepared with and without using the scalp and replace procedure (as described earlier in Chapter 3). Results indicate that the differences between the modified gradation samples and the original gradation samples for the σ_B versus M_r relationships are minimal.

Moisture content, dry unit weight, and degree of saturation, and homogenous sample M_r values for OGDC base, existing subbase, and subgrade materials are compared in Figure 38. Results indicate that increasing dry unit weight and decreasing moisture content generally increased M_r values. Comparison of M_r obtained on OGDC base material before and after back-saturation indicated that increasing saturation decreased the average M_r value by about 1.4 times, while it increased the E_s value by 1.7 times.

Pictures of a layered composite sample (base over subgrade) during and after testing are shown in Figure 39 and Figure 40, respectively. σ_B versus M_r along with corresponding “universal model” prediction curves for the layered composite sample are compared with the OGDC base layer homogenous sample in Figure 41. The M_r values between homogenous and layered composite samples are compared in a bar chart presented in Figure 42. The comparison reveals that the average M_r of layered composite sample is about 1.7 times lower than the average M_r of a homogenous layer OGDC sample at a similar density. The reason for this reduction in M_r in the layered composite sample is attributed to the weaker subgrade layer. This is an important finding and must be further studied with adequate testing in various combinations of layered composite sample configurations. Efforts are underway in this research study to further investigate the influence of layered composite soil layer configurations on M_r properties.

Table 6. Mr and UU test results for all samples

Sample	Mr Test									UU Test		
	γ_a (kN/m ³)	w (%)	Ave. Mr (MPa)	Mr at Stress States (MPa) [#]	Es (MPa)	ϵ_p (%)	k ₁	k ₂	k ₃	R ²	Su (kPa) [§]	Su @ $\epsilon = 1\%$ (kPa)
A4* (0.39–0.77 m)	17.09	16.6	26.7	26.1	1.4	2.04	996.0	0.64	-9.36	0.80	53.9	28.5
C2* (0.41–0.87 m)	17.17	19.1	41.1	55.9	11.3	0.55	1476.9	-0.13	-8.72	0.87	83.4	37.9
C2* (1.19–1.65 m)	16.78	20.5	29.7	28.5	4.1	1.03	770.5	0.57	-6.67	0.83	84.9	44.4
C4* (0.55–0.98 m)	16.85	21.4	75.9	67.9	17.0	0.36	961.3	0.39	-1.79	0.64	111.3	59.6
C4* (1.19–1.59 m)	16.93	19.0	40.2	42.7	4.8	0.96	924.8	0.33	-5.56	0.77	90.4	44.4
E2* (0.38–0.76 m)	16.70	22.2	22.3	23.7	2.0	1.74	666.9	0.39	-7.56	0.82	66.5	36.1
E2* (1.19–1.60 m)	17.07	21.4	66.9	77.9	21.1	0.28	935.1	-0.09	-1.96	0.58	132.8	63.6
E4* (0.48–1.40 m)	16.54	21.9	107.4	87.5	27.8	0.52	1777.3	0.71	-3.78	0.56	122.7	65.8
E4* (0.94–1.22 m)	16.54	21.5	45.1	57.9	5.5	0.73	1025.1	-0.07	-5.17	0.70	79.8	42.6
G1* (0.48–0.61 m)	16.82	20.2	59.6	60.0	14.3	0.37	825.3	0.20	-2.14	0.47	93.0	53.1
G1* (1.02–1.40 m)	16.65	21.3	72.3	69.2	14.1	0.38	944.2	0.27	-1.84	0.45	140.4	66.2
G3* (0.39–1.00 m)	16.45	22.2	66.9	101.3	10.3	0.49	1291.8	-0.56	-3.98	0.65	104.4	47.7
G3* (1.00–1.45 m)	16.65	21.0	86.6	87.7	60.0	0.16	1401.4	0.30	-3.12	0.54	130.8	73.8
Subgrade	17.58	18.4	96.6	89.2	31.4	0.21	1491.9	0.43	-3.05	0.64	170.1	91.2
Subgrade	18.30	9.2	147.7	116.2	92.0	0.11	1376.8	0.44	-0.11	0.36	533.6	337.7
Subgrade	18.95	13.8	203.0	233.8	142.7	0.08	2287.4	-0.21	-0.61	0.06	541/0	245.1

* = subgrade Shelby tube; # subgrade: $\sigma_3 = 14$ kPa (2 psi), $\sigma_{cyclic} = 41$ kPa (6 psi); §at axial strain $\epsilon = 5\%$ or at failure

Sample	γ_a (kN/m ³)	w (%)	Ave. M_r (MPa)	M_r Test							UU Test	
				M_r at Stress States (MPa) [#]	E_s (MPa)	ϵ_p (%)	k_1	k_2	k_3	R^2	S_u (kPa) [§]	S_u @ $\epsilon = 1\%$ (kPa)
Existing Sand Subbase	16.85	14.4	121.1	69.0	26.3	1.50	460.4	1.05	-0.61	0.96	82.9	81.4
Existing Sand Subbase	19.28	14.9	146.7	94.9	36.5	1.46	655.2	0.80	-0.26	0.97	76.0	75.0
OGDC Base	15.72	0.9	288.1	189.0	306.0	0.11	1244.1	0.68	0.15	0.92	262.4	261.3
OGDC Base	13.63	0.9	238.6	154.3	54.1	0.64	916.3	0.51	0.85	0.95	138.5	121.9
OGDC Base ^{SR}	16.45	1.3	214.7	133.0	73.6	0.69	852.4	0.78	0.06	0.98	146.2	118.1
OGDC Base ^{SR}	17.93	1.4	281.1	199.0	214.4	0.20	1564.6	0.78	-0.69	0.82	216.8	196.9
OGDC Base ⁺	16.21	3.3	154.9	88.4	128.3	0.30	555.1	0.95	-0.20	0.97	220.4	202.9
Layered Composite: OGDC Base/ Subgrade	16.65	1.6										
	17.37	15.0	125.8	111.6	37.5	1.35	1084.6	0.43	-0.78	0.72	179.1	154.1

[#] Base/subbase: $\sigma_3 = 35$ kPa (5 psi), $\sigma_{cyclic} = 103$ kPa (15 psi); ^{SR} = scalp and replace method; ⁺ = back saturated; [§]at axial strain $\epsilon = 5\%$ or at failure

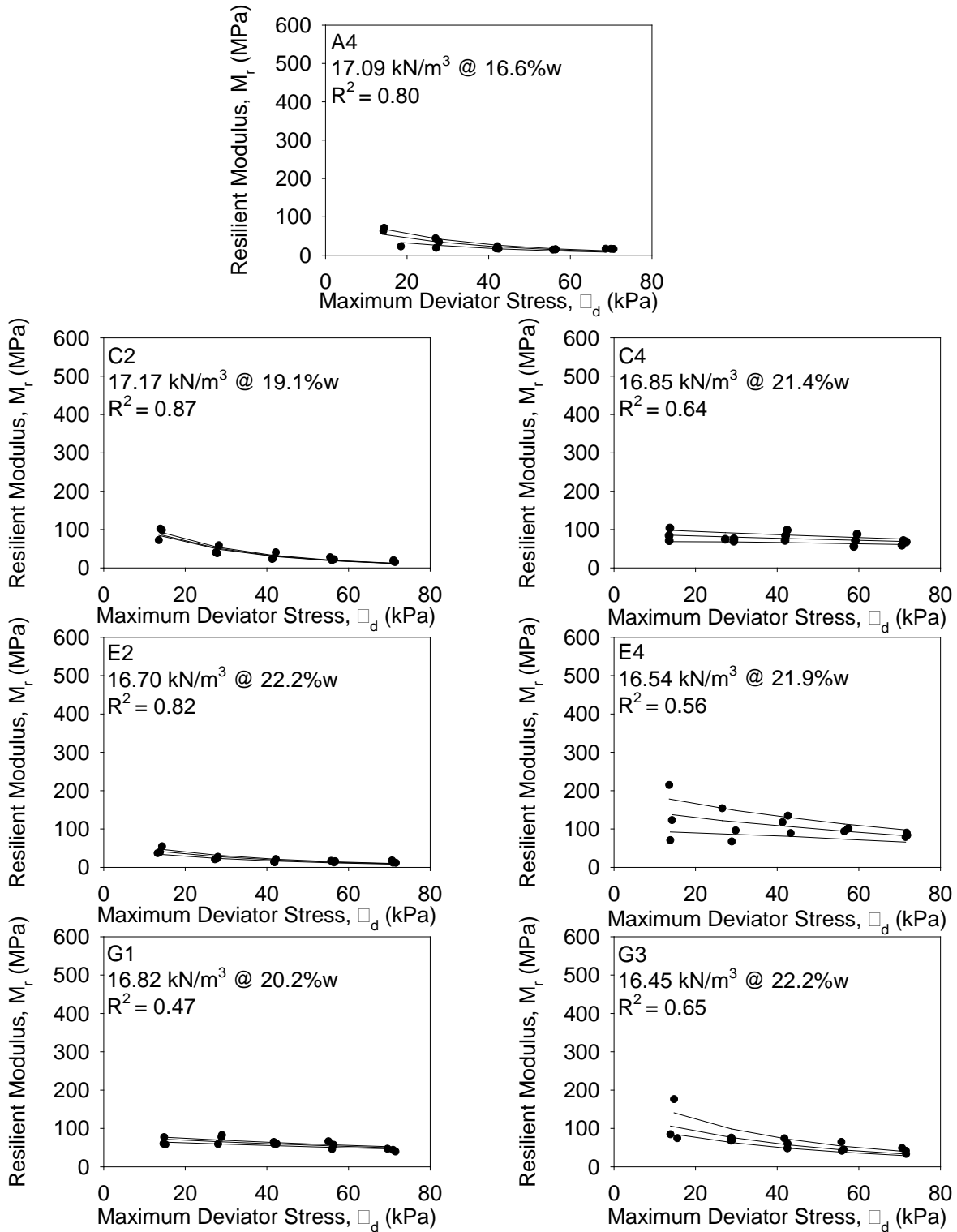


Figure 33. Summary of σ_d versus M_r for Shelby tubes taken 0.4 m to 1.0 m below the ground surface

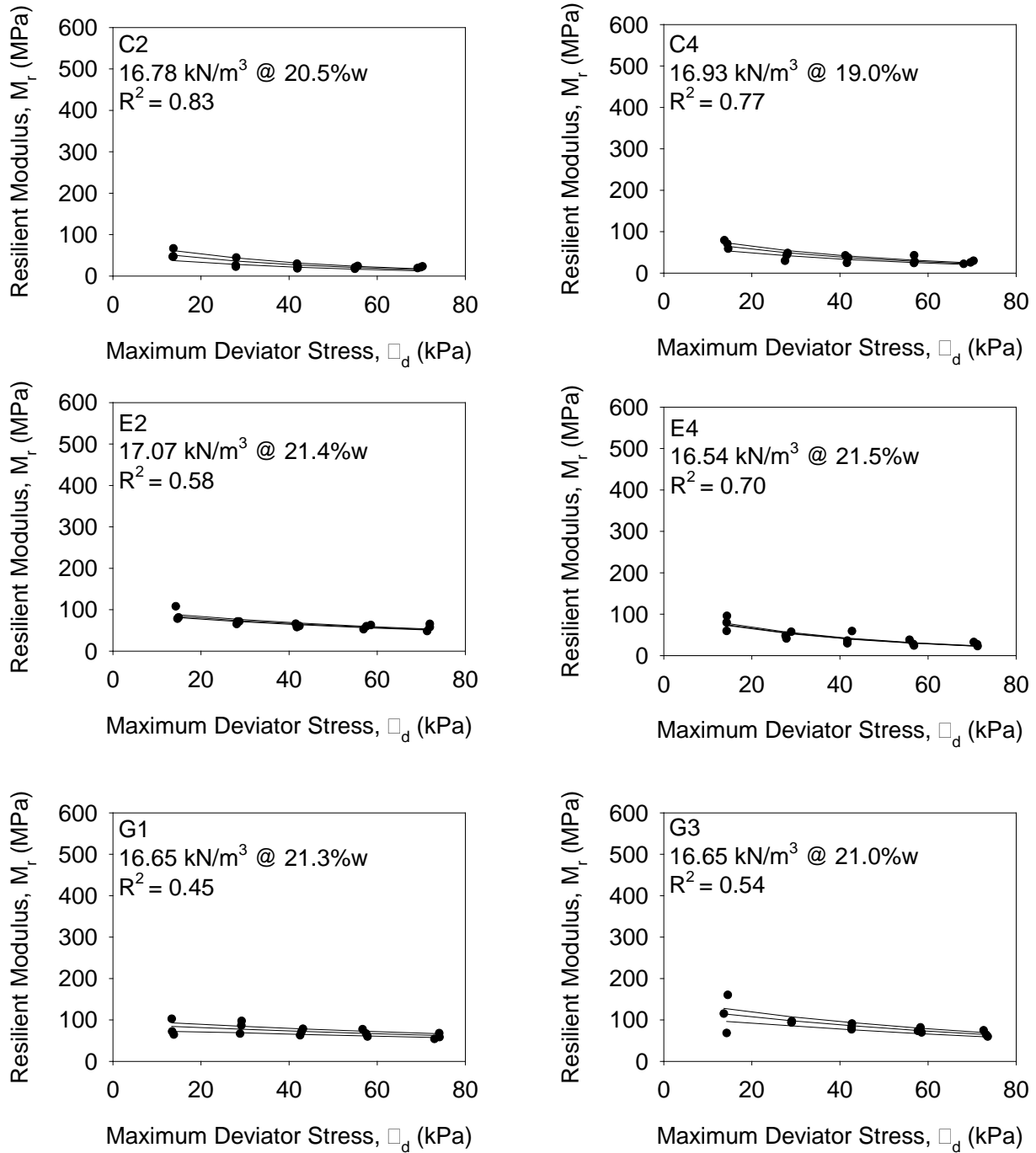


Figure 34. Summary of σ_d versus M_r for Shelby tubes taken 1.0 m to 1.7 m below the ground surface

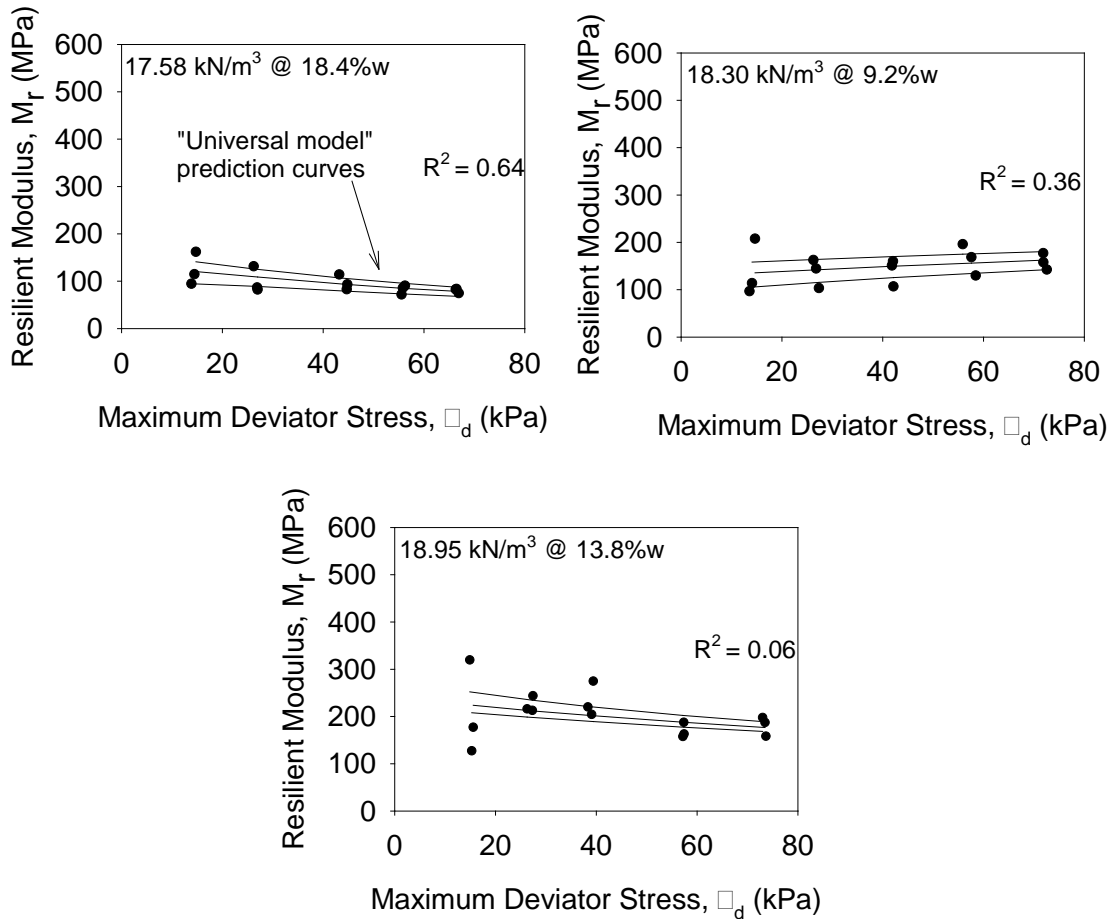


Figure 35. Summary of σ_d versus M_r for subgrade samples (compacted in laboratory)

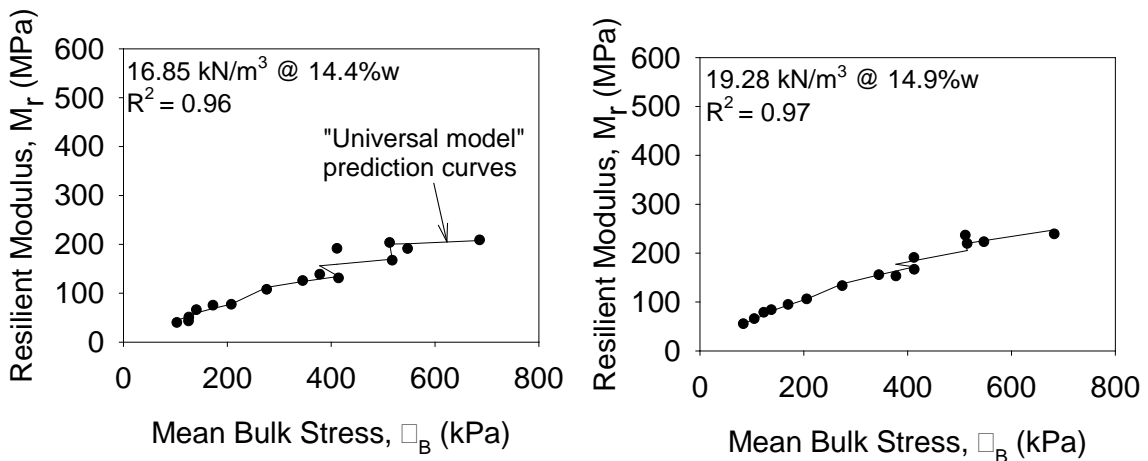


Figure 36. Summary of σ_B versus M_r for existing sand subbase samples

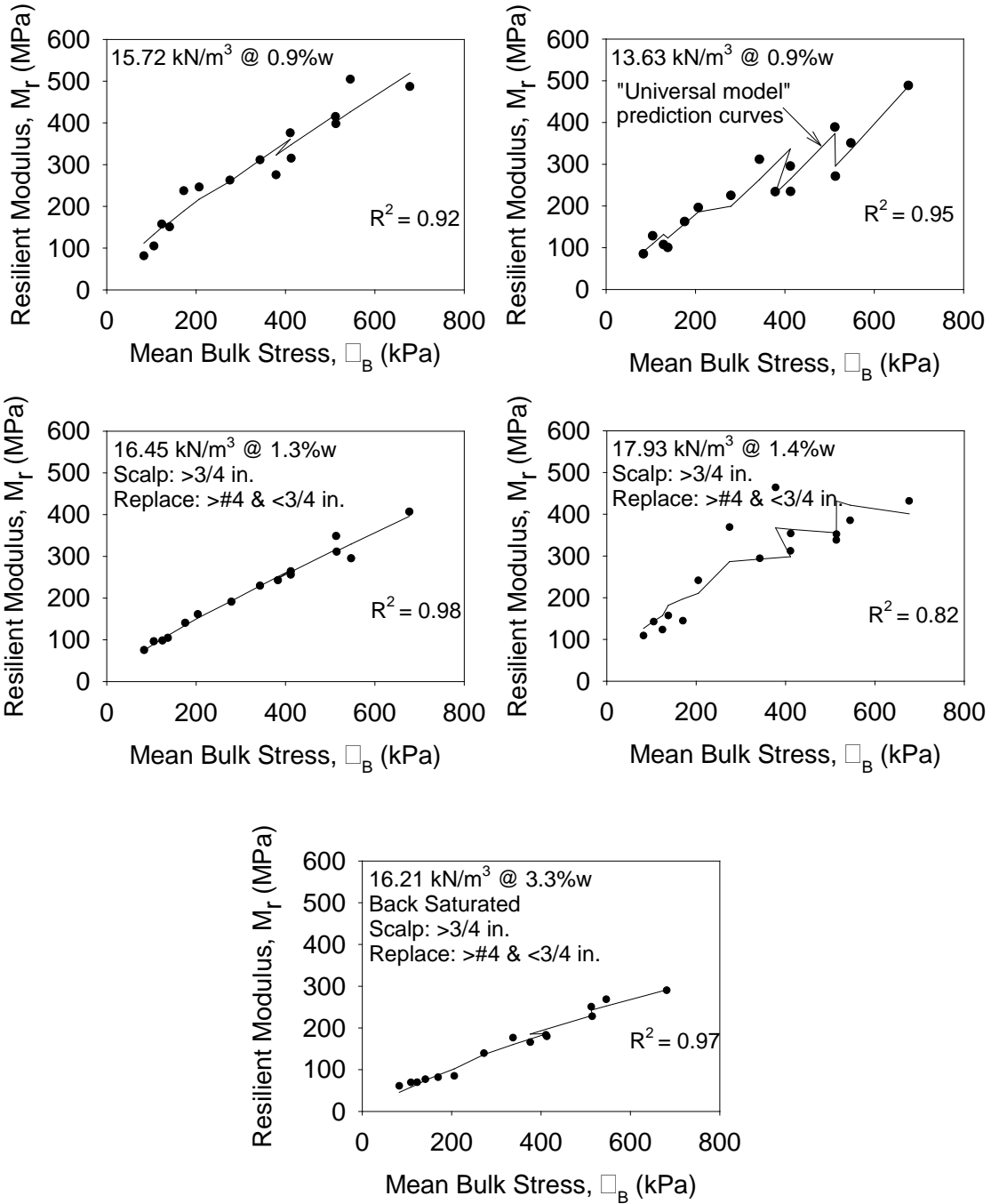


Figure 37. Summary of σ_B versus M_r for OGDC base samples

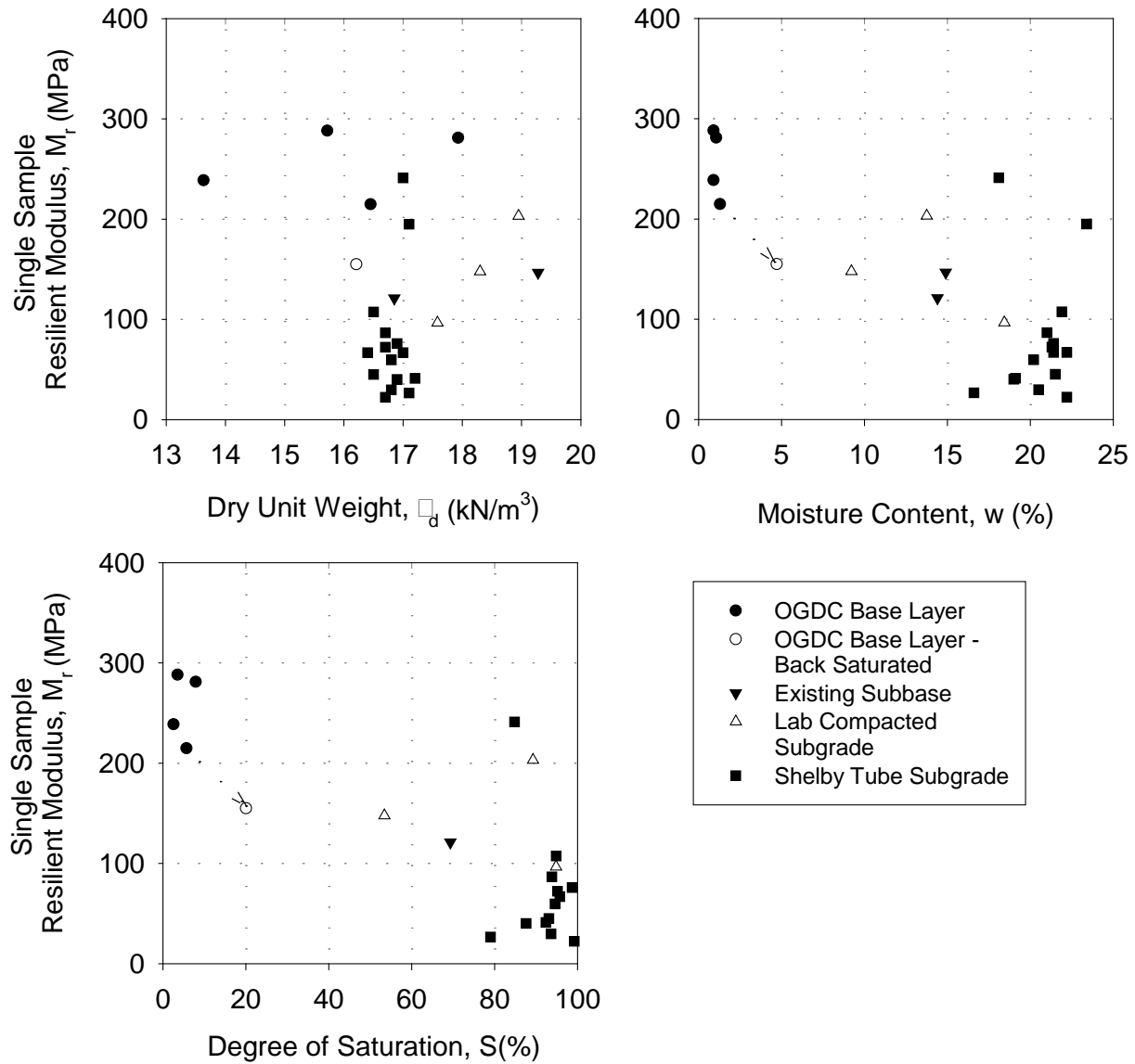


Figure 38. Relationships between dry unit weight, moisture content, and degree of saturation, and M_r on homogenous samples



Figure 39. Untrimmed base (16.65 kN/m^3 at 1.6% moisture) over subgrade (17.37 kN/m^3 at 15.0% moisture) during M_r testing



Figure 40. Untrimmed base (16.65 kN/m^3 at 1.6% moisture) over subgrade (17.37 kN/m^3 at 15.0% moisture) after M_r testing

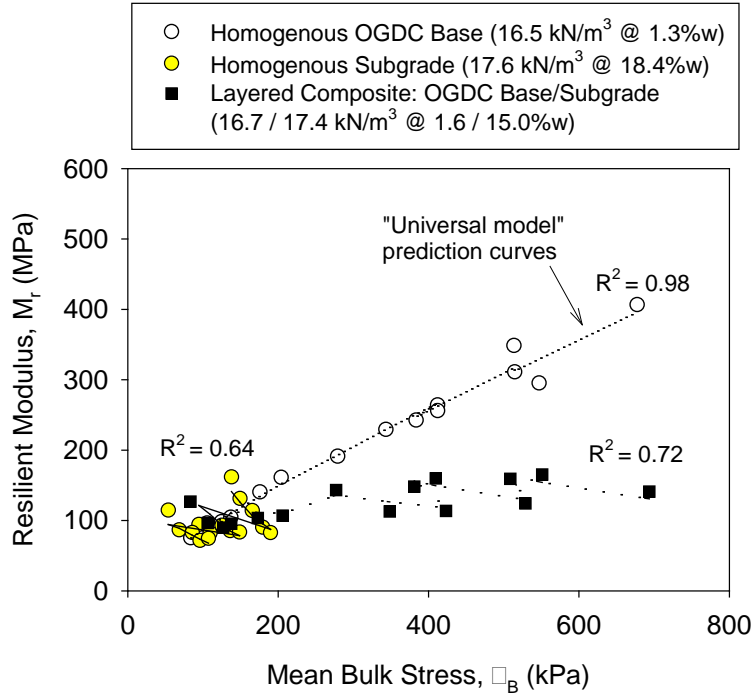


Figure 41. Comparison of σ_B versus M_r for layered composite sample and OGDC base and subgrade homogenous samples

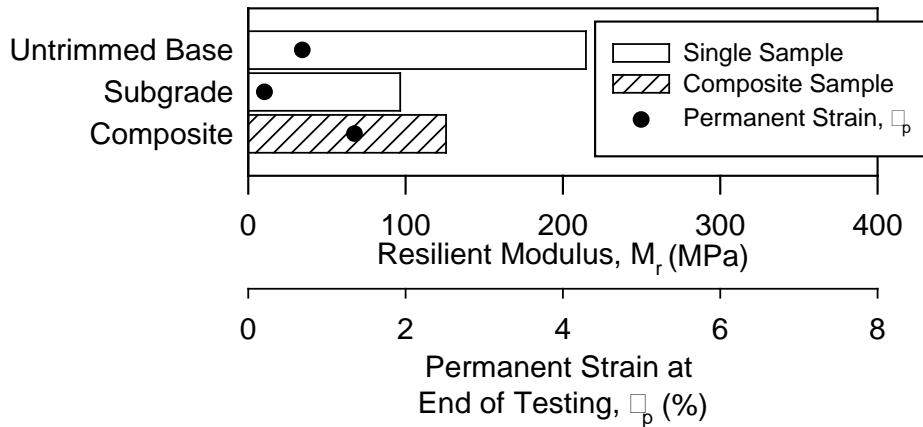


Figure 42. Comparison of homogenous and layered composite samples of base and subgrade $M_{r(T307)}$ values

Cyclic Triaxial and Aggregate Degradation Test Results

Cyclic triaxial testing with 100,000 loading cycles at a deviator stress level of 41.4 kPa (6 psi) or 62.0 kPa (9 psi) at a confining stress of 20.7 kPa (3 psi) was conducted on seven samples obtained from the OGDC layer. Particle size analysis tests were conducted on the samples before and after cyclic triaxial testing to evaluate the particle degradation under repeated loading. Each

cyclic load test was conducted with a unique series of test parameters to compare with others and evaluate the effect of a single test parameter. These parameters included: (a) fines content, (b) dry unit weight, and (c) deviator stress. Fines content was varied from 2% to 8% at every 2% increments without varying the compacted dry unit weight, moisture content, and deviator/confining stresses. Similarly, to evaluate the effect of dry unit weight, samples were prepared at a target 90% and 100% relative density with a target fines content of 2%. All samples were prepared at a target moisture content of about 3.3%, which is the mean value from field measurements. A summary of the test parameters and results is provided in Table 7.

The actual relative density (D_r) values varied from 105% to 107% on samples prepared with a target $D_r = 90\%$, and the actual D_r value was 119% for the sample prepared with a target of $D_r = 100\%$. The reason for these higher than anticipated densities is attributed to the differences in the gradation of the sample used in the testing versus the sample used in the relative density vibratory compaction test (note that the scalp and replace procedure was not used in the vibratory compaction test). The actual fines content varied from about 3.3% to 9.0% prior to triaxial testing.

Results from the cyclic triaxial tests are provided in Figure 43 and are summarized in Table 7. These results indicate that the permanent strain (ϵ_p) after 100,000 cycles generally increased from about 0.3 to 0.7% with increasing fines content from about 3% to 7%. Interestingly, the sample with 8% fines resulted in a ϵ_p of 0.3%. As expected, increasing dry unit weight from about 16.35 kN/m³ to 16.73 kN/m³ resulted in a decrease ϵ_p from about 0.4% to 0.2%, and increasing σ_d from 41.4 kPa to 62.0 kPa showed an increase in ϵ_p from about 0.3 to 0.7%.

Results from particle size analysis on samples before and after cyclic triaxial testing are summarized in Figure 44 and the gradation properties (i.e., D_{10} , D_{30} , D_{60} , and F_{200}) are provided in Table 7. These results did not indicate any considerable difference in gradation properties before and after the cyclic triaxial tests.

Similar cyclic triaxial and aggregate degradation testing is currently being performed on materials obtained from multiple project sites as part of this research. Statistical analysis combining results from various projects will be conducted to develop models to predict permanent deformation and aggregate degradation behavior based on test parameters and type of material.

Table 7. Summary of cyclic triaxial and degradation test results on OGDC base material

Parameter		Measurements					
Target F_{200} (%)		2.0	2.0	4.0	4.0	6.0	8.0
Nominal σ_d (kPa)		41.4	41.4	41.4	62.0	41.4	41.4
Nominal σ_c (kPa)		20.7	20.7	20.7	20.7	20.7	20.7
Target w (%)		3.30	3.30	3.30	3.30	3.30	3.30
Actual w (%)		3.62	3.25	3.64	3.52	3.37	3.40
Target γ_d (kN/m ³)		15.99	16.24	15.99	15.99	15.99	15.99
Target D_r (%)		90	100	90	90	90	90
Actual γ_d (kN/m ³)		16.35	16.73	16.37	16.40	16.48	16.40
Actual D_r (%)		105	119	106	107	110	107
Actual F_{200} (%)	Pre-test	3.3	3.3	4.5	4.5	6.9	9.0
	Post-test	3.3	3.6	5.0	4.7	7.1	9.0
D_{10} (mm)	Pre-test	0.6	0.5	0.5	0.5	0.2	0.1
	Post-test	0.6	0.5	0.4	0.5	0.2	0.1
D_{30} (mm)	Pre-test	4.0	4.0	4.7	4.7	3.4	3.4
	Post-test	4.9	3.9	4.5	4.9	3.2	3.4
D_{60} (mm)	Pre-test	8.4	9.0	9.5	9.5	8.9	9.1
	Post-test	9.9	9.0	9.5	10.2	9.0	8.9
ε_p (%) at the end of 100,000 cycles		0.4%	0.16%	0.32%	0.66%	0.71%	0.34%

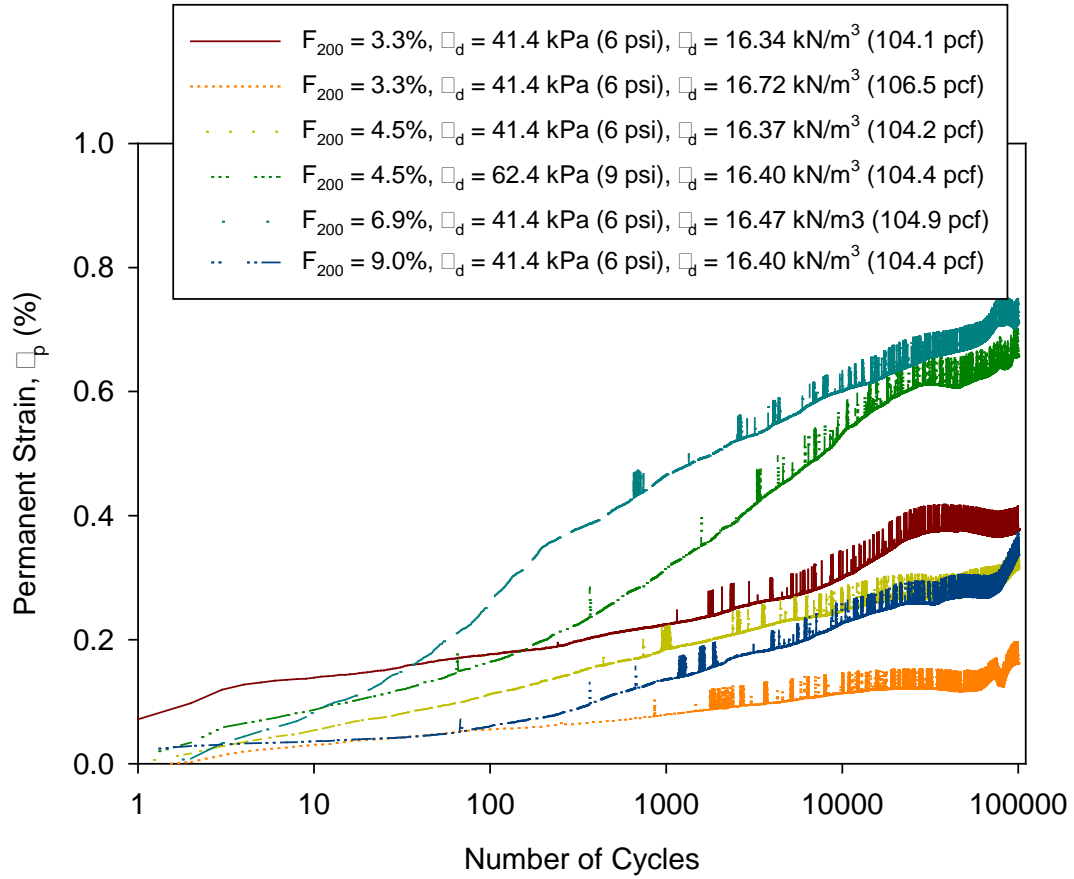


Figure 43. Results of cyclic triaxial tests on OGDC base material

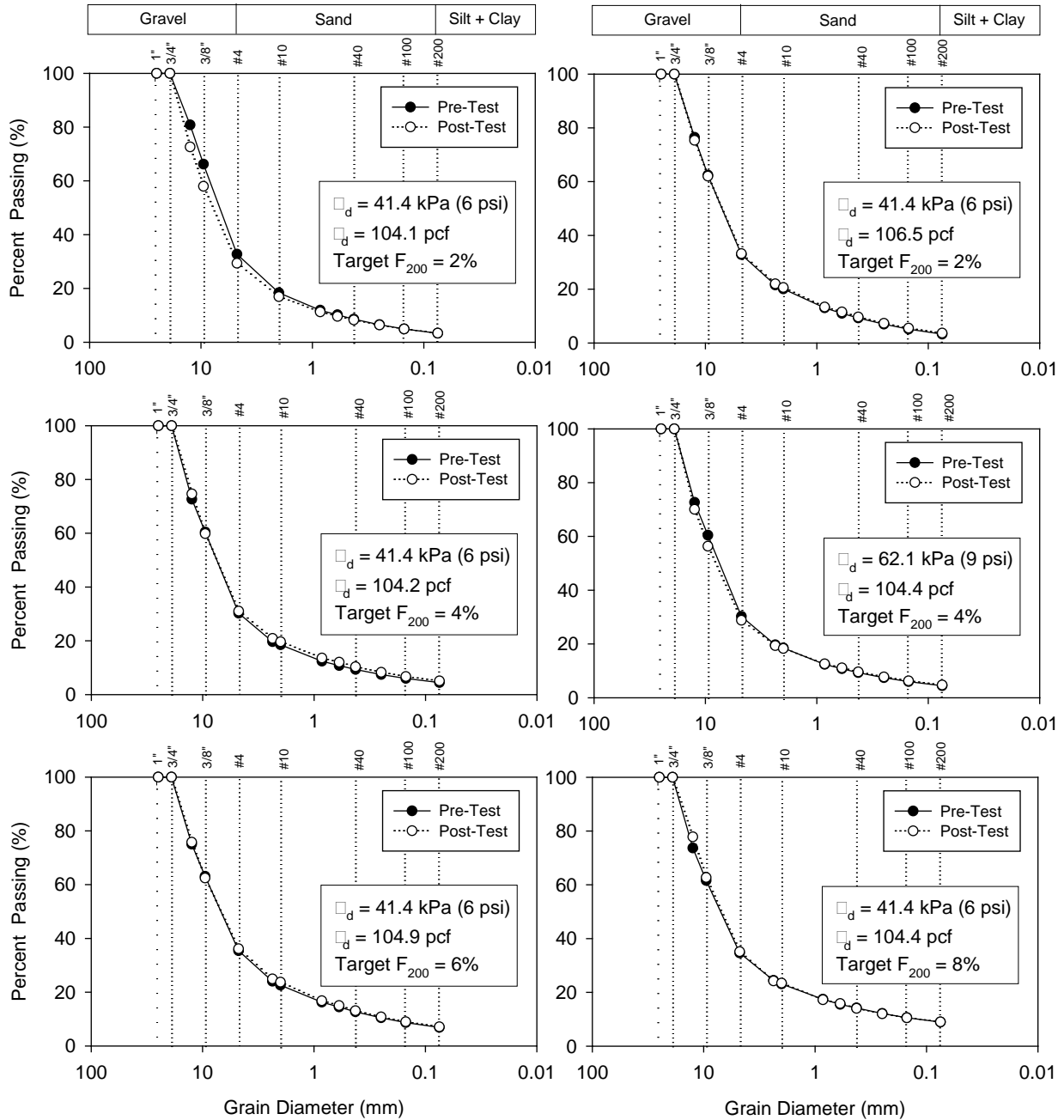


Figure 44. Particle size analysis test results of OGDC base material before and after cyclic triaxial tests

Laboratory Permeability Test Results

Laboratory permeability tests were performed using LSLP test equipment following the falling head test method. Three tests were performed to determine an average K_{sat} value. A sample was compacted in three lifts of equal thickness to reach a sample thickness of about 150 mm (6 in.). The sample was compacted using a Marshall hammer using 50 blows per layer. Visually, no

increase in density was noticed after 50 blows in each layer. The dry density achieved using this compaction method was about 14.77 kN/m^3 (94 pcf) and the material contained about 2% moisture content. Time t was recorded for the water head level to drop from about 90 to 50 cm. Using these values, the average $K_{\text{sat}} = 3.1 \text{ cm/s}$ was determined based on three consecutive tests on the same sample (K_{sat} ranged from 3.0 to 3.2 cm/s in the three tests performed).

Microstructural Analysis

A sample of OGDC steel slag aggregate material with 12.5 mm to 50 mm diameter chunks with varying color were chosen for microstructural analysis. Some samples were blown clean with an air duster to examine the surface (referred to as “rough surfaces” in the images). Others were rinsed with water in an ultrasonic bath, dried, embedded in epoxy, and ground to prepare a polished section (referred to as “polished surfaces” in the SEM images). Color stereo microscope images of all samples are presented in Appendix E. A wide range of colors varying from gray to light brown to dark brown and appearance were evident from the images. SEM images of one selected rough surface and one polished surface at different magnifications (7x, 25x, 100x, and 300x) are presented in Figure 45 and Figure 46, respectively.

Most pieces were quite porous, but some were quite dense and uniform. In rough form, the chunks showed macro porosity in the SEM. Most of the material was a uniform gray color in backscattered electron (BSE) images. Some areas showed light second phases indicating a higher content of heavy elements. The elemental analysis showed that the primary constituents of the slag material are composed of about 54% Oxygen (O), 16% Calcium (Ca), 14% Silica (Si), 8% Magnesium (Mg), 5% Aluminum (Al), among other minor amounts of elements. Figure 47 and Figure 48 show spatial distribution of elements for gray vesicular surface (at 300 x magnification) and polished surface B (at 400x magnification) samples, respectively. Figure 49 shows the intensity (counts per second/eV) versus the keV for polished surface A and polished surface B samples.

The composition of all samples was fairly consistent regardless of the visual appearance of the chunks. The polished sections showed granular structure and that porosity generally extended through the interior of the material. The grains were typically surrounded by another phase. Light material (i.e., Mn, Fe-rich) was found at the surfaces of the pores. Some sections (e.g., polished surface H) showed a fairly smooth material. It had some pores with isolated islands of light material, but did not show the clear granular nature evident in other samples (see Appendix E).

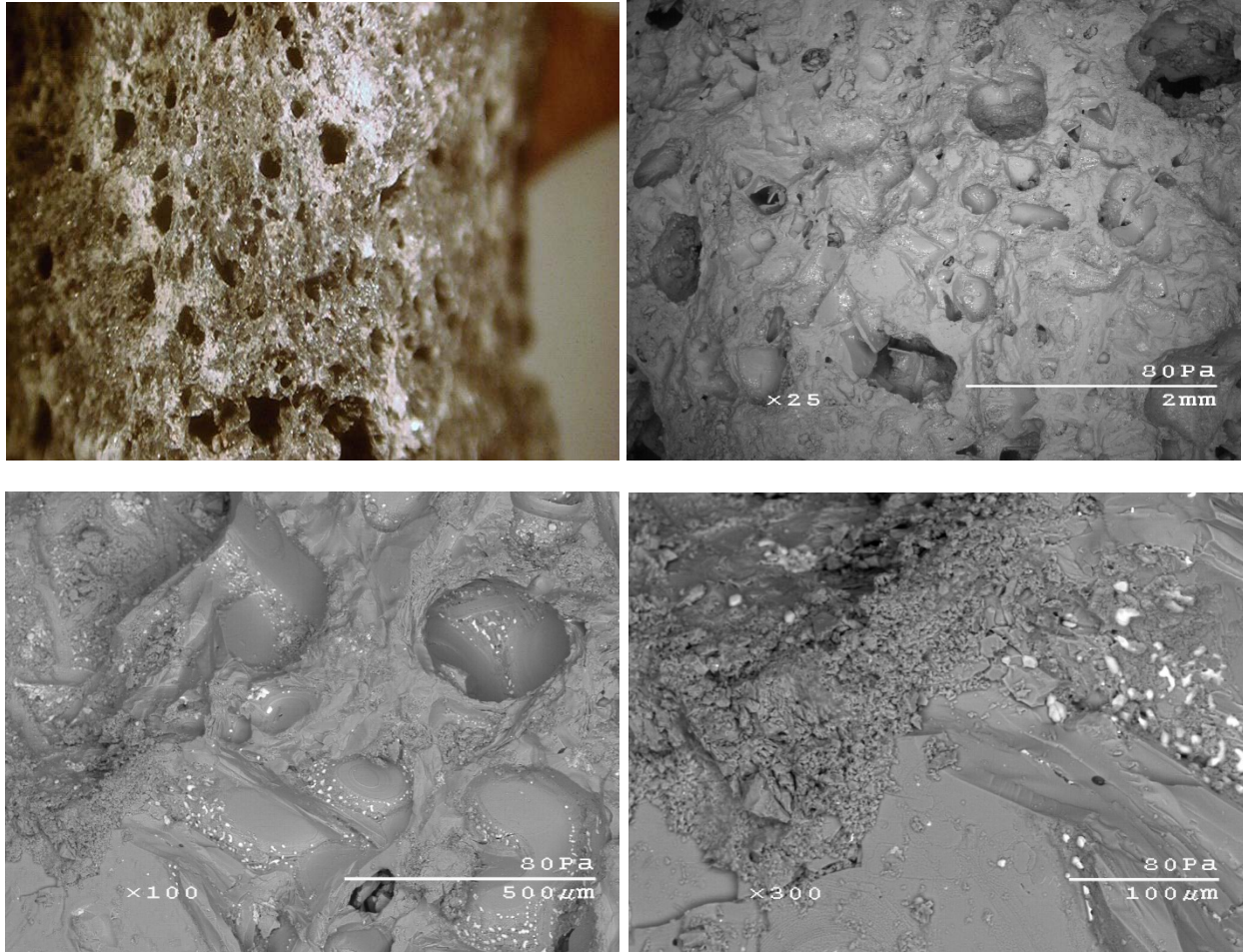


Figure 45. Color stereo microscope image of rough gray vesicular surface at 7x magnification, and SEM images at 7x, 25x, 100x, and 300x magnification

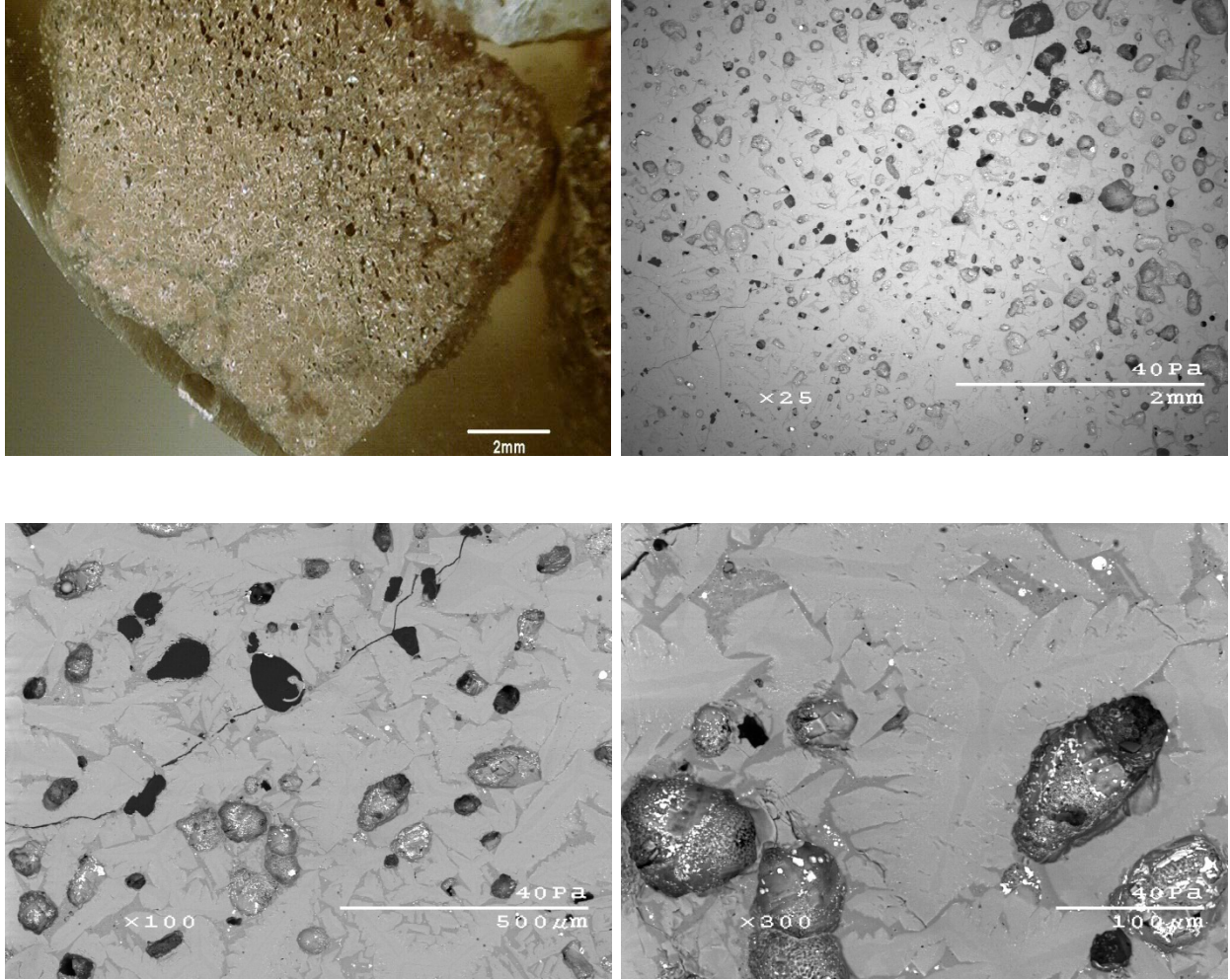


Figure 46. Color stereo microscope image of polished surface B at 7x magnification, and SEM images at 7x, 25x, 100x, and 300x magnification

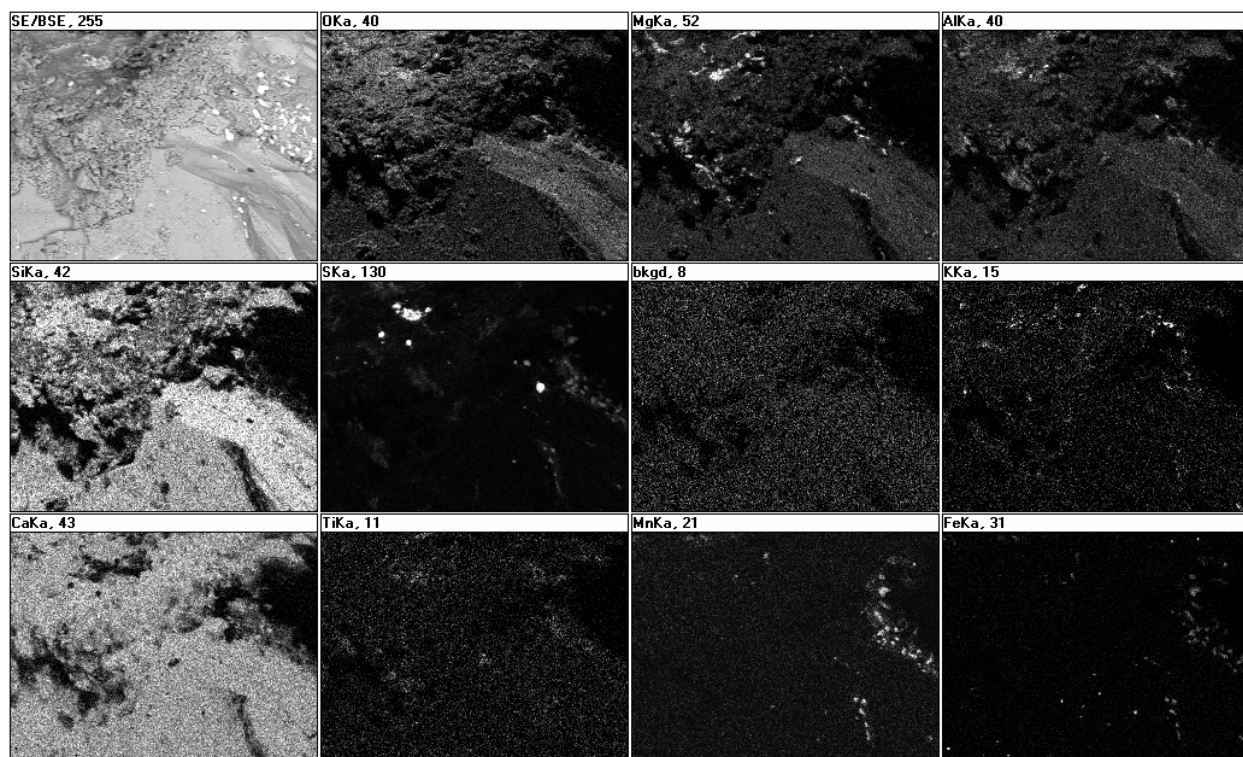


Figure 47. Elemental maps of gray vesicular surface at 300x magnification

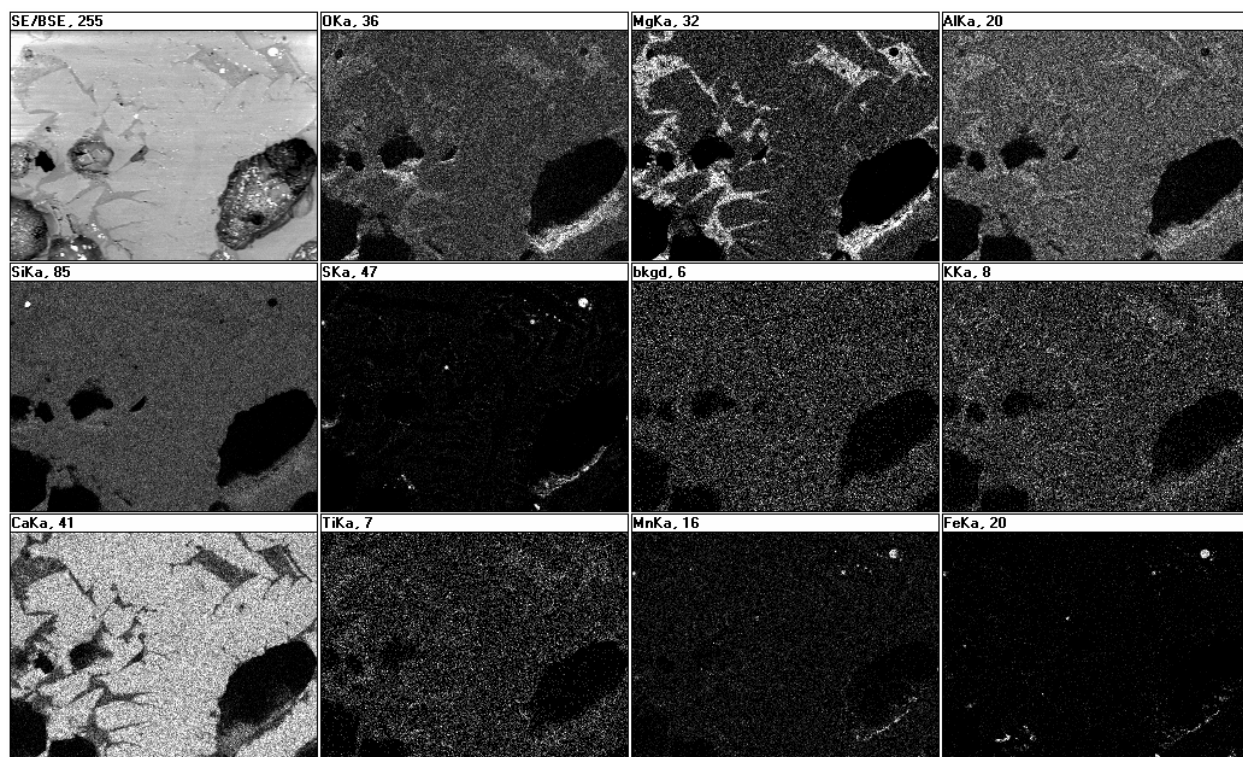


Figure 48. Elemental maps of polished surface B at 400x magnification

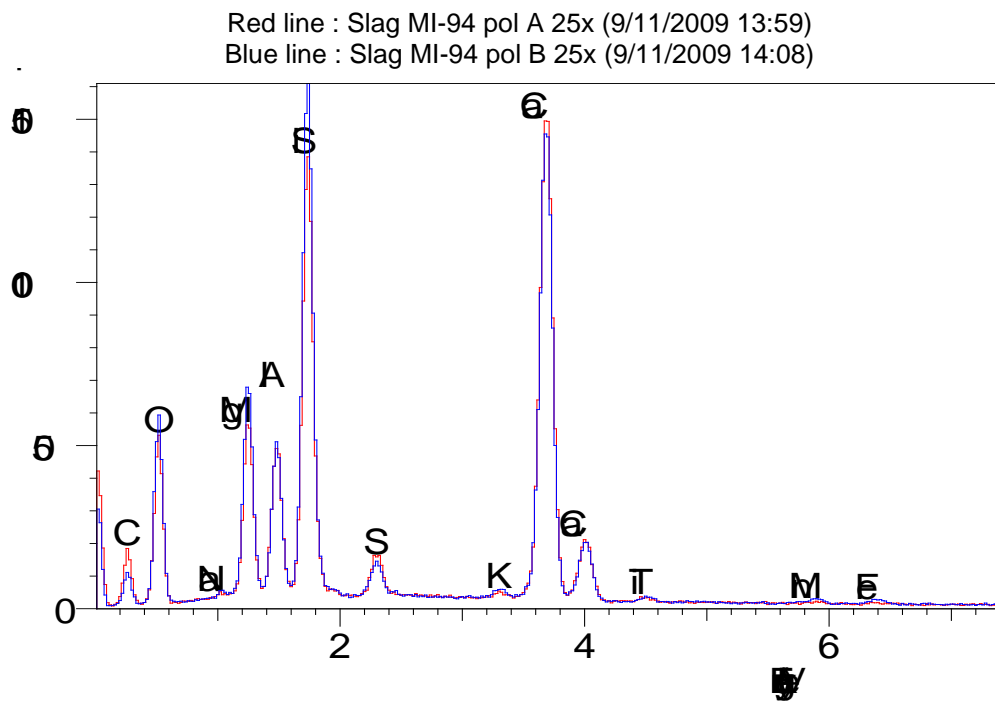


Figure 49. Elemental analysis of polished surfaces A and B at 25x magnification

CHAPTER 5. IN SITU TEST RESULTS

Description of Test Sections

A total of three TS were tested as part of this project. Of these, two TS consisted of areas with the newly constructed OGDC base layer, while one TS consisted investigating the conditions of the existing pavement and foundation layers. Various in situ testing methods were used in characterizing the pavement surface and foundation layer properties, and a summary of each TS is provided in Table 8.

Table 8. Summary of test sections and in situ testing

TS	Date	Location	Material	In situ Test Measurements	Comments
1a	5/27/2009	Sta. 804+00 to 813+00 [I-94 EB]	Newly constructed base	NG, DCP, LWD	Section tested after trimmed to grade.
1b	5/28/2009	Sta. 809+00 [I-94 EB] (7 m x 7 m area)	Newly constructed base	NG, DCP, LWD, GPT	Section tested after trimmed to grade. Testing was performed in 0.6 m x 0.6 m grid.
2a	5/27/2009	East of Adair rest area on-ramp	Existing PCC surface	FWD	FWD testing was performed on inner and outer lanes over a length of about 80 m.
2b	5/29/2009	East of Adair rest area on-ramp	Existing PCC surface, subbase and subgrade	FWD, GPT, DCP, LWD	Testing was performed in a grid pattern on the surface, and on existing subbase. Shelby tube samples of subgrade were obtained for M_r testing in laboratory.
3a	5/28/2009	Sta. 839+50 to 866+00	Newly constructed base	CMV, MDP, NG, DCP, LWD, FWD, PLT	Section tested prior to trimming. Rolling performed using low amplitude setting for two passes.
3b	5/28 – 5/29/2009	Sta. 866+00 to 890+00	Newly constructed base	CMV, MDP	
3c	6/1/2009	Sta. 959+00 to 969+00	Existing Subgrade	CMV, MDP	

Note: NG – nuclear gauge, DCP – dynamic cone penetrometer (DCP) test, LWD – Zorn light weight deflectometer with a 300 millimeter plate, GPT – gas permeameter test device, FWD – Kuab falling weight deflectometer (FWD), CMV – compaction meter value measured using CS-683 vibratory smooth drum roller, MDP – machine drive power measured using CS-683 vibratory smooth drum roller, PLT –static plate load test.

Geostatistical Data Analysis

Spatially referenced near continuous roller-integrated compaction measurements and in situ point measurements in a dense grid pattern were obtained in this study. These data sets provide an opportunity to quantify “non-uniformity” of compacted fill materials. Non-uniformity can be assessed using conventional univariate statistical methods (i.e., by statistical standard deviation (σ) and coefficient of variation (COV)), but they do not address the spatial aspect of non-uniformity. Vennapusa et al. (2010) demonstrated the use of semivariogram analysis in combination with conventional statistical analysis to evaluate non-uniformity in QC/QA during earthwork construction. A semivariogram is a plot of the average squared differences between data values as a function of separation distance, and is a common tool used in geostatistical studies to describe spatial variation. A typical semivariogram plot is presented in Figure 50.

The semivariogram $\gamma(h)$ is defined as one-half of the average squared differences between data values that are separated at a distance h (Isaaks and Srivastava 1989). If this calculation is repeated for many different values of h (as the sample data will support) the result can be graphically presented as experimental semivariogram, shown as circles in Figure 50. More details on experimental semivariogram calculation procedure are available elsewhere in the literature (e.g., Clark and Harper 2002, Isaaks and Srivastava 1989).

To obtain an algebraic expression for the relationship between separation distance and experimental semivariogram, a theoretical model is fit to the data. Some commonly used models include linear, spherical, exponential, and Gaussian models. A spherical model was used for data analysis in this report. Arithmetic expression of the spherical model and the spherical variogram are shown in Figure 50.

Three parameters are used to construct a theoretical semivariogram: sill ($C+C_0$); range (R); and nugget (C_0). These parameters are briefly described in Figure 50. More discussion on the theoretical models can be found elsewhere in the literature (e.g., Clark and Harper 2002, Isaaks and Srivastava 1989).

For the results presented in this report, the sill, range, and nugget values during theoretical model fitting were determined by checking the models for “goodness” using the modified Cressie goodness fit method (see Clark and Harper 2002) and cross-validation process (see Isaaks and Srivastava 1989). From a theoretical semivariogram model, a low “sill” and longer “range of influence” represent best conditions for uniformity, while the opposite represents an increasingly non-uniform condition.

Some of the results presented in this report revealed nested structures with short-range and long-range components in the experimental semivariograms. Nested structures have been observed in geological applications where different physical processes are responsible for spatial variations at different scales (see Chiles and Delfiner 1999). For the cases with nested structures, nested spherical variograms combining two spherical models (with two sill values and two range values) are fit to the experimental semivariogram data. A few previous studies (e.g., White et al. 2010b) have reported nested semivariograms with roller-integrated compaction measurements,

where the long-range component of the semivariogram was likely influenced by support conditions below the compaction layer, and the short-range component was likely due to the compaction layer properties.

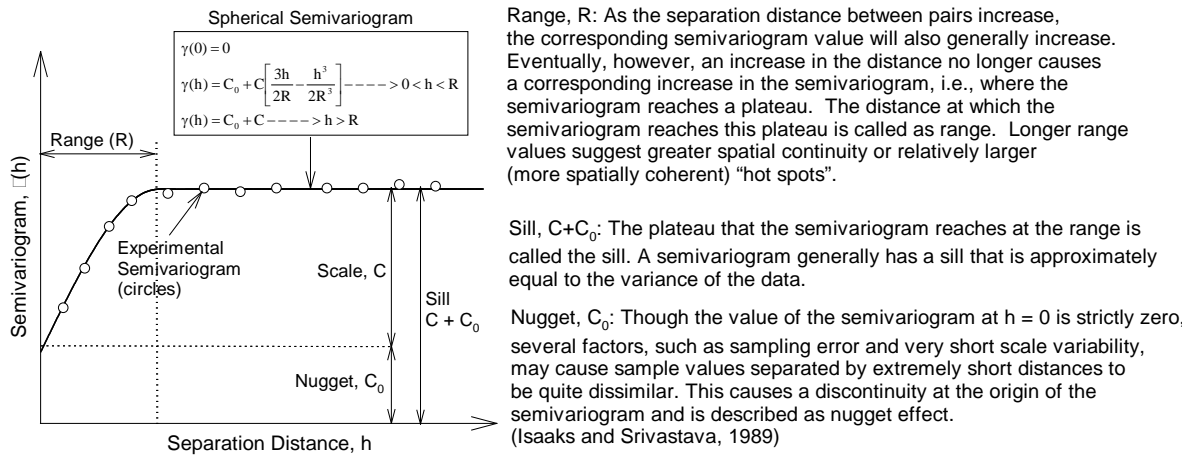


Figure 50. Description of a typical experimental and spherical semivariogram and its parameters

TS1 and TS3: Newly Constructed OGDC Base and Subgrade Layers

Test Sections Construction and Experimental Testing

TS1 involved testing the OGDC base layer on I-94 EB lanes between Sta. 804+00 and 813+00. The material was placed, compacted, and trimmed in this area prior to our testing. TS1-A involved testing every +50 station between Sta. 804+00 and 813+00 (Figure 51) along the centerline of the I-94 EB alignment and left and right of the centerline at about 4 m offsets. TS1-B involved testing a 7 m x 7 m area near Sta. 809+00 in a dense grid pattern (Figure 51, Figure 52) with 121 test points. NG, LWD, GPT, and DCP tests were conducted on this test section.

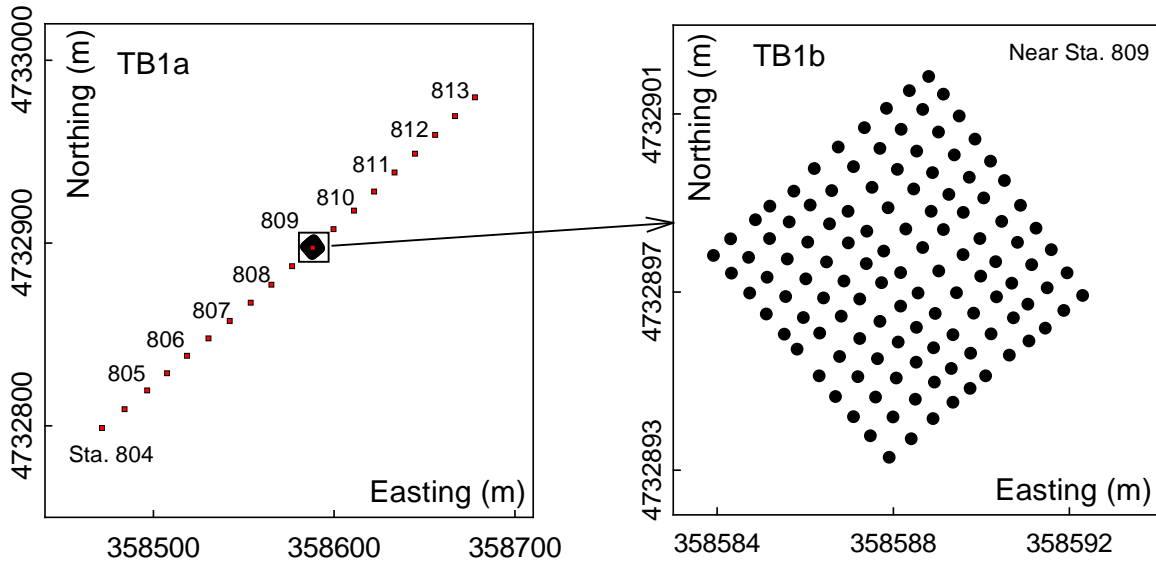


Figure 51. TS1: Plan view of in situ test locations



Figure 52. TS1-B: Photograph showing testing on the 0.6 m x 0.6 m grid pattern

TS3-A and TS3-B involved testing the OGDC base layer between Sta. 839+50 and 890+00. The material was placed and compacted in this area prior to our testing, but was not trimmed to the final grade. TS3-A involved testing using point measurements at every +50 station between Sta. 839+50 and 866+00 (Figure 53) along the center line of the I-94 EB alignment, and left and right of the center line at about 4 m offsets. NG, DCP, LWD, FWD, and PLT point tests were conducted on TS3-A.

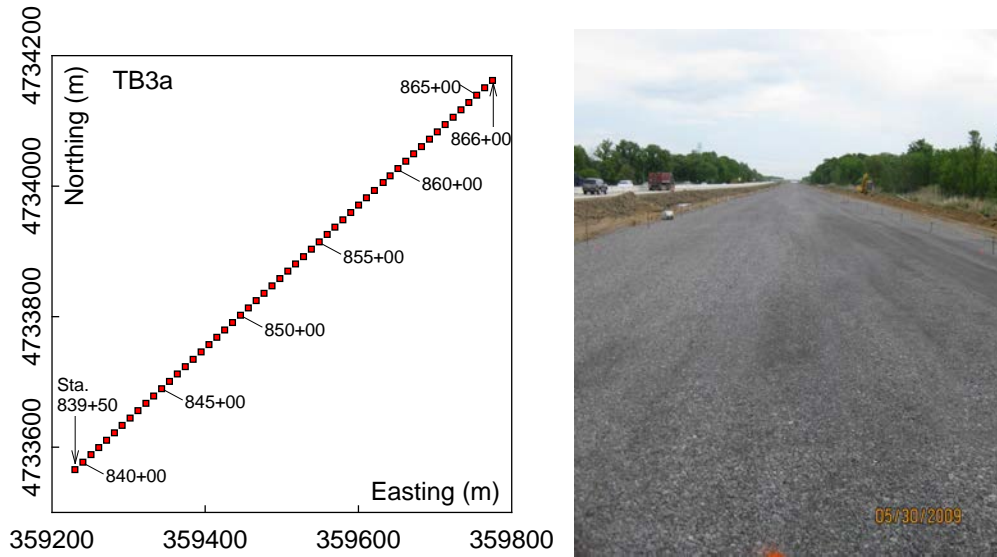


Figure 53. Plan view of in situ test locations on TS3-A (left) and photograph of TS3-A untrimmed OGDC base layer (right)

In addition, CMV and MDP_{40} roller-integrated measurements were obtained using the CS683 smooth drum roller in TSs 3a, 3b, and 3c. TS3b was located between Sta. 866+00 and 890+00. TS3c was located between Sta. 959+00 and 969+00 and consisted of compacted subgrade layer. Roller-integrated measurements were obtained for two roller passes on TS3-A, and one roller passes on TSs 3b and 3c. All roller passes were made using low amplitude (0.90 mm) and frequency = 30 Hz nominal settings at an average speed of about 4 km/h.

In Situ Point Test Results and Discussion

In situ test results from TS1-A are presented in Figure 54 through Figure 56. Results of the three tests performed at each +50 station and an average value of the three tests are presented in these figures. The 121 test points obtained near Sta. 809+00 (TS1-B) are also presented in these figures for reference. Figure 54 presents γ_d and w measurements obtained from NG test, and CBR of base and subgrade layer measurements obtained from DCP test (i.e., $DCP-CBR_{base}$, and $DCP-CBR_{subgrade}$) as point measurements with distance (note that each station is about 100 m apart).

Figure 55 presents in situ modulus measurements obtained from LWD test (E_{LWD-Z3}) on the OGDC base layer, estimated E_{SB} values of the OGDC base layer from DCP measurements, and estimated subgrade M_r values from DCP measurements. The estimated E_{SB} and M_r values were based on the charts presented in AASHTO (1993) (see Appendix B). The assumed E_{SB} and subgrade M_r values in design are shown in Figure 55 for reference and comparison. Using the E_{SB} and M_r values, and an average base layer thickness of 400 mm (15.7 in.) determined from DCP-CBR profiles (Figure 56), $k_{comp-AASHTO(1993)}$ values at each test location were determined to compare with the design k_{comp} values.

In situ test results from TS3-A are presented in Figure 57 through Figure 60. Results of the three tests performed at each +50 station and the average values of the three tests are presented in these figures. Figure 57 presents γ_d and w measurements obtained from NG tests; CBR of base and subgrade layer measurements obtained from DCP tests (i.e., DCP-CBR_{base}, and DCP-CBR_{subgrade}); and thickness of base layer (H_{Base}) based on DCP-CBR profiles as point measurements with distance. Figure 58 presents in situ modulus measurements obtained from FWD (E_{FWD-K3}); LWD (E_{LWD-Z3}); and PLT (E_{V1} and E_{V2}) tests on the OGDC base layer, estimated E_{SB} values from DCP measurements; and estimated subgrade M_r values from DCP measurements.

Using the E_{SB} and subgrade M_r values from DCP tests, and an average base layer thickness of 500 mm (19.7 in) determined from DCP profiles (Figure 59), $k_{comp-AASHTO(1993)}$ values at each test location were determined to compare with the design k_{comp} values. The same procedure to determine $k_{comp-AASHTO(1993)}$ was repeated using $E_{SB} = E_{LWD-Z3}$ and $E_{SB} = E_{FWD-K3}$, and the results are shown in Figure 60. Also included in Figure 60 are the k_{PLT*} measurements. The PLT was performed using a 300 mm (12 in.) diameter plate, but the k_{comp} used in the AASHTO (1993) design guide is based on a 720 mm (30 in.) diameter plate. Therefore, the measured k_{comp} values were corrected for plate size as described earlier in Chapter 3.

A summary of univariate statistics (i.e., mean μ , standard deviation σ , coefficient of variation COV) of the in situ point measurements from TS1-A and TS3-A is provided in Table 9.

NOTE: Three test points (at left, right, and center) at every +50 m station and *121 test points in a 0.6 m x 0.6 m grid at Sta. 809+00

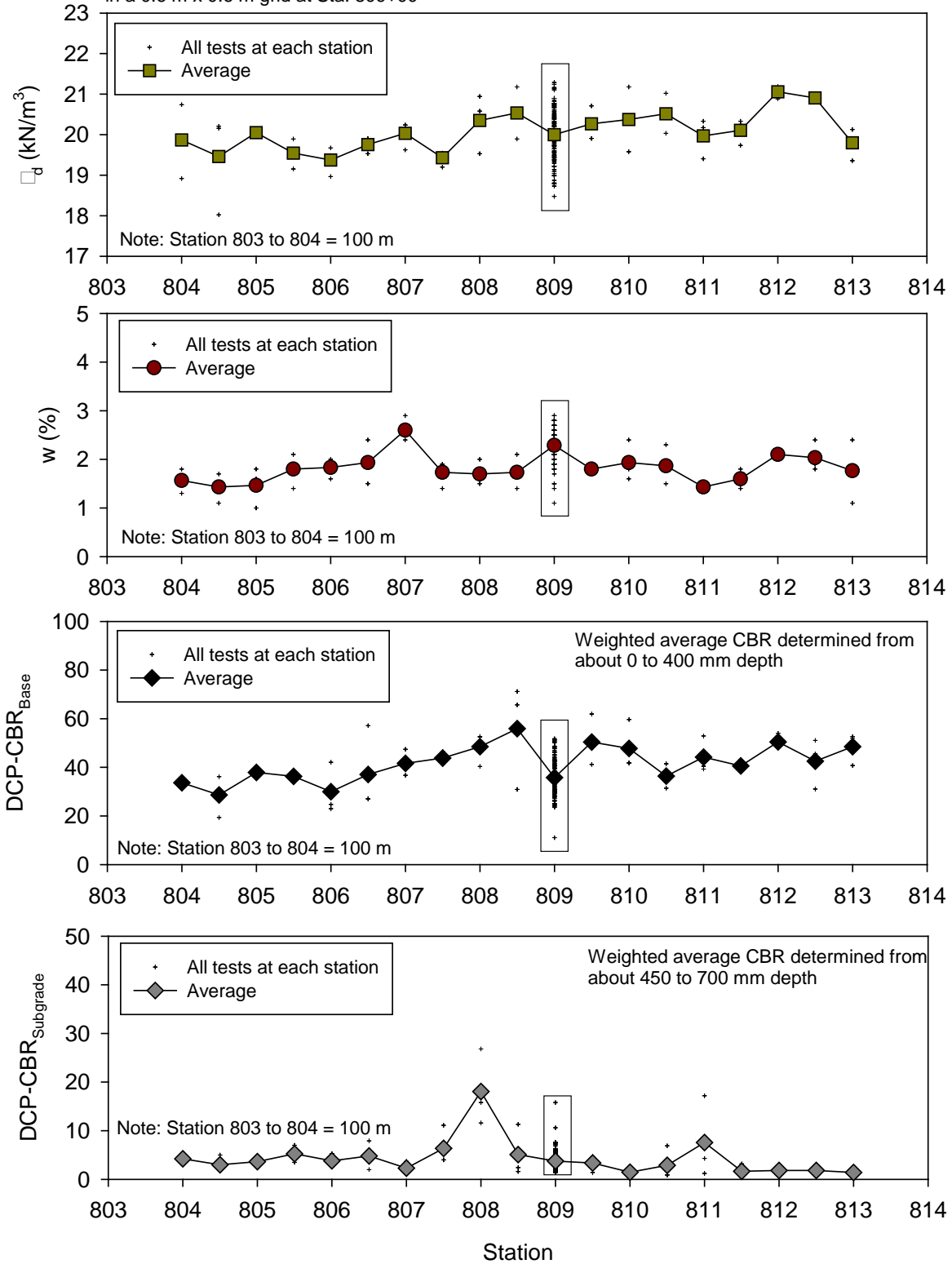


Figure 54. TS1-A: In situ NG and DCP test results from Sta. 804+00 to Sta. 814+00

NOTE: Three test points (at left, right, and center) at every +50 m station and *121 test points in a 0.6 m x 0.6 m grid at Sta. 809+00

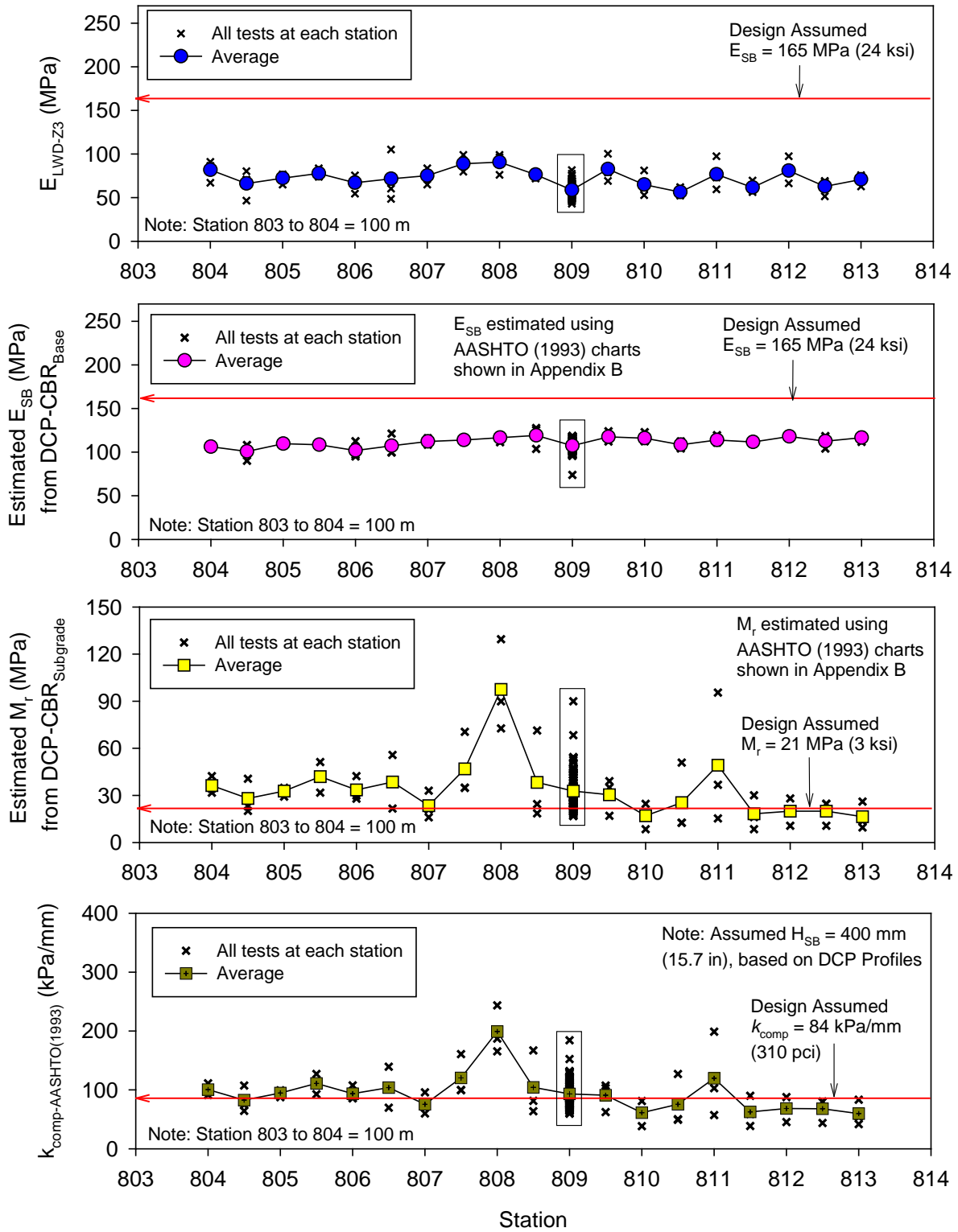


Figure 55. TS1-A: In situ modulus and estimated composite stiffness measurements from Sta. 804+00 to Sta. 814+00

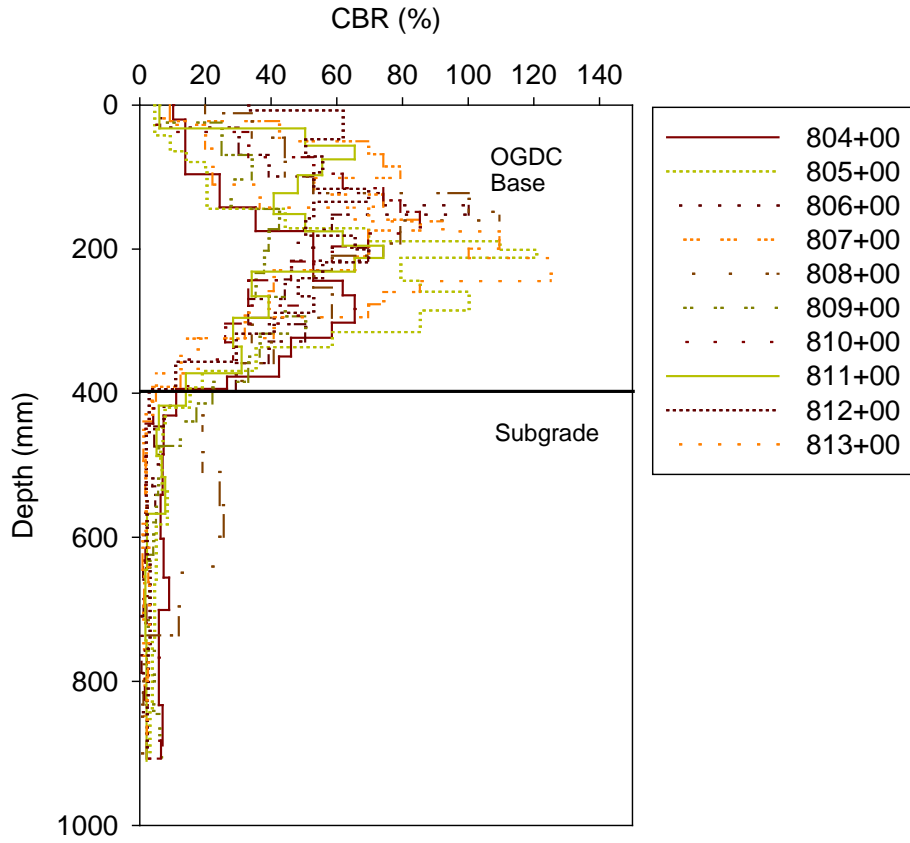


Figure 56. TS1-A: DCP-CBR profiles along centerline from Sta. 804+00 to Sta. 813+00

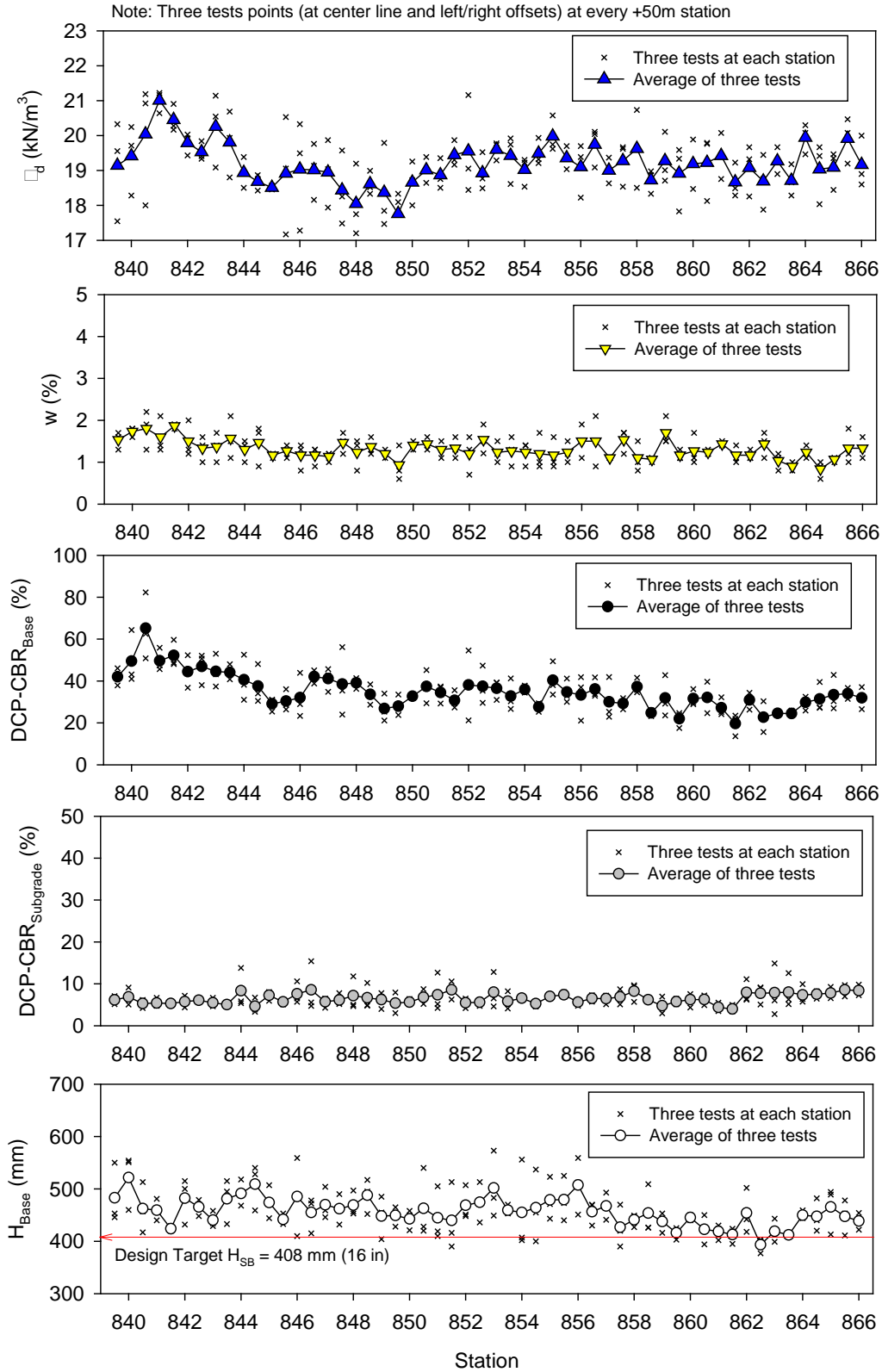


Figure 57. TS3-A In situ NG, DCP-CBR, and base layer thickness measurements on untrimmed OGDC base layer

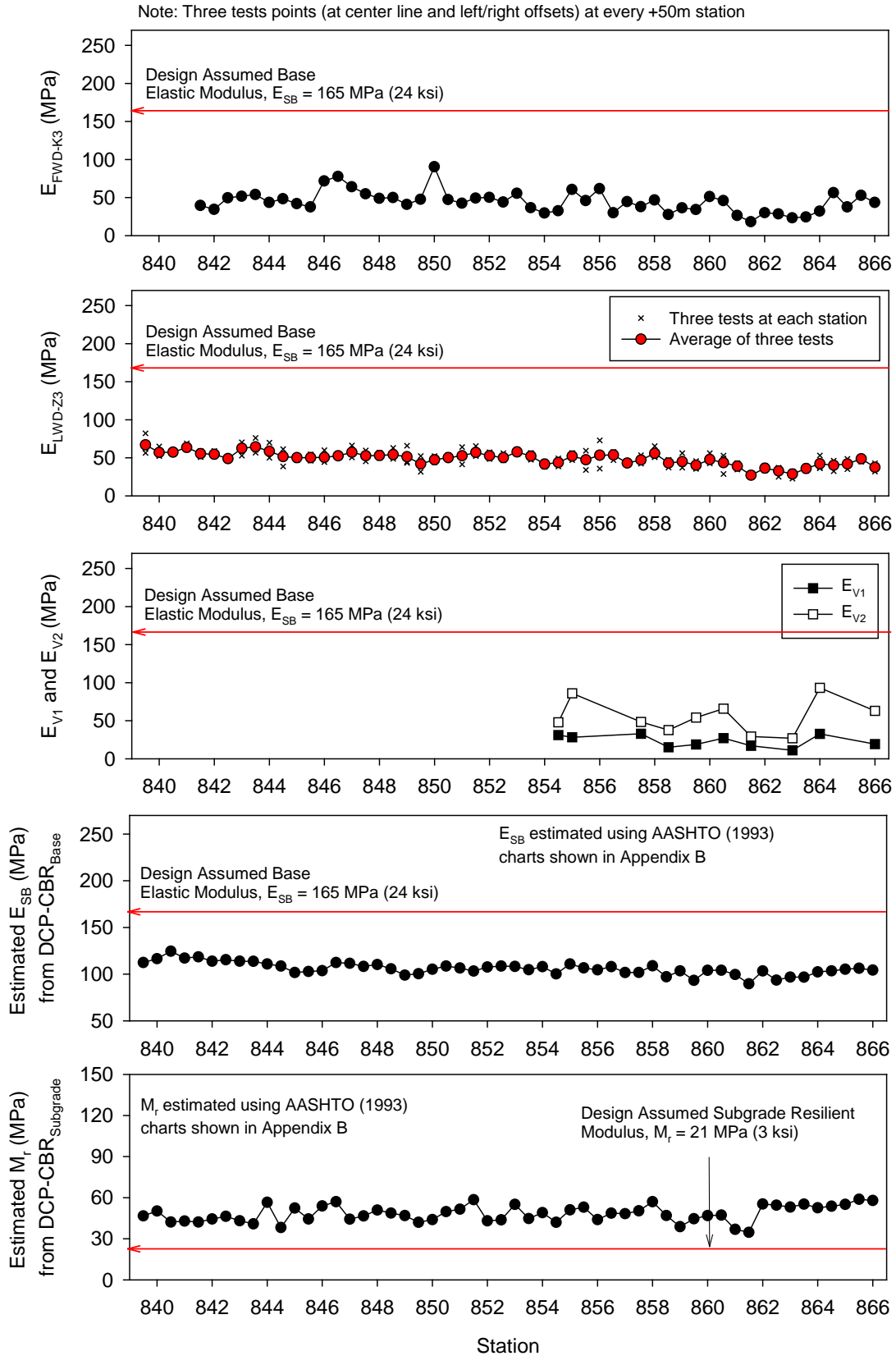


Figure 58. TS3-A: In situ modulus measurements on untrimmed OGDC base layer

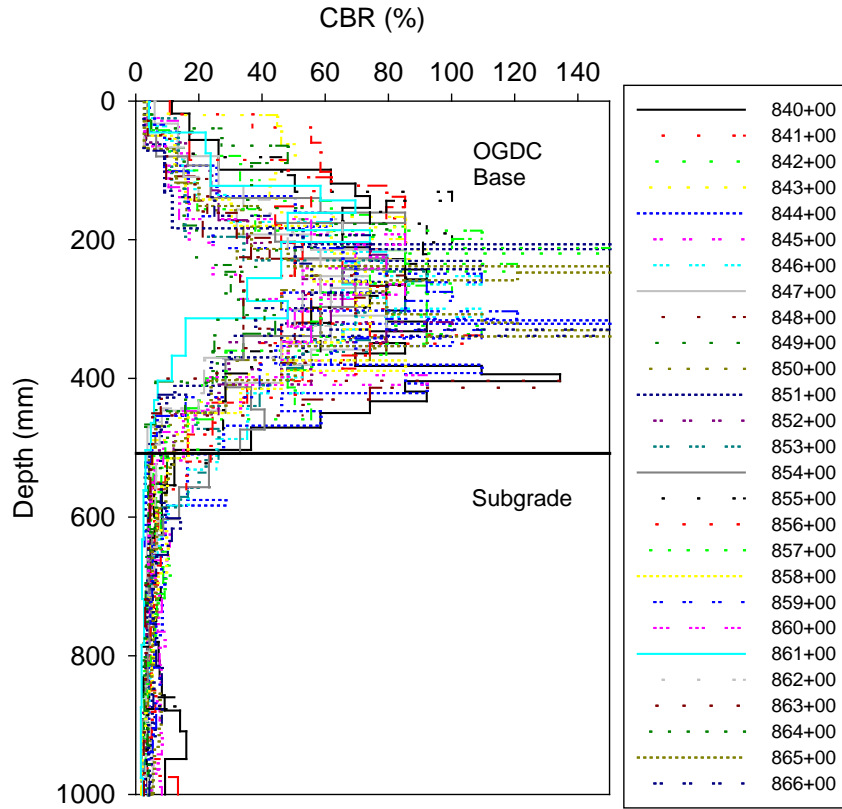


Figure 59. DCP-CBR profiles along centerline from Sta. 840+00 to Sta. 866+00 – TS3-A

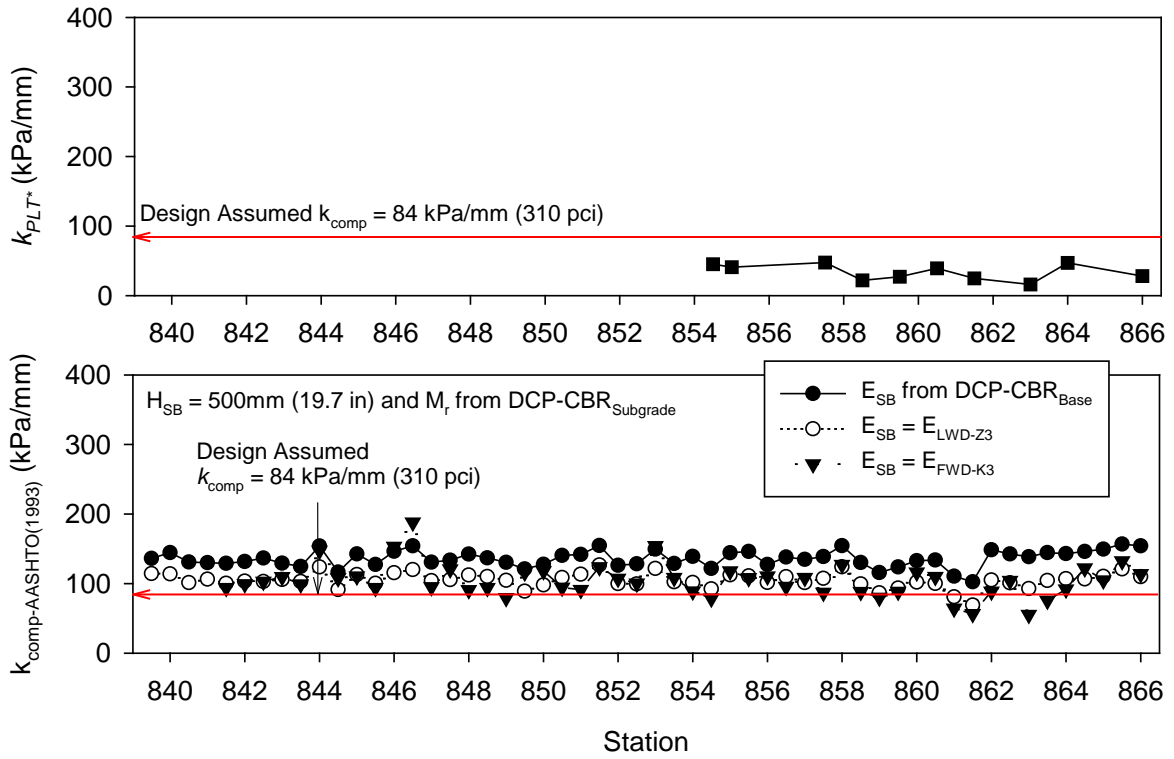


Figure 60. Comparison of estimated and measured k_{comp} – TS3-A

Table 9. TS1-A and TS3-A: Summary statistics of in situ test results

Measurement	n	μ	σ	COV (%)
TS1-A				
γ_d (kN/m ³)	175	20.02	0.63	3
w (%)	175	2.1	0.4	19
DCP-CBR _{Base} (%)	175	37.7	9.0	24
DCP-CBR _{Subgrade} (%)	175	4.0	3.1	79
K _{sat} (cm/s)	121	2.9	3.9	135
Fines (%)	121	3.7	1.4	37
E _{LWD-Z3} (MPa)	175	63.1	12.0	19
Estimated E _{SB} (MPa) [AASHTO 1993]	175	108.5	7.1	7
Estimated Subgrade M _r (MPa) [AASHTO 1993]	175	33.0	16.0	48
Estimated k _{comp-AASHTO(1993)}	175	93.0	28.9	31
TS3-A				
γ_d (kN/m ³)	162	19.21	0.88	5
w (%)	162	1.3	0.3	25
DCP-CBR _{Base} (%)	162	35.1	10.2	29
DCP-CBR _{Subgrade} (%)	162	6.5	2.2	34
E _{LWD-Z3} (MPa)	162	49.0	10.5	21
E _{FWD-K3} (MPa)	50	44.7	14.0	31
E _{V1} (MPa)	10	23.4	8.0	34
E _{V2} (MPa)	10	55.2	22.3	40
Estimated E _{SB} (MPa) [AASHTO 1993]	162	106.1	8.2	8
Estimated Subgrade M _r (MPa) [AASHTO 1993]	162	48.3	10.8	22
k _{PLT*} (kPa/mm)	10	33.8	11.5	34
Estimated k _{comp-AASHTO(1993)} ¹	162	136.0	21.3	16
Estimated k _{comp-AASHTO(1993)} ²	162	104.9	18.1	17
Estimated k _{comp-AASHTO(1993)} ³	50	104.4	24.1	23

¹Estimated using E_{SB} determined from DCP-CBR_{Base} using AASHTO (1993) empirical equations, ²Estimated using E_{SB} = E_{LWD-Z3}, ³Estimated using E_{SB}=E_{FWD-K3}.

Statistical Analysis of Dense Grid Point Testing – TS1-B

Test measurements obtained from TS1-B in a dense grid pattern with 121 tests over a plan area of about 7 m x 7 m provided a robust dataset to characterize the spatial characteristics of the measurements using geostatistical analysis. Kriged spatial contour maps, semivariograms, and histograms of each in situ point measurement are presented in Figure 61 through Figure 64. The spatial statistical parameters (i.e., sill, range, and nugget) are provided in the semivariogram plot of each figure.

With the exception of K_{sat} and DCP-CBR_{subgrade} measurements, all other measurements showed a clear spatial structure in the semivariogram plots without any need for data transformation. K_{sat}

measurements showed a log-normal distribution, therefore, the data was transformed to $\log(K)$ to develop a semivariogram. Similarly, transforming the data into a log scale resulted in a better spatial structure for $DCP-CBR_{\text{subgrade}}$. A spherical semivariogram model showed best fit for all the measurements.

Comparison of Kriged contour maps of K_{sat} and Fines in Figure 62 reveal that zones of high fines content (e.g., > 6%) match with zones of low K_{sat} (i.e., < 0.1 cm/s) and vice-versa. Previous studies have indicated that for granular materials, the permeability is highly governed by the percentage of fine particles passing the No. 200 sieve (Moulton 1980). AASHTO (1993) reports that K_{sat} of unbound granular materials decreases by two orders of magnitude with an increase in fines from 0 to 5% and a decrease by about four orders of magnitude with an increase in fines from 5% to 10%.

Relationships between fines content on K_{sat} based on the field measurements are presented in Figure 65. Exponential relationships showed the best fit for the trend in the data. A similar relationship was reported by Vennapusa et al. (2006) and is included in Figure 65 for reference. Based on the R^2 values, about 50% of the variation in K_{sat} is explained by the variation in fines content. Other parameters that influence K_{sat} include other gradation parameters (e.g., D_{10} , D_{60} , etc.), shape and orientation of aggregate particles and dry unit weight, as expected.

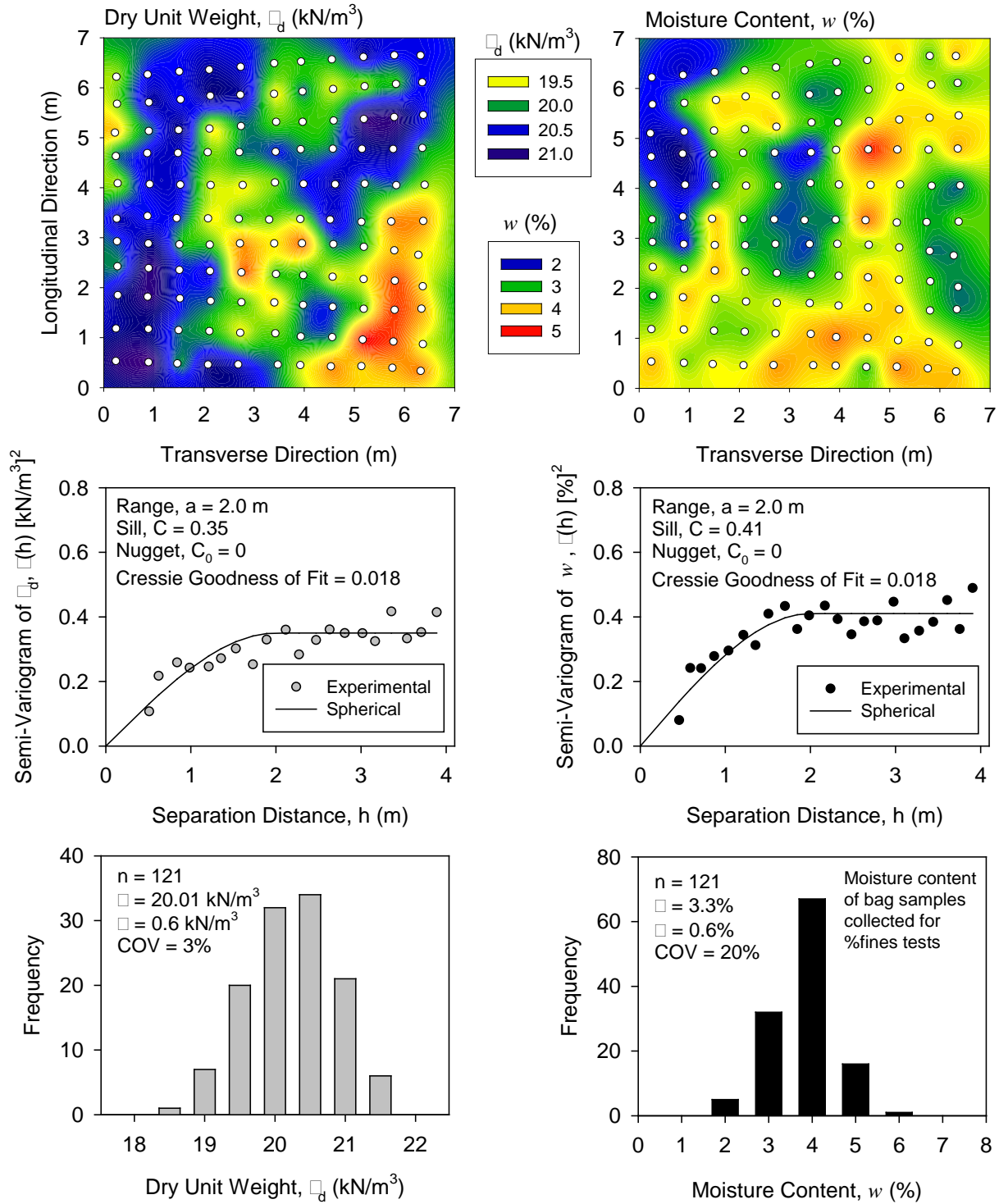


Figure 61. Kriged spatial contour map (top), semivariogram (middle), and histogram (bottom) plots of γ_d (left) and w (right) measurements – TS1-B

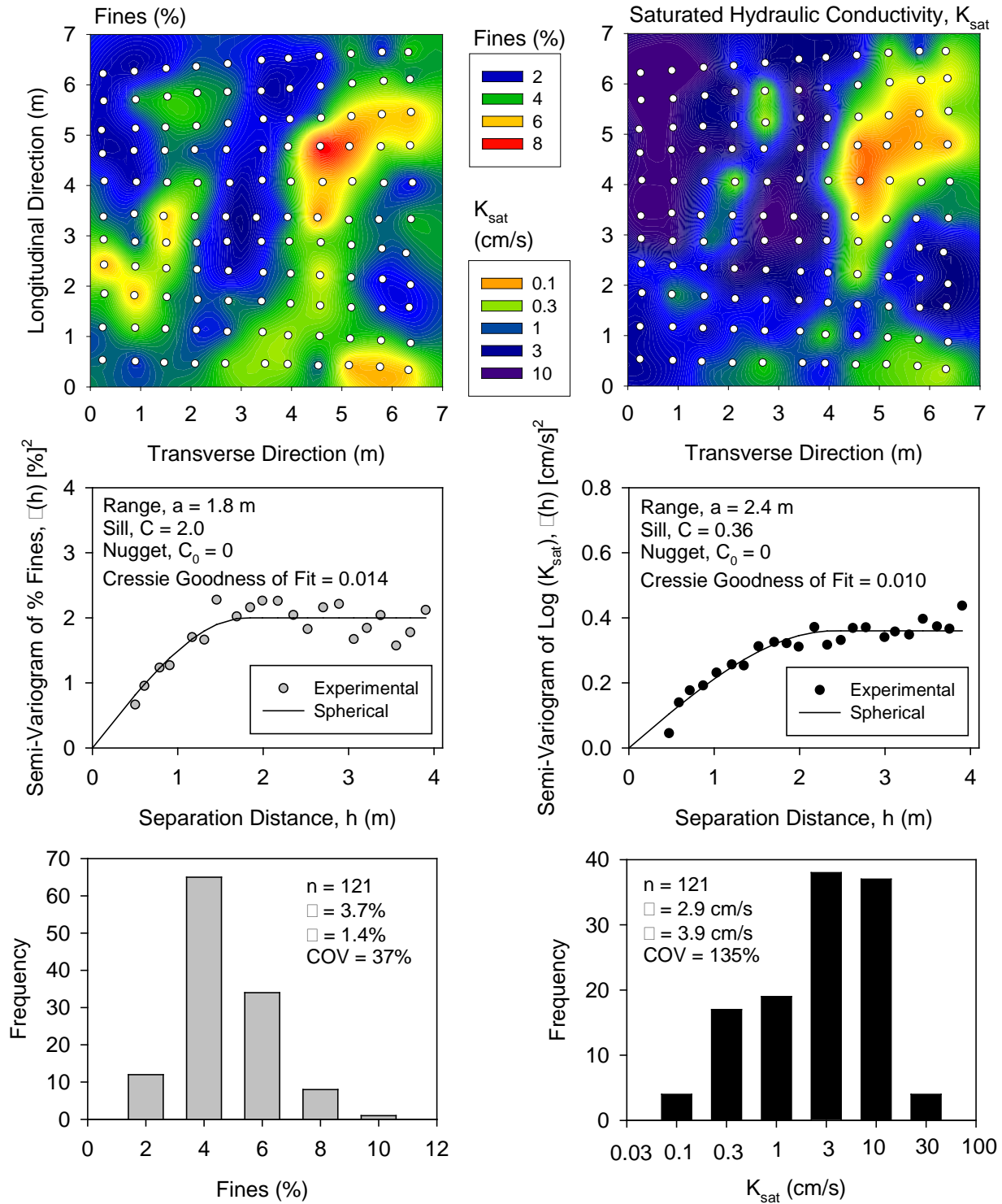


Figure 62. Kriged spatial contour map (top), semivariogram (middle), and histogram (bottom) plots of percent fines (left) and K_{sat} (right) measurements – TS1-B

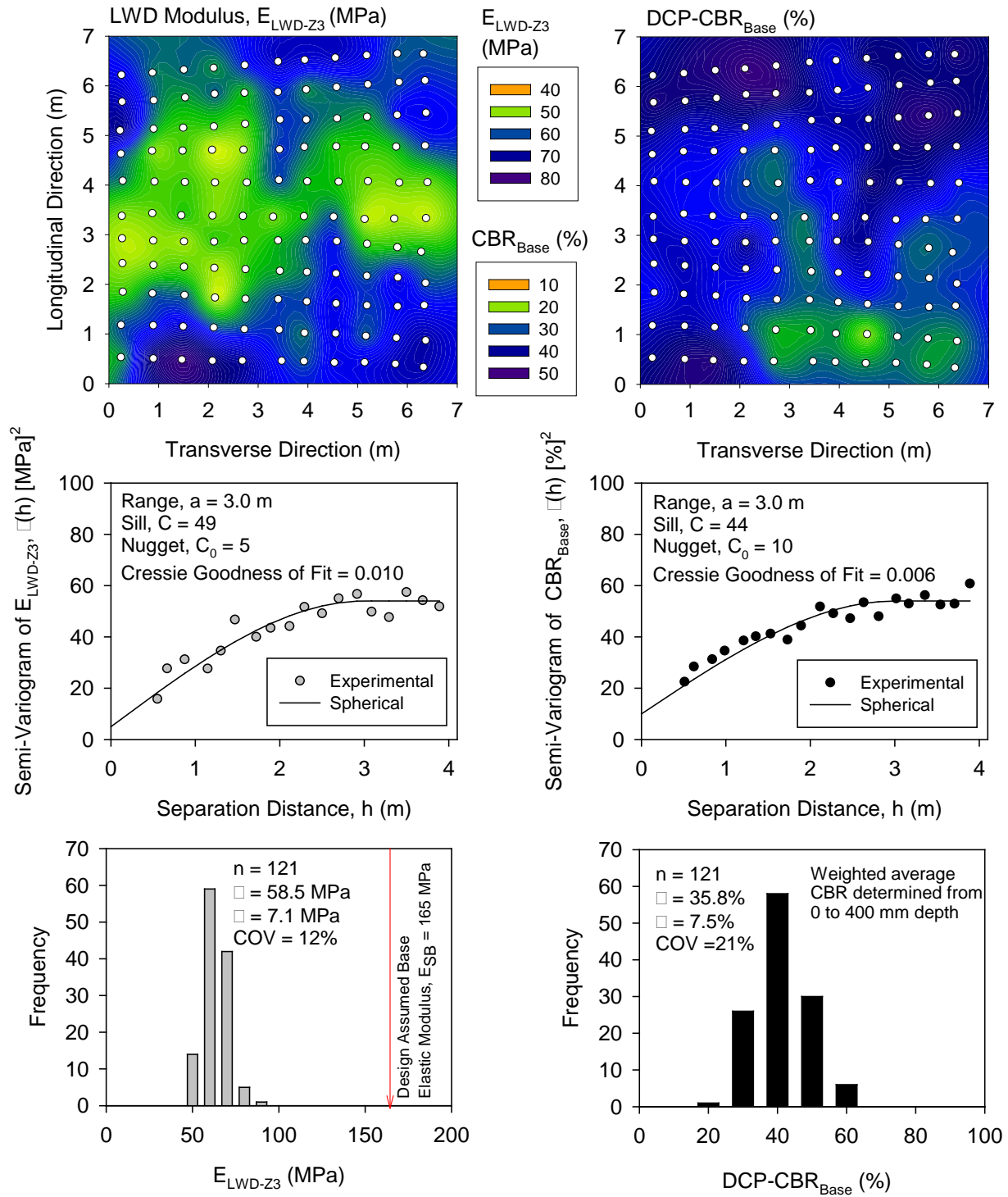


Figure 63. Kriged spatial contour map (top), semivariogram (middle), and histogram (bottom) plots of E_{LWD-Z3} (left) and $DCP-CBR_{Base}$ (right) measurements – TS1-B

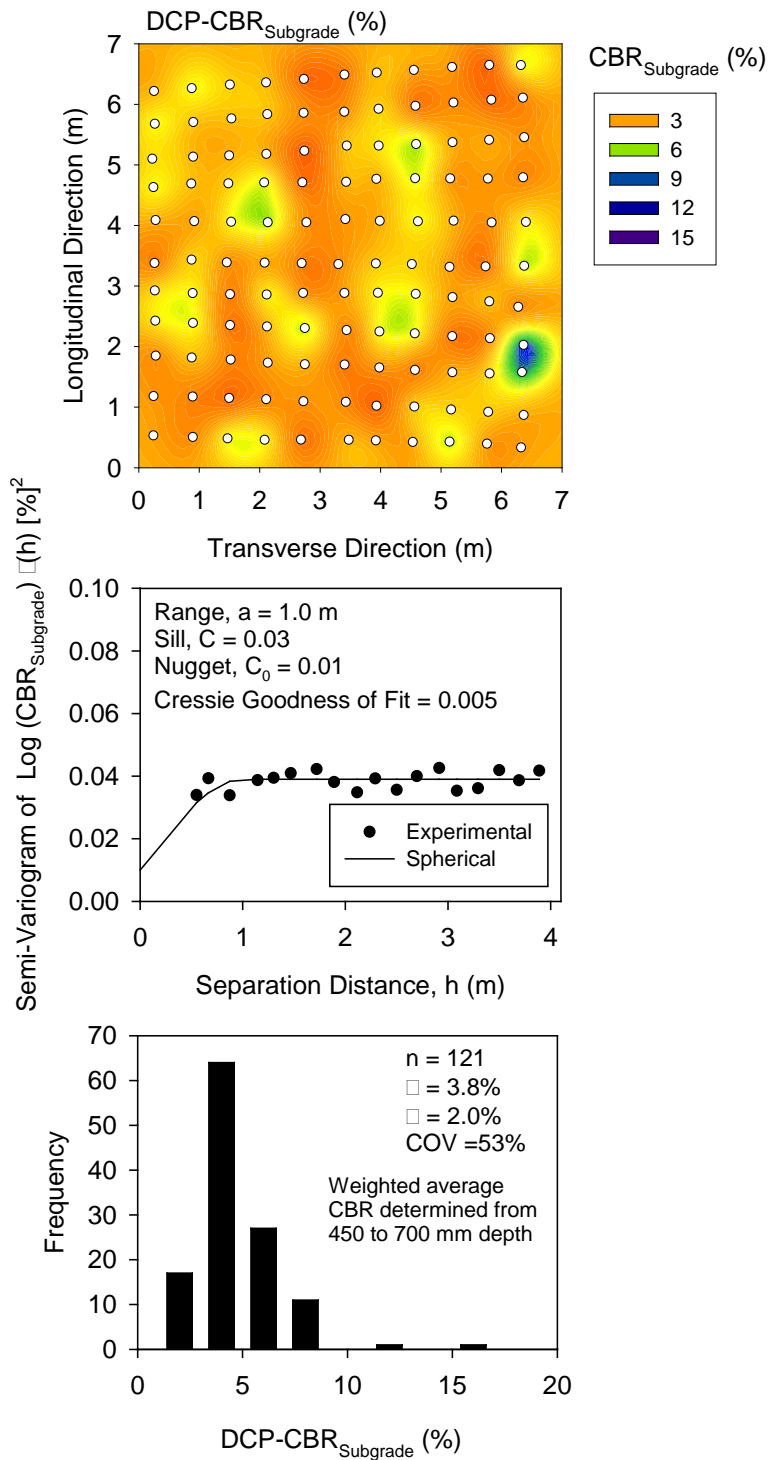


Figure 64. Kriged spatial contour map (top), semivariogram (middle), and histogram (bottom) plots of DCP-CBR_{Subgrade} measurements – TS1-B

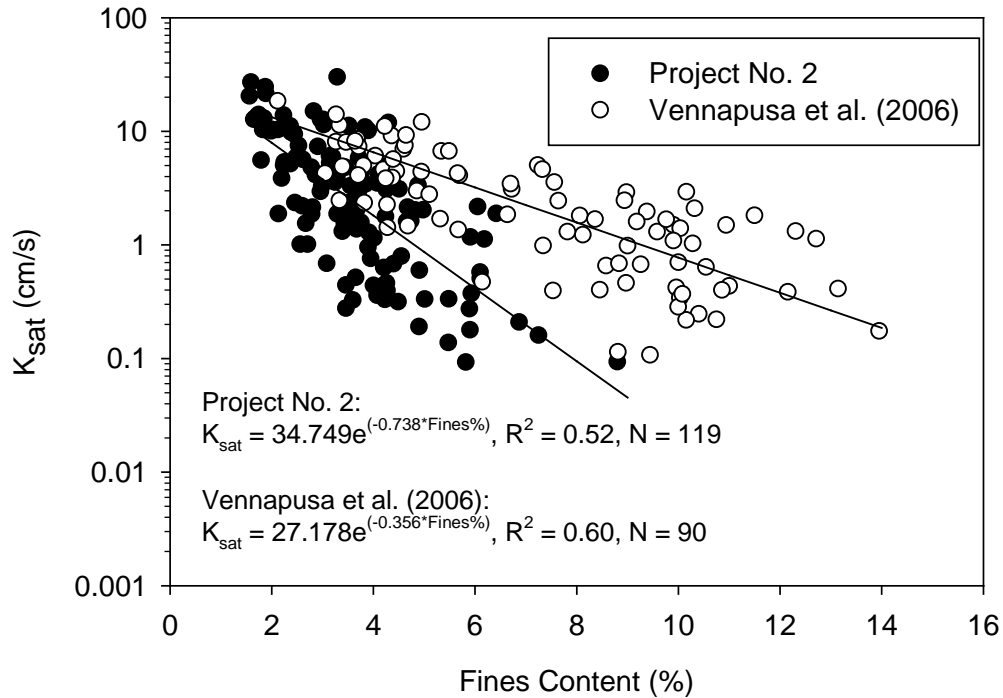


Figure 65. Effect of fines content on K_{sat} – TS1-B

Analysis of Roller-Integrated CMV and MDP₄₀ Measurements – TS3b

Roller-integrated CMV and MDP₄₀ measurements from roller passes 1 and 2 on TS3-A, and roller pass 1 on TSs 3b and 3c are shown in Figure 66. Histograms of CMV and MDP₄₀ measurements are shown in Figure 67 and Figure 68, respectively. Roller-integrated measurements are spatially referenced using GPS northing and easting measurements with virtually 100% coverage of compaction data. This data allowed characterizing spatial characteristics of compaction measurements, and therefore, semivariograms of CMV and MDP₄₀ measurements were developed, as shown in Figure 69. The univariate and spatial statistics of CMV and MDP₄₀ measurements are summarized in Table 10.

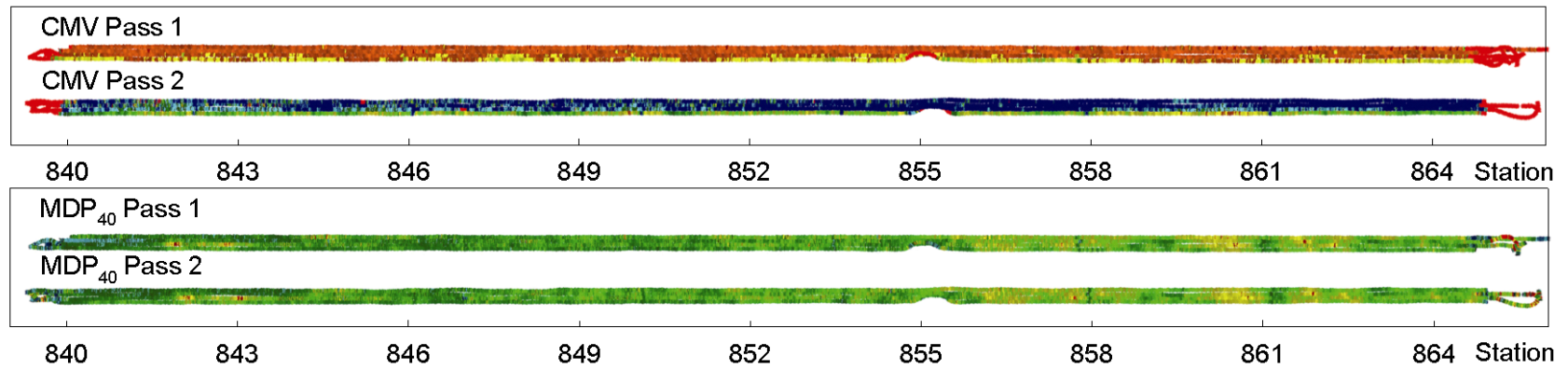
Some semivariograms of CMV and all semivariograms of MDP₄₀ measurements showed nested variograms with short-range and long-range components. These conditions were previously documented in other field studies (White et al. 2010b). It is likely that the long-range component is due to deeper underlying foundation variations. More research is warranted on this issue to further investigate the consequences of these different range spatial components on the performance of pavements.

Results from TS3-A indicated that CMV measurements increased on average by about 3.5 times from pass 1 to pass 2, while MDP₄₀ measurements did not show any considerable change. Further, the variability of CMV measurements also increased considerably from pass 1 to 2, as indicated by an increase in the standard deviation from 4.3 to 21.7 and an increase in the semivariogram sill value from about 19 to 480. MDP₄₀ measurements did not show any

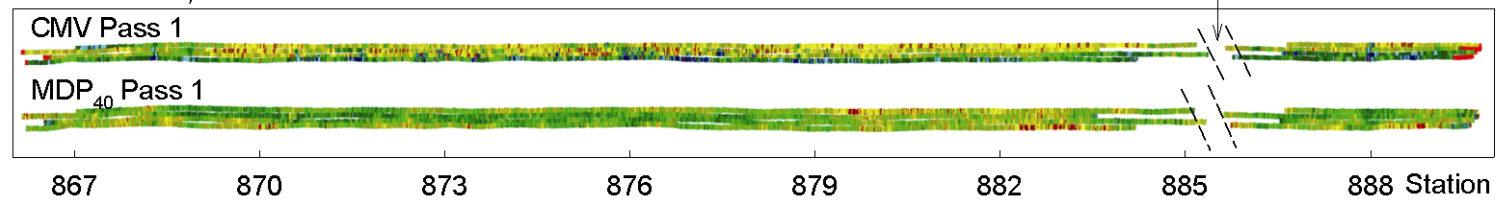
considerable changes in the variability between passes 1 and 2. TS3b showed about two times greater average CMV than TS3-A pass 1, and also showed comparatively more variability as indicated by higher standard deviation and semivariogram sill values than TS3-A pass 1.

Results obtained on TS3c (subgrade layer) showed CMV measurements that are significantly lower than on TSs 3a and 3b. Further, the variability observed in TS3c CMV measurements were also lower than on TSs 3a and 3b, as indicated by the comparatively lower standard deviation and semivariogram sill values. In contrast, the MDP₄₀ values showed significantly greater variability in TS3c compared to TSs 3a and 3b. The standard deviation of MDP₄₀ and semivariogram sill of MDP₄₀ on TS3c were about 14 and 235, respectively, while they are about 6 and 34 to 38 in TSs 3a and 3b.

OGDC Base, TB3a



OGDC Base, TB3b



Subgrade, TB3c

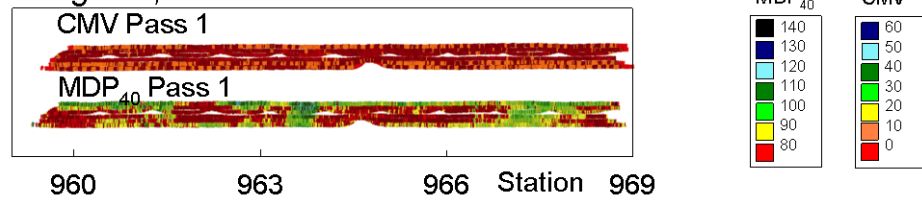


Figure 66. CMV and MDP₄₀ maps on untrimmed OGDC base and subgrade layers – TSs 3a, 3b, and 3c

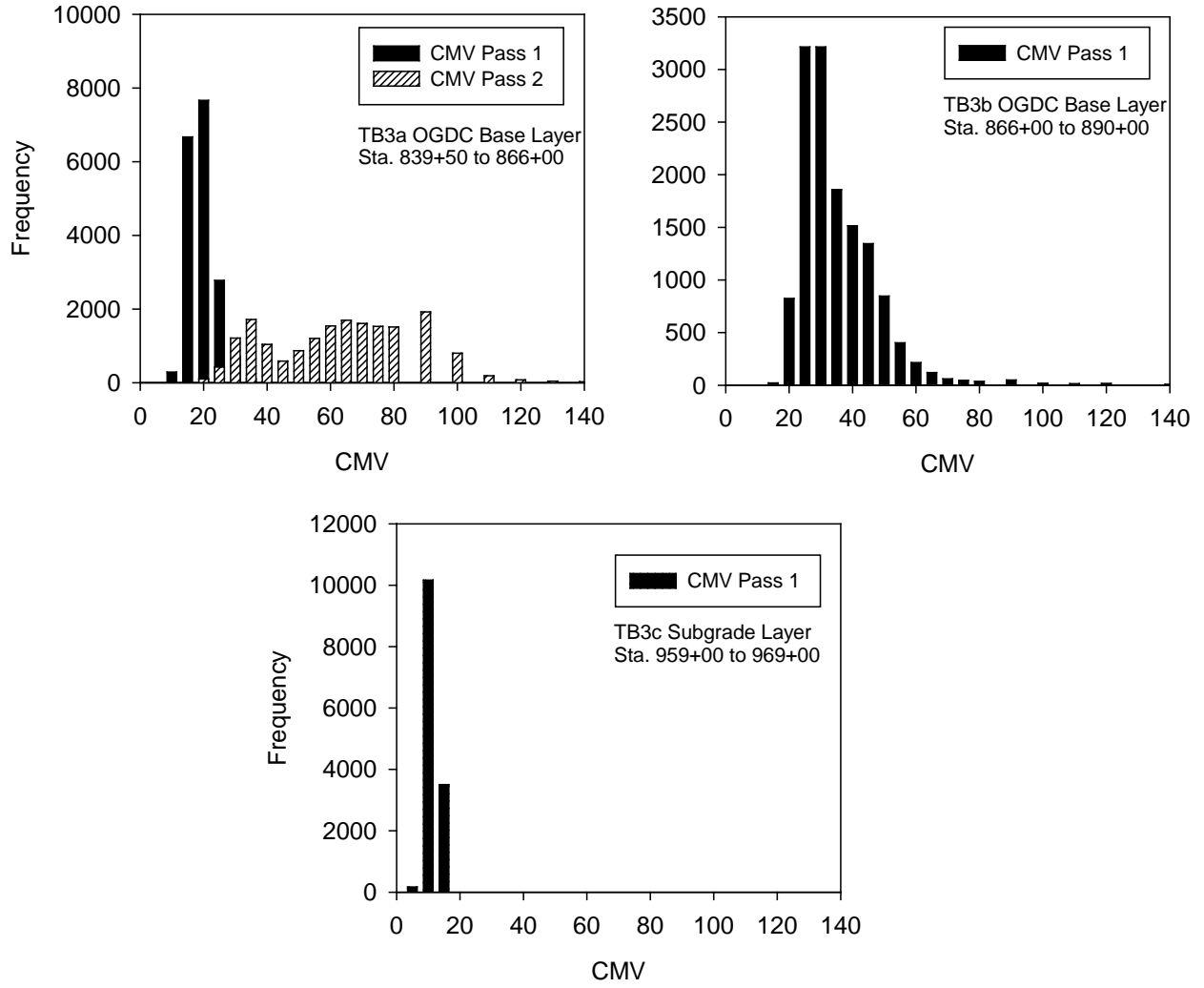


Figure 67. CMV histograms on untrimmed OGDC base and subgrade layers – TSs 3a, 3b, and 3c

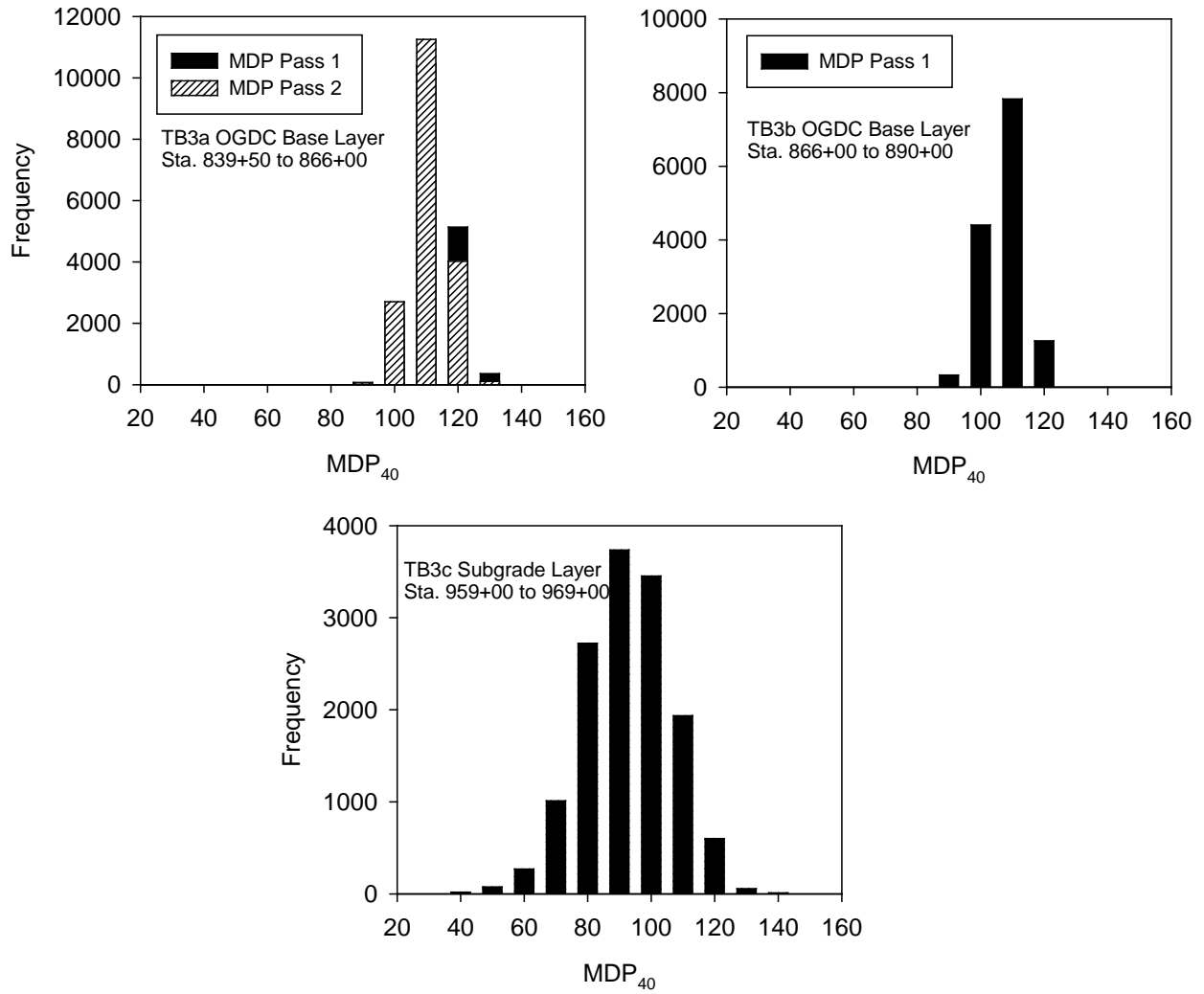


Figure 68. MDP₄₀ histograms on untrimmed OGDC base and subgrade layers – TSs 3a, 3b, and 3c

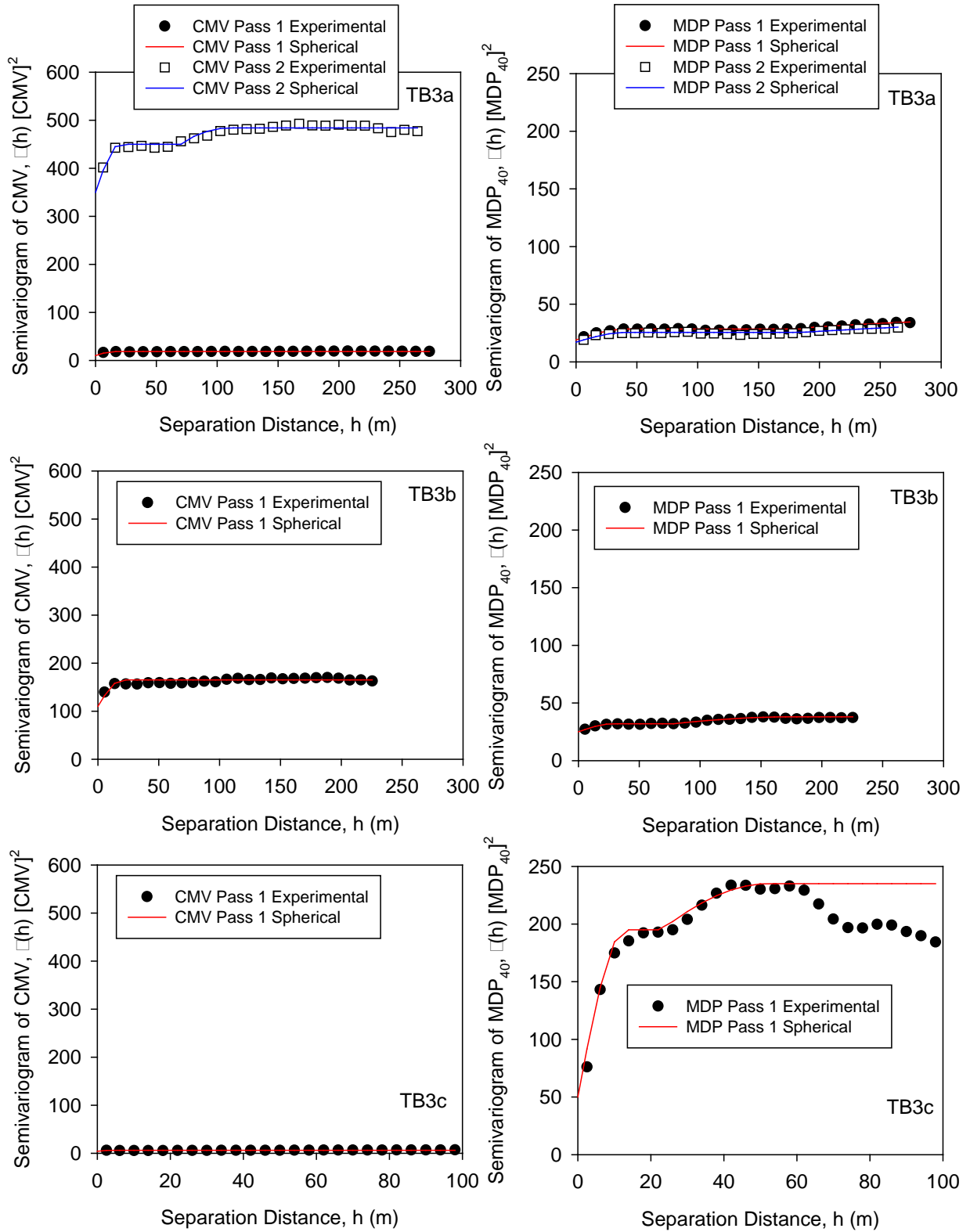


Figure 69. TS3-A, TS3-B, and TS3-C: Semivariograms of CMV (left column) and MDP40 (right column) measurements on untrimmed OGDC base and subgrade layers

Table 10. TS3-A, TS3-B, and TS3-C: CMV and MDP₄₀ measurements

TS	Measurement	Univariate Statistics				Spatial Statistics				
		n	μ	σ	COV (%)	Nugget ₁	Sill ₁	Range ₁ (m)	Sill ₂	Range ₂ (m)
TS3-A (OGDC Base Layer)	CMV (Pass 1)	18288	16.9	4.3	26	10	18.5	15	NA	
	CMV (Pass 2)	18157	59.8	21.7	36	350	450.0	20	480.0	110
	MDP ₄₀ (Pass 1)	18288	106.9	6.2	6	19	28.5	40	37.5	400
	MDP ₄₀ (Pass 2)	18157	105.9	5.7	5	17	25.5	40	33.5	400
TS3-B (OGDC Base Layer)	CMV (Pass 1)	13844	32.8	12.4	38	110	165.0	20	NA	
	MDP ₄₀ (Pass 1)	13844	102.3	6.0	6	25	32.0	28	38.0	175
TS3-C (Subgrade Layer)	CMV (Pass 1)	13887	8.9	2.8	31	4	6.0	3	NA	
	MDP ₄₀ (Pass 1)	13887	87.5	13.9	16	50	195.0	13	235.0	52

Comparisons of Design Value, In situ Measurements, and Laboratory Measurements

Comparisons of the measured, estimated, and design assumed modulus (i.e., base layer E_{SB} , subgrade M_r , and k_{comp}) values are presented in Figure 55, Figure 58, and Figure 60. A summary of the average values of in situ and laboratory measured values in comparison with the design values is provided in Table 11. These comparisons reveal some important aspects that are of high significance to this research project and are summarized as follows:

Base Layer Elastic Modulus (E_{SB})

The measured E_{SB} values (either by LWD or FWD or PLT) in TSs 1 and 3 locations did not meet the target design $E_{SB} = 165$ MPa (24 ksi). On average, the measured E_{SB} values were about 3 to 7 times lower than the design target value. Although estimated E_{SB} measurements from DCP-CBR_{Base} measurements resulted in higher values than LWD/FWD/PLT measurements, the E_{SB} were still about 1.5 times lower than the design target value. The laboratory determined E_{SB} values were, however, about 1.7 times higher than the design target value.

Subgrade Resilient Modulus (M_r)

A direct measurement of M_r was not obtained in the TS1 and TS3 subgrades; however, M_r tests were conducted on “undisturbed” samples obtained from TS2 subgrade. The results were summarized earlier in Chapter 4. Using the stress states recommended by NCHRP 1-28A (2002) for subgrade materials ($\sigma_3 = 14$ kPa (2 psi) and $\sigma_{cyclic} = 41$ kPa (6 psi)), an average $M_r = 61$ MPa (8.8 ksi) was determined from the laboratory tests, which exceeds the design target $M_r = 21$ MPa (3 ksi). The average in situ estimated M_r value from DCP-CBR_{Subgrade} measurements was about 41 MPa (5.9 ksi), which also exceeds the design target value.

Table 11. Design, in situ, and laboratory values

Design Parameter	Design Value	In Situ Measurements (Average)*	Laboratory Measurements (Average)**
Subgrade M_r	21 MPa (3.0 ksi)	41 MPa (5.9 ksi) ¹	61 MPa (8.8 ksi)
OGDC Base E_{SB}	165 MPa (24.0 ksi)	<i>Direct Measurement:</i> 56 MPa (8.1 ksi) ² 44 MPa (6.4 ksi) ³ 23 MPa (3.3 ksi) ⁴ 55 MPa (8.0 ksi) ⁵ <i>Estimated from DCP:</i> 107 MPa (15.5 ksi) ¹	288 MPa (41.8 ksi)
k_{comp}	84 kPa/mm (310 pci)	<i>Direct Measurement:</i> 34 kPa/mm (124 pci) ⁶ <i>Estimated Value:</i> 114 kPa/mm (420 pci) ⁷ 91 kPa/mm (336 pci) ⁸ 100 kPa/mm (369 pci) ⁹	<i>Estimated from average E_{SB} and M_r:</i> 163 kPa/mm (600 pci)
C_d	1.1 (Good to Excellent)	Good to Excellent based on the range of K_{sat} measurements in situ	Excellent based on laboratory K_{sat} measurement

*Average of all measurements obtained from TSs 1 and 3; **Average based on laboratory tests on all Shelby tube samples from subgrade and all laboratory compacted OGDC base material samples (without back-saturation); ¹Empirically estimated from charts presented in AASHTO (1993); ²Average of E_{LWD-Z3} measurements; ³Average of E_{FWD-K3} measurements; ⁴Average of E_{V1} measurements; ⁵Average of E_{V2} measurements; ⁶Based on plate load tests; ⁷Based on E_{SB} from DCP-CBR_{Base} measurements, subgrade M_r from DCP-CBR_{Subgrade} measurements, and H_{SB} from DCP profiles; ⁸Based on $E_{SB} = E_{LWD-Z3}$ measurements, subgrade M_r from DCP-CBR_{Subgrade} measurements, and H_{SB} from DCP profiles; ⁹Based on $E_{SB} = E_{FWD-K3}$ measurements, subgrade M_r from DCP-CBR_{Subgrade} measurements, and H_{SB} from DCP profiles.

Composite Modulus of Subgrade Reaction (k_{comp})

The k_{comp} values were determined in situ from PLT at 10 test locations. The average k_{PLT} * was about 34 kPa/mm (124 pci), which was about 2.5 times lower than the design target $k_{comp} = 84$ kPa/mm (310 pci). The k_{comp} value was also estimated to determine $k_{comp-AASHTO(1993)}$ using E_{SB} based on DCP, LWD, and FWD measurements. These estimated values ranged, depending on the selected E_{SB} value, from about 1.1 to 1.4 times the design value. The $k_{comp-AASHTO(1993)}$ determined using laboratory measurements was about 163 kPa/mm (600 pci), which is about 2 times higher than the design target value.

The results indicate that the k_{comp} values vary significantly (from about 2.5 times lower to 2 times higher than the design target value) based on the method or procedure used.

Drainage Coefficient (C_d)

The C_d value assumed in design = 1.1, which represents that the quality of drainage is rated as “good” to “excellent”. According to AASHTO (1993), if water is removed from the pavement system in one day, the quality of drainage is rated as “good” and if water is removed within two hours, the quality of drainage is rated as “excellent”.

Based on the pavement geometry (i.e., cross slope, width of the pavement, thickness of the base layer), the measured K_{sat} values from the field, and assuming an effective porosity = 0.3, time for a target 90% of drainage was calculated using “Pavement Drainage Estimator (PDE) Version 1.0,” an Excel-based Visual Basic program developed by Vennapusa (2004). A target of 90% drainage was selected in calculations. The time for 90% drainage was estimated as 1.4 days for $K_{sat} = 0.1$ cm/s (lower bound) to 0.1 hour for $K_{sat} = 30$ cm/s (upper bound). For an average $K_{sat} = 2.9$ cm/s, time for 90% drainage was estimated at about 1.1 hours. The average in situ $K_{sat} = 2.9$ cm/s compares well with the laboratory measured $K_{sat} = 3.1$ cm/s. Based on these estimates, the quality of the OGDC drainage layer can be rated as “good” to “excellent” and does meet the design requirements.

TS2: Existing PCC Surface, Subbase, and Subgrade

Experimental Testing

TS2 involved testing the existing PCC surface layer and the foundation layers. TS2-A involved conducting FWD tests at the center of the panel and at selected joints along the inner and outer lanes of I-94 EB existing pavement over an 80 m long area (Figure 71). TS2-B involved conducting FWD testing in dense grid pattern on PCC surface with 203 tests in a 7.4 m x 13.4 m area consisting of two PCC panels and a patching area (Figure 71). After testing on the PCC surface, the pavement panels were removed to expose the underlying foundation layers (Figure 77). A gravelly sand base layer of about 100 mm in thickness (4 in.) was encountered directly beneath the PCC surface. No tests were performed on the base layer as the layer was disturbed during the pavement removal process (Figure 77). A trench was carefully excavated down to the existing sand subbase layer at 28 test locations to conduct LWD tests (Figure 77). DCP tests were conducted through the disturbed base layer at all 28 test locations extending down to the subgrade layer. GPT test measurements were obtained at 8 selected locations on the subbase layer.

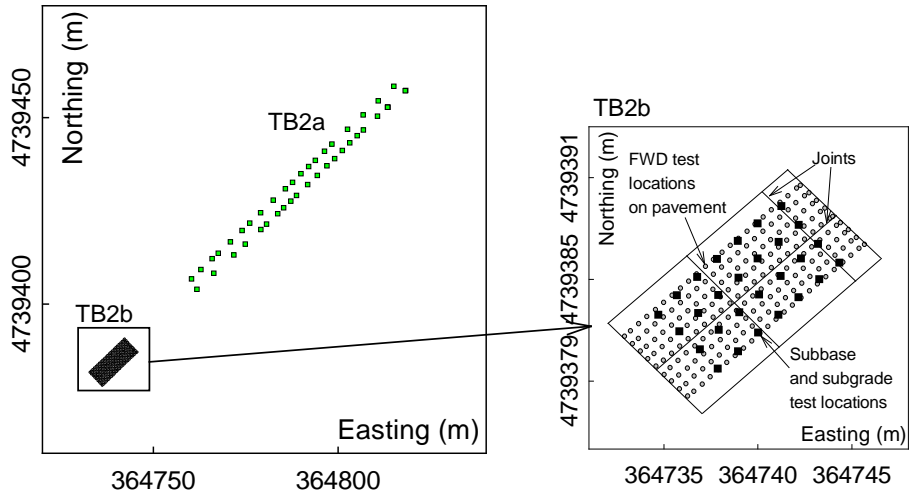


Figure 70. TS2: Plan view showing in situ test locations (left) and detailed view of TS2-B (right)



Figure 71. TS2-B: Laying out the test grid (left) and Kuab FWD testing on the grid (right)



Figure 72. TS2-B: Bucket loader in place for excavating existing pavement



Figure 73. TS2-B: Bucket loader excavating existing pavement



Figure 74. Measuring the existing pavement depth



Figure 75. TS2-B: Preparing test locations for in situ testing (foreground) and the MDOT drilling rig obtaining Shelby tube samples



Figure 76. TS2-B: Air permeameter testing device



Figure 77. TS2-B: Plate load testing in progress

In Situ Test Results and Discussion

FWD deflection basin parameters (i.e., D_0 , SCI, BDI, BCI, and Intercept) from tests conducted at the center of the panel on TS2a are presented in Figure 78. LTE, D_0 , and Intercept measurements from FWD tests conducted at joints are presented in Figure 79. According to McCracken (2008), intercept ≥ 0.05 mm indicates presence of void beneath the pavement. Results indicated that all intercept measurements (both at joints and at center of the panel) were below the 0.05 mm (50 μm or 2 mils) target limit. The LTE at the joints varied from about 38% to 100%, with 6 out of 8 measurements below 70%. A summary of univariate statistics (i.e., mean μ , standard deviation σ , and coefficient of variation COV) of TS2a measurements is provided in Table 12.

Kriged spatial contour maps of FWD deflection basin parameters from tests conducted in a dense grid pattern on TS2-B are presented in Figure 80. Semivariograms used to develop these contour maps are provided in Figure 81. A spherical variograms showed the best fit for all of the measurements. The semivariogram range of all FWD deflection basin parameters was about the same (2 to 3 m), while the sill values varied between the parameters. Histogram plots of the FWD deflection basin parameters are provided in Figure 82.

Kriged spatial contour maps of in situ point measurements on the existing subbase and subgrade layers are presented in Figure 83. Semivariograms of these measurements are provided in Figure 84, and histogram plots of the measurements are presented in Figure 85. The experimental semivariograms did not show a clear spatial structure, so a theoretical semivariogram could not be fit to the data. The Kriged contour maps were developed only for visualization purposes without the use of a semivariogram. DCP-CBR profiles (Figure 86) were used to determine the DCP-CBR_{Subbase} and DCP-CBR_{Subgrade}. A summary of the univariate statistics of these measurements are provided in Table 12.

On average, the E_{LWD-Z3} on the existing sand subbase is about two times lower than the E_{LWD-Z3} on the newly constructed OGDC base layer. Laboratory M_r tests also revealed similar differences as noted earlier in Chapter 4 (Table 6). On average, M_r (at a selected stress state for base/subbase layers) of the existing subbase layer is about two times lower than M_r of the OGDC base layer. The average DCP-CBR_{Subbase} is about 18 times lower than the average DCP-CBR_{Base} (on the OGDC base layer from TSs 1 and 3). The DCP-CBR_{Subgrade} from TS2-B is about the same as the DCP-CBR_{Subgrade} from TSs 1 and 3. The K_{sat} of the existing subbase layer was on average about an order of magnitude lower than on the OGDC base layer (TS1).

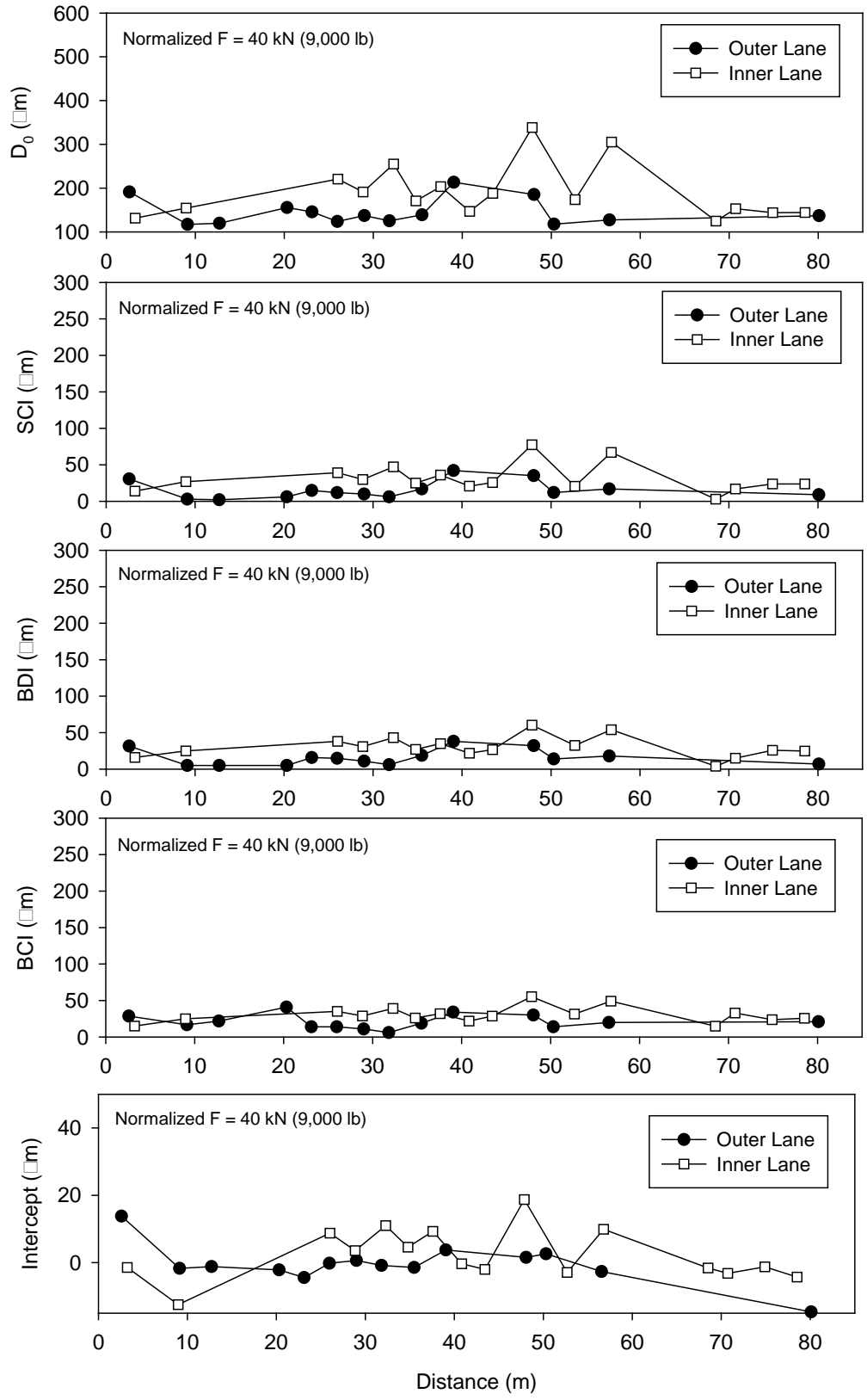


Figure 78. Results from FWD tests at the center of pavement panels from TS2a

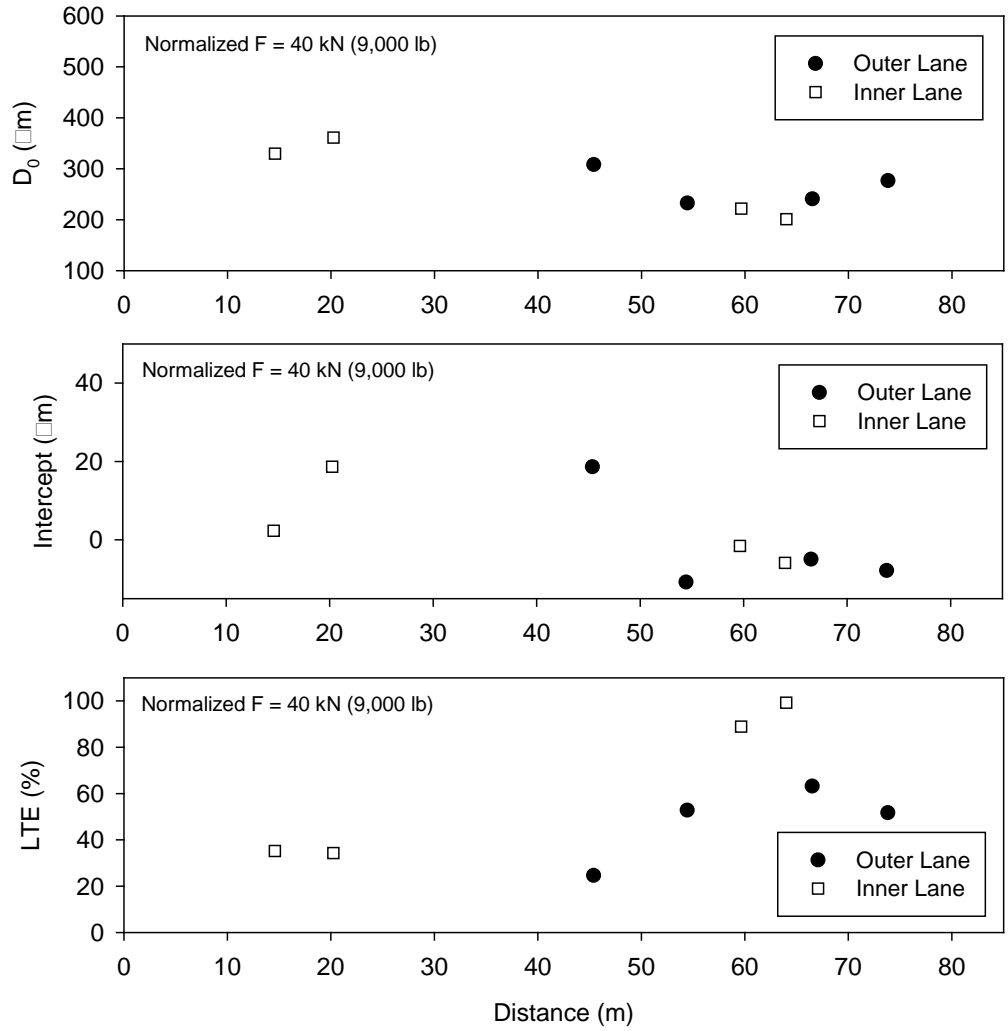


Figure 79. Results from FWD tests at pavement joints from TS2a

Table 12. TS2: Summary statistics of in situ test results

Test Bed	Measurement	Univariate Statistics				Spatial Statistics		
		n	μ	σ	COV (%)	Nugget	Sill	Range (m)
TS2-A (measurements at center of the PCC panels)	D ₀ (μm)	30	169.3	54.1	32			
	SCI (μm)	30	23.8	17.8	75			
	BDI (μm)	30	23.4	14.5	62			
	BCI (μm)	30	25.8	11.2	43			
	Intercept, I (μm)	30	1.0	7.0	712		NA	
TS2-A (measurements near joints)	D ₀ (μm)	8	271.5	57.0	21			
	Intercept, I (μm)	8	1.1	11.5	1086			
	LTE (%)	8	88	33	37			
TS2-B (Spatial area on PCC surface)	D ₀ (μm)	203	175.5	73.7	42	0	7500	3.0
	SCI (μm)	203	14.5	10.4	72	25	100	3.0
	BDI (μm)	203	19.9	10.3	52	25	85	2.0
	BCI (μm)	203	22.8	10.1	44	10	120	2.2
	Intercept, I (μm)	203	6.1	13.4	221	0	260	3.0
TS2-B (Spatial area on subbase and subgrade)	E _{LWD-Z3} (MPa)	28	26.9	6.9	26			
	DCP-CBR _{Subbase} (%)	28	5.2	1.1	22			
	DCP-CBR _{Subgrade} (%)	28	6.1	2.7	45			
	K _{sat} (cm/s)	8	0.12	0.06	53			

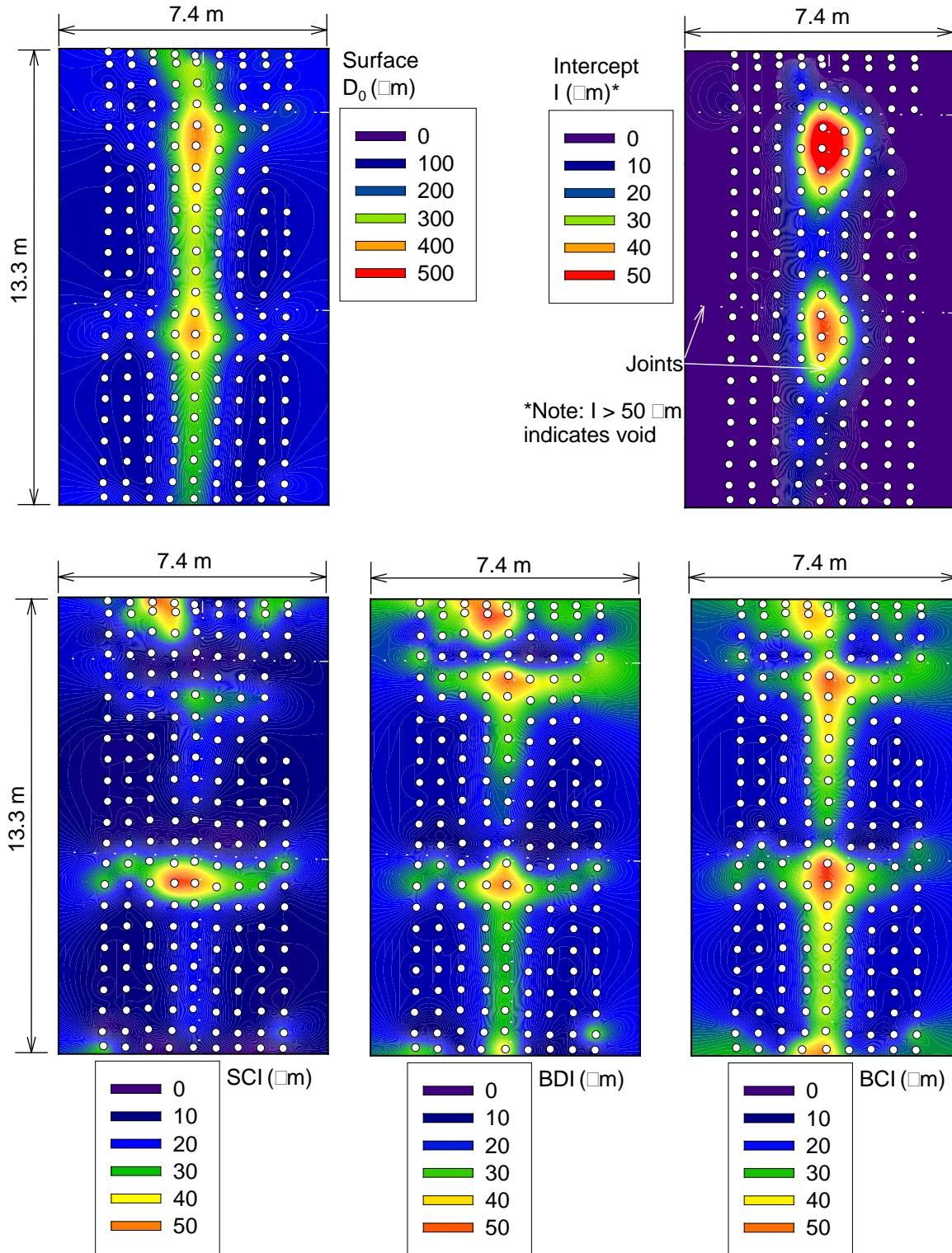


Figure 80. Kriged spatial contour maps of FWD test results (normalized for $F = 40 \text{ kN}$ (9000 lbs)) on pavement surface from TS2-B

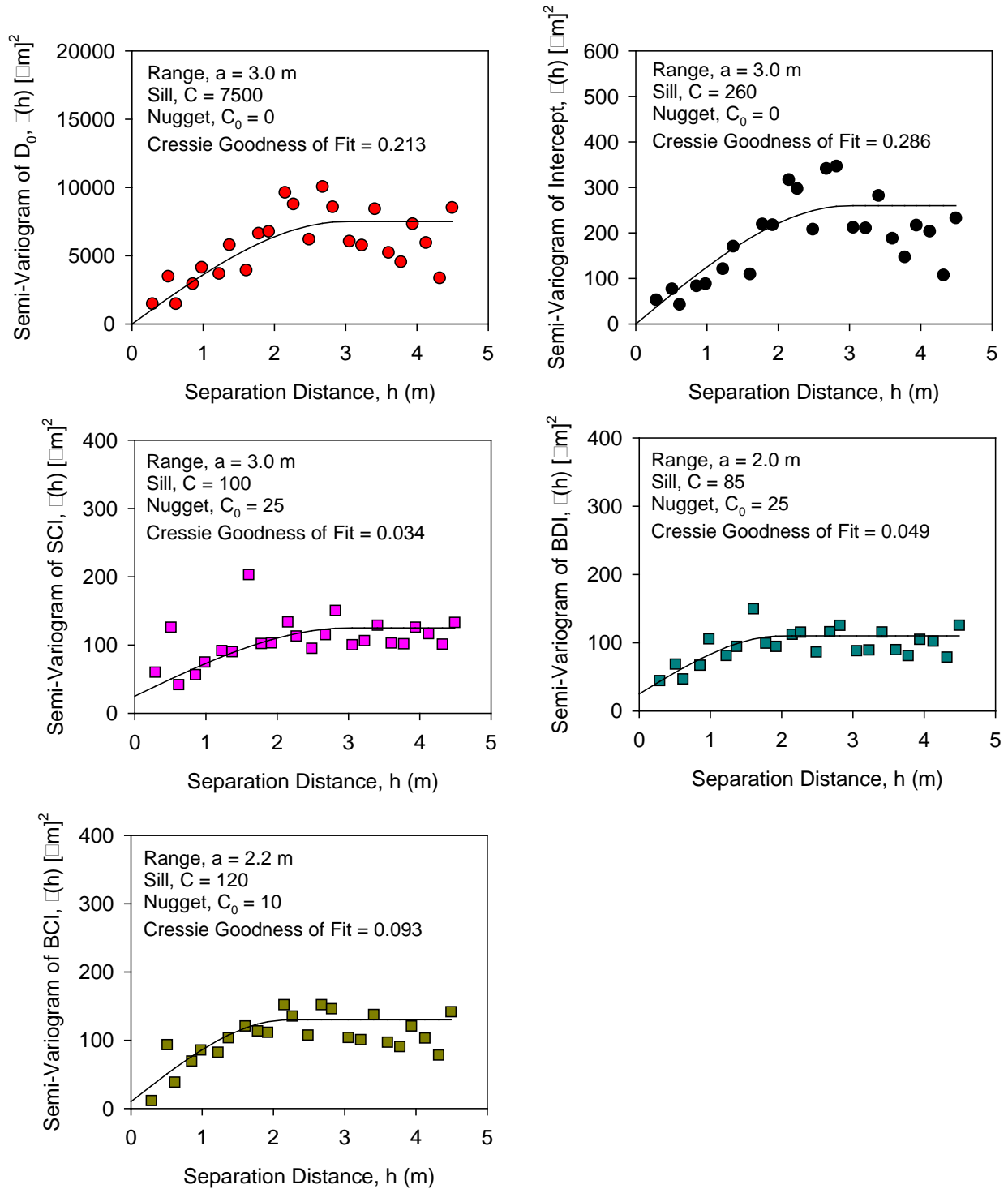


Figure 81. Semivariograms of FWD test results (normalized for F = 40 kN (9000 lbs)) on pavement surface from TS2-B

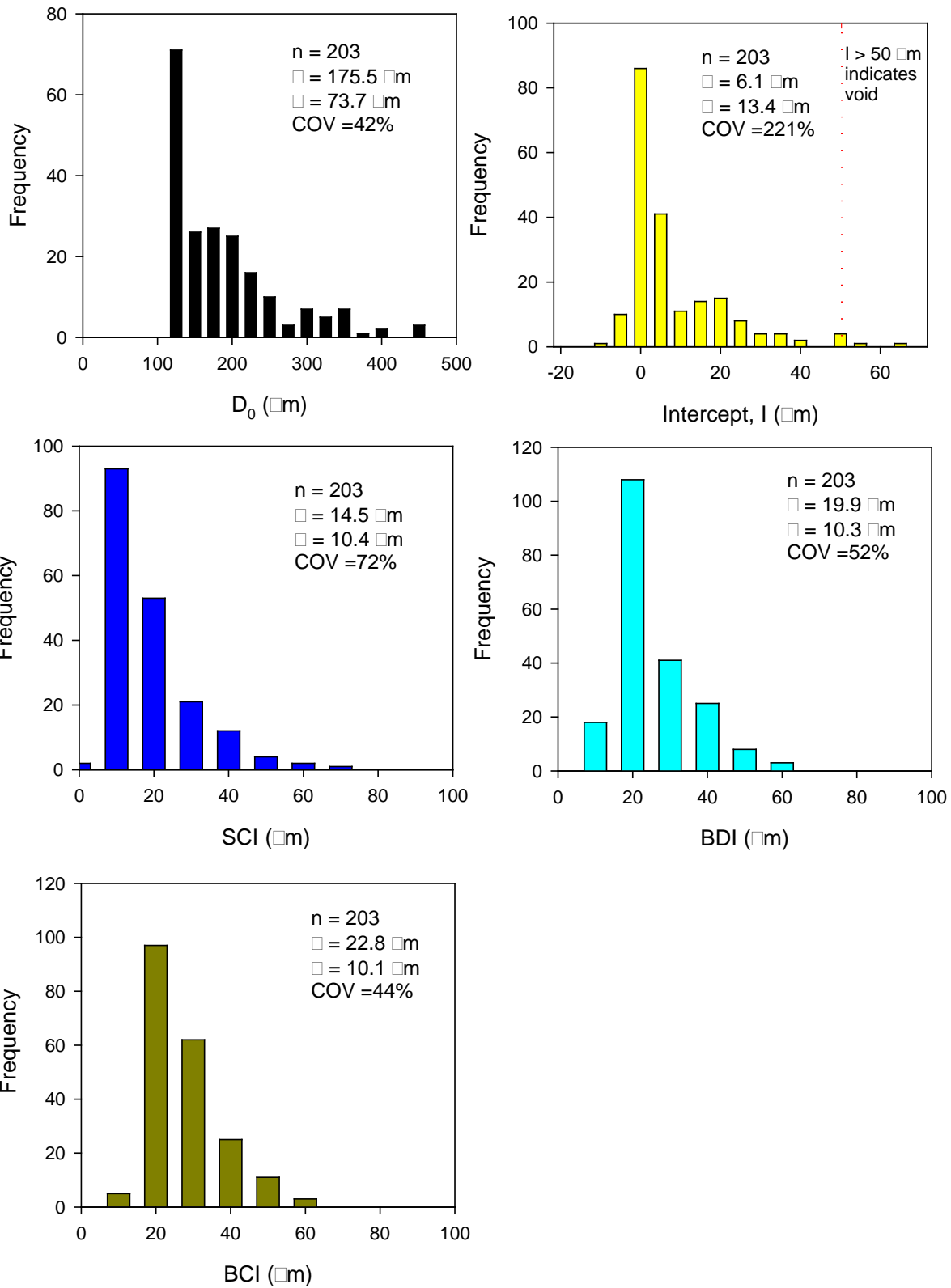


Figure 82. Histograms of FWD test results (normalized for F = 40 kN (9000 lbs)) on pavement surface from TS2-B

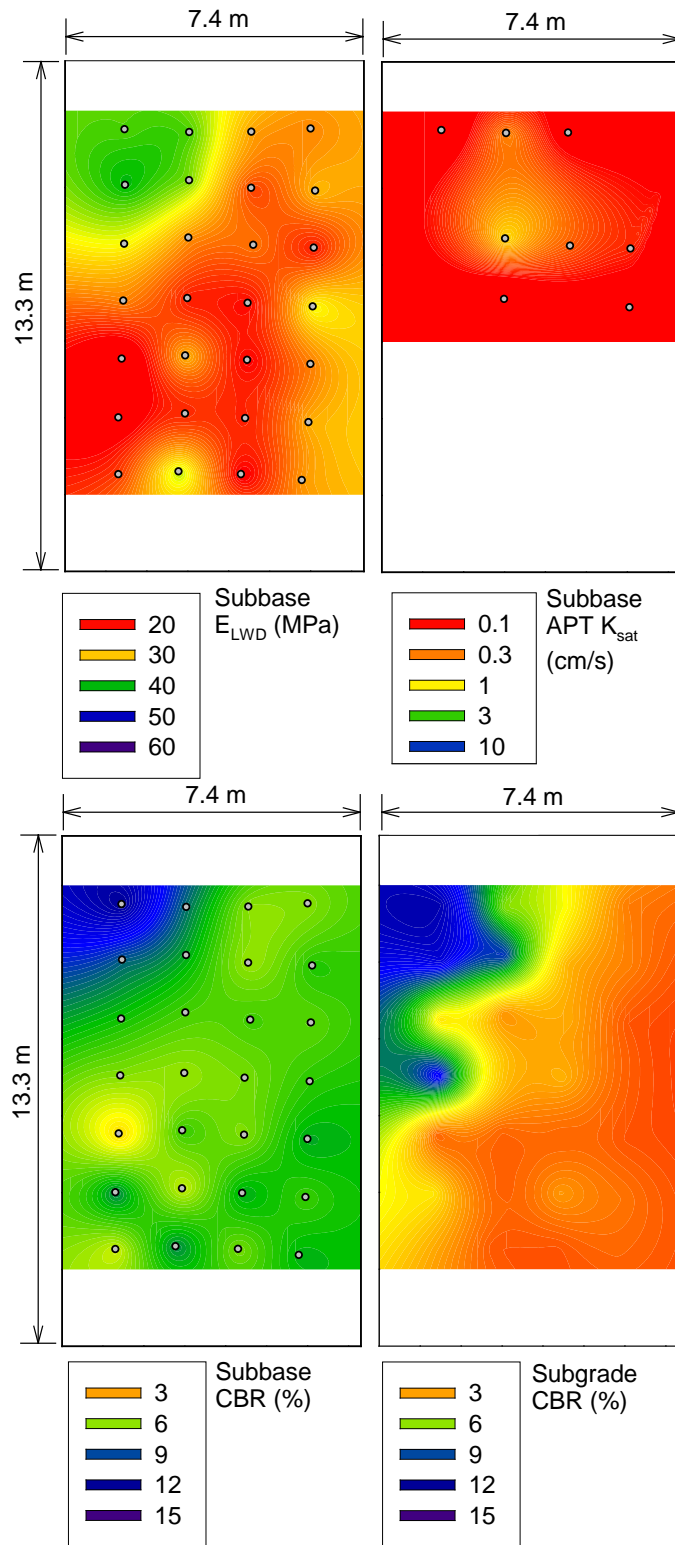


Figure 83. Kriged spatial contour maps of in situ point measurements on the existing subbase and subgrade layers from TS2-B

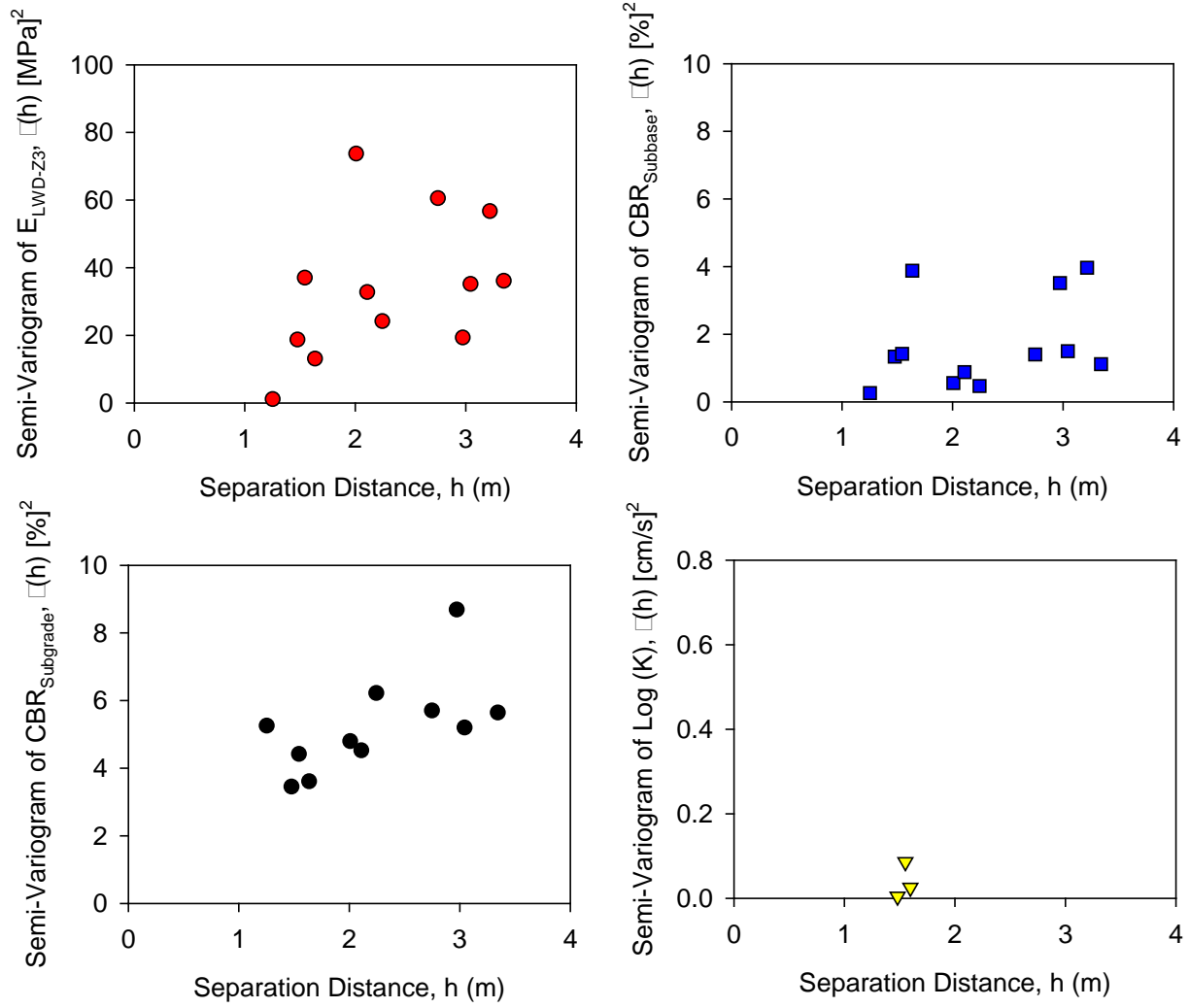


Figure 84. Semivariograms of in situ point measurements on existing subbase and subgrade layers from TS2-B

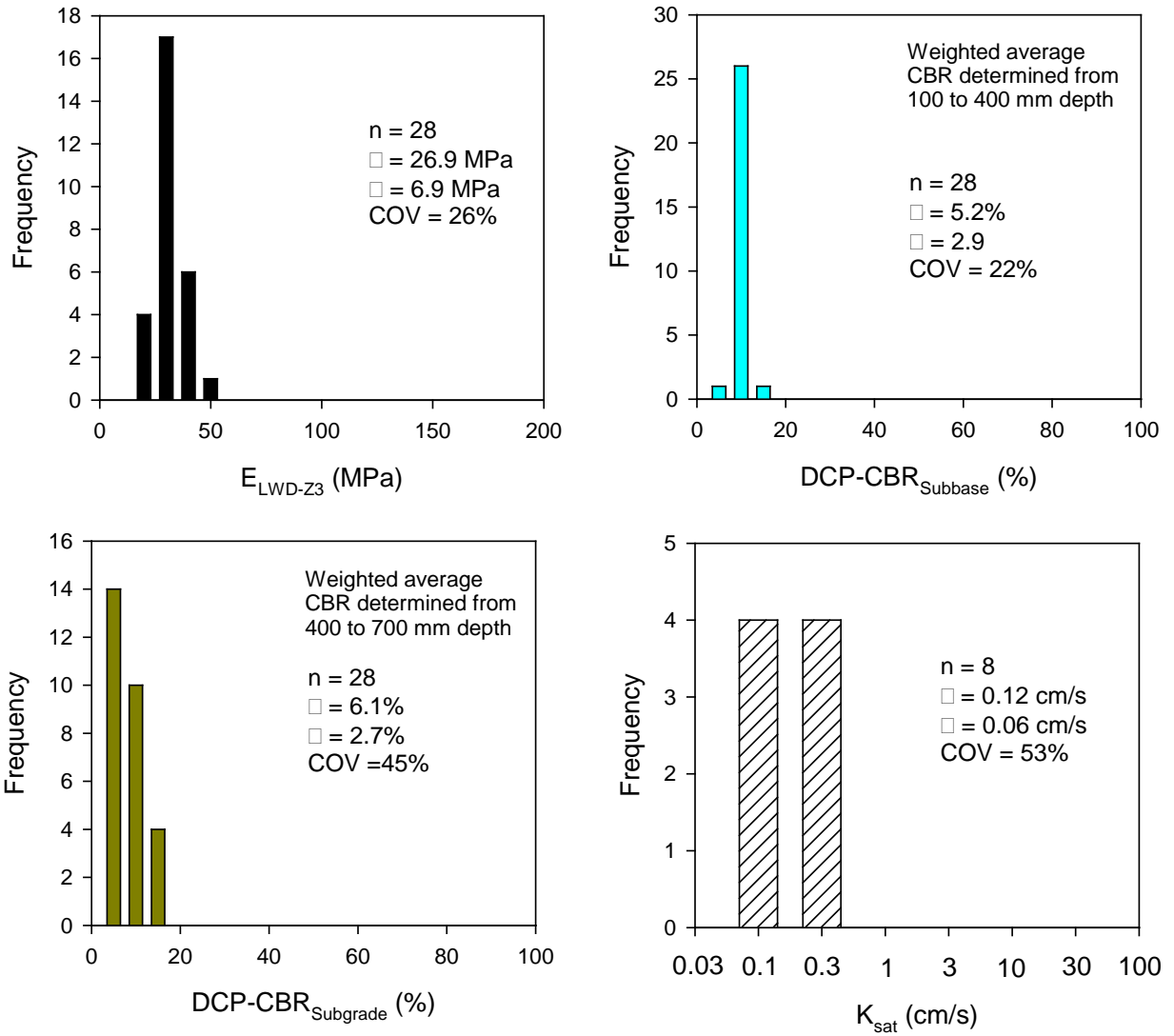


Figure 85. Histograms of in situ point measurements on existing subbase and subgrade layers from TS2-B

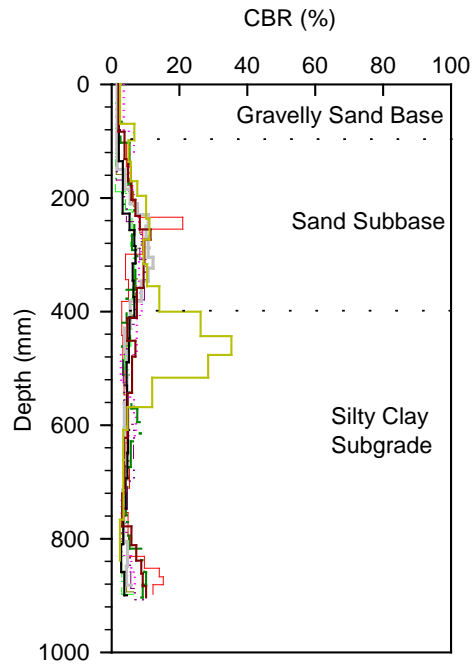


Figure 86. DCP-CBR profiles on the existing foundation layers from TS2-B

CHAPTER 6. SUMMARY AND CONCLUSIONS

This report presents results and analysis from a field study conducted on the I-94 between mile posts 23.0 and 6.1 in St. Clair and Macomb Counties, Michigan. The project involved construction of a 280 mm (11 in.) thick jointed PCC pavement, by undercutting the existing foundation layers to a depth of about 690 mm (27 in.) for placement of an open-graded drainage course (OGDC) layer composed of recycled steel slag, over the subgrade with a geotextile separation layer at the subgrade/OGDC layer interface. Review of construction bid documents indicated that the construction cost of the foundation layers (i.e., excavation, OGDC base layer, geotextile separator) was about 50% (\$5,424,275) of the total cost of the project (\$10,918,175).

Field testing was conducted on three test sections. Two of the test sections consisted of compacted OGDC base layer, while one test section consisted of existing pavement/ foundation layers. In situ testing was conducted by using point test methods (i.e., NG, LWD, FWD, DCP, PLT) and using roller-integrated compaction monitoring method to obtain 100% coverage over the OGDC base layer. Field point testing was conducted by spacing the test measurements about 50 to 100 m apart to capture the variability along the road alignment. Testing was also conducted in a dense grid pattern (spaced at about 0.6 to 1.5 m) to capture spatial variability over a small area. Geostatistical semivariogram analysis was performed to analyze the point test data from dense grid pattern testing to characterize and quantify spatial non-uniformity of the PCC surface and foundation layer properties. Geostatistical analysis was also performed on spatially referenced roller-integrated compaction measurements to quantify spatial non-uniformity of the foundation layers.

Comparing measured properties from laboratory and in situ testing with the design assumed values revealed the following:

- The measured E_{SB} values (either by LWD or FWD or PLT) and the estimated E_{SB} values (from DCP measurements) were on average about 1.5 to 7 times lower than the design target value. The laboratory determined E_{SB} values were, however, about 1.7 times higher than the design target value. It must be noted that the E_{SB} values obtained by LWD, FWD, and PLT represent a composite response in situ with the influence of both base layer and the underlying subgrade layer stiffness.
- M_r tests conducted on “undisturbed” in situ subgrade layer samples showed an average $M_r = 61$ MPa (8.8 ksi), which exceeds the design target $M_r = 21$ MPa (3 ksi). The average in situ estimated M_r value from DCP-CBR_{Subgrade} measurements was about 41 MPa (5.9 ksi), which also exceeds the design target value.
- The k_{comp} values determined in situ from PLT showed an average k_{PLT^*} of about 34 kPa/mm (124 pci), which was about 2.5 times lower than the design target $k_{comp} = 84$ kPa/mm (310 pci). The $k_{comp-AASHTO(1993)}$ values were estimated using E_{SB} based on DCP, LWD, and FWD measurements. These estimated values ranged from about 1.1 to 1.4 times the design target k_{comp} , depending on the selected E_{SB} value. The $k_{comp-AASHTO(1993)}$ determined using laboratory

measurements was about 163 kPa/mm (600 pci), which is about 2 times higher than the design target k_{comp} value. These results indicate that k_{comp} values vary significantly based on the method or procedure used.

- The C_d value assumed in design = 1.1, which represents that the quality of drainage is “good” to “excellent” according to AASHTO (1993). Based on the pavement geometry and the range of K_{sat} values obtained from field, the time for 90% of drainage ranged from 0.1 hour to 1.4 days. For an average $K_{sat} = 2.9$ cm/s, time for 90% drainage was estimated at about 1.1 hours. The average in situ $K_{sat} = 2.9$ cm/s compared well with the laboratory measured $K_{sat} = 3.1$ cm/s. These times for 90% drainage estimates indicate that the quality of the OGDC drainage layer is “good” to “excellent” according to AASHTO (1993) and therefore that it meets the design requirements.

Laboratory testing was conducted on foundation layer materials obtained from the field to determine index properties, moisture-dry unit weight relationships from compaction tests, resilient modulus, and aggregate degradation under cyclic loading. The resilient tests were conducted on homogenous samples as well as composite samples (i.e., OGDC base over subgrade) to assess its influence on the resilient modulus values. In addition, microstructural analysis using SEM on OGDC base layer material samples was performed. Some key findings from laboratory testing are as follows:

- Results indicated that the M_r of OGDC base layer material increased with increasing bulk stresses, as expected for granular materials. M_r of subgrade materials decreased with increasing deviator stress, as expected for non-granular materials. Increasing moisture content decreased M_r and increasing dry unit weight increased M_r for both subbase and subgrade materials.
- Comparison of M_r obtained on OGDC base material before and after back-saturation indicated that increasing saturation decreased the average M_r value by about 1.4 times.
- The comparison of homogenous and composite M_r test results revealed that the average M_r of composite sample is about 1.7 times lower than the average M_r of a homogenous layer OGDC sample at a similar density. The reason for this reduction in M_r in the composite sample is attributed to the weaker subgrade layer.
- Cyclic triaxial testing (up to 100,000 cycles) and corresponding aggregate degradation tests were conducted on OGDC base layer material samples compacted to different target dry unit weights, fines content, moisture content, and deviator/confining stress combinations. Results indicated very low permanent strains (< 0.7%) after 100,000 cycles for the recycled steel slag material used in the OGDC base layer for this project. No considerable aggregate degradation was found after 100,000 cycles on any of the OGDC base layer samples tested.

REFERENCES

- AASHTO T-307. (1999). "Standard method of test for determining the resilient modulus of soils and aggregate materials" American Association of State Highway and Transportation Officials (AASHTO), Washington, DC.
- AASHTO. (1993). *AASHTO design guide for design of pavement structures*. American Association of State Highway and Transportation Officials, Washington DC.
- Andrei, D., Witzak, M. W., Schwartz, C. W., and Uzan, J. (2004). "Harmonized resilient modulus test method for unbound pavement materials." *Transportation Research Record: Journal of the Transportation Research Board*. No. 1874, Transportation Research Board of the National Academies, Washington, DC, 29-37.
- ASTM C136-06. (2010). "Standard test method for sieve analysis of fine and coarse aggregates." American Standards for Testing Methods (ASTM), West Conshohocken, PA.
- ASTM D422-63. (2010). "Standard Test Method for Particle-Size Analysis of Soils." American Standards for Testing Methods (ASTM), West Conshohocken, PA.
- ASTM D698-07e1. (2010). "Standard test method for laboratory compaction characteristics of soil using standard effort (12,400 ft-lbf/ft³ (600 kN-m/m³))." American Standards for Testing Methods (ASTM), West Conshohocken, PA.
- ASTM D1557-09. (2010). "Standard test method for laboratory compaction characteristics of soil using modified effort (56,000 ft-lbf/ft³ (2,700 kN-m/m³))." American Standards for Testing Methods (ASTM), West Conshohocken, PA.
- ASTM D1587-08. (2010). "Standard practice for thin-walled tube sampling of soils for geotechnical purposes." American Standards for Testing Methods (ASTM), West Conshohocken, PA.
- ASTM D2487-10 (2010). "Standard test method for classification of soil for engineering purposes (unified soil classification system)." American Standards for Testing Methods (ASTM), West Conshohocken, PA.
- ASTM D3282-09 (2010). "Standard test method for classification of soils and soil-aggregate mixtures for highway construction purposes." American Standards for Testing Methods (ASTM), West Conshohocken, PA.
- ASTM D4253-00. (2010). "Standard test methods for maximum index density and unit weight of soils using a vibratory table." American Standards for Testing Methods (ASTM), West Conshohocken, PA.
- ASTM D4254-00. (2010). "Standard test methods for minimum index density and unit weight of soils and calculation of relative density." American Standards for Testing Methods (ASTM), West Conshohocken, PA.
- ASTM D4318-10. (2010). "Standard test methods for liquid limit, plastic limit, and plasticity index of soils." American Standards for Testing Methods (ASTM), West Conshohocken, PA.
- ASTM D4767-04 (2010). "Standard test method for consolidated undrained triaxial compression test for cohesive soils." American Standards for Testing Methods (ASTM), West Conshohocken, PA.
- ASTM D6951-03 (2010). "Standard test method for use of the dynamic cone penetrometer in shallow pavement applications." American Standards for Testing Methods (ASTM), West Conshohocken, PA.

- ASTM D6938-08a. “Standard test method for in-place density and water content of soil and soil-aggregate by nuclear methods (shallow depth).” American Standards for Testing Methods (ASTM), West Conshohocken, PA.
- Brandl, H., and D. Adam. (1997). “Sophisticated continuous compaction control of soils and granular materials.” Proceedings of the 14th International Conference of Soil Mechanics and Foundation Engineering. Hamburg, Germany, 1-6.
- Chilès Chilès, J. P., and P. Delfiner. (1999). *Geostatistics – Modeling Spatial Uncertainty*. John Wiley & Sons, Inc., New York.
- Clark, I., and W. Harper. (2002). *Practical geostatistics 2000*. 3rd reprint, Ecosse North America Llc, Columbus, Ohio.
- Floss,R., G. Bräu, M. Gahbauer, N. Gruber, and J. Obermayer. (1991). Dynamische Verdichtungsprüfung bei Erd-und Straßenbauten. *Prüfamnt für Grundbau, Boden-und Felsmechanik Technische Universität München*, Heft 612, München, Germany (in German).
- Horak, E. (1987). Aspects of deflection basin parameters used in a mechanistic rehabilitation design procedure for flexible pavements in South Africa. PhD Dissertation, University of Pretoria, South Africa.
- Huang H.Y. (2004). *Pavement Analysis and Design*, 2nd Edition, Pearson Prentice Hall, NJ.
- Isaaks, E. H., and R. M. Srivastava. (1989). *An introduction to applied geostatistics*. Oxford University Press, New York.
- Kilareski, W. P., and B. A. Anani. (1982). Evaluation of In Situ Moduli and Pavement Life from Deflection Basins. Fifth International Conference of Asphalt Pavements, University of Michigan, Ann Arbor, MI.
- McCracken, J. K. (2008). Seasonal analysis of the response of jointed plain concrete pavements to FWD and truck loads. MS Thesis, University of Pittsburg, Pittsburgh, Pennsylvania.
- MDOT (2005). *Pavement design and selection manual*. Prepared by Pavement Management Unit and Construction and Technology Division, Michigan Department of Transportation. <http://www.michigan.gov/documents/mdot/MDOT_Pavement_Design_and_Selection_Manual_257723_7.pdf> (Accessed, February 2015).
- NCHRP 1-28A. (2002). *Recommended standard method for routine resilient modulus testing of unbound granular base/subgrade materials and subgrade soils – NCHRP protocol 1-28A*, National Cooperative Highway Research Program.
- Mohammad, L. N., A. Herath, R. Gudishala, M. Y. Abu-Farsakh, and K. Alshibli. (2008). *Development of Models to Estimate the Subgrade and Subbase Layers’ Resilient Modulus from In Situ Devices Test Results for Construction Control*. Final report submitted to Louisiana Department of Transportation and Development, Louisiana Transportation Research Center, Baton Rouge, LA.
- Moulton, L. K (1980). *Highway Subdrainage Design*. Report No. FHWA-TS-80-224. Federal Highway Administration, Washington, DC.
- Powell, W. D., J. F. Potter, H. C. Mayhew, and M. E. Nunn. (1984). *The structural design of bituminous roads*. Report LR1132. Transport and Road Research Laboratory, UK.
- Quintus, V. H. L., and A. L. Simpson. (2002). *Backcalculation of Layer Parameters for LTPP Test Sections, Volume II: Layered Elastic Analysis for Flexible and Rigid Pavements, Research Report, Long-Term Pavement Performance Program*, Report No. FHWA-RD-01-113, Federal Highway Administration, Washington, DC, October 2002.

- Samaras, A. A., R. Lamm, and J. Treiterer. (1991). "Application of continuous dynamic compaction control for earthworks in railroad construction." *Transportation Research Record: Journal of the Transportation Research Board*. No. 1309, Transportation Research Board of the National Academies, Washington, DC, 42-46.
- Sandström, Å. (1994). *Numerical simulation of a vibratory roller on cohesionless soil*. Internal Report, Geodynamik, Stockholm, Sweden.
- Sandström Å., and C. B. Pettersson. (2004). Intelligent systems for QA/QC in soil compaction, *Proceedings of the TRB 2004 Annual Meeting* (CD-ROM), Transportation Research Board, Washington, DC.
- Substad, R. N. (2002). *LTPP Data Analysis: Feasibility of Using FWD Deflection Data to Characterize Pavement Construction Quality*. NCHRP Web Document 52, Project No. 20-50(9), National Cooperative Highway Research Program, Transportation Research Board of the National Academies, Washington, DC.
- Terzaghi, K., and R. B. Peck. (1967). *Soil mechanics in engineering practice*, 2nd Ed., John Wiley & Sons, Inc., New York.
- Thompson, M., and D. White. (2008). "Estimating compaction of cohesive soils from machine drive power." *Journal of Geotechnical and Geoenvironmental Engineering*, ASCE, 134(12), 1771-1777.
- Til, V. C. J., B. A. McCullough, Vallerga, and R. G. Hicks. (1972). *Evaluation of AASHTO Interim Guides for Design of Pavement Structures*. NCHRP 128, Highway Research Board.
- Vandenbossche, J. M. (2005). "Effects of slab temperature profiles on the use of falling weight deflectometer data to monitor joint performance and detect voids." *Transportation Research Record: Journal of the Transportation Research Board*. No. 2005, Transportation Research Board of the National Academies, Washington, DC, pp. 75-85.
- Vennapusa, P. (2004). *Determination of the Optimum Base Characteristics for Pavements*. Master's Thesis, Department of Civil Construction and Environmental Engineering, Iowa State University, Ames, Iowa.
- Vennapusa, P., and D. J. White. (2009). "Comparison of light weight deflectometer measurements for pavement foundation materials." *Geotechnical Testing Journal*, ASTM, 32(3), 239-251.
- Vennapusa, P., D. J. White, J. Siekmeier, and R. Embacher. (2011). "In-situ mechanistic characterization of granular pavement foundation layers." *International Journal of Pavement Engineering* (in print).
- Vennapusa, P., D. J. White, and M. Morris. (2010). "Geostatistical analysis of spatial referenced roller-integrated compaction measurements." *Journal of Geotechnical and Geoenvironmental Engineering*, ASCE, 136(6), 813-822
- Vennapusa, P., D. J. White, and C. T. Jahren. (2006). In situ permeability of unbound granular bases using the air permeameter test. Proceedings of the 85th Annual Transportation Research Board Conference, CD-ROM Paper # 06-1729, Transportation Research Board, Washington, DC.
- Vennapusa, P., D. J. White, and H. Gieselmann. (2009). Influence of support conditions on roller-integrated machine drive power measurements for granular base. International Foundation Congress and Equipment Exposition 2009 (IFCEE 09). March 15-19, Orlando, FL.

- White, D. J., and M. Thompson. (2008). "Relationships between in situ and roller-integrated compaction measurements for granular soils." *Journal of Geotechnical and Geoenvironmental Engineering*, ASCE, 134(2), 1763-1770.
- White, D. J., P. Vennapusa, and C. T. Jahren. (2004). *Determination of the Optimum Base Characteristics for Pavements*. Final Report, Iowa DOT Project TR-482, Center for Transportation Research and Education Project 02-119, Iowa State University, Ames, IA.
- White, D. J., E. Jaselskis, V. Schaefer, T. Cackler, (2005). "Real-time compaction monitoring in cohesive soils from machine response." *Transportation Research Record: Journal of the Transportation Research Board*. No. 1936, Transportation Research Board of the National Academies,, Washington DC, 173-180.
- White, D. J., P. Vennapusa, M. T. Suleiman., and C. T. Jahren. (2007). "An in situ device for rapid determination of permeability for granular bases." *Geotechnical Testing Journal*, 30(4), 282-291.
- White, D. J., P. Vennapusa, D. Eichner, H. Gieselman, L. Zhao, and C. T. Jahren. (2010a). *Rapid, self-contained in situ permeameter for field QA/QC of pavement base/subbase materials*. NCHRP 1-130 IDEA Project, Transportation Research Board, Washington, DC.
- White, D. J., Vennapusa, P., Gieselman, H., Zhang, J., Goldsmith, R., Johanson, L., and Quist, S. (2010b). *Accelerated Implementation of Intelligent Compaction Monitoring Technology for Embankment Subgrade Soils, Aggregate Base, and Asphalt Pavement Materials*. TPF-5(128) – *New York IC Demonstration Field Project*, ER10-01, Report submitted to The Transtec Group, FHWA, January.
- Witczak, M. W., and Uzan, J. (1988). *The universal airport design system – Report I of IV: Granular material characterization*. Department of Civil Engineering, University of Maryland, College Park. MD.
- Zapata and W. N. Houston. (2008). *Calibration and Validation of the Enhanced Integrated Climatic Model for Pavement Design*. NCHRP Report 602, Transportation Research Board, Washington, DC.
- Zorn, G. (2003). *Operating manual: Light drop-weight tester ZFG2000*, Zorn Stendal, Germany.

APPENDIX A: MDOT OFFICE MEMORANDUM (FEBRUARY 29, 2008): PAVEMENT SELECTION

EOC Approved by email 3/14/2008



OFFICE MEMORANDUM

DATE: February 29, 2008

TO: Brenda J. O'Brien
Engineer of Construction and Technology

FROM: Benjamin F. Krom
Pavement Selection Engineer

SUBJECT: **Pavement Selection: Reconstruct Jointed Plain Concrete Pavement**
CS 50112 & 77111, JN 100701
Reconstruct I-94: W of St. Clair/Macomb CoL to E of St. Clair Highway
CS 50112: BMP 5.650 to MP 6.165
CS 77111: MP 0.000 to EMP 6.510

I am requesting that the referenced project be placed on the agenda for the next Engineering Operations Committee (EOC) meeting. The subject project is programmed for letting in August of 2008, with a May 2008 plan completion.

The reconstruction alternatives being considered are a Hot Mix Asphalt Pavement (HMA Alt #1) and a Jointed Plain Concrete Pavement (JPCP Alt #2). The pavement designs being considered are as follows:

Alternative #1: Reconstruct with Hot Mix Asphalt Pavement

- 2" HMA, Gap-Graded Superpave, Top Course (mainline & inside shoulder)
- 2.5" HMA, 4E30, Leveling Course (mainline & inside shoulder)
- 6" HMA, 3E30, Base Course (mainline & inside shoulder)
- 2" HMA, 5E3, Top Course (outside shoulder)
- 2.5" HMA, 4E3, Leveling Course (outside shoulder)
- 6" HMA, 3E3, Base Course (outside shoulder)
- 16" Open-Graded Drainage Course
- Geotextile Separator
- 8" Sand Subbase
- 6" dia. Underdrain System
- 34.5" Total Section Thickness

Present Value Initial Construction Cost	\$1,010,802/directional mile
Present Value Initial User Cost	\$499,860/directional mile
Present Value Maintenance Cost	\$127,428/directional mile

Equivalent Uniform Annual Cost (EUAC)\$89,536/directional mile

Alternative #2: Reconstruct with Jointed Plain Concrete Pavement

10.5"	Non-Reinforced Concrete Pavement, P1 Modified, with 14' joint spacing
16"	Open Graded Drainage Course
	Geotextile Separator
6" dia.	Open-Graded Underdrain System
26.5"	Total Thickness

Present Value Initial Construction Cost	\$819,071/directional mile
Present Value Initial User Cost	\$375,461/directional mile
Present Value Maintenance Cost	\$76,707/directional mile

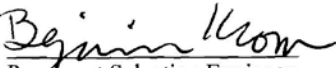
Equivalent Uniform Annual Cost (EUAC) \$69,484/directional mile

The pavement designs for both alternatives are based on the 1993 AASHTO "Guide for Design of Pavement Structures" and use the AASHTO pavement software DARWin Version 3.01, 1997. The Equivalent Uniform Annual Cost calculation is based on the revised pavement selection process as approved by the EOC on June 3, 1999.

The estimated construction costs are based on historical averages from similar projects. User costs are calculated using MDOT's Construction Congestion Cost model, which was developed by the University of Michigan.

Conclusion

Pavement selection was determined using the procedures outlined in the MDOT Pavement Design and Selection Manual. Department policy requires that the pavement alternative with the lowest EUAC, **Alternative #2: Reconstruct with Jointed Plain Concrete Pavement**, be selected. Final pavement selection requires approval by the Engineering Operations Committee.


Benjamin Kwon
Pavement Selection Engineer

cc: C. Bleech
K. Kennedy
P. Schafer
M. Eacker
A. Iftikhar
M. Grazioli
N. Bandara

PROJECT SUMMARY

Project Location

This project includes 7.025 miles of I-94 reconstruction from west of the Saint Clair/Macomb County Line to east of Saint Clair Highway. The existing section is a 4 lane divided freeway consisting of 12' paved lanes, an 9' paved outside shoulder and a 4' paved inside shoulder in each direction. The proposed section increases the outside shoulder to 12' and the inside shoulder to 5'.

Existing Pavement and Condition Data

The existing typical cross section consists of, on average, 9.6" of jointed reinforced concrete pavement and 14.1" of sand subbase. Only 17% of the cores showed a distinguishable aggregate base layer. EB I-94 between Belle River and Allington Road has, on average, 3" of HMA over the above described pavement section. The existing sand is of insufficient depth to be used for the proposed pavement designs.

Average Ride Quality (2007)

RQI \geq 70 Poor

73 EB I-94

73 WB I-94

Average Remaining Service Life (2007)

RSL < 3 Poor

4 EB I-94

4 WB I-94

Traffic

35,750 ADT (2008 two-way)

4,469 Commercial ADT (2008 two-way)

Growth Rate: 1.5% compound

22.50 million Design ESAL's – Rigid – 20 years

14.90 million Design ESAL's – Flexible – 20 years

Directional Distribution Factor – 55%

Different 18 Kip axle equivalency factors (ESAL's) are used for the designs of Flexible and Rigid pavements because each pavement type experiences a different loss of serviceability from the passage of identical vehicles. Work done at the AASHO test road resulted in the creation of pavement design formulas that account for these differences. Proper use of these formulas requires that different ESAL's be used for Flexible and Rigid pavements, although the anticipated traffic is identical. The Engineering Operations Committee has approved the use of different ESAL factors for Flexible and Rigid pavement designs.

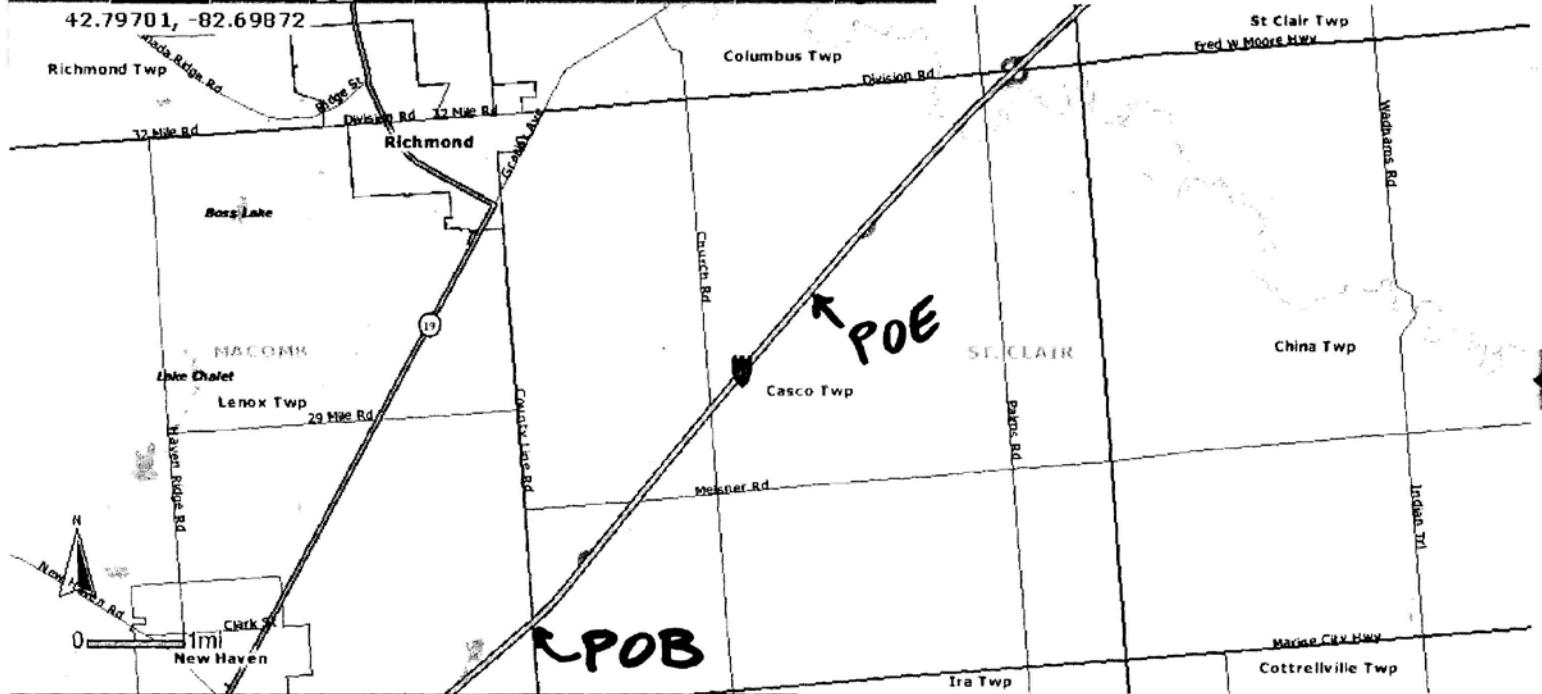
Hourly volumes for 24 hour periods, shown in the appendix, are based on distributions appearing in Table 3.2 of FHWA publication "Life Cycle Cost Analysis in Pavement Design". User costs for succeeding maintenance activities are based on the values shown in Table A, page 17, of the appendix.

Soils

The Regional Soils Specialist recommends a subgrade soil resilient modulus of 3,000 psi be used for design purposes. This is based on site observations and the soil conditions encountered during the soils investigation. For more information, refer to pages 20-23 of the appendix.

Construction Staging and Maintaining Traffic

For information refer to the maintaining traffic memo in the appendix.



APPENDIX A – TABLE OF CONTENTS

1	EUAC Summary
2-3	Initial Costs
4	Pavement Preservation Strategy
5-6	Proposed Reconstruction Typical
7-10	Construction Time Estimates
11	Traffic Information
12-14	Maintaining Traffic Memo
15	User Cost Summary
16	User Cost Output Sheet
17	User Costs for Maintenance Activities
18-19	AASHTO DARWin Pavement Design
20-23	Recommendation for Subgrade Mr
24-25	Modulus of Subgrade Reaction

EUAC Summary
I-94 Reconstruction

<u>Alternative</u>	<u>PV Initial Construction Cost</u>	<u>PV Initial User Cost</u>	<u>PV Maintenance Cost</u>	<u>n</u>	<u>EUAC</u>
#1: HMA	\$1,010,802	\$499,860	\$127,428	26	\$89,536
#2: JPCP	\$819,071	\$375,461	\$76,707	26	\$69,484

$$EUAC = NPV * (i * (1+i)^n) / ((1+i)^n - 1)$$

Note: All costs are per directional mile

NPV = Net Present Value

i = Real Discount Rate (2008: 2.8%)

n = Number of years

PV = Present Value

EUAC = Equivalent Uniform Annual Cost

PROJECT COSTING ALTERNATIVE #1: HMA PAVEMENT

REGION NO.	CONTROL SECTION	JOB NUMBER	BMP	EMP	LETTING DATE	PROJECT DESCRIPTION:
7	77111	100701	0.053	4.330	1-Aug-2008	I-94: from Saint Clair/Macomb County Line to Meldrum Road
Metro			Length =	4.277	Miles	

PAY ITEM CODE	PAY ITEM DESCRIPTION	LANE (0=OS, 1=ML1, 2=ML2, ..., 6=IS)	WIDTH (Ft)	DEPTH (Inches)	# OF RUNS or Jt SPACE (Ft)	ENTER QUANTITY	UNITS	CALC'D QUANTITY	UNIT PRICE	TOTAL COST (Per Dir. Mile)
										\$1,010,801.88
5020057	HMA, 5E3	Outside Shoulder	0	12	2		Ton	774.4	\$54.71	\$42,367.42
5020051	HMA, 4E3	Outside Shoulder	0	12	2.5		Ton	968.0	\$50.86	\$49,232.48
5020045	HMA, 3E3	Outside Shoulder	0	12	6		Ton	2323.2	\$44.05	\$102,336.96
3037011	Open-Graded Dr Cse, 16 inch	Outside Shoulder	0	12			Syd	7040.0	\$8.30	\$58,432.00
3030020	Geotextile Separator	Outside Shoulder	0	12			Syd	7040.0	\$1.07	\$7,532.80
3010002	Subbase, CIP	Outside Shoulder	0	12	8		Cyd	1564.4	\$7.60	\$11,889.78
2050016	Excavation, Earth	Outside Shoulder	0	12	28.8		Cyd	5632.0	\$4.02	\$22,640.64
5027031	Gap-Graded Superpave	MainLine1	1	12	2		Ton	774.4	\$52.26	\$40,470.14
5020053	HMA, 4E30	MainLine1	1	12	2.5		Ton	968.0	\$55.56	\$53,782.08
5020047	HMA, 3E30	MainLine1	1	12	6		Ton	2323.2	\$44.86	\$104,218.75
3037011	Open-Graded Dr Cse, 16 inch	MainLine1	1	12			Syd	7040.0	\$8.30	\$58,432.00
3030020	Geotextile Separator	MainLine1	1	12			Syd	7040.0	\$1.07	\$7,532.80
3010002	Subbase, CIP	MainLine1	1	12	8		Cyd	1564.4	\$7.60	\$11,889.78
2050016	Excavation, Earth	MainLine1	1	12	24.9		Cyd	4869.3	\$4.02	\$19,574.72
5027031	Gap-Graded Superpave	MainLine2	2	12	2		Ton	774.4	\$52.26	\$40,470.14
5020053	HMA, 4E30	MainLine2	2	12	2.5		Ton	968.0	\$55.56	\$53,782.08
5020047	HMA, 3E30	MainLine2	2	12	6		Ton	2323.2	\$44.86	\$104,218.75
3037011	Open-Graded Dr Cse, 16 inch	MainLine2	2	12			Syd	7040.0	\$8.30	\$58,432.00
3030020	Geotextile Separator	MainLine2	2	12			Syd	7040.0	\$1.07	\$7,532.80
3010002	Subbase, CIP	MainLine2	2	12	8		Cyd	1564.4	\$7.60	\$11,889.78
2050016	Excavation, Earth	MainLine2	2	12	24.9		Cyd	4869.3	\$4.02	\$19,574.72
5027031	Gap-Graded Superpave	Inside Shoulder	6	5	2		Ton	322.7	\$52.26	\$16,862.56
5020053	HMA, 4E30	Inside Shoulder	6	5	2.5		Ton	403.3	\$55.56	\$22,409.20
5020047	HMA, 3E30	Inside Shoulder	6	5	6		Ton	968.0	\$44.86	\$43,424.48
3037011	Open-Graded Dr Cse, 16 inch	Inside Shoulder	6	5			Syd	2933.3	\$8.30	\$24,346.67
3030020	Geotextile Separator	Inside Shoulder	6	5			Syd	2933.3	\$1.07	\$3,138.67
3010002	Subbase, CIP	Inside Shoulder	6	5	8		Cyd	651.9	\$7.60	\$4,954.07
2050016	Excavation, Earth	Inside Shoulder	6	5	28.8		Cyd	2346.7	\$4.02	\$9,433.60

2

PROJECT COSTING ALTERNATIVE #2: JPCP PAVEMENT

REGION NO.	CONTROL SECTION	JOB NUMBER	BMP	EMP	LETTING DATE	PROJECT DESCRIPTION:
7 Metro	77111	100701	0.053 Length =	4.330 4.277 Miles	1-Aug-2008	I-94: from Saint Clair/Macomb County Line to Meldrum Road

PAY ITEM CODE	PAY ITEM DESCRIPTION	LANE (0=OS, 1=ML1, 2=ML2,..., 6=IS)	WIDTH (Ft)	DEPTH (Inches)	# OF RUNS or Jt SPACE (Ft)	ENTER QUANTITY	UNITS	CALC'D QUANTITY	UNIT PRICE	TOTAL COST (Per Dir. Mile)
										\$819,070.59
6020109	Conc Pavt, Nonreinf, 10 1/2 inch	Outside Shoulder	0	12			Syd	7040.0	\$17.98	\$126,579.20
3037011	Open-Graded Dr Cse, 16 inch	Outside Shoulder	0	12			Syd	7040.0	\$8.30	\$58,432.00
3030020	Geotextile Separator	Outside Shoulder	0	12			Syd	7040.0	\$1.07	\$7,532.80
6020201	Joint, Contraction, C3p	Outside Shoulder	0	12	14		Ft	4525.7	\$2.62	\$11,857.37
2050016	Excavation, Earth	Outside Shoulder	0	12			Cyd	4067.6	\$4.02	\$16,351.57
6020109	Conc Pavt, Nonreinf, 10 1/2 inch	MainLine1	1	12			Syd	7040.0	\$17.98	\$126,579.20
3037011	Open-Graded Dr Cse, 16 inch	MainLine1	1	12			Syd	7040.0	\$8.30	\$58,432.00
3030020	Geotextile Separator	MainLine1	1	12			Syd	7040.0	\$1.07	\$7,532.80
6020200	Joint, Contraction, Cp	MainLine1	1	12	14		Ft	4525.7	\$10.46	\$47,338.97
2050016	Excavation, Earth	MainLine1	1	12			Cyd	3304.9	\$4.02	\$13,285.65
6020109	Conc Pavt, Nonreinf, 10 1/2 inch	MainLine2	2	12			Syd	7040.0	\$17.98	\$126,579.20
3037011	Open-Graded Dr Cse, 16 inch	MainLine2	2	12			Syd	7040.0	\$8.30	\$58,432.00
3030020	Geotextile Separator	MainLine2	2	12			Syd	7040.0	\$1.07	\$7,532.80
6020200	Joint, Contraction, Cp	MainLine2	2	12	14		Ft	4525.7	\$10.46	\$47,338.97
2050016	Excavation, Earth	MainLine2	2	12			Cyd	3304.9	\$4.02	\$13,285.65
6020109	Conc Pavt, Nonreinf, 10 1/2 inch	Inside Shoulder	6	5			Syd	2933.3	\$17.98	\$52,741.33
3037011	Open-Graded Dr Cse, 16 inch	Inside Shoulder	6	5			Syd	2933.3	\$8.30	\$24,346.67
3030020	Geotextile Separator	Inside Shoulder	6	5			Syd	2933.3	\$1.07	\$3,138.67
6020201	Joint, Contraction, C3p	Inside Shoulder	6	5	14		Ft	1885.7	\$2.62	\$4,940.57
2050016	Excavation, Earth	Inside Shoulder	6	5			Cyd	1694.8	\$4.02	\$6,813.16

Alternative #1: HMA Pavement Preservation Strategy

I-94 Reconstruction

Facility: Freeway/Divided Highway

Fix Type: New/Reconstruction - Flexible HMA Pavement

<u>Activity</u>	<u>Approx. Age</u>	<u>Cost per Lane-Mile</u>	<u>Number of Lanes</u>	<u>Present Value per Directional Mile</u>
Maintenance	10	\$33,789 Agency \$67 User Cost	2	\$51,373
Maintenance	13	\$54,384 Agency \$67 User Cost	2	\$76,055
Rehabilitation or Reconstruction	26			
Total PV=				\$127,428

Alternative #2: JPCP Pavement Preservation Strategy

I-94 Reconstruction

Facility: Freeway/Divided Highway

Fix Type: New/Reconstruction - Rigid Concrete Pavement

<u>Activity</u>	<u>Approx. Age</u>	<u>Cost per Lane-Mile</u>	<u>Number of Lanes</u>	<u>Present Value per Directional Mile</u>
Maintenance	9	\$13,516 Agency \$115 User Cost	2	\$21,263
Maintenance	15	\$41,834 Agency \$115 User Cost	2	\$55,444
Rehabilitation or Reconstruction	26			
Total PV=				\$76,707

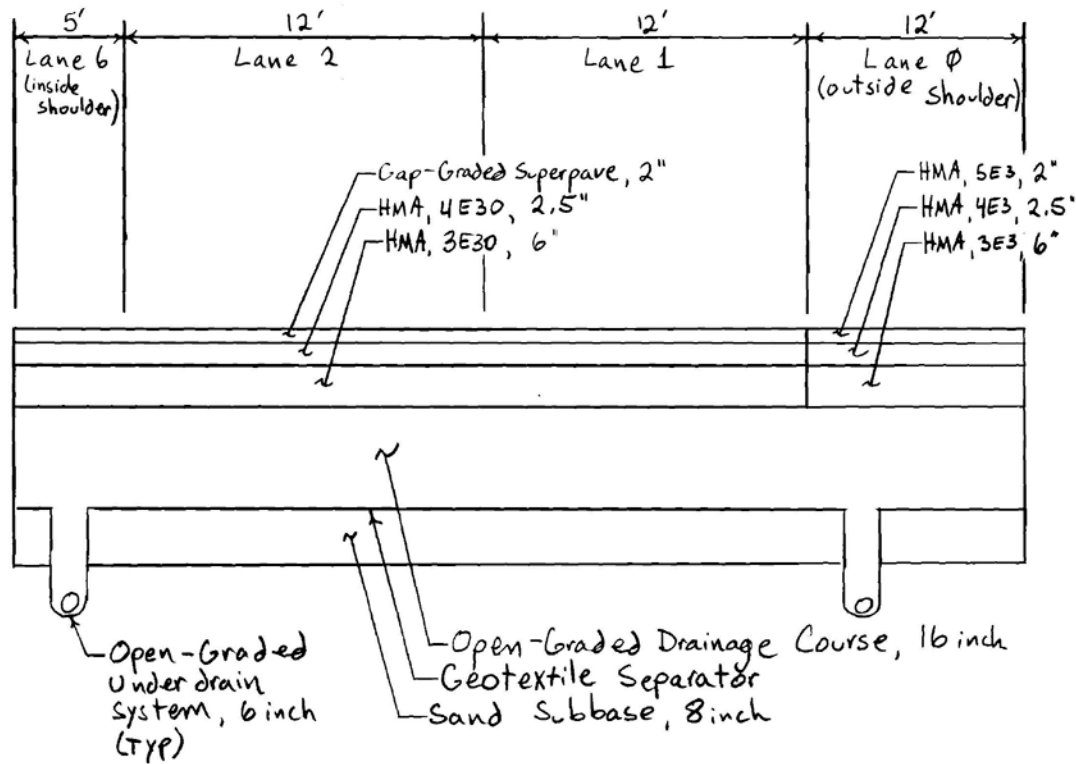
Present Value (PV) = (Agency Maint. Cost + User Maint. Cost)/(1+i)ⁿ

i = Real Discount Rate (2008: 2.8%)

n = Year of rehabilitation or reconstruction

4

Alternative #1: HMA Reconstruction



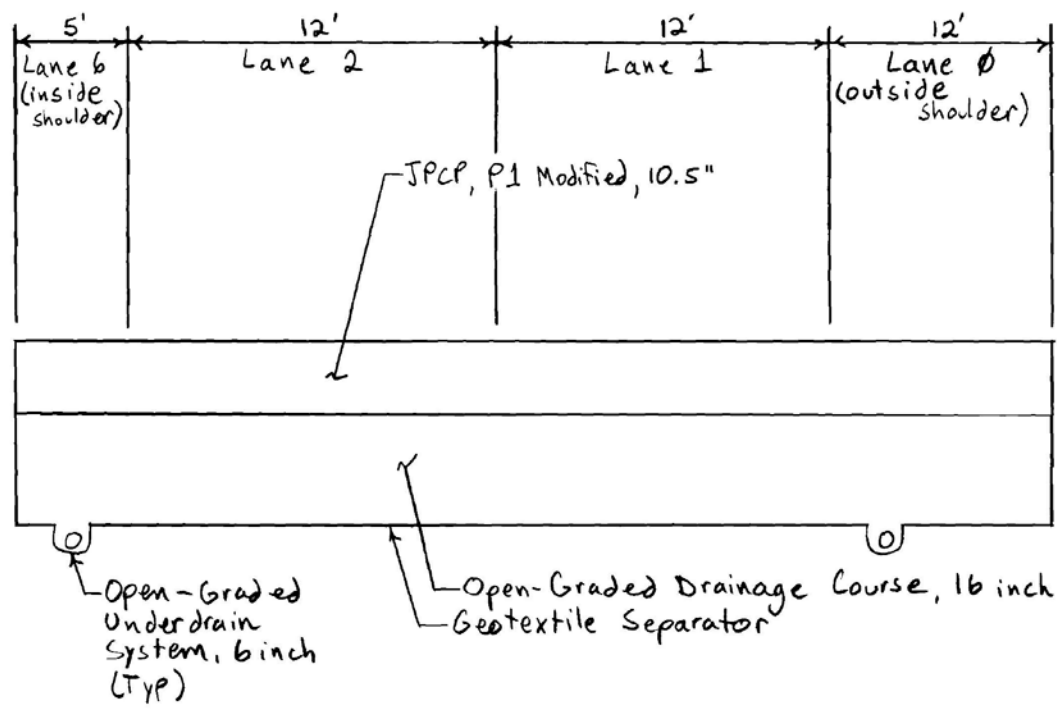
77111

100701

B/L 2/12/2008

5

Alternative #2: JPCP Reconstruction



77111

100701

BK

2/12/2008

PROJECT COSTING ALTERNATIVE #1: HMA PAVEMENT WORKPLAN

STAGE 1	STAGE 2	STAGE 3	STAGE 4
CONST WB LANES:	CONST EB LANES:		
0	0		
1	1		
2	2		
6	6		

STAGE 1

Pay Item	Total per Dir. Mi.	Production Rate	Production Days	Project Length	Total Production Days
Excavation, Earth	17717	Cyd 2600	Cyd/day 6.8	x 7.025 Miles =	47.9
Subbase, CIP	5345	Cyd 2600	Cyd/day 2.1	x 7.025 Miles =	14.4
Geotextile Separator	24053	Syd 6100	Syd/day 3.9	x 7.025 Miles =	27.7
(1) Open-Graded Dr Cse, 16 inch	24053	Syd 6100	Syd/day 3.9	x 7.025 Miles =	27.7
(2) Open-Graded Dr Cse, 16 inch	24053	Syd 6100	Syd/day 3.9	x 7.025 Miles =	27.7
HMA, 3E30	5614	Ton 2000	Ton/day 2.8	x 7.025 Miles =	19.7
HMA, 4E30	2339	Ton 2000	Ton/day 1.2	x 7.025 Miles =	8.2
Gap-Graded Superpave	1871	Ton 2000	Ton/day 0.9	x 7.025 Miles =	6.6
HMA, 3E3	2323	Ton 2000	Ton/day 1.2	x 7.025 Miles =	8.2
HMA, 4E3	968	Ton 2000	Ton/day 0.5	x 7.025 Miles =	3.4
HMA, 5E3	774	Ton 2000	Ton/day 0.4	x 7.025 Miles =	2.7

STAGE 2

Pay Item	Total per Dir. Mi.	Production Rate	Production Days	Project Length	Total Production Days
Excavation, Earth	17717	Cyd 2600	Cyd/day 6.8	x 7.025 Miles =	47.9
Subbase, CIP	5345	Cyd 2600	Cyd/day 2.1	x 7.025 Miles =	14.4
Geotextile Separator	24053	Syd 6100	Syd/day 3.9	x 7.025 Miles =	27.7
(1) Open-Graded Dr Cse, 16 inch	24053	Syd 6100	Syd/day 3.9	x 7.025 Miles =	27.7
(2) Open-Graded Dr Cse, 16 inch	24053	Syd 6100	Syd/day 3.9	x 7.025 Miles =	27.7
HMA, 3E30	5614	Ton 2000	Ton/day 2.8	x 7.025 Miles =	19.7
HMA, 4E30	2339	Ton 2000	Ton/day 1.2	x 7.025 Miles =	8.2
Gap-Graded Superpave	1871	Ton 2000	Ton/day 0.9	x 7.025 Miles =	6.6
HMA, 3E3	2323	Ton 2000	Ton/day 1.2	x 7.025 Miles =	8.2
HMA, 4E3	968	Ton 2000	Ton/day 0.5	x 7.025 Miles =	3.4
HMA, 5E3	774	Ton 2000	Ton/day 0.4	x 7.025 Miles =	2.7

(1) and (2) state which lift of material is being placed

7

PROJECT COSTING ALTERNATIVE #2: JPCP PAVEMENT WORKPLAN

STAGE 1 CONST WB LANES:	STAGE 2 CONST EB LANES:	STAGE 3	STAGE 4
0	0		
1	1		
2	2		
6	6		

STAGE 1

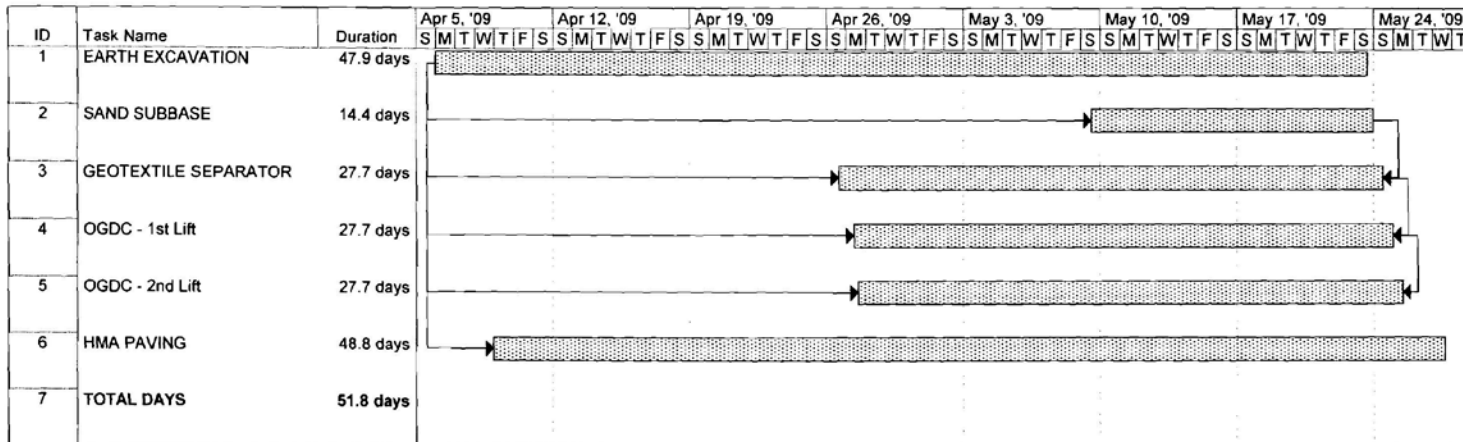
Pay Item	Total per Dir. Mi.	Production Rate	Production Days	Project Length	Total Production Days
Excavation, Earth	12372	Cyd 2600	Cyd/day 4.8	x 7.025 Miles =	33.4
Geotextile Separator	24053	Syd 6100	Syd/day 3.9	x 7.025 Miles =	27.7
(1) Open-Graded Dr Cse, 16 inch	24053	Syd 6100	Syd/day 3.9	x 7.025 Miles =	27.7
(2) Open-Graded Dr Cse, 16 inch	24053	Syd 6100	Syd/day 3.9	x 7.025 Miles =	27.7
Conc Pavt, Nonreinf, 10 1/2 inc	24053	Syd 7700	Syd/day 3.1	x 7.025 Miles =	21.9
Joint, Contraction, Cp	9051	Ft	Ft/day	x 7.025 Miles =	1.5
Joint, Contraction, C3p	6411	Ft	Ft/day	x 7.025 Miles =	1.5

STAGE 2

Pay Item	Total per Dir. Mi.	Production Rate	Production Days	Project Length	Total Production Days
Excavation, Earth	12372	Cyd 2600	Cyd/day 4.8	x 7.025 Miles =	33.4
Geotextile Separator	24053	Syd 6100	Syd/day 3.9	x 7.025 Miles =	27.7
(1) Open-Graded Dr Cse, 16 inch	24053	Syd 6100	Syd/day 3.9	x 7.025 Miles =	27.7
(2) Open-Graded Dr Cse, 16 inch	24053	Syd 6100	Syd/day 3.9	x 7.025 Miles =	27.7
Conc Pavt, Nonreinf, 10 1/2 inc	24053	Syd 7700	Syd/day 3.1	x 7.025 Miles =	21.9
Joint, Contraction, Cp	9051	Ft	Ft/day	x 7.025 Miles =	1.5
Joint, Contraction, C3p	6411	Ft	Ft/day	x 7.025 Miles =	1.5

(1) and (2) state which lift of material is being placed

8



I-94 From St. Clair/Macomb Co Line to Meldrum Road
 CS 77111 JN 100701
 HMA Reconstruction: Stages 1 & 2



Alternative 1: HMA
 Stages 1 & 2

ID	Task Name	Duration	Apr 5, '09							Apr 12, '09							Apr 19, '09							Apr 26, '09							May 3, '09							May 10, '09						
			S	M	T	W	T	F	S	S	M	T	W	T	F	S	S	M	T	W	T	F	S	S	M	T	W	T	F	S	S	M	T	W	T	F	S	S	M	T	W	T	F	S
1	EARTH EXCAVATION	33.4 days																																										
2	GEOTEXTILE SEPARATOR	27.7 days																																										
3	OGDC - 1st Lift	27.7 days																																										
4	OGDC - 2nd Lift	27.7 days																																										
5	CONCRETE PAVING	21.9 days																																										
6	JOINTS AND CURE	3 days																																										
7	TOTAL DAYS	38.9 days																																										

I-94 from St. Clair/Macomb Co Line to Meldrum Road
CS 77111 JN 100701
JPCP Reconstruction: Stages 1 & 2

Task		Milestone		External Tasks	
Split		Summary		External Milestone	
Progress		Project Summary		Deadline	

Alternative 2: JPCP
Stages 1 & 2



OFFICE MEMORANDUM

DATE: November 28, 2007

TO: Mohammed Huque, Scott Singer
Port Huron TSC

FROM: Ed Waddell
Project Planning Division

SUBJECT: Traffic Analysis Request #1959, Job #100701
I-94 from St. Clair S.C.L. to Meldrum Road (CS 77111 MP 0.0 to 4.33)

The following tables depict the traffic data requested for this project. Please let me know if there are any questions.

Interstate 94, from 26 Mile Road to Fred Moore Highway				
		Base Year	Construction Year	Design Year
		2007	2009	2029
ADT		35,500	36,000	42,000
Directional ADT		17,750	18,000	21,000
NorthEastbound Peaks AM: 11-12 PM: 5-6	AM	1288	1309	1518
	PM	2448	2488	2885
Southwestbound Peaks AM: 6-7 PM: 2-3	AM	2428	2468	2861
	PM	1492	1516	1758
% Commercial of ADT				12.5%
% Commercial of DHV				7%
ESAL Calculations				
		RIGID	FLEXIBLE	
2009 Commercial ADT		4500	4500	
Growth Rate		1.5%	1.5%	
Directional Distribution		55%	55%	
Lane Distribution		90%	90%	
Average ESAL		1.22	0.81	
Initial Year ESAL (2-way)		2.0 million	1.3 million	
Total ESALs (2009-2029)		22.8 million	15.1 million	



OFFICE MEMORANDUM

DATE: January 24, 2008

TO: Brenda J. O'Brien
Engineer of Construction and Technology

FROM: Gregory Johnson
Metro Region Engineer

SUBJECT: Maintaining Traffic Requirements for Life Cycle Cost Analysis
CS 77111 - JN 100701, I-94 from South County Line to Meldrum Road.

This project includes the reconstruction of I-94 from the South St. Clair County Line to Meldrum Road (including the ramps to the west bound rest area). All existing drainage culverts will be replaced as part of this project. The project also includes sign replacement and ROW fence replacement within the roadway reconstruction limits of I-94.

The project is located in Casco Township, in St. Clair County. It was programmed for the 2009 construction season, with cross over work being done in the late summer/fall of 2008.

The recommended method of maintaining traffic for the reconstruction of I-94 is to close and construct one side of the freeway while maintaining traffic on the opposite side. Temporary freeway crossovers are proposed south of County Line Road and north of Meldrum Road. Ramp crossovers are also recommended at the Rest Area to be able to keep it open during construction.

Lane widths on I-94 will be reduced to 11 feet (min) during construction. Temporary concrete barrier (TCB) will be used to separate eastbound and westbound I-94 traffic. One foot of shy distance is recommended between the traffic lanes and the barrier wall.

12

Staging Summary

Maintaining Traffic work prior to JN 100701A (JN 78488A)

- Cold mill existing outside of EB I-94 shoulders to make them drivable.
- Construct temporary median and ramp crossovers.

Stage 1 Construction:

- Install temporary concrete barrier.
- Reconstruct WB I-94 from the POB to the POE.

Stage 1 Traffic:

- Close the left lane of EB and WB I-94. Shift the WB lane of traffic on to the inside lane of EB I-94. Maintain one lane of traffic in each direction.

Stage 2 Construction:

- Reconstruct EB I-94 from the POB to POE.

Stage 2 Traffic:

- Close the left lane of EB and WB I-94. Shift the EB lane of traffic on to the inside lane of WB I-94. Maintain one lane of traffic in each direction.

Stage 3 Construction:

- Remove temporary freeway crossovers and restore median to original configuration prior to construction.

Stage 3 Traffic:

- Close left lane of NB I-75 for removal of crossovers.

Factors Involved in the Decision to Close and Construct One Side of the Freeway While Maintaining Traffic On the Other Side

This method was chosen for the following reasons:

1. Construction is on one side of the freeway, giving the Contractor full access to the entire work zone. This will make it easier for the contractor to construct the project and will ultimately result in a superior product.
2. It is safer for the Contractor and motorists to have the work zone on one side of the freeway.
3. The work is to be completed in one construction season.
4. It enables one lane of traffic to be maintained both eastbound and westbound on I-94 with minimal work.

It is assumed that with a January 2009 letting, construction will begin during late winter/early spring of 2009 and will be completed prior to the end of the 2009 construction season on November 15th.

For questions pertaining to this project, please don't hesitate to contact Mr. Scott Singer at (810) 985-5011.

Gregory Johnson
Metro Region Engineer

cc: T. Kratofil
M. Grazioli
P. Williams
D. Weber

USER COST SUMMARY

Weekday \$29,330 Weekend \$45,234

Alternative #1: Flexible HMA Pavement

Stage 1 = 51.8 days

EB:	Weekdays:	38 days @	\$29,330 per day =	\$1,114,534
	Weekends:	14 days @	\$45,234 per day =	\$633,272
WB:	Weekdays:	38 days @	\$29,330 per day =	\$1,114,534
	Weekends:	14 days @	\$45,234 per day =	\$633,272

Stage 2 = 51.8 days

EB:	Weekdays:	37 days @	\$29,330 per day =	\$1,085,204
	Weekends:	15 days @	\$45,234 per day =	\$678,505
WB:	Weekdays:	37 days @	\$29,330 per day =	\$1,085,204
	Weekends:	15 days @	\$45,234 per day =	\$678,505
				Total = \$7,023,031

Total Initial User Cost = \$7,023,031 / (2 * 7.025 dir-mile) = **\$499,860 /dir-mile**

Alternative #2: Rigid JPCP Pavement

Stage 1 = 38.9 days

EB:	Weekdays:	29 days @	\$29,330 per day =	\$850,566
	Weekends:	10 days @	\$45,234 per day =	\$452,337
WB:	Weekdays:	29 days @	\$29,330 per day =	\$850,566
	Weekends:	10 days @	\$45,234 per day =	\$452,337

Stage 2 = 38.9 days

EB:	Weekdays:	27 days @	\$29,330 per day =	\$791,906
	Weekends:	12 days @	\$45,234 per day =	\$542,804
WB:	Weekdays:	27 days @	\$29,330 per day =	\$791,906
	Weekends:	12 days @	\$45,234 per day =	\$542,804
				Total = \$5,275,225

Total Initial User Cost = \$5,275,225 / (2 * 7.025 dir-mile) = **\$375,461 /dir-mile**

15

SummaryView

period length (min) 60				PROJECT INFORMATION				REPORT INFORMATION				
annual traffic growth (%) 1.50%				PROJECT TITLE I-94 From St. Clair/Macomb CoL to Meldrum Road				REPORT TITLE DETAILED USER COST REPORT SUMMARY SHEET				
years of growth				C.S. 77111				DIVISION C&T				
VEHICLE INPUT				JOB # 100701				REPORT BY BK				
design demand (%) 87.5% 12.5%				START DATE				REPORT DATE 2/13/2008				
user cost per hour (\$/V hr) \$15.75 \$27.79				NOTES: One lane of traffic will be maintained in each direction using temporary crossovers. WB reconstructed first, followed by EB.								
user cost per mile, (\$/V mi) \$0.505 \$1.63				user cost per cancellation, (\$/V)								
METHOD INPUT				METHOD 1		METHOD 2		METHOD 3		METHOD 4		
method title				One Lane Open								
DISTANCE AND SPEED (mi) (mph)				distance	speed	distance	speed	distance	speed	distance	speed	
work zone				5.8	see delay		see delay		see delay		see delay	
normal travel				5.8	70.0							
diversion												
SPEED DELAY				threshold	range	threshold	range	threshold	range	threshold	range	
capacity for speed delay (V/period)				1395								
speed (when D=0) (mph)				45								
speed (when D=C) (mph)				34								
DECREASE TO DEMAND				threshold	range	threshold	range	threshold	range	threshold	range	
capacity for decreases to design demand (V/period)												
canceled cars (with no delay) (%)												
canceled trucks (with no delay) (%)												
canceled cars (with delay) (%/min)												
canceled trucks (with delay) (%/min)												
diverted cars (with no delay) (%)												
diverted trucks (with no delay) (%)												
diverted cars (with delay) (%/min)												
diverted trucks (with delay) (%/min)												
OTHER USER COST INPUT				cars	trucks	cars	trucks	cars	trucks	cars	trucks	
other user cost per actual demand (\$/V)				\$0.00	\$0.00	\$0.00	\$0.00	\$0.00	\$0.00	\$0.00	\$0.00	
user cost per diversion (\$/V)				\$0.00	\$0.00	\$0.00	\$0.00	\$0.00	\$0.00	\$0.00	\$0.00	
PERIOD INPUT				backup at start (V)		0		0		0		
direction:	weekday	weekend	weekday	weekend	weekday	weekend	weekday	weekend	weekday	weekend	weekday	weekend
period	historical demand	design demand	historical demand	design demand	capacity	capacity	capacity	capacity	capacity	capacity	capacity	capacity
(hr)	(V/period)	(V/period)	(V/period)	(V/period)	(V/period)	(V/period)	(V/period)	(V/period)	(V/period)	(V/period)	(V/period)	(V/period)
12 A	302	358	302	358	1395	1395						
1 A	249	295	249	295	1395	1395						
2 A	231	274	231	274	1395	1395						
3 A	231	274	231	274	1395	1395						
4 A	249	295	249	295	1395	1395						
5 A	373	442	373	442	1395	1395						
6 A	658	779	658	779	1395	1395						
7 A	871	1032	871	1032	1395	1395						
8 A	871	1032	871	1032	1395	1395						
9 A	924	1095	924	1095	1395	1395						
10 A	978	1158	978	1158	1395	1395						
11 A	1031	1221	1031	1221	1395	1395						
12 P	1013	1200	1013	1200	1395	1395						
1 P	1049	1242	1049	1242	1395	1395						
2 P	1120	1327	1120	1327	1395	1395						
3 P	1227	1453	1227	1453	1395	1395						
4 P	1280	1516	1280	1516	1395	1395						
5 P	1173	1390	1173	1390	1395	1395						
6 P	942	1116	942	1116	1395	1395						
7 P	782	927	782	927	1395	1395						
8 P	676	800	676	800	1395	1395						
9 P	604	716	604	716	1395	1395						
10 P	516	611	516	611	1395	1395						
11 P	427	505	427	505	1395	1395						
Total	17777.667	21059.142	17778	21059	33480	33480	0	0	0	0	0	0
SUMMARY OUTPUT				traffic method		One Lane Open						
direction				weekday	weekend	weekday	weekend	weekday	weekend	weekday	weekend	
total user cost				\$19,875	\$32,761							
user cost of delays				\$19,875	\$32,761							
user cost of decreases				\$0	\$0							
maximum backup (V)				0	179							
maximum backup length (lane mi)				0.0	1.0							
maximum delay (min)				4.8	13.0							
total delay, except diversions (V hr)				1152	1899							
average delay, except diversions (min)				3.9	5.4							
total vehicles canceled(V)				0	0							
total vehicles diverted (V)				0	0							
total decrease in demand (V)				0	0							
% decrease in demand				0.0%	0.0%							
delay per diverted vehicle (min)				0.0	0.0							
total diversion delay (V hr)				0	0							
total delay, including diversions (V hr)				1,152	1,899							
average delay, including diversions (min)				3.9	5.4							
user cost / design demand				\$1.12	\$1.56							
delay cost / actual demand				\$1.12	\$1.56							
Auto	ON	Print	ON	Nox	OK	validity of output	VALID	VALID	NOT VALID	NOT VALID	NOT VALID	NOT VALID

TABLE A
User Costs for Maintenance Activities

Total ADT	Facility	User \$/day	Day/In-mile Bit	Day/In-mile Concrete	Bituminous User \$/In-mile	Concrete User \$/In-mile
0 to 40,000	Fwy.*	\$191	0.35	0.6	\$67	\$115
40,001 to 80,000	Fwy.*	\$321	0.35	0.6	\$112	\$193
80,001 to 120,000	Fwy.*	\$658	0.35	0.6	\$230	\$395
0 to 40,000	Divided Hwy.*	\$288	0.35	0.6	\$101	\$173
40,001 to 80,000	Divided Hwy.*	\$489	0.35	0.6	\$171	\$293
80,001 to 120,000	Divided Hwy.*	\$909	0.35	0.6	\$318	\$545

* User costs based on a one lane closure.

Computations:

Maintenance for HMA

1 lane-mile @ 165 lbs/syd (12 ft/lane)
 Production = 1650 Ton/day
 $(165 \text{ lbs/syd} \times 12 \text{ ft/ln} \times 5280 \text{ ft/mile} \times \text{syd}/9 \text{ sft}) / (2000 \text{ lbs/Ton}) = 581 \text{ Ton/In-mile}$
 $(581 \text{ Ton/In-mile}) / 1650 \text{ Ton/day} = 0.35 \text{ day/In-mile}$

Maintenance for Concrete

1 lane-mile @ 30 patches/In-mile
 Production = 50 patches/day
 $(30 \text{ patches/In-mile}) / (50 \text{ patches/day}) = 0.6 \text{ day/In-mile}$

1993 AASHTO Pavement Design
DARWin Pavement Design and Analysis System

A Proprietary AASHTOWare
Computer Software Product
 Michigan Department of Transportation
 8885 Ricks Rd.
 Lansing, MI
 USA

Flexible Structural Design Module

CS 77111, JN 100701 I-94 from south county line to Meldrum Rd.
 HMA Reconstruct

Flexible Structural Design

18-kip ESALs Over Initial Performance Period	14,900,000
Initial Serviceability	4.5
Terminal Serviceability	2.5
Reliability Level	95 %
Overall Standard Deviation	0.49
Roadbed Soil Resilient Modulus	3,000 psi
Stage Construction	1
 Calculated Design Structural Number	 7.08 in

Specified Layer Design

<u>Layer</u>	<u>Material Description</u>	Struct Coef. (Ai)	Drain Coef. (Mi)	Thickness (Di)(in)	Width (ft)	Calculated SN (in)
1	Gap Graded Superpave Top Course	0.42	1	1.9	-	0.80
2	4E30 Leveling Course	0.42	1	2.5	-	1.05
3	3E30 Base Course	0.36	1	6	-	2.16
4	Open Graded Drainage Course	0.13	1.1	16	-	2.29
5	Sand Subbase	0.1	1	8	-	0.80
Total	-	-	-	34.40	-	7.10

1993 AASHTO Pavement Design

DARWin Pavement Design and Analysis System

A Proprietary AASHTOWare Computer Software Product

Michigan Department of Transportation
8885 Ricks Rd.
Lansing, MI
USA

Rigid Structural Design Module

CS 77111, JN 100701 I-94 from south countyl line to Meldrum Rd.
Concrete Reconstruct

Rigid Structural Design

Pavement Type	JPCP
18-kip ESALs Over Initial Performance Period	22,500,000
Initial Serviceability	4.5
Terminal Serviceability	2.5
28-day Mean PCC Modulus of Rupture	670 psi
28-day Mean Elastic Modulus of Slab	4,200,000 psi
Mean Effective k-value	190 psi/in
Reliability Level	95 %
Overall Standard Deviation	0.39
Load Transfer Coefficient, J	2.7
Overall Drainage Coefficient, Cd	1.1
Calculated Design Thickness	10.33 in



OFFICE MEMORANDUM

DATE: February 11, 2008

TO: Benjamin Krom
Pavement Selection Engineer

FROM: Adnan Iftikhar
Area Soils Engineer
Metro Region – Construction & Technology

SUBJECT: CS 77111, JN 100701C: I-94 Reconstruction from Macomb/St. Clair County
Line North-Easterly to Meldrum Road. BMP 0.053 EMP 4.33
Request for Life Cycle Cost Analysis

Please begin performing the Life Cycle Cost Analysis (LCCA) for this reconstruction project. This project was originally scheduled for 09/15/08 Plan Completion with a 01/09/09 letting. However, currently it is on an expedited schedule with letting tentatively planned for August, 2008. Project management duties are expected to be taken over by the MDOT Port Huron TSC.

The I-94 roadway within the project limits has twenty year design 18 Kip ESAL loadings of 22.8 Million for rigid, and 15.1 Million for flexible pavement options. Both rigid and flexible options have commercial growth rate of 1.5% and directional distribution factor of 50% (copy of Traffic Report is attached).

Soils Recommendation

The following is recommended for the pavement design and LCCA. All recommendations are based on analysis of field investigation data.

Soil Resilient Modulus (M_r) = 3000 psi

HMA Option:

Remove existing pavement and grade to required depth
Open Graded Drainage Course (OGDC), 16 inches
Sand Subbase, 8 inches (New)
Open Graded Underdrains, 6 inch diameter
Geotextile Separator

Concrete Option:

Remove existing pavement and grade to required depth
Open Graded Drainage Course (OGDC), 16 inch
Open Graded Underdrains, 6 inch diameter
Geotextile Separator

20

Ben Krom
 LCCA Request for:
 CS 77111, JN 100701C
 I-94 Reconstruction from
 Macomb/St. Clair County Line to Meldrum Road
 February 11, 2008
 Page 2

Pavement History

Two lanes of rigid pavement in both eastbound and westbound were constructed in 1963 to 1964. A rehabilitation work, comprising of full depth concrete patching and partial depth bituminous repairs, was undertaken in mid-1990s. Eastbound roadway between Belle River and Allington Road received a HMA overlay in the mid-1990s. Both inside and outside shoulders along eastbound and westbound roadways are HMA and are in fair condition with some signs of oxidation on pavement surface and some low to medium severity raveling and some low to medium severity cracking.

Results from Pavement Cores

A total of 35 pavement cores were available for the I-94 roadway within the project limits. Out of the 35, 18 cores were taken on EB & WB I-94 mainline lanes. The remaining 17 cores were taken on the NB and SB I-75 Shoulders. The tables below provide summary of the various layer thicknesses.

EB I-94 Mainline Lanes

	Average	Maximum	Minimum
Concrete	9.6	10.8	8.4
Aggregate Base	0	0	0
Sand Subbase	14.7	18.0	13.2

Note: Three mainline cores taken between Belle River and Allington Road showed 3 inches thick HMA layer on top of concrete.

WB I-94 Mainline Lanes

	Average	Maximum	Minimum
Concrete	9.6	9.6	9.6
Aggregate Base*	4.4	6.0	3.6
Sand Subbase	13.5	20.4	8.4

*: Only three cores on WB mainline lanes showed Aggregate Base.

Ben Krom
 LCCA Request for:
 CS 77111, JN 100701C
 I-94 Reconstruction from
 Macomb/St. Clair County Line to Meldrum Road
 February 11, 2008
 Page 3

I-94 Shoulder Lanes

	Average	Maximum	Minimum
HMA	5.7	7.2	2.4
Aggregate Base	6.3	9.6	3.6
Sand Subbase	14.7	28.8	8.4

Note: One core that was taken along EB I-94 Right shoulder in the vicinity of Fred Moor Highway interchange showed 9 inches of concrete under HMA.

Sand Subbase

Due to use of 16 inch OGDC layer, the retention (or replacement) of existing sand subbase is not deemed an issue, for the concrete option. The existing pavement will be removed to required depth (including existing sand subbase, if necessary), and replaced with OGDC and concrete pavement. Any remaining portion of existing sand subbase after grading will be left in place.

Out of the total 35 cores available for I-94 roadway within the project limits, 34 (i.e. 97%) show that the existing sand subbase will not be available in the required thickness (after grading) to warrant retention as part of the reconstructed HMA pavement. Therefore, the existing sand subbase will be removed and replaced, for the HMA option.

Out of a total of 12 samples that were obtained from existing sand subbase within the project limits; 10 samples met CL IIA specifications.

Subgrade Conditions

It is assumed that the pavement removal and excavation would be to approximate depths of 27 and 35 inches below top of existing pavement for the concrete and asphalt sections, respectively.

At the 27 inch level (concrete option), the subgrade soil classification varies from brown to gray, stiff to very stiff, silty CLAY with trace sand and gravel (77% of boring locations); to brown to gray, stiff to very stiff, silty CLAY with trace sand and organics (23% of boring locations). Three cores showed 3 to 4 inches of sand at the estimated clay grade elevation. Approximately half the cores showed mottling within the silty Clay layer. The Soil Resilient modulus is based

Ben Krom
LCCA Request for:
CS 77111, JN 100701C
I-94 Reconstruction from
Macomb/St. Clair County Line to Meldrum Road
February 11, 2008
Page 4

on brown to gray, stiff to very stiff, silty CLAY with trace sand and organics at or within 6 inches of proposed subgrade level.

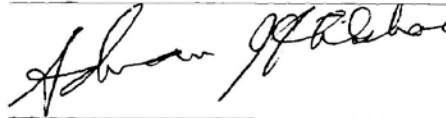
At the 35 inch level (asphalt option), the subgrade soil classification varies from brown to gray, stiff to very stiff, silty CLAY with trace sand and gravel (80% of boring locations); to brown to gray, stiff to very stiff, silty CLAY with trace sand and organics (20% of boring locations). One core showed 3 to 4 inches of sand at the estimated clay grade elevation. Approximately half the cores showed mottling within the silty Clay layer. The Soil Resilient modulus is based on brown to gray, stiff to very stiff, silty CLAY with trace sand and organics at or within 6 inches of proposed subgrade level.

Almost all the cores reveal competent subgrade material in the form of stiff, brown gray, silty CLAY at the estimated clay grade levels (HMA & concrete pavement options) to depths of five feet below top of existing pavement. One core logged a sand subbase thickness of greater than 24 inches indicating previous undercut areas. It is anticipated that minimal subgrade correction will be required.

If you have any questions, please do not hesitate to call me at (248) 483-5167, or e-mail me at IFTIKHARA@MICHIGAN.GOV.

Sincerely,

METRO REGION SOILS & MATERIALS OFFICE



Adnan Iftikhar

Attached: Copy of Boring Logs
Copy of Traffic Report

cc: N. Bandara
M. Grazioli

C.S. 7711, JN 100701

Highway Pavement Structural Design

II-39

$D = 16''$
 $E = 24,000 \text{ psi}$
 $M_R = 3600 \text{ psi}$

Example:

$k = 310 \text{ pci}$

$D_{SB} = 6 \text{ inches}$
 $E_{SB} = 20,000 \text{ psi}$
 $M_R = 7,000 \text{ psi}$
Solution: $k_s = 400 \text{ pci}$

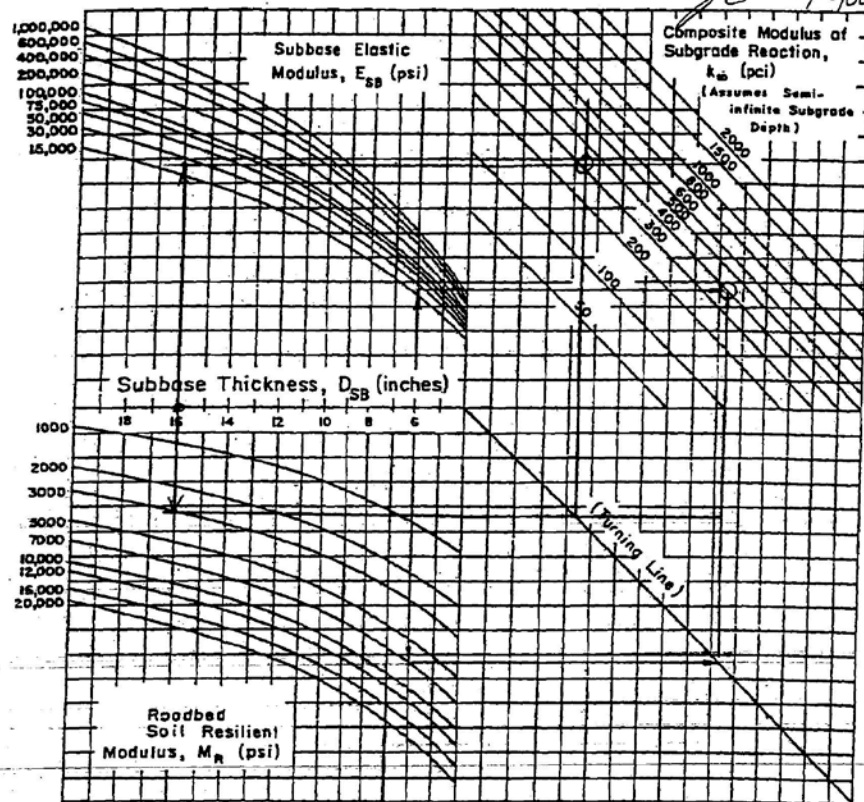


Figure 3.3. Chart for Estimating Composite Modulus of Subgrade Reaction, k_s , Assuming a Semi-Infinite Subgrade Depth. (For practical purposes, a semi-infinite depth is considered to be greater than 10 feet below the surface of the subgrade.)

CS 77111, JN 100701

II-42

$k = 310 \text{ pci}$

$k_{\text{eff}} = 190 \text{ pci}$

Design of Pavement Structures

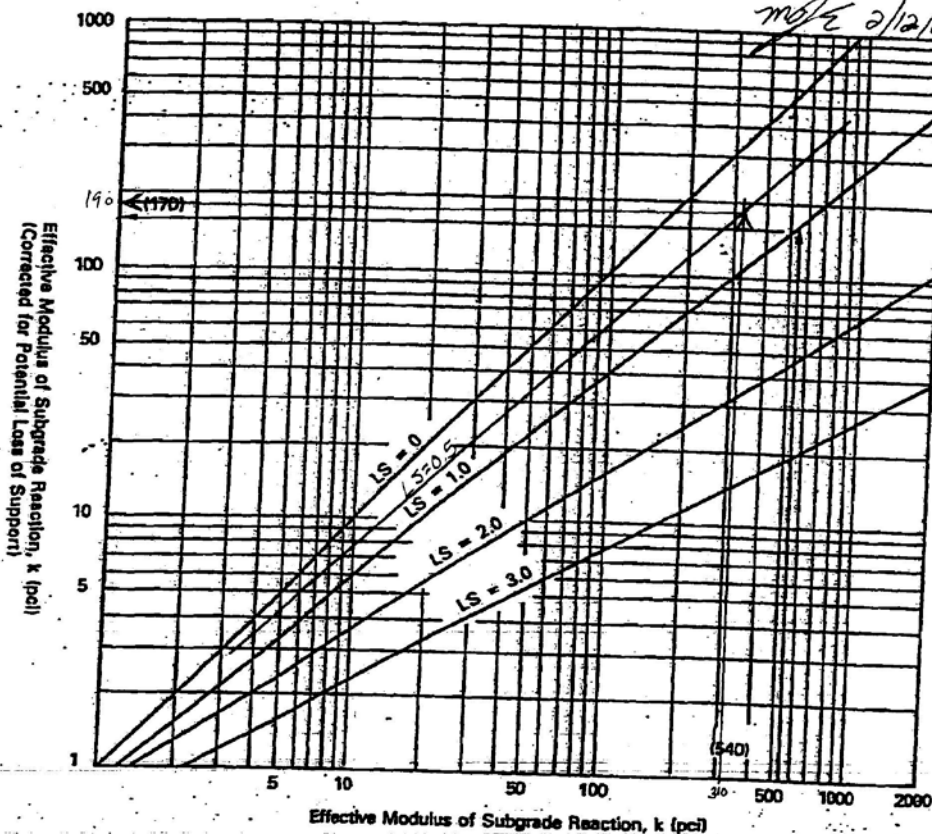
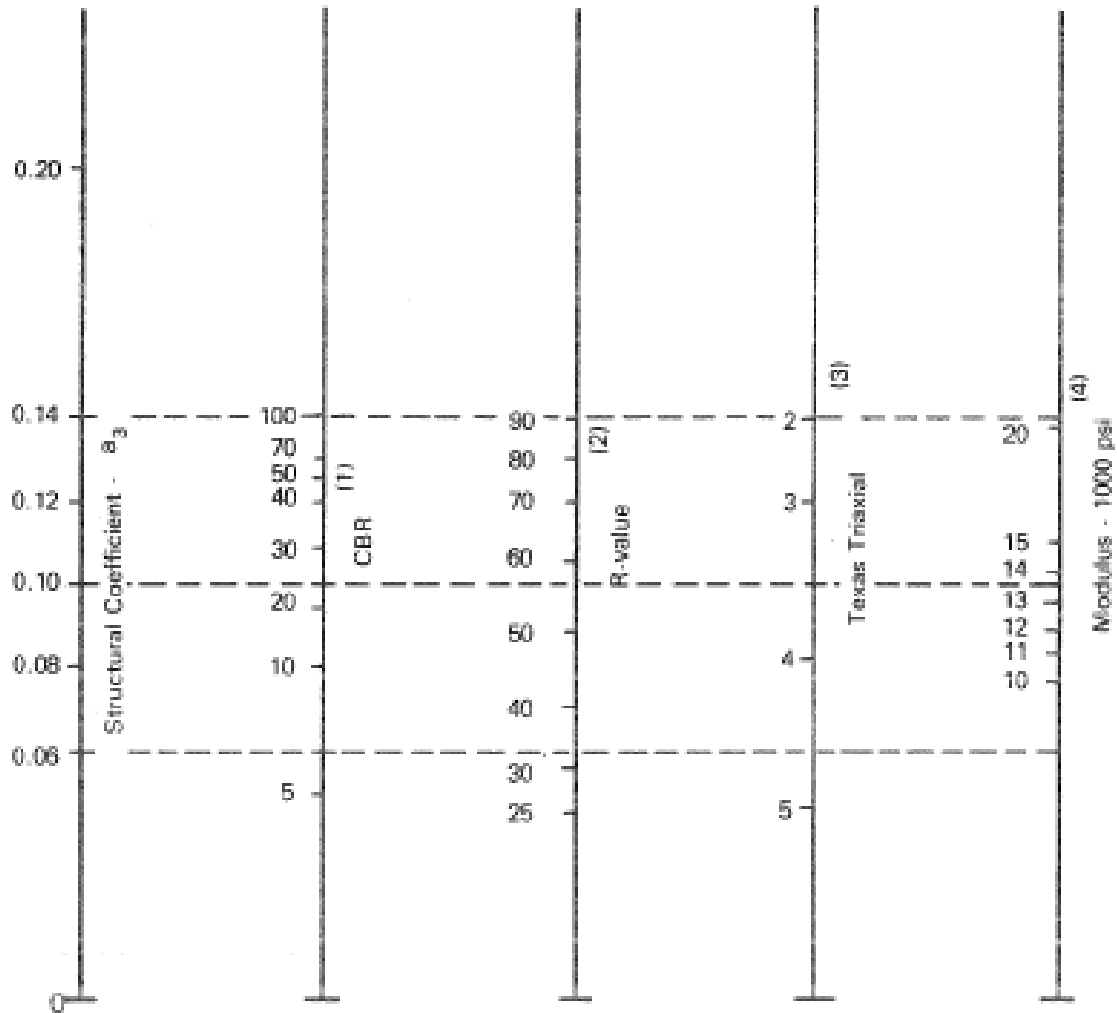


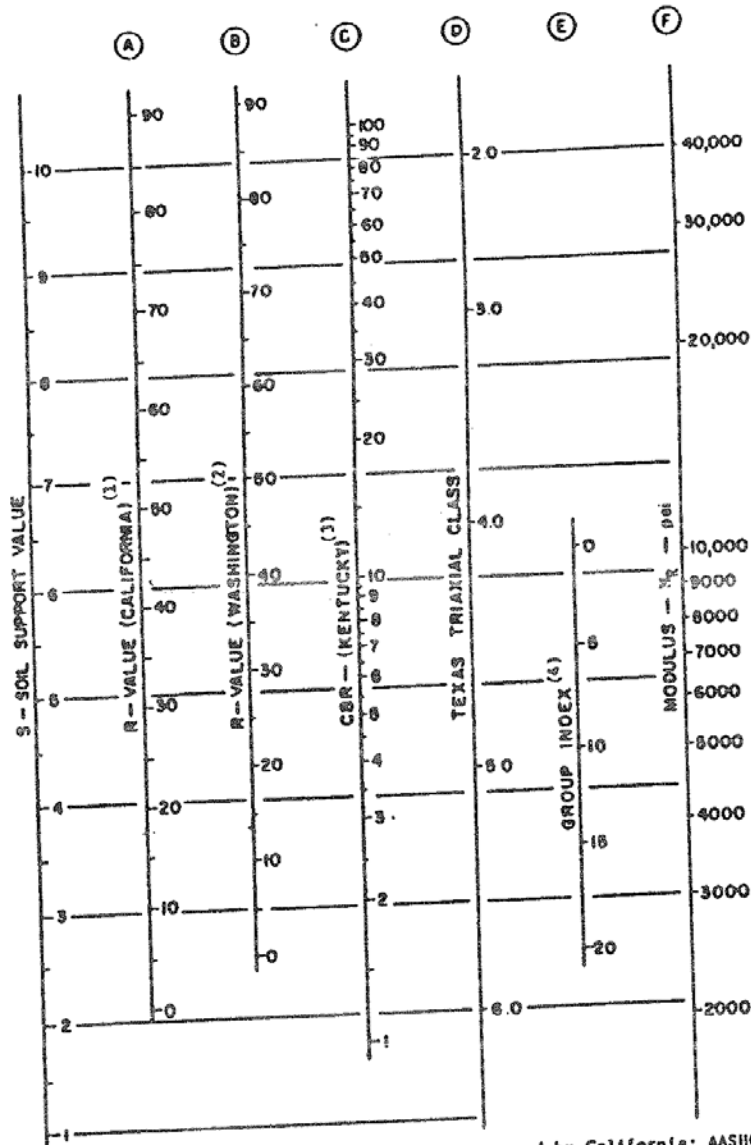
Figure 3.6. Correction of Effective Modulus of Subgrade Reaction for Potential Loss of Subbase Support (6)

APPENDIX B: AASHTO 1972, AASHTO (1993), AND PCA (1984) DESIGN CHARTS



- (1) Scale derived from correlations from Illinois.
- (2) Scale derived from correlations obtained from The Asphalt Institute, California, New Mexico and Wyoming.
- (3) Scale derived from correlations obtained from Texas.
- (4) Scale derived on NCHRP project (3).

Figure 87. Chart to estimate modulus of subbase layer (E_{SB}) from CBR (from AASHTO 1993 based on results from Til et al. 1972)



(1) The correlation is with the design curves used by California; AASHTO designation is T-173-60, and exudation pressure is 240 psi. See Ivey, F.M., and Carmany, R.M., "The Factors Underlying the Rational Design of Pavements." *Proc. HRB*, Vol. 28 (1948) pp. 101-136.

(2) The correlation is with the design curves used by Washington Dept. of Highways; exudation pressure is 300 psi. See "Flexible Pavement Design Correlation Study." *HRB Bull.* 133 (1956).

(3) The correlation is with the CRR design curves developed by Kentucky. See Drake, W.B., and Havens, J.H., "Re-Evaluation of Kentucky Flexible Pavement Design Criterion." *HRB Bull.* 233 (1959) pp. 33-56. The following conditions apply to the laboratory-modified CRR: specimen is to be molded at or near the optimum moisture content as determined by AASHTO T-99; dynamic compaction is to be used with a hammer weight of 10 lb dropped from a height of 18 in.; specimen is to be compacted in five equal layers with each layer receiving 10 blows; specimen is to be soaked for 4 days.

(4) This scale has been developed by comparison between the California R-value and the Group Index determined by the procedure in *Proc. HRB* Vol. 25 (1945) pp. 376-392.

Figure 88. Chart to estimate M_r of subgrade from CBR (from AASHTO 1993 Appendix FF)

Example:

$D_{SB} = 6$ inches
 $E_{SB} = 20,000$ psi
 $M_R = 7,000$ psi
 Solution: $k_{\infty} = 400$ pci

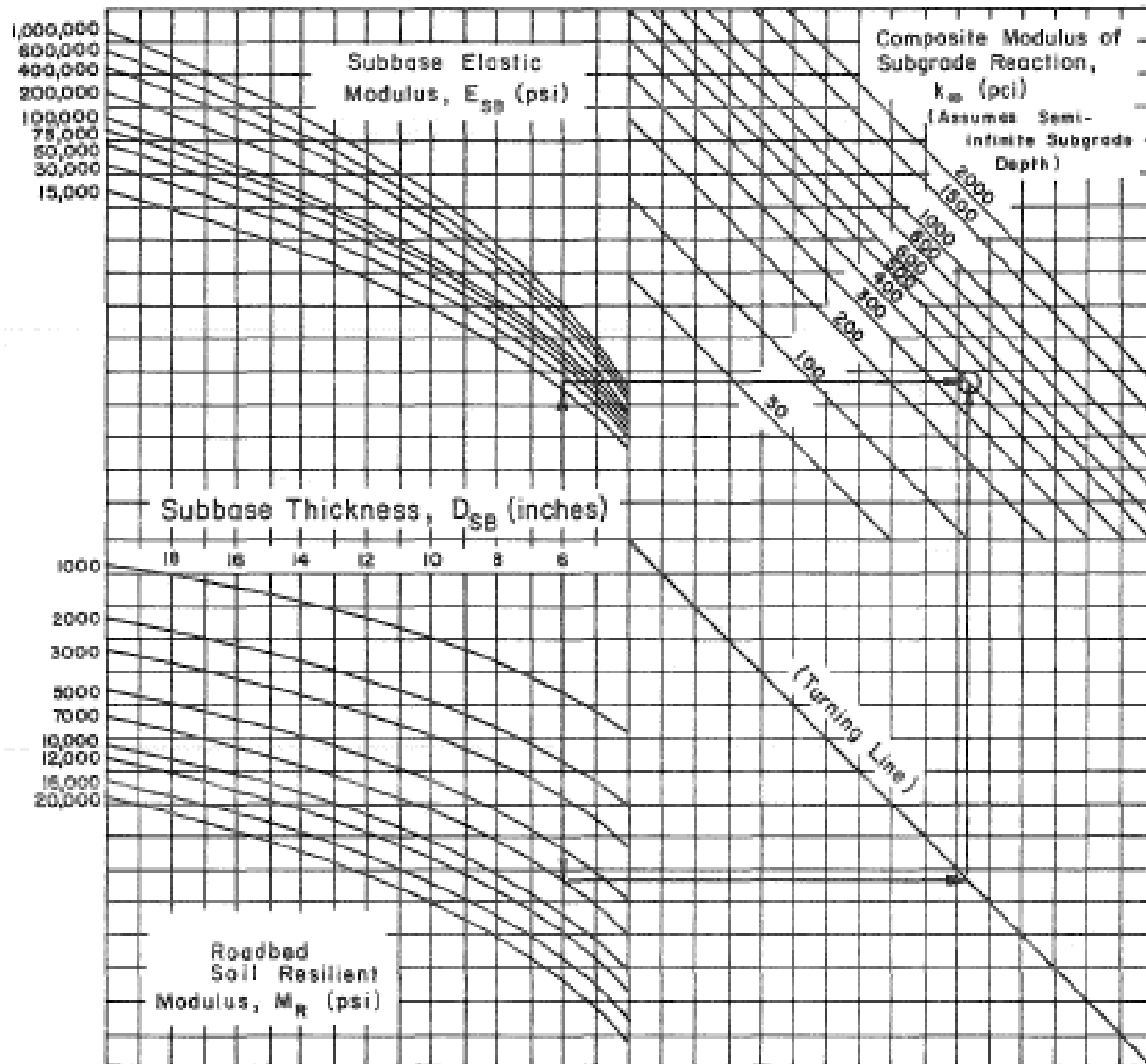


Figure 3.3. Chart for Estimating Composite Modulus of Subgrade Reaction, k_{∞} , Assuming a Semi-Infinite Subgrade Depth. (For practical purposes, a semi-infinite depth is considered to be greater than 10 feet below the surface of the subgrade.)

Figure 89. Chart for estimating composite modulus of subgrade reaction (k_{comp} -AASHTO(1993)) assuming a semi-infinite subgrade depth (from AASHTO 1993)

APPENDIX C: MDOT FIELD MOISTURE/DENSITY REPORTS, AGGREGATE INSPECTION REPORT, AND MDOT DENSITY GUIDELINES

pg 142
 RL 301

Michigan Department
 of Transportation
 65528 (11-03)

MOISTURE AND DENSITY DETERMINATION NUCLEAR METHOD

DISTRIBUTION: ORIGINAL - Project Engineer, COPIES - Area Density Supervisor, Density Technology (Lansing).
 * SEE REVERSE SIDE

DATE 7-13-09	CONTROL SECTION ID 77111	JOB NUMBER 100701A	ROUTE NO. or STREET I-94 E.B. RECON	GAUGE NO. 60378
DENSITY INSPECTOR DELOU JOHNSON	CERTIFICATION NO. 10997-0413	PROJECT ENGINEER (MDOT) MIKE FRANKHOUSE	PROJECT MANAGER HARRY YOUNG	PHONE NO. 810-985-5011

DETERMINATION OF IN-PLACE DENSITY

TEST NO.	DETERMINATION OF IN-PLACE DENSITY										LOCATION OF TEST			
	WET DENSITY		MOISTURE				DRY DENSITY				STATION	DISTANCE FROM I FT.	DEPTH INCH	ITEM OF WORK
	COUNTS SEC	TEST DEPTH INCH	WET DENSITY PCF	COUNTS IMC	MOIS- TURE PCF	MOIS- TURE %	DRY DENSITY PCF	MAX DENSITY PCF	PERCENT OF COM- PACTION					
1	2234	6	141.5	54	2.8	2.0	138.7	142.2	97.6	1089+00	15		.92	SS
2	2854	6	132.4	41	1.7	1.3	128.7	142.2	90.5	1094+00	15		.92	SS
3	2263	6	138.9	65	3.7	2.7	135.2	142.2	95.1	1099+00	15		.92	SS
4	3166	6	125.6	43	1.8	1.5	123.8	133.9	92.5	1104+00	15		.92	SS SLAG
5	941	9	145.3	116	7.9	5.8	137.3	142.5	96.4	902+00		25	0	SA
6	1039	9	141.8	86	5.4	4.0	136.4	142.5	95.7	907+00		25	0	SA
7	1116	9	139.2	84	5.3	3.9	133.9	142.5	94.0	912+00		25	0	SA
8	1025	9	142.3	89	5.7	4.1	136.6	142.5	95.9	917+00		25	0	SA
9	1061	9	141.0	87	5.5	4.1	135.5	142.5	95.1	922+00		25	0	SA
10	1165	9	137.7	75	4.5	3.4	133.2	142.5	93.5	927+00		25	0	SA
7-13-2	2421	6	137.8	51	2.5	1.9	135.3	142.2	95.1	1094+00	15		.92	SS

DETERMINATION OF MAXIMUM DENSITY (Soil & Bituminous)

TEST NO.	MOIS- TURE %	VOLUME MOLD CU. FT.	DETERMINATION						MAX DENSITY PCF	OPTIMUM MOISTURE %	NOTE	
			WET SOIL MOLD PCF	MOLD PCF	WET SOIL PCF	WET SOIL PCF	COMPACTED SOIL WET PCF	CHART STANDARDS			DENSITY	MOISTURE
1	5.4	.0450	4980	1985	2995	6.60	146.7	142.2	6.9	3238	745	
4	5.8	.0450	4823	1985	2838	6.26	139.0	139.9	8.3	3173	716	
5	5.8	.0450	5019	1985	3034	6.69	148.6	142.5	6.8	3214	724	

REMARKS
 TEST #1 4G OPEN GRADED LIMESTONE 4853, 4900, 4945, 4977, (4980)
 TEST #4 4G OPEN GRADED SLAG 4780, 4805, 4820, (4823)
 TEST #5 23A 5001, 5017, (5019)
 DENSITY INSPECTOR'S SIGNATURE: DELOU JOHNSON
 AGENCY/COMPANY: T.Y.M.E. ENGINEERING

Clear/Sunny
 51° - 79°

pg 142
FILE 301

Michigan Department
of Transportation
05929 (1-03)

MOISTURE AND DENSITY DETERMINATION NUCLEAR METHOD

DISTRIBUTION ORIGINAL - Project Engineer, GOPIES - Area Density Supervisor, Density Technology (Lansing).
*SEE REVERSE SIDE

DATE 7-13-09	CONTROL SECTION NO 77111	JOB NUMBER 100701A	ROUTE NO. or STREET I-94 E.B. RECON	GAUGE NO. 60378
DENSITY INSPECTOR DELEN JOHNSON	CERTIFICATION NO. 10997-0413	PROJECT ENGINEER (POET) MIKE FRANKHOUSE	PROJECT MANAGER HARRY YOLINS	PHONE NO. 810-985-5011

DETERMINATION OF IN-PLACE DENSITY

TEST NO.	WET DENSITY			MOISTURE			DRY DENSITY			PERCENT OF COMPACTION	STATION	LOCATION OF TEST		DEPTH BELOW PLAN GRADE FT.	ITEM OF WORK
	COUNTS (DC)	TEST DEPTH (inch)	WET DENSITY (pcf)	COUNTS (MC)	MOISTURE (pcf)	MOISTURE (%)	DRY DENSITY (pcf)	MAX DENSITY (pcf)	DISTANCE FROM LEFT FT.			DISTANCE FROM RIGHT FT.			
													1		
1	2234	6	141.5	54	2.8	2.0	138.7	142.2	97.6	1089+00	5		.92	SS	
2	2854	6	130.4	41	1.7	1.3	128.7	142.2	90.5	1094+00	15		.92	SS	
3	2363	6	138.9	65	3.7	2.7	135.2	142.2	95.1	1099+00	15		.92	SS	
4	3166	6	125.6	43	1.8	1.5	123.8	133.9	92.5	1104+00	15		.92	SS SLAG	
5	941	9	145.3	116	7.9	5.8	137.3	142.5	96.4	902+00		25	C	SA	
6	1039	9	141.8	86	5.4	4.0	136.4	142.5	95.7	907+00		25	C	SA	
7	1116	9	139.2	84	5.3	3.9	133.9	142.5	94.0	912+00		25	C	SA	
8	1025	9	142.3	89	5.7	4.1	136.6	142.5	95.9	917+00		25	C	SA	
9	1061	9	141.0	87	5.5	4.1	135.5	142.5	95.1	922+00		25	C	SA	
10	1165	9	137.7	75	4.5	3.4	133.2	142.5	93.5	927+00		25	C	SA	
7-13-2	2421	6	137.8	51	2.5	1.9	135.3	142.2	95.1	1094+00	5		.92	SS	

DETERMINATION OF MAXIMUM DENSITY (Soil & Bituminous)

TEST NO.	MOISTURE %	VOLUME MOULD CU. FT.	DENSITY DETERMINATION						MAX DENSITY (pcf)	OPTIMUM MOISTURE %
			WET SOIL - MOULD (pcf)	MOLD (pcf)	WET SOIL (pcf)	WET SOIL (pcf)	COMPACTED SOIL, WET (pcf)	MAX DENSITY (pcf)		
A	B	C	D	E	F	G	H	I	J	
1	5.4	.0450	4980	1985	2995	6.60	146.7	142.2	6.9	
4	5.8	.0450	4823	1985	2838	6.26	139.0	133.9	8.3	
5	5.8	.0450	5019	1985	3034	6.69	148.6	142.5	6.8	

NOTE:
To convert (g) to (lbs.)
Wt. (g) ÷ 453.59 = Wt. (lbs.)
To convert (m³) to (ft³)
Vol. (m³) × 35.3147 = Vol. (ft³)

CHART STANDARDS	
DENSITY	MOISTURE
5238	745
3173	716
OPERATING STANDARDS	
DENSITY	MOISTURE
5214	724

BITUMINOUS MIX DESIGN PCF

REMARKS

TEST #1 4G OPEN GRADED LIMESTONE 4853, 4900, 4945, 4977, 4980

TEST #4 4G OPEN GRADED SLAG 4780, 4805, 4820, 4823

TEST #5 23A 5001, 5017, 5019

Clear / Lowway
5' - 7.8'

NEED TO ESTABLISH NEW M.D. BRISTLE INCREASED > 1.5%

pg 1 of 2
FILE 301

Michigan Department of Transportation
DESIGN (1103)

MOISTURE AND DENSITY DETERMINATION NUCLEAR METHOD

DISTRIBUTION - ORIGINAL - Project Engineer, COPIES - Area Density Supervisor, Density Technology (Lansing)
*SEE REVERSE SIDE

DATE 7-15-09	CONTROL SECTION # 77111	JOB NUMBER 100701A	ROUTE NO. or STREET I-94 E.B. Lecon	TRAVERSE NO. 60378
DENSITY INSPECTOR DELOON JOHNSON	CERTIFICATION NO. 10997-0413	PROJECT ENGINEER (MDO) MIKE FRANKHOUSE	PROJECT MANAGER LARRY YOUNG	PHONE NO. 313-985-5111

DETERMINATION OF IN-PLACE DENSITY

TEST NO.	WET DENSITY			MOISTURE			DRY DENSITY				LOCATION OF TEST			
	COUNTS (CO)	TEST DEPTH (in)	WET DENSITY (pcf)	COUNTS (in)	MOISTURE (pcf)	MOISTURE (%)	DRY DENSITY (pcf)	MAX DENSITY (pcf)	PERCENT OF COMPACTION	STATION	DISTANCE FROM		DEPTH BELOW PLAN OR AS BUILT (ft)	ITEM OF WORK
											LEFT	RIGHT		
1	2061	6	145.1	65	3.7	2.6	141.4	143.1	98.8	139+86	E		.92	SS
2	2058	6	145.2	55	2.8	2.0	142.3	143.1	99.5	144+00	R		.92	SS
3	2416	6	138.0	62	3.4	2.5	134.6	143.1	94.1	149+00		3	.92	SS
745 3	2277	6	140.6	64	3.6	2.6	137.0	143.1	95.7	149+00		3	.92	SS
4	2350	6	139.2	56	2.9	2.1	136.3	143.1	95.2	154+00	E		.92	SS
5	1361	10	122.1	98	6.4	5.5	115.6	121.9	94.9	996+62	39		1.0	E
745 5	1316	10	123.3	104	6.9	5.9	116.4	121.9	95.5	996+62	39		1.0	E
6	3066	6	127.2	38	1.4	1.1	125.7	130.8	96.1	159+00		2	.92	SS
744 11	3229	4	137.8	138			7.6	140.4	98.1	804+10	22		.33	CAB
7	2253	6	141.1	47	2.2	1.6	139.0	143.1	97.1	262+75		4	.92	SS
8	2785	6	131.1	150			8.9	129.4	101.3	804+50	39		.33	CAB

DETERMINATION OF MAXIMUM DENSITY (Soil & Bituminous)

TEST NO.	MOISTURE (%)	VOLUME MOLD (cu. ft.)	DENSITY DETERMINATION								OPTIMUM MOISTURE (%)	CHART STANDARDS	
			WET SOIL MOLD (pcf)	MOLD (pcf)	WET SOIL (pcf)	WET SOIL (pcf)	COMPACTED SOIL WET (pcf)	MAX DENSITY (pcf)	OPERATING STANDARDS	DENSITY		MOISTURE	
1	5.4	.0450	5001	1985	3016	6.65	147.8	143.1	6.7	6.7	3238	745	
5	5.5	.0450	4585	1985	2600	5.73	127.4	121.9	11.3	11.3	3173	716	
6	6.0	.0450	4775	1985	2790	6.15	136.7	130.8	9.0	9.0			
8	8.9	.0337	4134	2006	2128	4.69	139.2	129.4	9.5	9.5	3217	724	
9	3.5	.0337	4091	2006	2085	4.60	136.4	140.4	6.8	6.8			

REMARKS

TEST #1 46 LOW GRADED LIMESTONE 4925, 4955, 4987, 4999 (5001)

TEST #5 SAND 4577 (4585) TEST #6 CRUSHED CONCRETE 4134

TEST #6 46 OPEN GRADED 4650, 4695, 4723, 4735, 4760, 4770, (4775)

pg. 1 of 3

Michigan Department of Transportation
05825 (11/03)

MOISTURE AND DENSITY DETERMINATION NUCLEAR METHOD

FILE NO.

DISTRIBUTION: ORIGINAL - Project Engineer, COPIES - Area Density Supervisor, Density Technology (Training).
*SEE REVERSE SIDE

DATE 7-17-09	CONTR. SECTION ID 77111	JOB NUMBER 100701A	ROUTE NO. & STREET I-94 E.B. RECON.	CAUSE NO. 60378
DENSITY INSPECTOR DELLON JOHNSON	CERTIFICATION NO. 10997-0413	PROJECT ENGINEER (MOOT) MIKE FRANKHOUSE	PROJECT MANAGER LARRY YOUNG	PHONE NO. 313-985-5611

DETERMINATION OF IN-PLACE DENSITY

TEST NO.	WET DENSITY			MOISTURE			DRY DENSITY			LOCATION OF TEST				
	COUNTS	DEPTH Inch	WET DENSITY pcf	COUNTS	MOIS- TURE pcf	MOIS- TURE %	DRY DENSITY pcf	MAX DENSITY pcf	PERCENT OF COM- PACTION	STATION	DISTANCE FROM LEFT RIGHT		DEPTH BELOW PLAN GRADE ft	ITEM OF WORK
											12	13		
1	3121	4	139.7	73	4.3	3.2	135.4	141.9	95.4	1062+00	18		.42	SA
2	3141	4	139.3	73	4.3	3.2	135.0	141.9	95.1	1067+00	18		.42	SA
3	2832	4	144.7	86	5.4	3.9	139.3	141.9	98.2	1072+00	18		.42	SA
4	2768	4	145.8	92	5.9	4.2	139.9	141.9	98.6	1077+00	18		.42	SA
5	2897	4	143.5	89	5.6	4.1	137.9	141.9	97.2	1082+00	18		.42	SA
6	3062	4	140.7	70	4.1	3.0	136.6	141.9	96.3	1087+00	18		.42	SA
7	3073	4	140.4	91	5.8	4.3	134.6	140.4	95.9	1121+75	18		0	SA
8	3360	4	135.7	89	5.6	4.3	130.1	140.4	92.7	1117+00	18		0	SA
9	2906	4	143.3	100	6.6	4.8	136.7	140.4	97.4	1112+00	18		0	SA
10	3037	4	141.0	100	6.6	4.9	134.4	140.4	95.7	1107+00	18		0	SA
11	3017	4	141.3	101	6.6	4.9	134.7	140.4	95.9	1102+00	18		0	SA

✓ CHECKED MO. TWICE. GAUGE READ 101" @ 0.4"

DETERMINATION OF MAXIMUM DENSITY (Soil & Bituminous)

TEST NO.	MOIS- TURE %	VOLUME MOLD CU. FT.	WET SOIL				WET SOIL pcf	COMPACTED SOIL WET pcf	MAX DENSITY pcf	OPTIMUM MOISTURE %	CHART STANDARDS	
			WET SOIL MOLD g	MOLD g	WET SOIL g	WET SOIL lbs.					DENSITY	MOISTURE
1	5.8%	.0450	5005	1985	3020	6.66	148.0	141.9	6.9	3238	745	
7	6.8%	.0450	5037	1985	3052	6.73	149.5	140.4	7.1	3173	716	
										OPERATING STANDARDS		
										DENSITY	MOISTURE	
										3209	726	
BITUMINOUS MIX DESIGN PCF												

REMARKS
 TEST #4 46 OPEN-GRADED LIMESTONE 4952, 4977, 4995, 5000, 5005
 TEST #7 234 5013, 5029, 5037

DENSITY INSPECTOR SIGNATURE: *[Signature]*
 AGENCY/COMPANY: TIME ENGINEERING

3243

Michigan Department of Transportation
3582B (11/03)

MOISTURE AND DENSITY DETERMINATION
NUCLEAR METHOD

FILE 301

DISTRIBUTION: ORIGINAL - Project Engineer, COPIES - Area Density Supervisor, Density Technology (Lansing).
*SEE REVERSE SIDE

DATE 7-17-09	CONTROL SECTION # 77111	JOB NUMBER 100701A	ROUTE NO. or STREET I-94 E.B. RECON	GALVAN # 60378
DENSITY INSPECTOR DELOAN JOHNSON	CERTIFICATION NO. 10997-0413	PROJECT ENGINEER (INDOT) MIKE FRANKHOUSE	PROJECT MANAGER LARRY YOUNG	PHONE NO. 313-985-5011

DETERMINATION OF IN-PLACE DENSITY

ORIGINAL CHECK	WET DENSITY			MOISTURE			DRY DENSITY			LOCATION OF TEST				
	COUNTS (CP)	TEST DEPTH (in)	WET DENSITY (pcf)	COUNTS (MC)	MOISTURE (pcf)	MOISTURE (%)	DRY DENSITY (pcf)	MAX. DENSITY (pcf)	PERCENT OF COMPACTION	STATION	DISTANCE FROM E		DEPTH BELOW PLAN GRADE (ft)	ITEM OF WORK
											LEFT	RIGHT		
12	2970	4	142.1	101	6.6	4.9	135.5	140.4	96.5	1097+00	18		0	SA
13	2862	4	144.1	103	6.8	5.0	137.2	140.4	97.8	1092+00	18		0	SA
7-178	2952	4	142.5	94	6.1	4.4	136.4	140.4	97.2	1117+00	18		0	SA
14	3071	4	140.4	95	6.1	4.6	134.3	140.4	95.6	1087+00	18		0	SA
15	3057	4	140.7	98	6.4	4.8	134.3	140.4	95.8	1082+00	18		0	SA
16	2992	4	141.8	102	6.7	5.0	135.0	140.4	96.2	1077+00	18		0	SA
17	3019	4	141.3	101	6.6	4.9	134.7	140.4	95.9	1072+00	18		0	SA
18	2919	4	143.0	105	7.0	5.1	136.1	140.4	96.9	1067+00	18		0	SA
19	2971	4	142.1	98	6.4	4.7	135.7	140.4	96.7	1062+00	18		0	SA
20	2810	4	145.0	108	7.2	5.2	137.8	140.4	98.1	1057+00	18		0	SA
21	2670	4	147.6	108	7.2	5.1	140.4	140.4	100.0	1052+00	18		0	SA

↑ RECORDED AND TRACED

DETERMINATION OF MAXIMUM DENSITY (Soil & Bituminous)

TEST NO	MOISTURE %	VOLUME MOLD (cu. ft.)	DENSITY DETERMINATION							
			WET SOIL + MOLD (g)	MOLD (g)	WET SOIL (g)	WET SOIL (lbs.)	COMPACTED SOIL WET (pcf)	MAX DENSITY (pcf)	OPTIMUM MOISTURE (%)	
A	B	C	D	E	F	G	H	I	J	
7	6.86	0.450	5037	1985	3052	6.73	149.5	140.4	7.1	

NOTE:
To convert (g) to (lbs.):
Wt. (g) ÷ 453.59 = Wt. (lbs.)
To convert (cm³) to (ft³):
Vol. (cm³) ÷ 0.02832 = Vol. (ft³)

CHART STANDARDS	
DENSITY	MOISTURE
3238	745
3173	716
OPERATING STANDARDS	
DENSITY	MOISTURE
3209	726

BITUMINOUS MIX DESIGN P&F

REMARKS

DENSITY INSPECTOR'S SIGNATURE

AGENCY/COMPANY

[Signature] TUNE ENGINEERING

Pg. 3 of 3

Michigan Department of Transportation
MS10D (11/02)

MOISTURE AND DENSITY DETERMINATION NUCLEAR METHOD

FILE 301

DISTRIBUTION: ORIGINAL - Project Engineer, COPIES - Area Density Supervisor, Density Technology (Lansing).
* SEE REVERSE SIDE

DATE 7-7-69	CONTROL SECTION ID 7711	JOB NUMBER 100701A	ROUTE NO. or STREET I-94 E.B. RECON.	GAUGE NO. 60378
DENSITY INSPECTOR DEWON JOHNSON	CERTIFICATION NO. 10997-0413	PROJECT ENGINEER (M.D.T.) MIKE FRANKHOUSE	PROJECT MANAGER LARRY YOUNG	PHONE NO. 510-985-5011

DETERMINATION OF IN-PLACE DENSITY

TEST NO.	WET DENSITY			MOISTURE			DRY DENSITY			LOCATION OF TEST					
	CORRECTED COUNTS	DEPTH INCH	WET DENSITY PCF	MOISTURE PCF	MOISTURE %	DRY DENSITY PCF	MAX DENSITY PCF	PERCENT OF COMPACTION	STATION	DISTANCE FROM E		DEPTH BELOW PLAN GRADE FT	ITEM OF WORK		
										LEFT	RIGHT				
22	2405	6	138.0	55	2.8	2.1	135.2	141.9	95.3	1089+25		19	92 SS		
23	3050	4	140.7	105	7.0	5.2	133.8	140.4	95.3	1047+00		18	0 SA		
24	2963	4	142.3	102	6.7	5.0	135.5	140.4	96.5	1042+00		18	0 SA		
25	2341	6	139.3	48	2.2	1.6	137.0	141.9	96.6	147+65		12	92 SS		
26	2053	6	145.1	64	3.6	2.5	141.6	141.9	99.8	152+00		12	92 SS		
27	2772	6	131.7	36	1.3	1.0	130.4	133.8	97.5	157+00		12	92 SS		
28	2621	6	134.2	41	1.7	1.3	132.5	133.8	99.1	162+00		12	92 SS		
29	2767	6	131.8	33	1.0	0.8	130.8	133.8	97.7	1113+50		18	92 SS		
30	2633	6	134.0	42	1.8	1.3	132.2	133.8	98.8	1118+50		18	92 SS		

GRADE AREA

DETERMINATION OF MAXIMUM DENSITY (Soil & Bituminous)

TEST NO.	MOISTURE %	VOLUME MOLD CU. FT.	WET SOIL		MOLD		WET SOIL		MAX DENSITY PCF	OPTIMUM MOISTURE %
			WET SOIL + MOLD	MOLD	WET SOIL	WET SOIL				
A	B	C	D	E	F	G	H	I	J	
27	5.8%	.0450	4821	1985	2836	6.25	138.9	133.8	8.4	
1	5.8%	.0450	5005	1985	3020	6.66	148.0	141.9	6.9	
7	6.8%	.0450	5037	1985	3052	6.73	149.5	140.4	7.1	

NOTE:
To convert (g/cc) to (pcf):
pcf = (g/cc) x 62.428
To convert (pcf) to (g/cc):
g/cc = pcf / 62.428

CHART STANDARDS

DENSITY	MOISTURE
3235	745
3173	716

OPERATING STANDARDS

DENSITY	MOISTURE
3209	726

BITUMINOUS MIX DESIGN PCF

Pg. 1
Pg. 1

REMARKS

TEST #27 UG OPEN GRADED SLAG 4778, 4795, 4815, 4821

DENSITY INSPECTOR'S SIGNATURE

AGENCY/COMPANY

TUNE ENGINEERING

MOISTURE AND DENSITY DETERMINATION NUCLEAR METHOD

DISTRIBUTION: ORIGINAL - Project Engineer, COPIES - Area Density Supervisor, Density Technology (Lansing).
*SEE REVERSE SIDE

DATE 7-9-09	CONTR. SECTION ID 77111	JOB NUMBER 100701A	ROUTE NO. & STREET I-94 E.B., RECON	GAUGE NO. 60378
DENSITY INSPECTOR DELOE JOHNSON	CERTIFICATION NO. 10997-2413	PROJECT ENGINEER (MGT.) MIKE FRANKHOUSE	PROJECT MANAGER LARRY YOUNG	PHONE NO. 510-985-5011

CORRECTED CHECK	DETERMINATION OF IN-PLACE DENSITY											LOCATION OF TEST				
	WET DENSITY			MOISTURE				DRY DENSITY				STATION	DISTANCE FROM E		DEPTH BELOW PLAN GRADE FT	ITEM OF WORK
	COUNTS (CG)	TEST DEPTH (inch)	WET DENSITY (pcf)	COUNTS (MO)	MOISTURE (pcf)	MOISTURE (%)	DRY DENSITY (pcf)	MAX DENSITY (pcf)	PERCENT OF COMPACTION	FT	RIGHT					
1	799	11	130.1	135	9.4	7.8	120.7	124.8	99.1	121+66	2	2.25	BE			
2	3018	6	128.0	48	2.2	1.8	125.7	130.7	96.2	121+50	2	1.58	SS			
3	2879	6	130.2	38	1.4	1.1	128.8	130.7	98.5	121+75	3	.92	SS			

DETERMINATION OF MAXIMUM DENSITY (Soil & Bituminous)										NOTE:		
TEST NO.	MOISTURE %	VOLUME MOULD (cu. ft)	DENSITY DETERMINATION						MAX DENSITY (pcf)	OPTIMUM MOISTURE %	CHART STANDARDS	
			WET SOIL + MOULD (g)	MOULD (g)	WET SOIL (g)	WET SOIL (lbs.)	COMPACTED SOIL WET (pcf)	DENSITY			MOISTURE	
A	B	C	D	E	F	G	H	I	J			
1	7.8	.0450	4650	1985	2665	5.88	130.6	121.8	11.3	3235	745	
2	5.4	.0450	4748	1985	2763	6.09	135.4	130.7	9.0	3173	716	

OPERATING STANDARDS
DENSITY: 3225 MOISTURE: 730
BITUMINOUS MIX DESIGN PCF

REMARKS
TEST #1 Sand 4625, 4626, 4625, 4650
TEST #2 461 OPEN GRADED SLAG 4650, 4688, 4713, 4730, 4742, 4746

DENSITY INSPECTOR'S SIGNATURE: *[Signature]*
AGENCY/COMPANY: *[Signature]*
TYPE ENGINEERING

MOISTURE AND DENSITY DETERMINATION NUCLEAR METHOD

DISTRIBUTION: ORIGINAL - Project Engineer, COPIES - Area Density Supervisor, Density Technician (as applicable)
* SEE REVERSE SIDE

DATE 7-21-69	CONTROL SECTION NO. 77111	JOB NUMBER 100701A	ROUTE NO. or STREET I-94 E.B. RECON	PLAN NO. 66578
DENSITY INSPECTOR DEAN JOHNSON	CERTIFICATION NO. 10997-0413	PROJECT ENGINEER (MDD) MIKE FRANKHOUSE	PROJECT MANAGER LARRY YOUNG	PHONE NO. 985-5011

DETERMINATION OF IN-PLACE DENSITY

TEST NO.	WET DENSITY			MOISTURE			DRY DENSITY			PERCENT OF COMPACTION	STATION	LOCATION OF TEST		DEPTH BELOW GRADE FT.	TEMP OF WORK
	COUNTS / SEC	TEST DEPTH INCH	WET DENSITY PCF	COUNTS / MC	MOISTURE PCF	MOISTURE %	DRY DENSITY PCF	MAX. DENSITY PCF	DISTANCE FROM LEFT FT.			DISTANCE FROM RIGHT FT.			
													1		
1	3056	6	127.0	335		8.1	126.5	100.4	996+72	45		33	CAB		
2	3180	6	125.5	49	2.4	1.9	123.2	127.7	96.4	123+61	13		92	SS	
3	2125	6	143.8	62	3.4	2.4	140.4	142.9	98.3	120+97		8	92	SS	

DETERMINATION OF MAXIMUM DENSITY (Soil & Bituminous)

TEST NO.	MOISTURE %	VOLUME MOLD CU FT	DENSITY DETERMINATION						MAX DENSITY PCF	OPTIMUM MOISTURE %
			WET SOIL - MOLD	MOLD	WET SOIL	WET SOIL	COMPACTED SOIL WET	SOIL WET		
A	B	C	D	E	F	G	H	I	J	
1	8.1	.0387	4011	2006	2005	4.42	131.2	126.5	10.5	
2	5.8	.0450	4715	1985	2730	6.02	133.7	127.7	9.7	
3	5.0	.0450	4965	1965	2980	6.57	146.0	142.9	6.8	

CHART STANDARDS

DENSITY	MOISTURE
3238	745

OPERATING STANDARDS

DENSITY	MOISTURE
3225	722

BITUMINOUS MAX DESIGN PCF

REMARKS:
 TEST #1 CRUSHED CONCRETE TEST #2 4" OPEN GRADED LWS 4660, 4698, 4710, 4715
 TEST #3 4" OF LIMESTONE 4910, 4946, 4960, 4965
 PROJECT ENGINEER

Michigan Department of Transportation
 (313) 221-1000

MOISTURE AND DENSITY DETERMINATION NUCLEAR METHOD

FILE NO.

DISTRIBUTION: ORIGINAL - Project Engineer, COPIES - Area Density Supervisor, Density Technology (Lansing)
 * SEE REVERSE SIDE

DATE: 7-22-09 CONTROL SECTION ID: 77111 JOB NUMBER: 10A701A ROUTE NO. OR STRESS: I-94 E B RECEN CASE NO.: 60378
 DENSITY INSPECTOR: DELON JOHNSON CERTIFICATION NO.: 10997-0413 PROJECT ENGINEER (MOOT): MIKE FRANKHOUSE PROJECT MANAGER: LARRY VALLIN
 PHONE NO.: 866-945-5011

DETERMINATION OF IN-PLACE DENSITY

TEST NO.	WET DENSITY			MOISTURE			DRY DENSITY			LOCATION OF TEST				
	COUNTS SEC	DEPTH INCH	DENSITY PCF	COUNTS MC	MOISTURE PCF	MOISTURE %	DRY DENSITY PCF	MAX DENSITY PCF	PERCENT OF COMPACTION	STATION	DISTANCE FROM S FT	DISTANCE FROM R FT	DEPTH BELOW PLAN GRADE FT	TEMP OF WORK °F
1	2976	4	142.2	82	5.1	3.7	137.1	141.7	96.8	10+0+00		25	42	SA
2	2615	4	145.1	86	5.4	3.9	139.6	141.7	98.6	1005+00		25	42	SA
3	2635	4	148.4	103	6.8	4.8	141.5	141.7	99.9	1015+00		25	42	SA
4	3361	4	135.8	92	5.9	4.6	129.9	141.7	91.7	1020+00		25	42	SA
7-22 4	2954	4	142.5	98	6.4	4.7	136.1	141.7	96.0	1024+00		25	42	SA
5	2934	4	142.9	83	5.2	3.8	137.8	141.7	97.2	1025+00		25	42	SA
6	2627	4	148.5	98	6.4	4.5	142.1	141.7	100.3	1030+00		25	42	SA
7	3396	4	135.4	64	3.6	2.7	131.8	141.7	93.0	1035+00		25	42	SA
8	2934	4	142.9	85	5.3	3.9	137.6	141.7	97.1	1040+00		25	42	SA
7-22 7	2931	4	143.0	69	4.0	2.9	139.0	141.7	98.1	1035+00		25	42	SA
9	3122	4	139.8	71	4.2	3.1	135.6	141.7	95.7	1045+00		25	42	SA

DETERMINATION OF MAXIMUM DENSITY (Soil & Bituminous)

TEST NO.	MOISTURE %	VOLUME MOLD CU FT	WET SOIL		WET SOIL		WET SOIL Wt. GR.	COMPACTED SOIL WET PCF	MAX DENSITY PCF	OPTIMUM MOISTURE %
			WET SOIL Wt. GR.	MOLD	WET SOIL Wt. GR.	MOLD				
A	B	C	D	E	F	G	H	I	J	
1	5.2	0.450	4954	1985	2969	6.55	145.5	141.7	69	

NOTE:
 To convert (g) to (lbs.):
 1 g = 0.002205 lb (avoirdupois)
 To convert (m³) to (ft³):
 1 m³ = 35.3147 ft³

CHART STANDARDS

DENSITY	MOISTURE
3258	745
3173	716

OPERATING STANDARDS

DENSITY	MOISTURE
3214	724

RETURN TO: S & DESIGN PCF

REMARKS: TEST #S 46 CG LIMESTONE 4817, 4866, 4900, 4931, 4947, 4950

DENSITY INSPECTOR SIGNATURE: *[Signature]* AGENCY CONTACT: TIME ENGINEERING

Michigan Department of Transportation
 6600 15150

MOISTURE AND DENSITY DETERMINATION
 NUCLEAR METHOD

FILE 301

DISTRIBUTION: ORIGINAL - Project Engineer, COPIES - Area Density Supervisor, Density Technology (Lansing)
 * SEE REVERSE SIDE

DATE: 7-22-09 CONTROL SECTION: 7711 JOB NUMBER: 100701A (ROUTE NO. OF STREET): I-94 E.B. RECON GAUGE NO: 00378
 DENSITY INSPECTOR: DELEN JOHNSON CERTIFICATION NO.: 0097-0413 PROJECT ENGINEER (MOOT): MIKE FRANKHOUSE PROJECT MANAGER: LARRY YOUNG PROJECT NO.: 810 995-SC11

DETERMINATION OF IN-PLACE DENSITY

TEST NO.	WET DENSITY			MOISTURE			DRY DENSITY			LOCATION OF TEST			
	COUNTS	DEPTH (in)	WET DENSITY (pcf)	COUNTS (MC)	MOIS-TURE (pcf)	MOIS-TURE (%)	DRY DENSITY (pcf)	MAX DENSITY (pcf)	PERCENT OF COM-PACTION	STATION	DISTANCE FROM E RIGHT	DEPTH BELOW PLAN GRADE (ft)	TEMP OF WORK
10	2864	4	144.1	98	6.4	4.7	137.7	142.0	97.0	1005+00	25	0	SA
11	2911	4	143.3	98	6.4	4.7	136.9	142.0	96.4	1010+00	25	0	SA
12	2980	4	142.0	105	7.0	5.2	135.0	142.0	95.1	1015+00	25	0	SA
13	2888	4	143.7	101	6.7	4.9	137.0	142.0	96.5	1020+00	25	0	SA
14	2700	4	147.1	110	7.4	5.3	139.7	142.0	98.4	1025+00	25	0	SA
15	2817	4	144.9	107	7.2	5.2	137.8	142.0	97.0	1030+00	25	0	SA
16	3067	4	140.6	94	6.1	4.5	134.5	142.0	94.7	1035+00	25	0	SA
17	3010	4	141.6	93	6.0	4.4	135.6	142.0	95.5	1035+00	25	0	SA
18	2921	4	143.1	105	7.0	5.1	136.1	142.0	95.8	1040+00	25	0	SA
19	2673	4	147.6	107	7.2	5.1	140.5	142.0	98.9	1045+00	25	0	SA
19	3120	4	139.8	71	4.2	3.1	135.6	142.0	95.5	1071+75	25	4 1/2	SA

pass

DETERMINATION OF MAXIMUM DENSITY (Soil & Bituminous)

TEST NO.	MOIS-TURE (%)	VOLUME MOLD (cu. ft.)	WET SOIL		MOLD		WET SOIL		COMPACTED SOIL WET (pcf)	MAX DENSITY (pcf)	OPTIMUM MOISTURE (%)
			WET SOIL (lb)	A	B	C	D	E			
10	6.36	.0450	5045	1985	3060	6.75	149.9	142.0	6.9		
19	5.48	.0450	4942	1985	2957	6.52	144.9	140.6	7.1		

NOTE:
 To convert (g) to (lbs.):
 Wt. (g) ÷ 453.59 = Wt. (lbs.)
 To convert (m³) to (ft³):
 Vol. (m³) × 35.3147 = Vol. (ft³)

CHART STANDARDS

DENSITY	MOISTURE
3238	745
3173	716

OPERATING STANDARDS

DENSITY	MOISTURE
3214	724

BITUMINOUS MIX DESIGN POF

REMARKS:
 TEST #10 23A 4910, 4935, 4940, 5015, 5039, 5045
 TEST #19 46 CG SLAG 4857, 4892, 4940, 4942
 DENSITY INSPECTOR: DELEN JOHNSON PROJECT ENGINEER: MIKE FRANKHOUSE
 TIME ENGINEERING

pg. 3 of 3

Michigan Department of Transportation
MDOT (11/03)

MOISTURE AND DENSITY DETERMINATION NUCLEAR METHOD

FILE 301

DISTRIBUTION: ORIGINAL - Project Engineer, COPIES - Area Density Supervisor, Density Technology (email)
*SEE REVERSE SIDE

DATE 7-22-09	CONTRACT SECTION NO. 77111	JOB NUMBER 100701A	ROUTE NO. & STREET I-94 E B RECON	SHEET NO. 60378
DENSITY INSPECTOR DELOU JOHNSON	CERTIFICATION NO. 109977-0413	PROJECT ENGINEER/MDOT MIKE FRANKHOUSE	PROJECT MANAGER LARRY YOUNG 810-985-5011	PHONE NO.

DETERMINATION OF IN-PLACE DENSITY

TEST NO.	WET DENSITY			MOISTURE			DRY DENSITY			STATION	LOCATION OF TEST			ITEM OF WORK
	COUNTS PER MINUTE	TEST DEPTH INCH	WET DENSITY PCF	COUNTS PER MINUTE	MOISTURE %	DRY DENSITY PCF	MAX DENSITY PCF	PERCENT OF COMPACTION	DISTANCE FROM E		DISTANCE FROM W	DEPTH BELOW PLAN GRADE FT		
													1	
20	3131	4	139.6	64	3.6	2.6	136.0	140.6	96.7	1075+20	25	42	SA	
21	3007	4	141.7	67	3.8	2.8	137.9	140.6	98.1	1076+30	25	42	SA	
22	3206	4	138.4	71	4.2	3.1	134.2	140.6	95.4	1081+30	25	42	SA	
23	2879	4	143.8	105	7.0	5.1	136.8	142.0	96.4	1071+78	25	C	SA	

DETERMINATION OF MAXIMUM DENSITY (Soil & Bituminous)

TEST NO.	MOISTURE %	VOLUME MOULD CU FT	DENSITY DETERMINATION					MAX DENSITY PCF	OPTIMUM MOISTURE %
			WET SOIL + MOULD	MOULD	WET SOIL	WET SOIL	COMPACTED SOIL WET SOIL		
A	B	C	D	E	F	G	H	I	
19	5.4	0.450	49.42	1.985	29.57	6.52	144.9	140.6	7.1

NOTE:
To convert lb to kg: 1 lb = 0.45359 kg
To convert cu ft to m³: 1 cu ft = 0.0283168 m³
To convert % to g/100g: 1% = 10 g/100g

CHART STANDARDS

DENSITY	MOISTURE
3258	745
3173	716

OPERATING STANDARDS

DENSITY	MOISTURE
3214	724

BITUMINOUS VIA DESIGN PCF

REMARKS

DENSITY INSPECTOR'S SIGNATURE

[Signature]

ASPIRE MANAGER

TUNE ENGINEERING

pg 1 of 2

Michigan Department of Transportation
 (4428711-001)

MOISTURE AND DENSITY DETERMINATION NUCLEAR METHOD

FL 110

DISTRIBUTION ORIGINAL Project Engineer COPIES Area Density Supervisor Density Technology Training
 *SEE REVERSE SIDE

DATE: 7-23-09 CONTROL SECTION ID: 77111 JOB NUMBER: 100701A ROUTE NO & STREET: I-94 E.B. RECON DISTRICT: 40378
 DENSITY INSPECTOR: DELON JOHNSON CERTIFICATION NO.: 0997-0413 PROJECT ENGINEER/AGGT: MIKE FRANKHOUSE PROJECT MANAGER: LARRY YOUNG PHONE NO.: 56-985-5011

TEST NO.	WET DENSITY			MOISTURE			DRY DENSITY			PERCENT OF COMPACTION	LOCATION OF TEST		
	COUNTS	TEST DEPT. (in)	WET DENSITY (pcf)	COUNT'S (in)	MOISTURE (pcf)	MOISTURE (%)	DRY DENSITY (pcf)	MAX DENSITY (pcf)	STATION		DISTANCE FROM E. FT.	DEPTH (ft)	ITEM OF WORK
1	2917	4	143.2	90	5.8	4.2	137.9	142.0	95.7	107+00	25	SA	
2	3064	4	140.7	84	5.3	3.9	135.4	141.5	95.7	107+00	25	SA	
7-23 2	3271	4	137.2	92	5.9	4.5	131.3	141.5	93.0	102+50	7	SA	
3	3040	4	141.0	93	6.0	4.5	135.0	141.5	95.4	102+50	7	SA	
4	3091	4	140.3	65	3.7	2.7	136.6	141.5	96.5	107+50	7	SA	
5	3118	4	139.8	70	4.1	3.0	135.7	141.5	95.9	112+50	7	SA	
6	2974	4	142.2	86	5.4	4.0	136.8	141.5	96.6	117+50	14	SA	
7	4179	4	124.3	56	2.9	2.4	121.4	137.9	98.0	1086+00	25	SA	
8	2633	4	148.4	99	6.5	4.6	141.9	141.5	100.3	122+50	13	SA	
7-23 8	3274	4	137.2	86	5.4	4.1	131.7	141.5	93.1	204+50	7	SA	
9	2711	4	146.9	92	5.9	4.2	141.0	141.5	99.6	204+50	7	SA	

TEST NO.	MOISTURE (%)	VOLUME MOULD (cu ft)	WET SOIL		MOLD		WET SOIL		COMPACTED SOIL WET (pcf)	MAX DENSITY (pcf)	OPTIMUM MOISTURE (%)
			WET SOIL (pcf)	MOULD (pcf)	WET SOIL (pcf)	WET SOIL (pcf)					
1	5.6	.0450	4979	1985	2994	6.60	146.7	141.5	7.0	3173	716
6	5.0	.0450	4856	1985	2371	6.33	140.7	137.9	7.6	3213	721

REMARKS:
 TEST #2 234 4912 4997 4970 (4979)
 TEST #6 46 06 5.26 4790 4842 4855 (4856)
 DENSITY INSPECTOR'S SIGNATURE: [Signature] TIME ENGINEERING

Michigan Department
of Transportation
USEE 1103

MOISTURE AND DENSITY DETERMINATION
NUCLEAR METHOD

DISTRIBUTION: ORIGINAL Project Engineer COPIES - Area Density Supervisor Density Technology (Lansing)
*SEE REVERSE SIDE

DATE: 7-22-09 CONTRACT SECTION: T7111 JOB NUMBER: 100701A ROUTE NO. & STREET: I-94, E.B. RECON. DIST. OR NO.: 60378
 DENSITY INSPECTOR: DELOON, JOHNSON IDENTIFICATION NO.: 10997-0413 PROJECT ENGINEER (SIC): MIKE FRANKHOUSE PROJECT MANAGER: LARRY YOUNG
 PROJECT MANAGER PHONE NO.: 910-985-5011

DETERMINATION OF IN-PLACE DENSITY

TEST NO.	WET DENSITY			MOISTURE			DRY DENSITY			PERCENT OF COMPACTION	LOCATION OF TEST			DEPTH BELOW PLAN GRADE (ft)	TEMP OF WORK (°F)
	COUNTS (SC)	TEST DEPTH (in)	WET DENSITY (pcf)	COUNTS (SC)	MOISTURE (pcf)	MOISTURE (%)	DRY DENSITY (pcf)	MAX DENSITY (pcf)	STATION		DISTANCE FROM L (ft)	DISTANCE FROM R (ft)	DEPTH (ft)		
9	2961	4	142.4	111	6.7	4.9	135.7	141.5	95.9	126+65	1	14	.42	SA	
10	2888	4	143.7	90	5.8	4.2	137.9	141.5	97.5	1069+00	25	14	.42	SA	
11	3044	4	141.0	91	5.9	4.3	135.1	141.5	95.5	109+00	15	14	.42	SA	
12	3115	4	139.8	83	5.2	3.9	134.6	141.5	95.7	202+25	1	14	.42	SA	

DETERMINATION OF MAXIMUM DENSITY (Soil & Bituminous)

TEST NO.	MOISTURE (%)	VOLUME MOULD (cu ft)	WET SOIL - MOULD		WET SOIL (lb)	WET SOIL (pcf)	COMPACTED SOIL WET (pcf)	MAX DENSITY (pcf)	OPTIMUM MOISTURE (%)
			W	D					
56	5.6	.0450	4979	1985	2994	6.60	146.7	141.5	7.0

NOTE:
 1. 100 wet (lb) to (kg)
 2. 100 wet (kg) to (lb)
 3. To convert (pcf) to (kg/m³)
 4. To convert (pcf) to (lb/ft³)

CHART STANDARDS

DENSITY	MOISTURE
3238	745
3173	716

OPERATING STANDARDS

DENSITY	MOISTURE
3213	721

BITUMINOUS MIX DESIGN (pcf)

REMARKS

INSPECTOR'S SIGNATURE: *[Signature]* AREA CHIEF: *[Signature]* TYPE ENGINEERING

AGGREGATE INSPECTION REPORT

Michigan Department
Of Transportation
1500 (109)

PLEASE PRINT

DISTRIBUTION ORIGINAL - Project Engineer, COPY - Testing Laboratory, Region Materials Supervisor, Region Materials Supervisor - Using Region (when applicable)

CONTROL SECTION		JOB NUMBER 100701		PROJECT ENGINEER MIKE FRANKHOUSE, P.E.		CONTRACTOR JOHN CARLO, INC			
MATERIAL 4G Slag	PIT NUMBER 82-17		PIT NAME D.L. C. LEVY (DIX)		PRODUCER TEST STRIP		TONS REPRESENTED		
DATE SAMPLED 6/6/2009		SAMPLED BY Michael Cornacchia			SAMPLED FROM I-94 TEST STRIP			REPORT NUMBER	
DATE TESTED 6/7/2009		NAME OF TESTER Michael Cornacchia			SIGNATURE <i>Michael J. Cornacchia</i>		REPORT NUMBER		
TEST RESULTS					TEST RESULTS				
SIEVE	RETAINED WEIGHT	FRACTIONAL % RETAINED	CUMULATIVE % RETAINED	RESULTS % PASSING	SPEC. % PASSING	WEIGHT	RESULTS %	SPEC %	
6 INCH	0.0	0.0	0.0	100		INITIAL WEIGHT OF SAMPLE	4277.0		
3 INCH	0.0	0.0	0.0	100		WEIGHT AFTER WASHING	4133.0		
2 INCH	0.0	0.0	0.0	100	100%	LOSS BY WASHING (L.B.W.)	144.0	3.4	8.0 max
1 1/2 INCH	0.0	0.0	0.0	100		PICK WEIGHT			
1 INCH	508.0	11.9	11.9	88		FINESS MODULUS			
3/4 INCH	763.0	17.8	29.7	70	55-85	ORGANIC PLATE NUMBER			
1/2 INCH	784.0	17.9	47.6	52	35-70%	CRUSHED MATERIAL %	0.0	0	
3/8 INCH	432.0	10.1	57.7	42		SOFT PARTICLES	0.0	0.0	
NO. 4	733.0	17.1	74.8	25		CHERT PARTICLES	0.0	0.0	
NO. 6	339.0	7.9	82.7	17	10-30%	SUM OF SOFT AND CHERT	0.0	0.0	
NO. 16	230.0	5.4	88.1	12		CLAY IRONSTONE	0.0	0.0	
NO. 30	125.0	2.9	91.0	9	5-23%	FLAT			
NO. 60						ELONGATION			
NO. 100									
PAN	239.0	5.6	96.6	3	8.0 max				
L.B.W.	144.0	3.4	100.0			Meels			
TOTAL	4277.0	100.0				Project Engineer not fed.	Contractor notified		
Remarks									
STATION 891+50 TO 900+50									

FILE COPY

DENSITY GUIDELINES

	% DENSITY	ITEM OF WORK	DEPTH
Original Ground			
Road Embankment Areas (if specified)	90.0	OG	9"
Bridges — Within the limits as shown on the plans	95.0	OG	9"
Cut Areas			
Cuts requiring Sand Subbase	95.0	CS	9"
Cuts not requiring Sand Subbase	95.0	CN	12"
Subgrade for Bituminous Base, Aggregate Base and Concrete Widening	95.0	SG	9"
Embankments			
Regular	95.0	E	
Abutments with Piling	95.0	AP	
Abutments without Piling — Within the limits for Structure Embankment as shown on the plans	100.0	AN	
Foundation Undercut Backfill for retaining Walls, Grade Separations or Bridges	100.0	FB	
Backfill for Bridges, Culverts, Sewers, Manholes, Catch Basins, Edge Drains, and Subgrade Undercuts	95.0	B	
Subbase	95.0	S	
Subbase for Slope Paving	90.0	SP	
Aggregate Base — Concrete	95.0	SS	
Aggregate Base — Bituminous	98.0	AB	
Bituminous Aggregate Base (pulverized Bituminous used as Aggregate Base)	98.0	BAB	
Recycled Concrete Aggregate Base - used under Concrete Pavement	95.0	CAC	
Recycled Concrete Aggregate Base - used under Bituminous Pavement	98.0	CAB	
Shoulders — Class I	98.0	SAA	
Shoulders — Class II and III	95.0	SA	
Bituminous Stabilization	98.0	BS	
Bituminous Paving — Base Course	97.0	BB	
Bituminous Paving — Leveling Course	97.0	BL	
Bituminous Paving — Top Course	97.0	BT	

APPENDIX D: STRESS-STRAIN CURVES FROM RESILIENT MODULUS TESTING

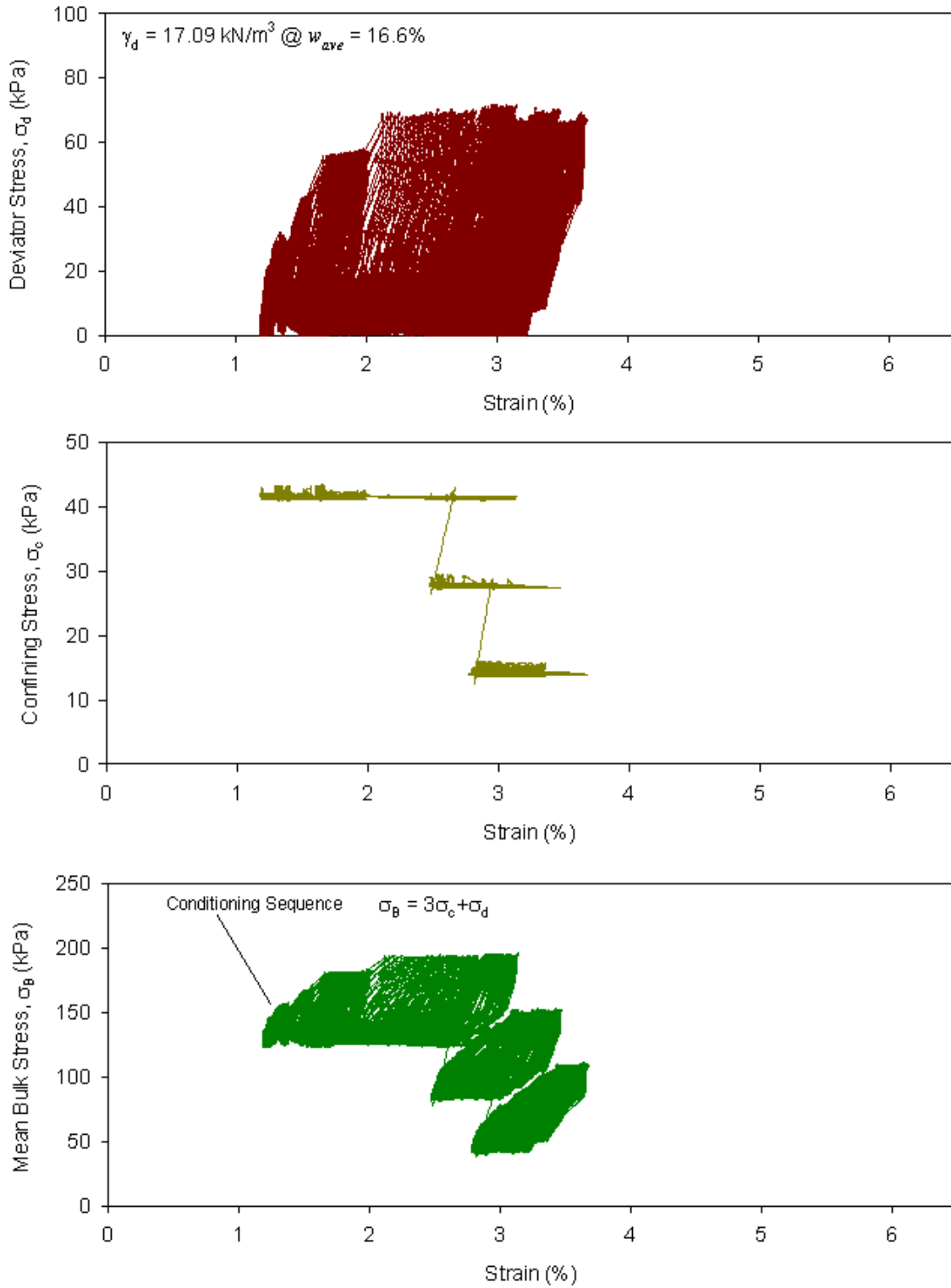


Figure 90. Cyclic stress-strain curves from M_R test for Shelby tube A4 (0.4–1.0 m)

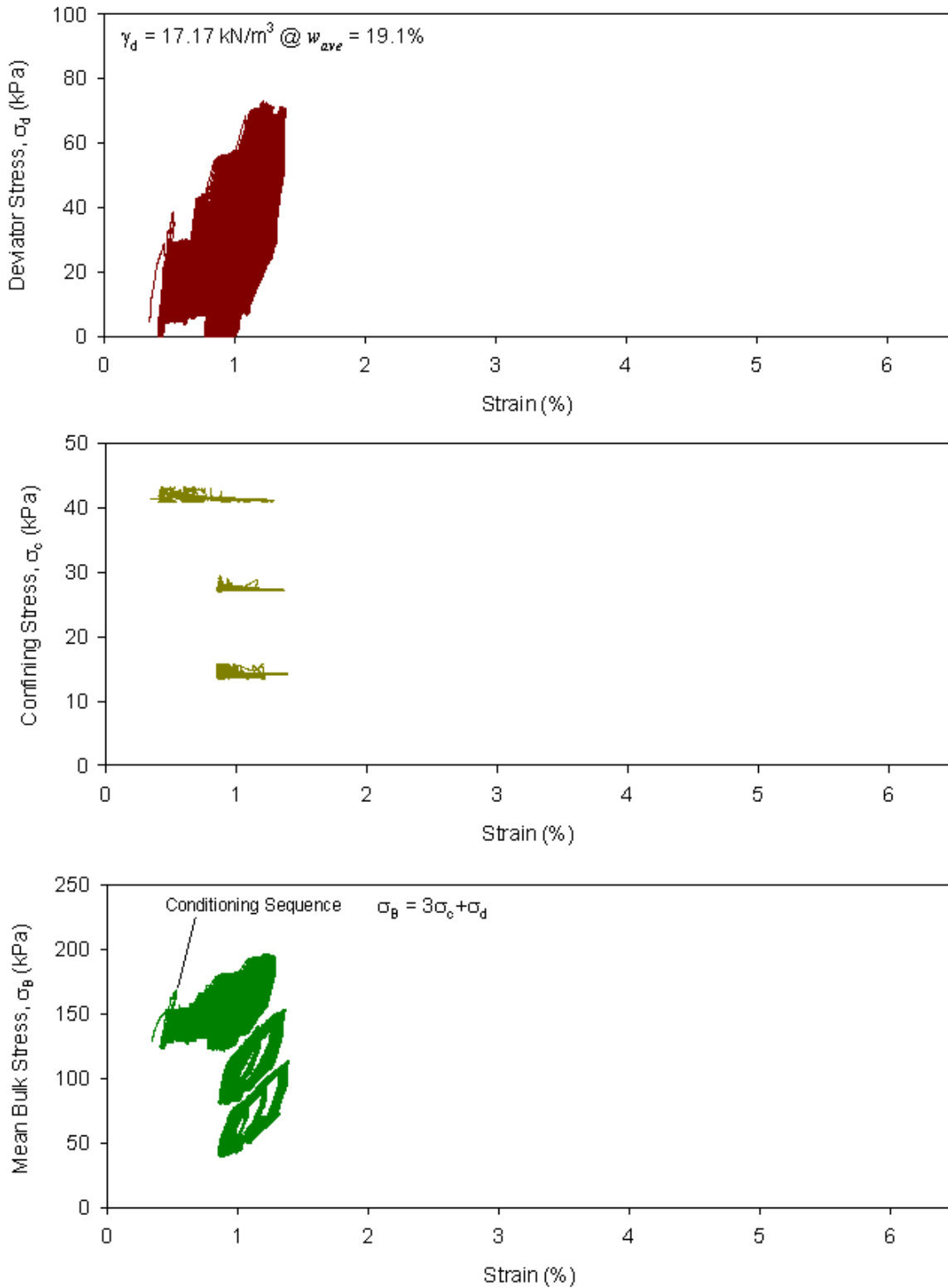


Figure 91. Cyclic stress-strain curves from M_r test for Shelby tube C2 (0.4–1.0 m)

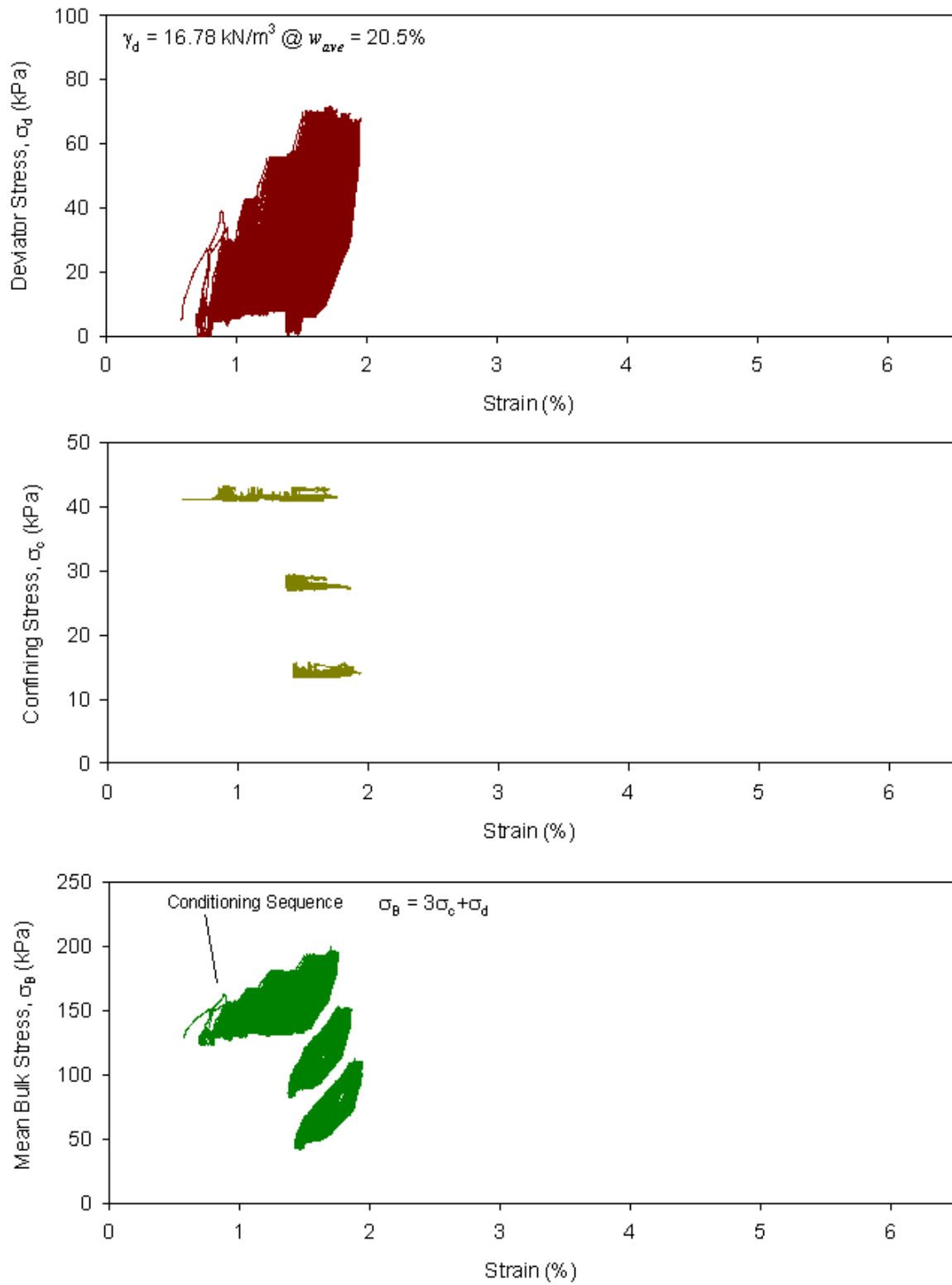


Figure 92. Cyclic stress-strain curves from M_r test for Shelby tube C2 (1.0–1.7 m)

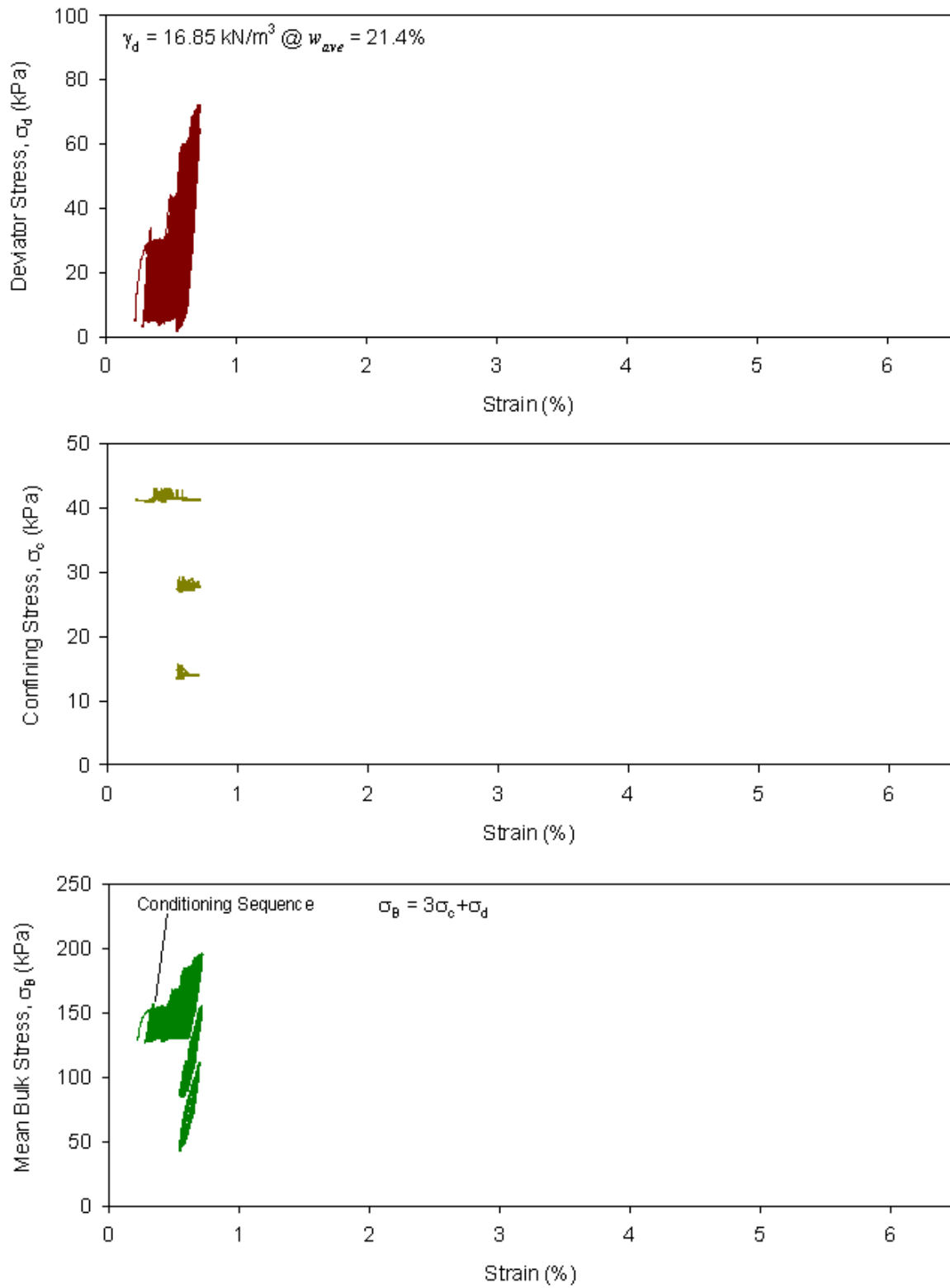


Figure 93. Cyclic stress-strain curves from Mr test for Shelby tube C4 (0.4–1.0 m)

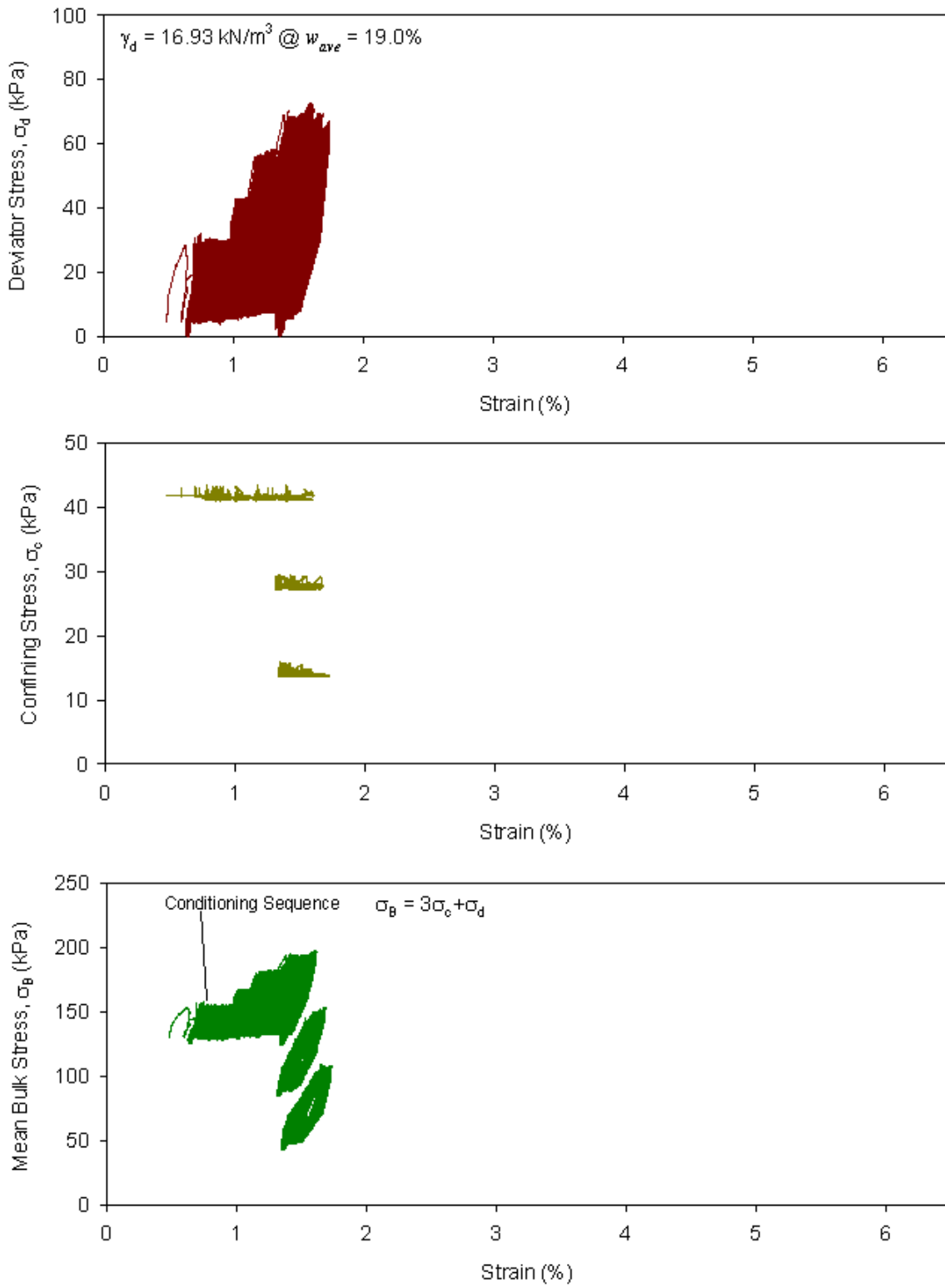


Figure 94. Cyclic stress-strain curves from M_r test for Shelby tube C4 (1.0–1.7 m)

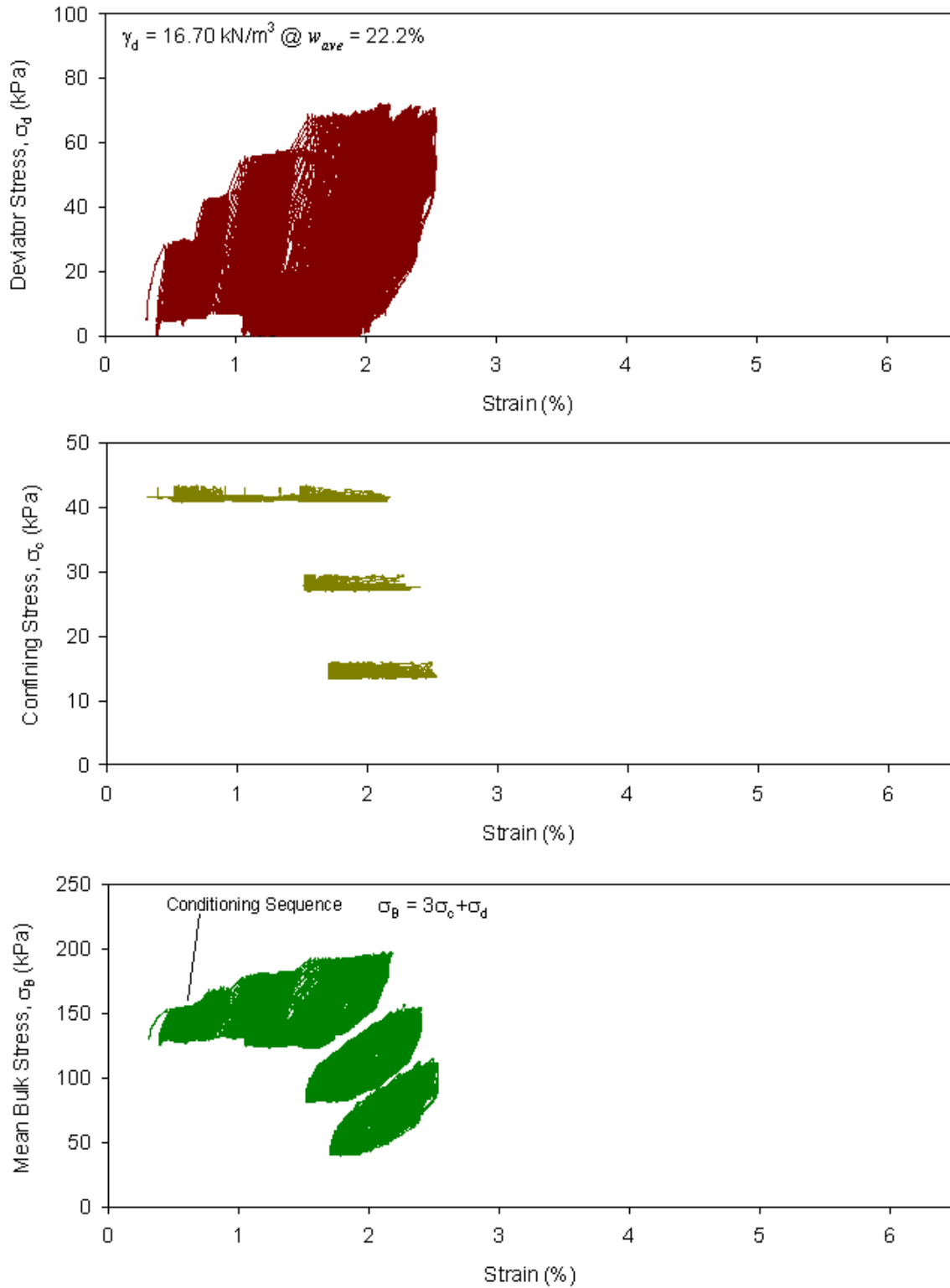


Figure 95. Cyclic stress-strain curves from M_r test for Shelby tube E2 (0.4–1.0 m)

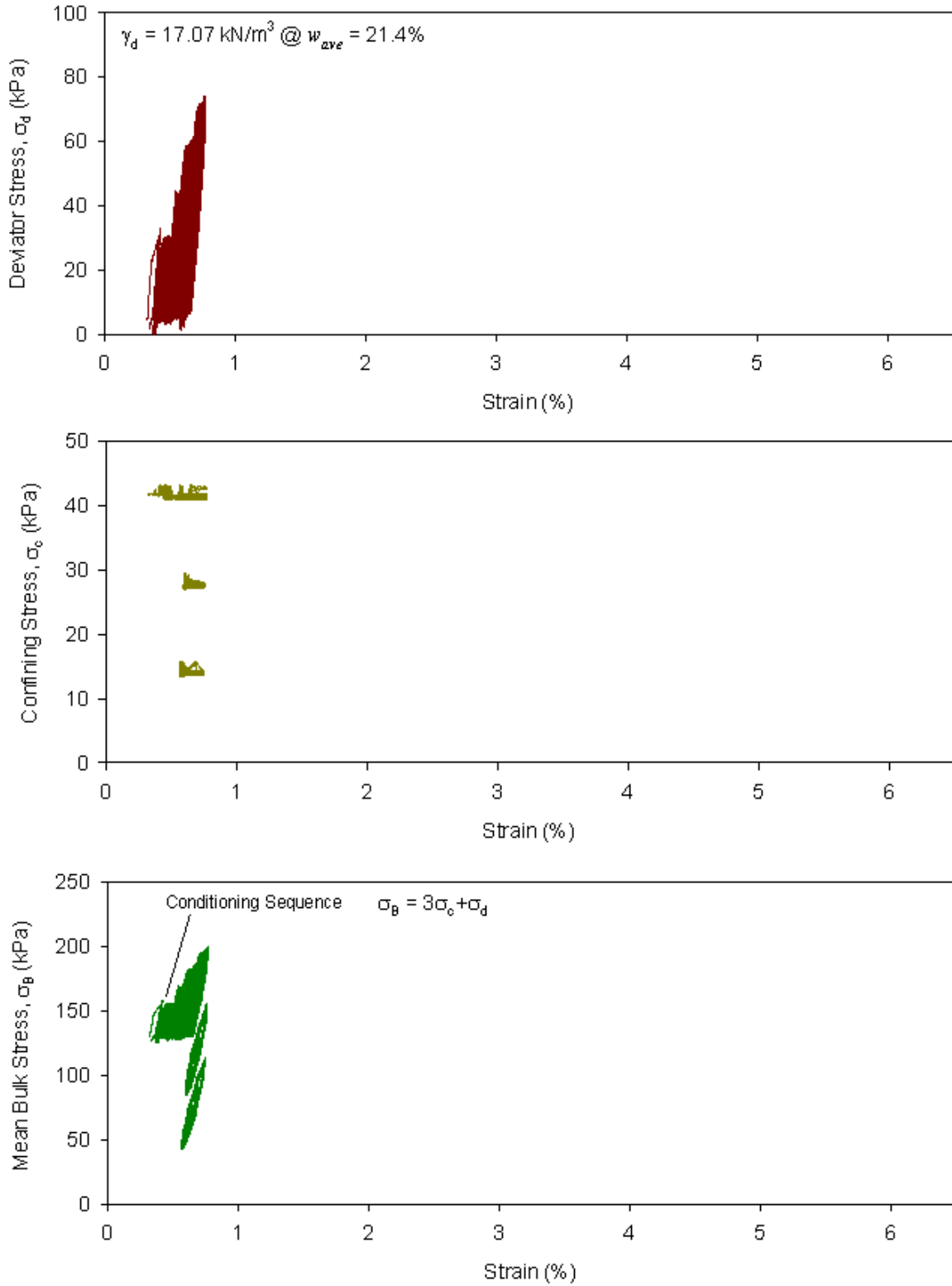


Figure 96. Cyclic stress-strain curves from M_r test for Shelby tube E2 (1.0–1.7 m)

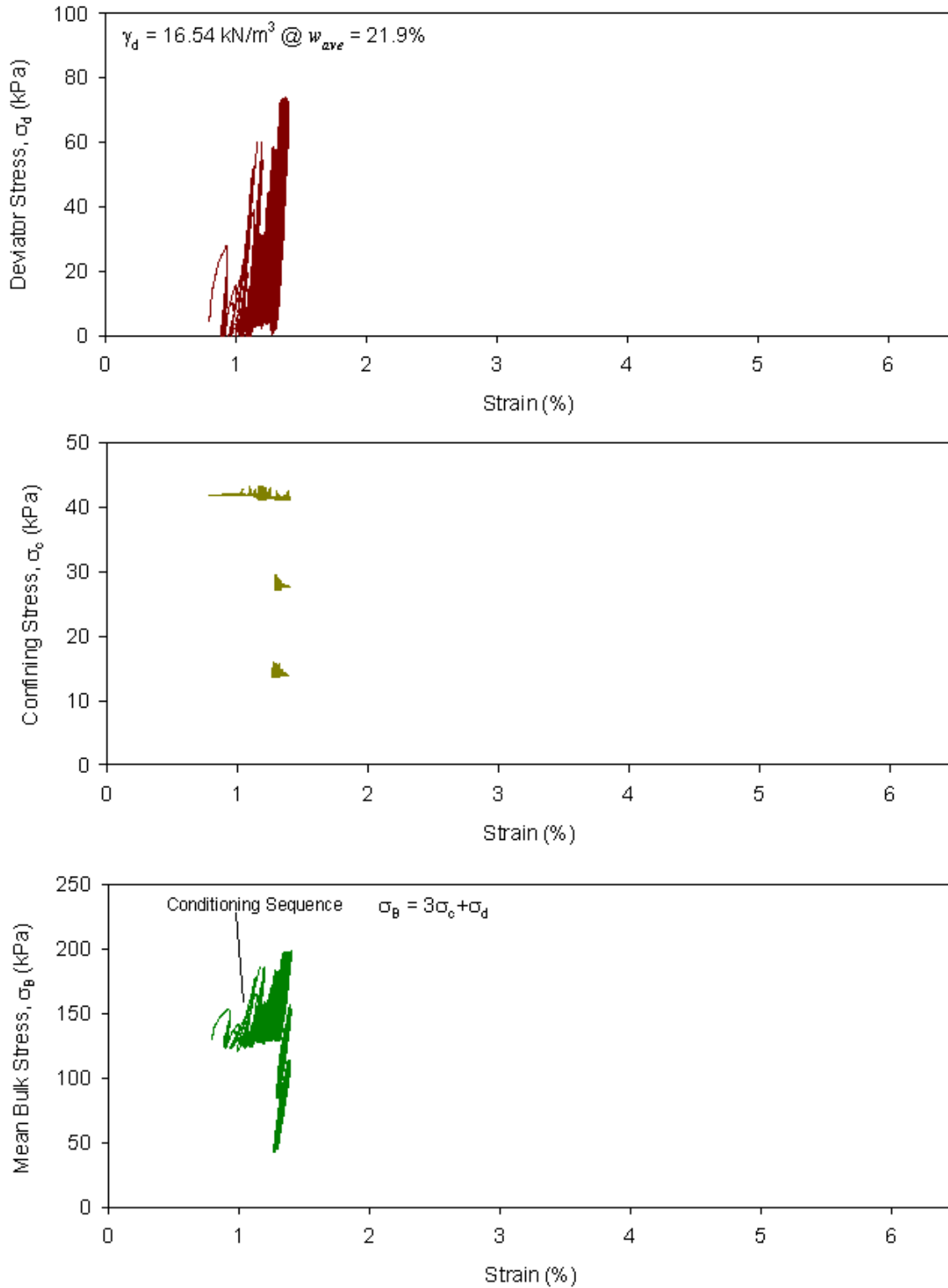


Figure 97. Cyclic stress-strain curves from M_r test for Shelby tube E4 (0.4–1.0 m)

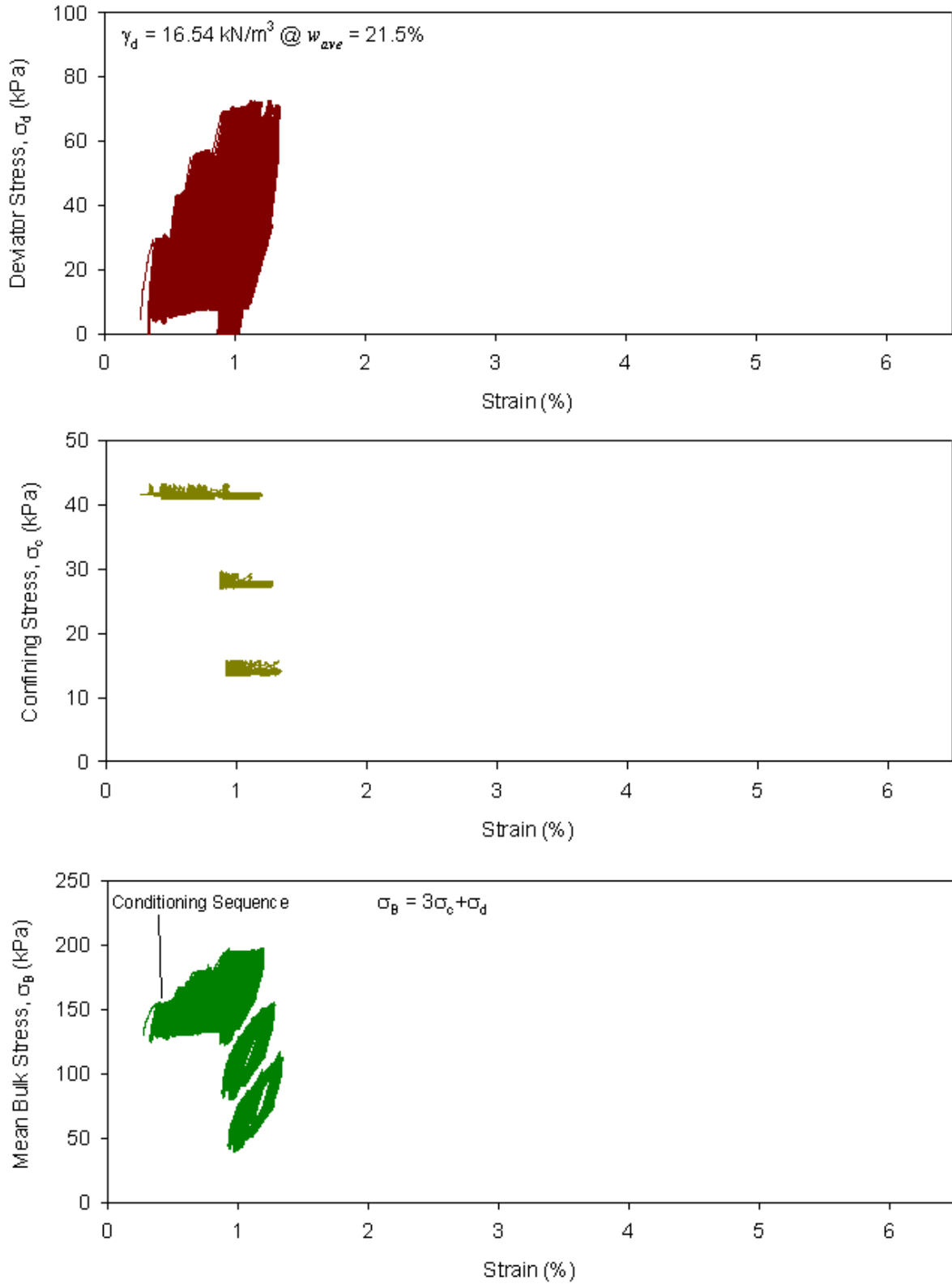


Figure 98. Cyclic stress-strain curves from M_r test for Shelby tube E4 (1.0–1.7 m)

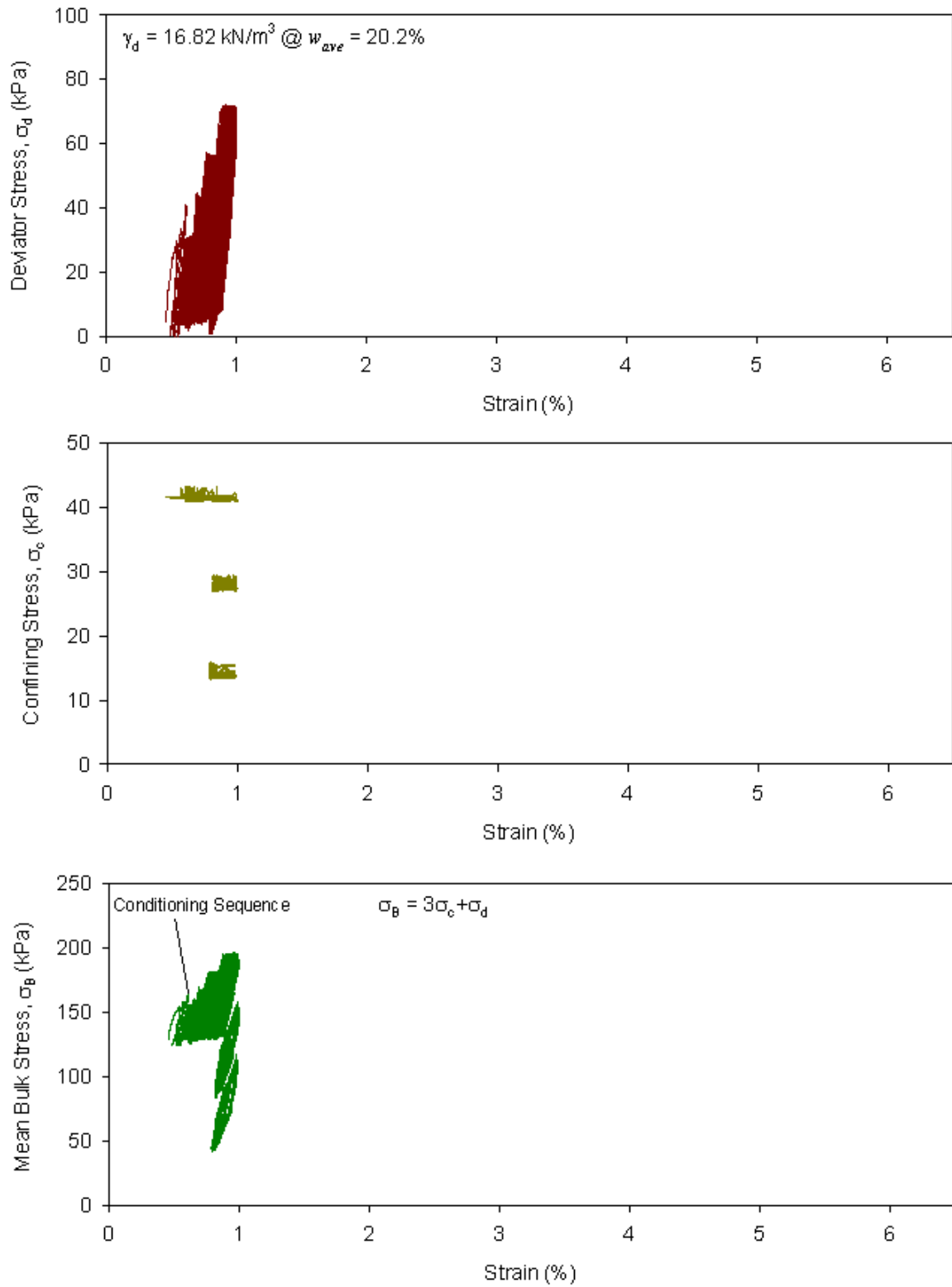


Figure 99. Cyclic stress-strain curves from M_r test for Shelby tube G1 (0.4–1.0 m)

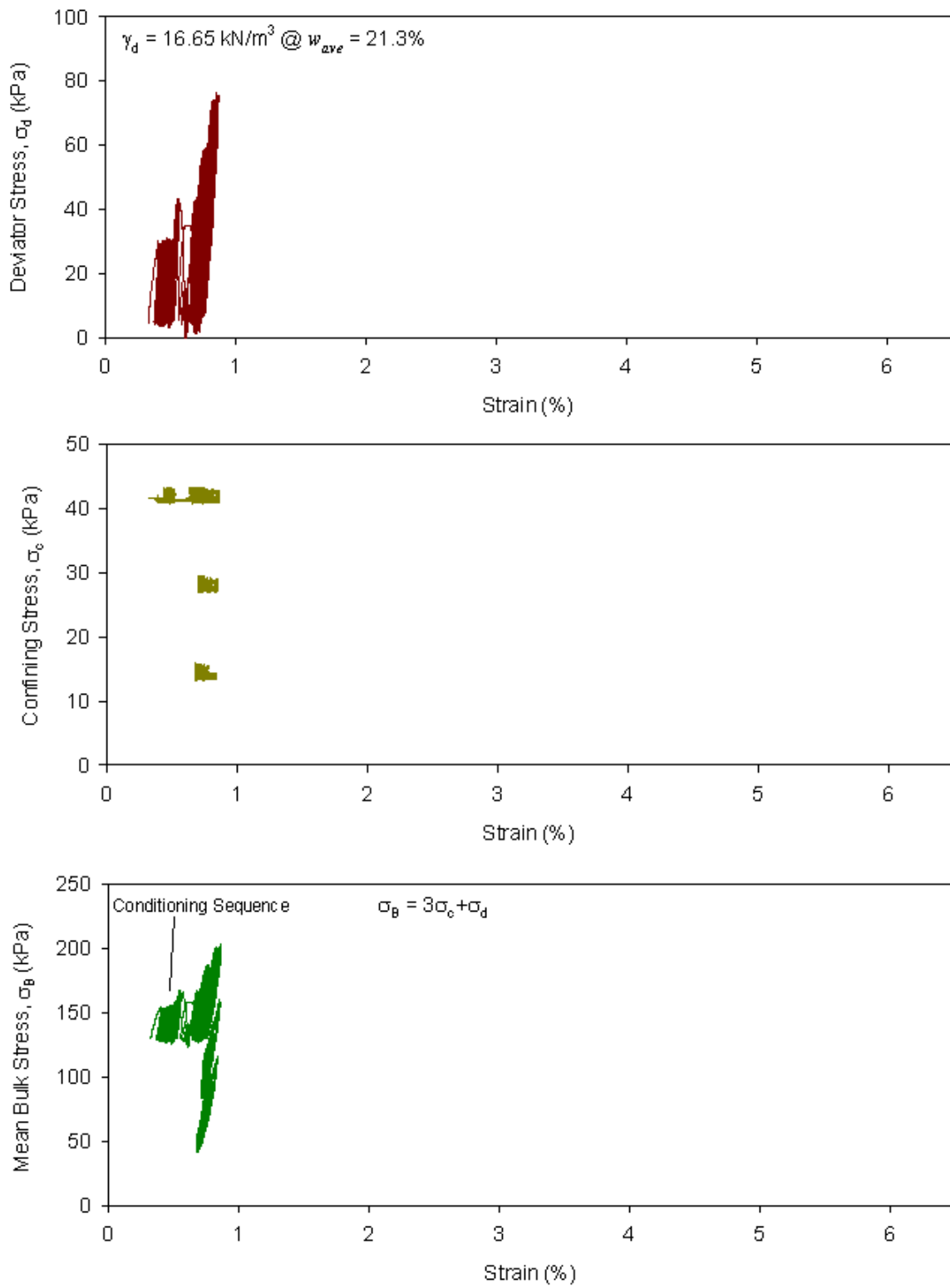


Figure 100. Cyclic stress-strain curves from M_R test for Shelby tube G1 (1.0–1.7 m)

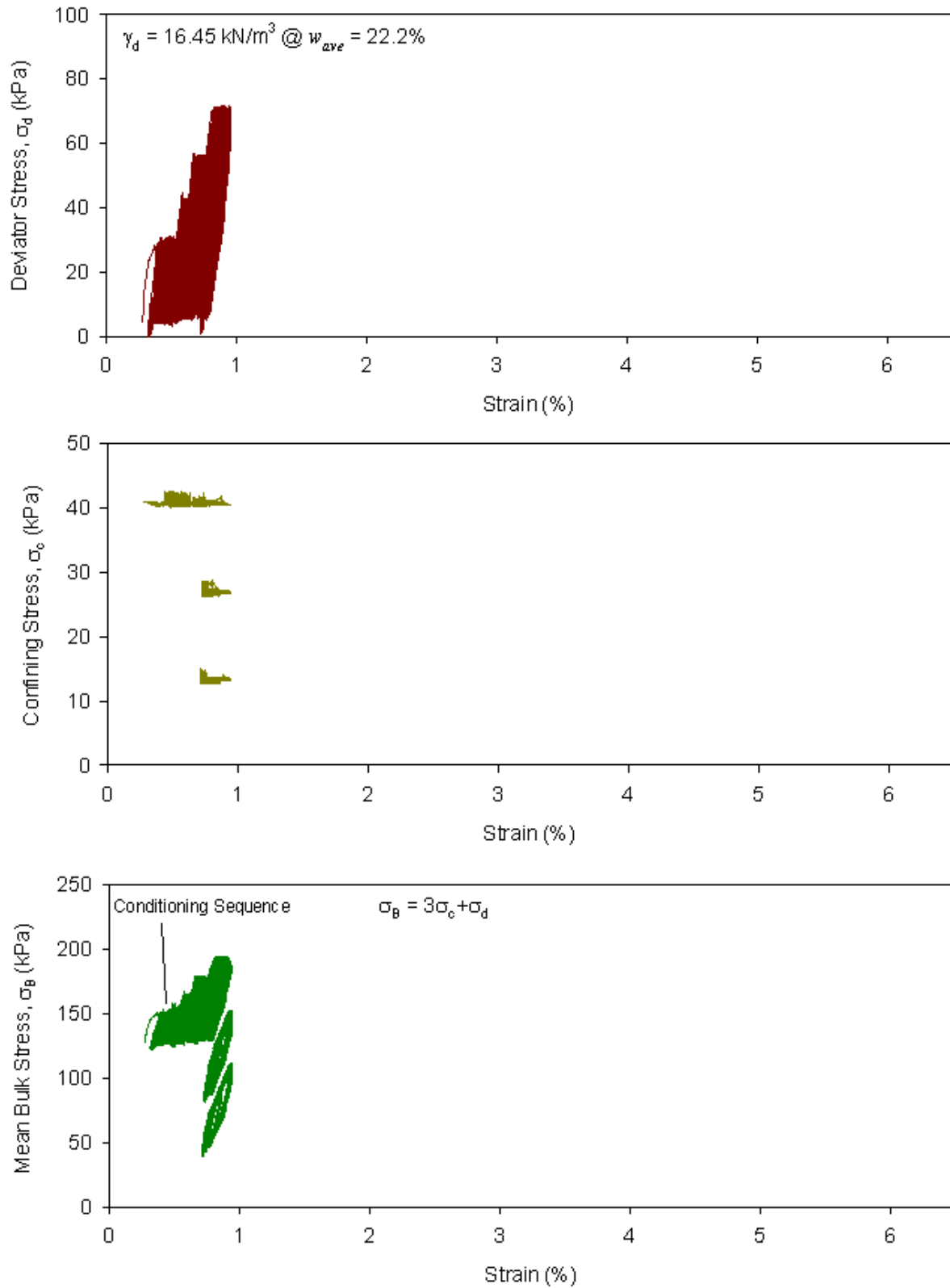


Figure 101. Cyclic stress-strain curves from M_r test for Shelby tube G3 (0.4–1.0 m)

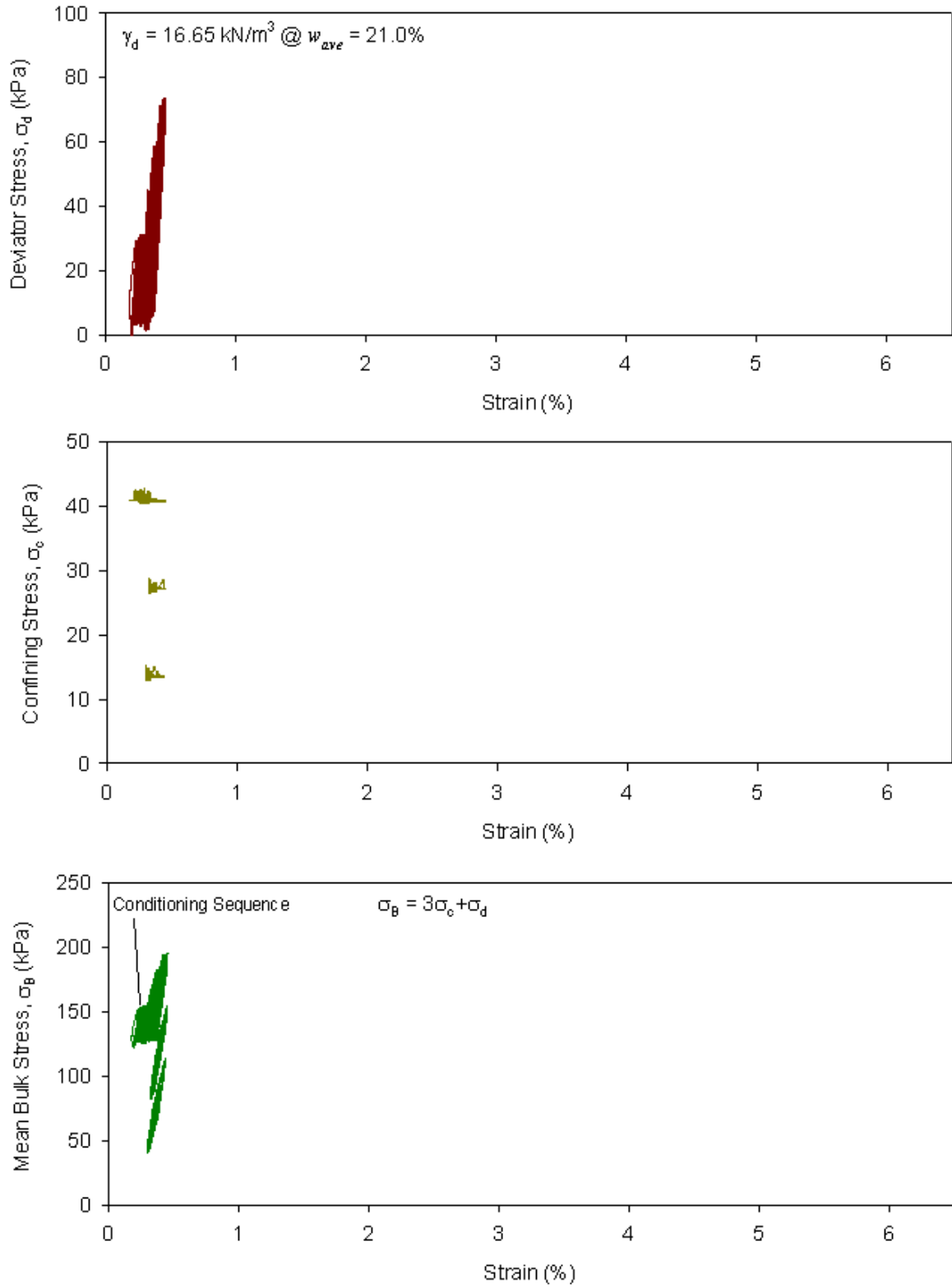


Figure 102. Cyclic stress-strain curves from M_R test for Shelby tube G3 (1.0–1.7 m)

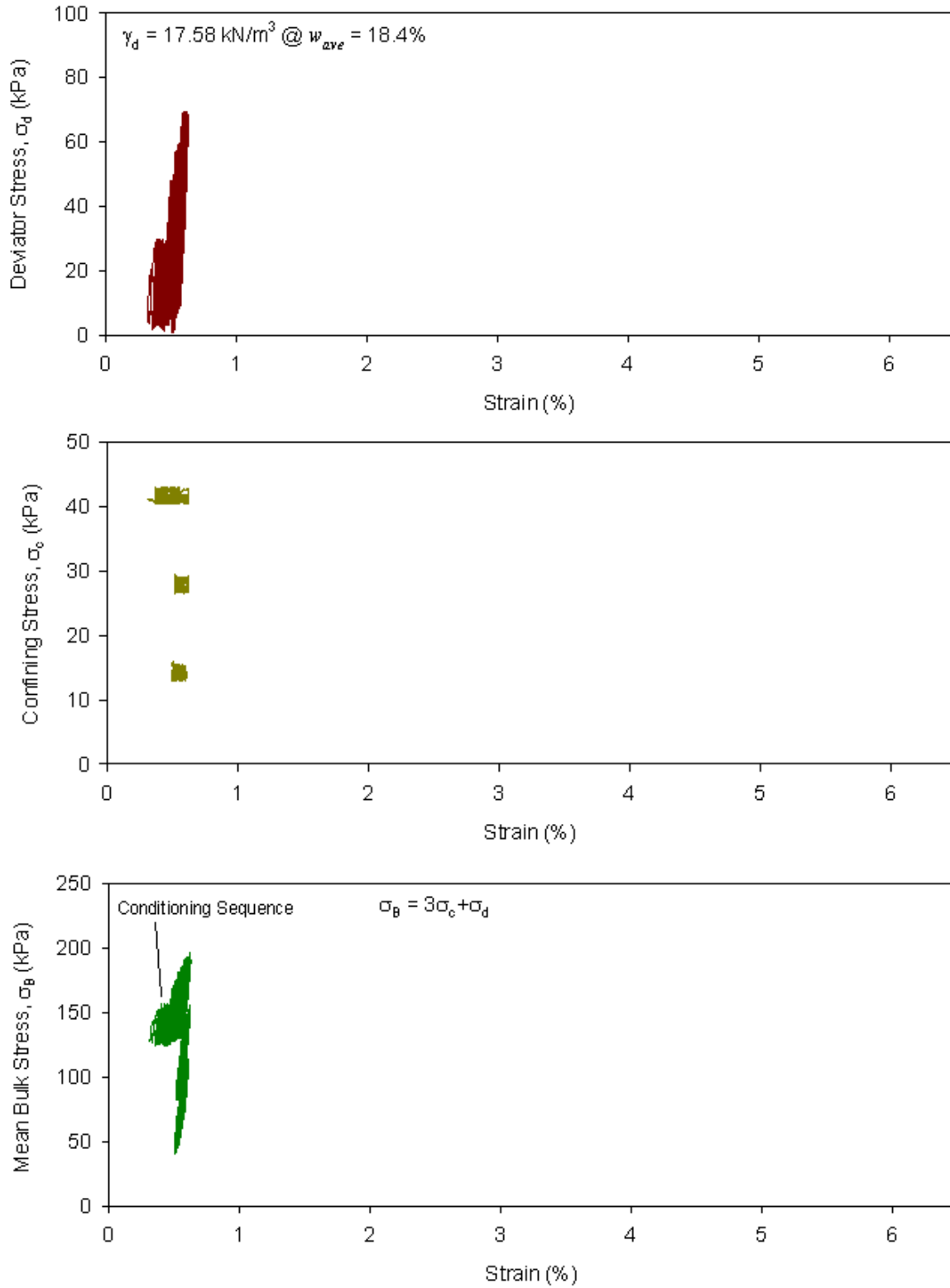


Figure 103. Cyclic stress-strain curves from Mr test for subgrade sample 17.85 kN/m³ @ 18.4% moisture

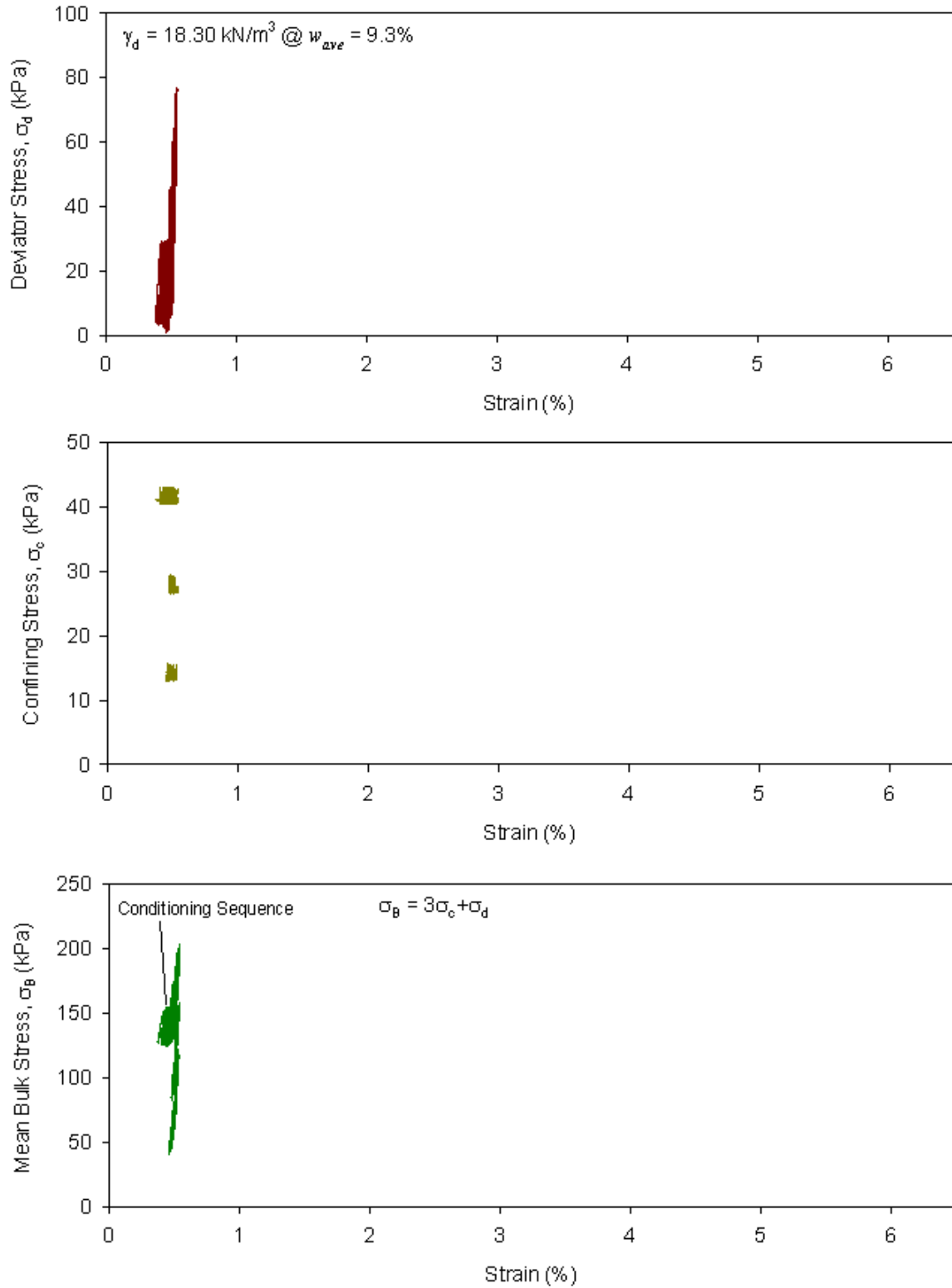


Figure 104. Cyclic stress-strain curves from M_R test for subgrade sample $18.30 \text{ kN/m}^3 @ 9.3\%$ moisture

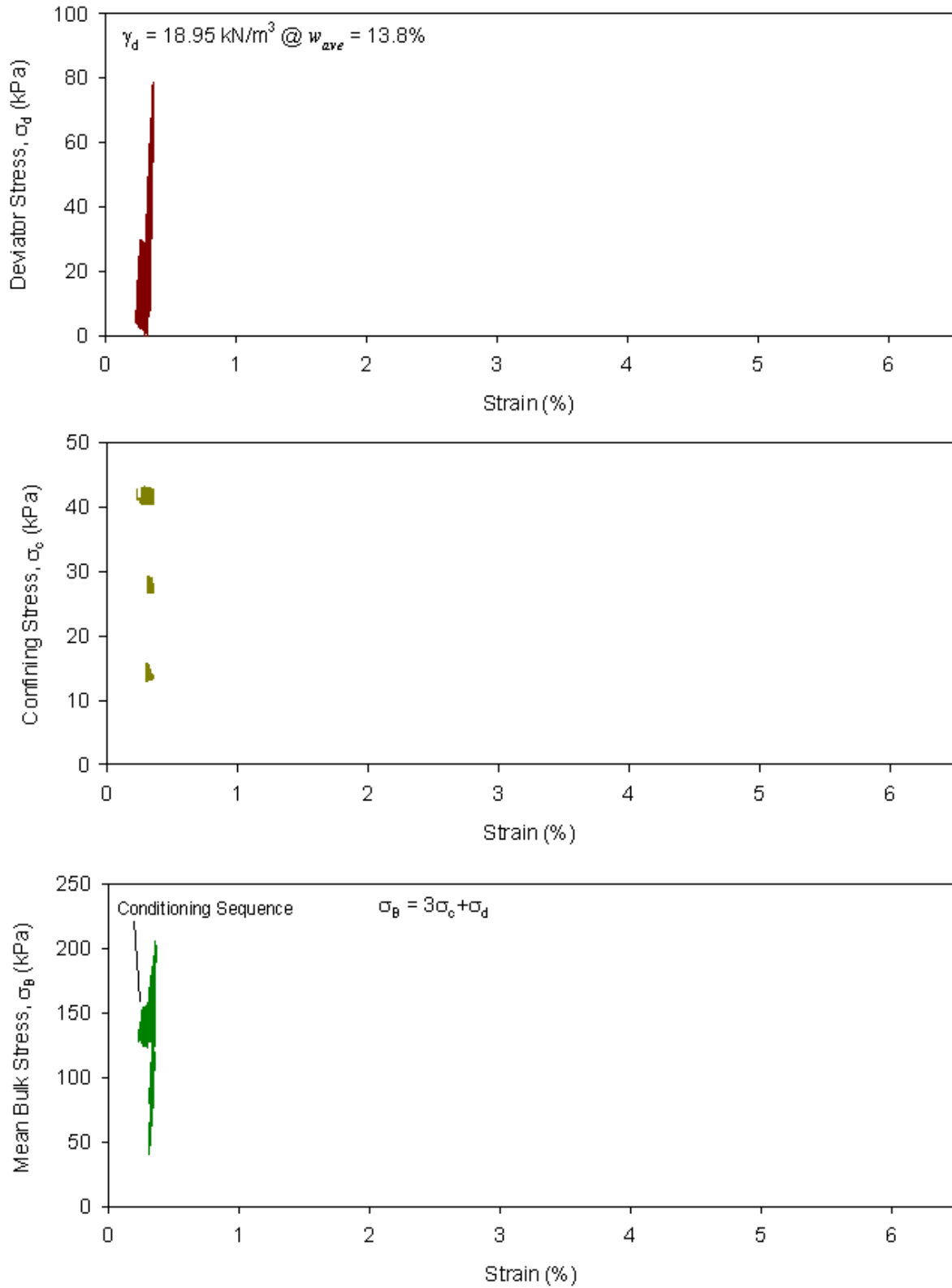


Figure 105. Cyclic stress-strain curves from M_r test for subgrade sample $18.95 \text{ kN/m}^3 @ 13.8\%$ moisture

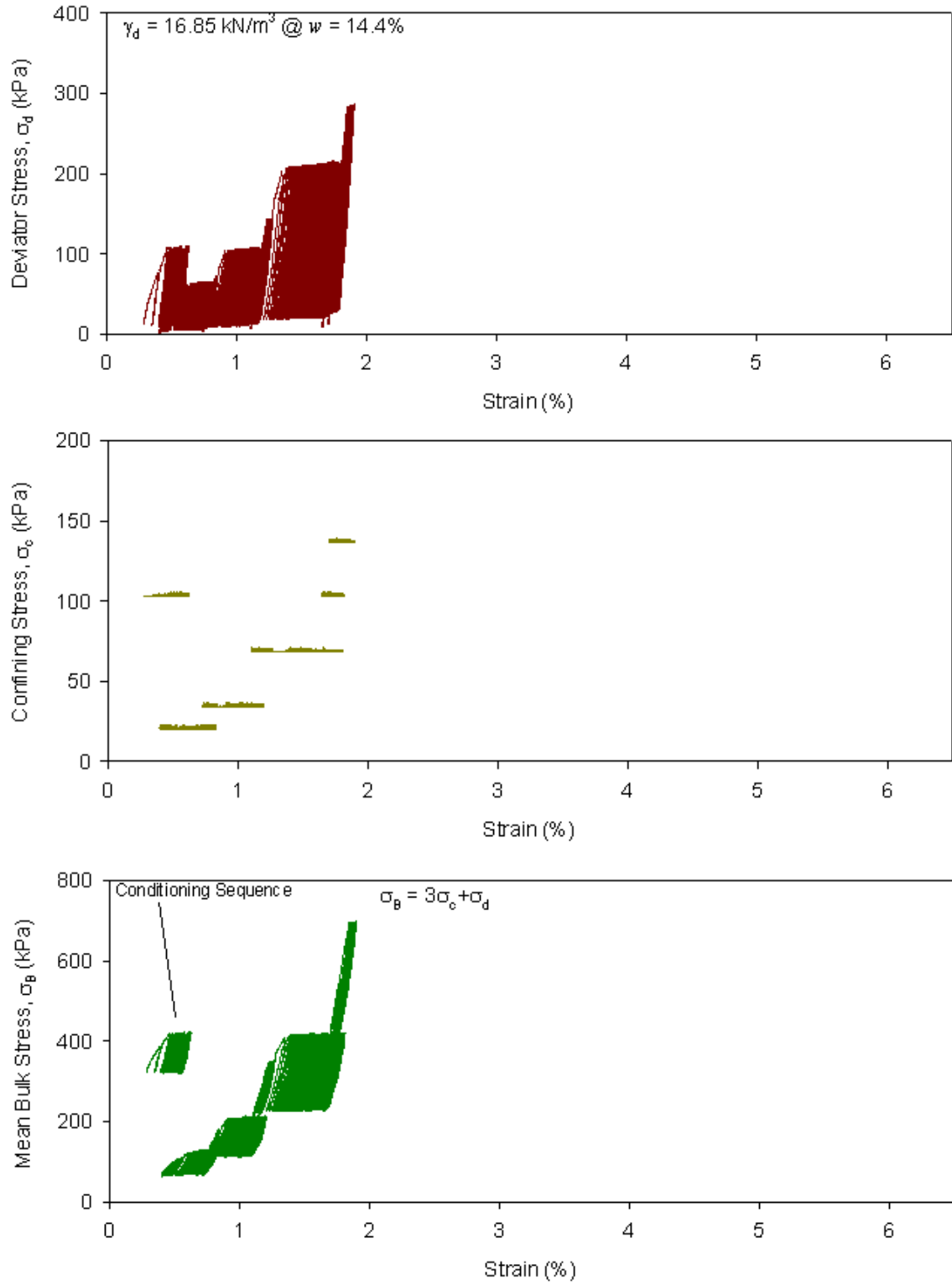


Figure 106. Cyclic stress-strain curves from M_R test for existing sand subbase sample $16.85 \text{ kN/m}^3 @ 14.4\%$ moisture

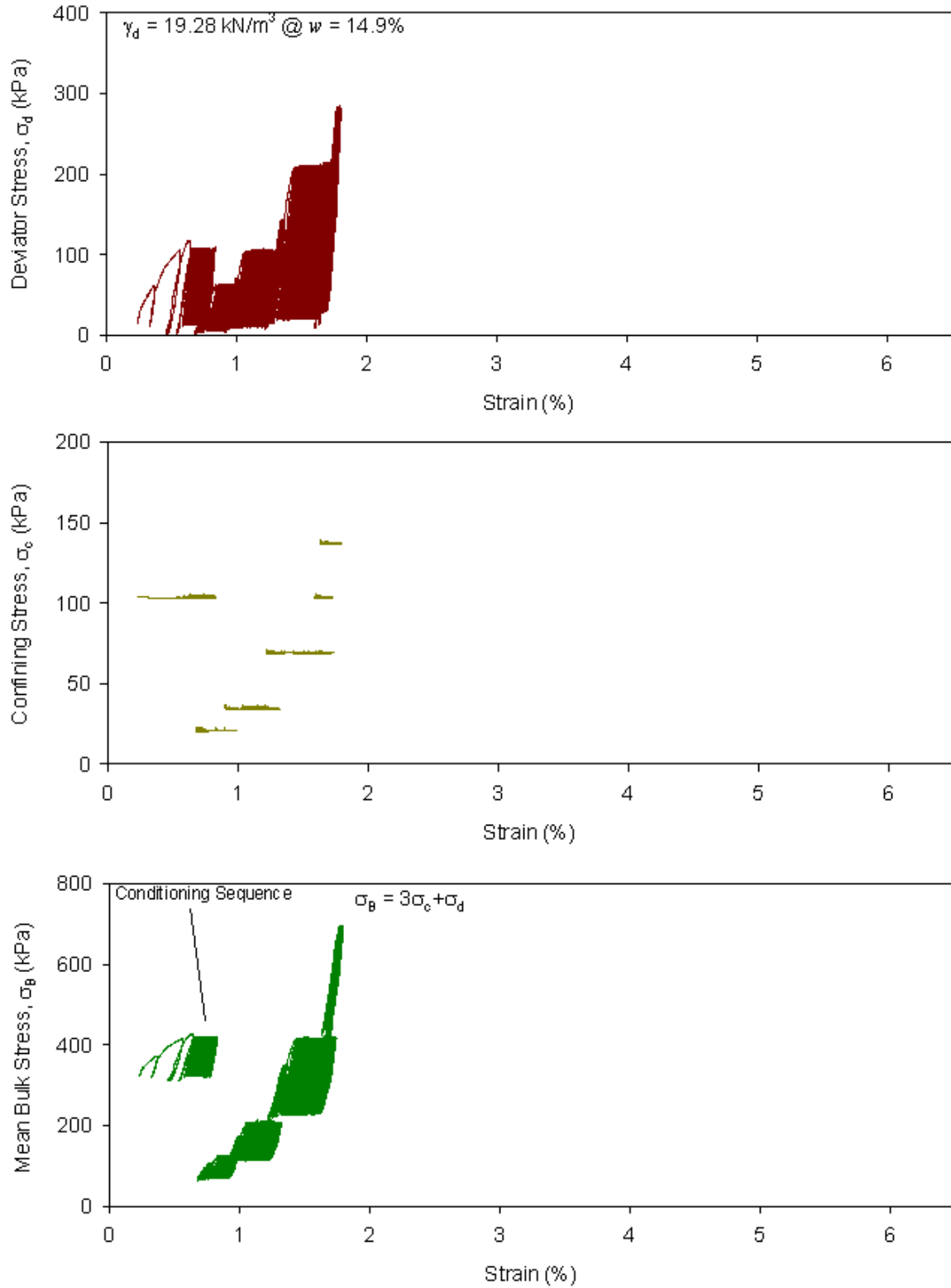


Figure 107. Cyclic stress-strain curves from M_r test for existing sand subbase sample $19.28 \text{ kN/m}^3 @ 14.9\%$ moisture

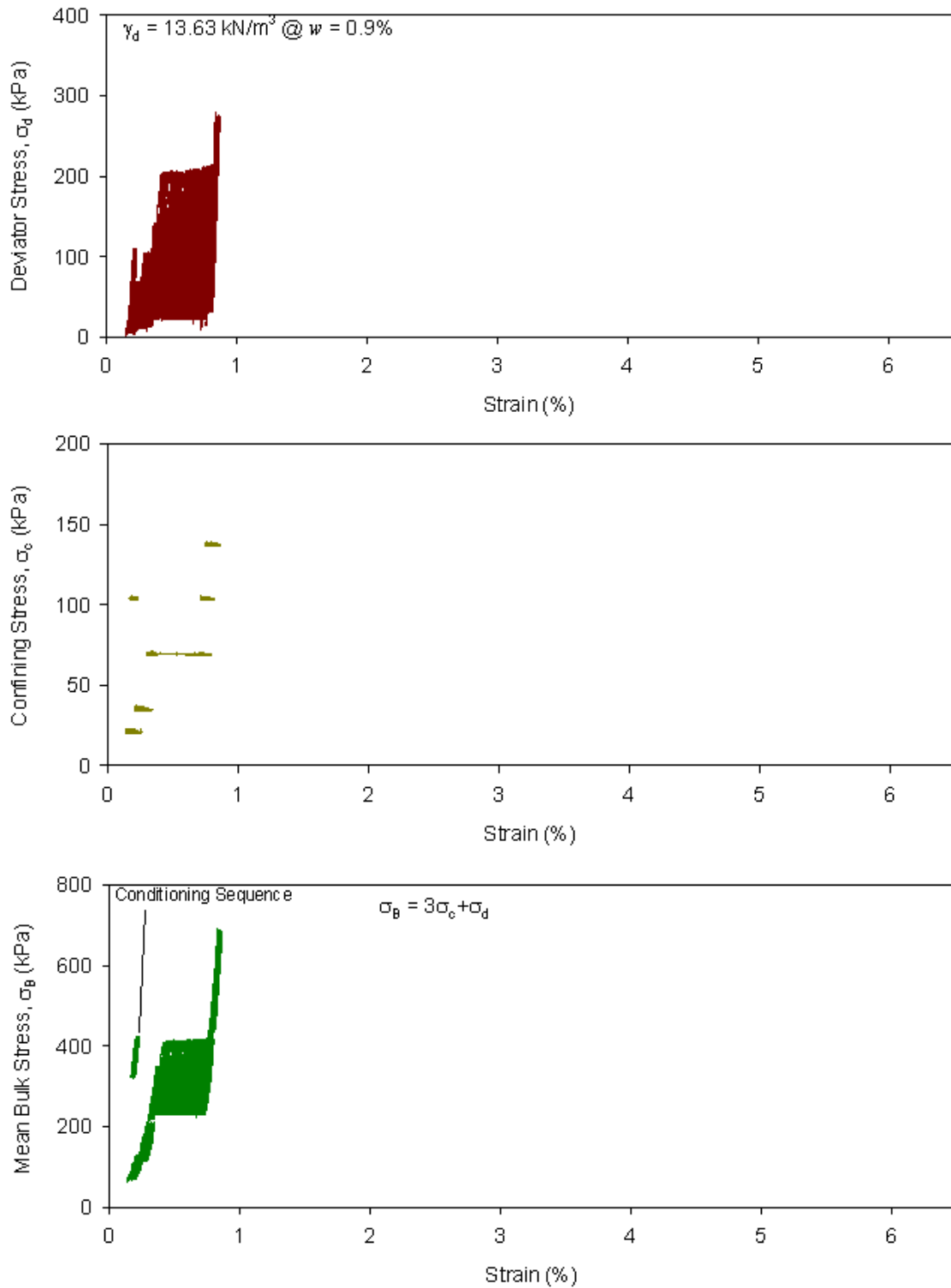


Figure 108. Cyclic stress-strain curves from M_r test for untrimmed base sample $13.63 \text{ kN/m}^3 @ 0.9\%$ moisture

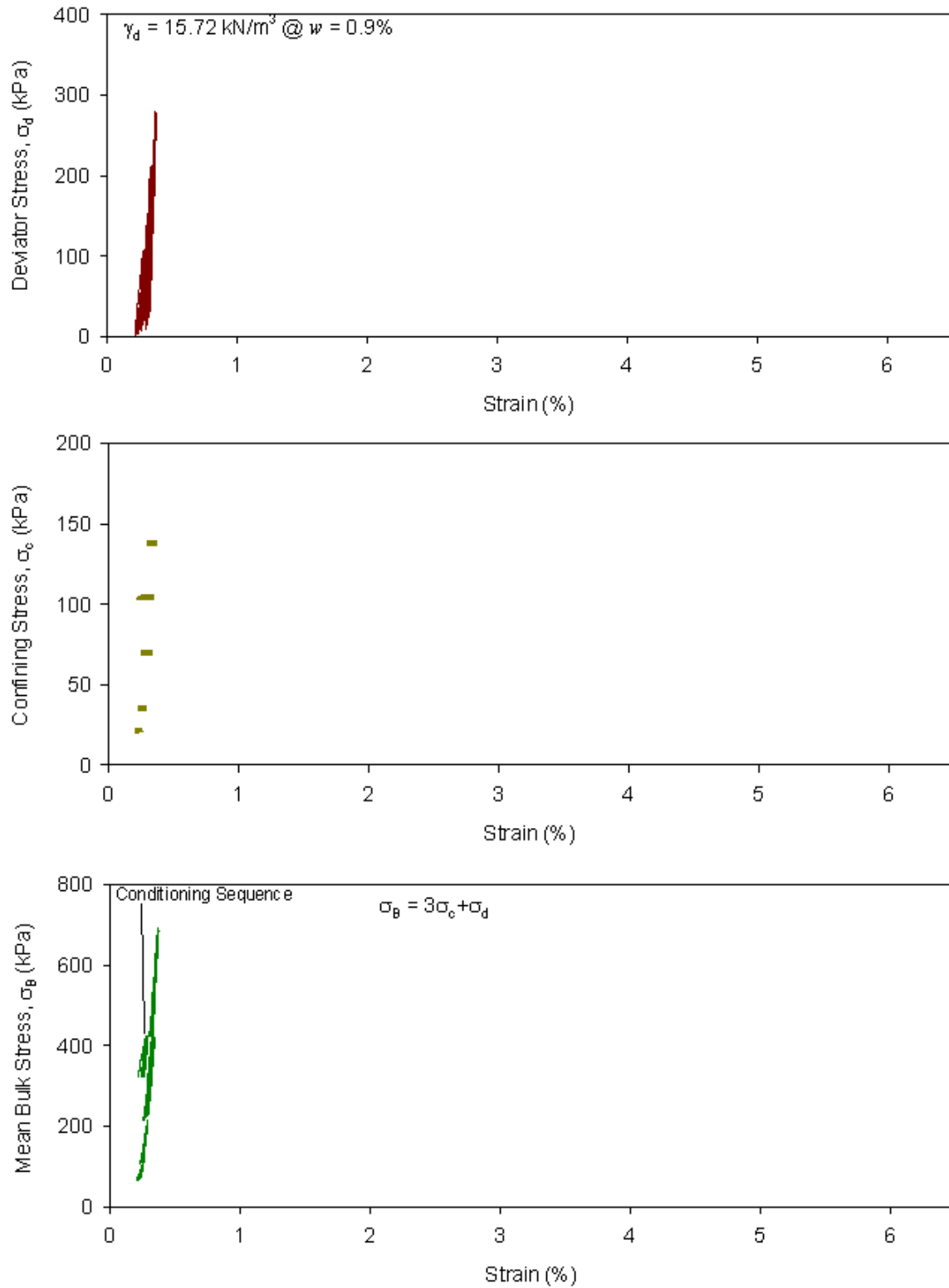


Figure 109. Cyclic stress-strain curves from M_r test for untrimmed base sample $15.72 \text{ kN/m}^3 @ 0.9\%$ moisture

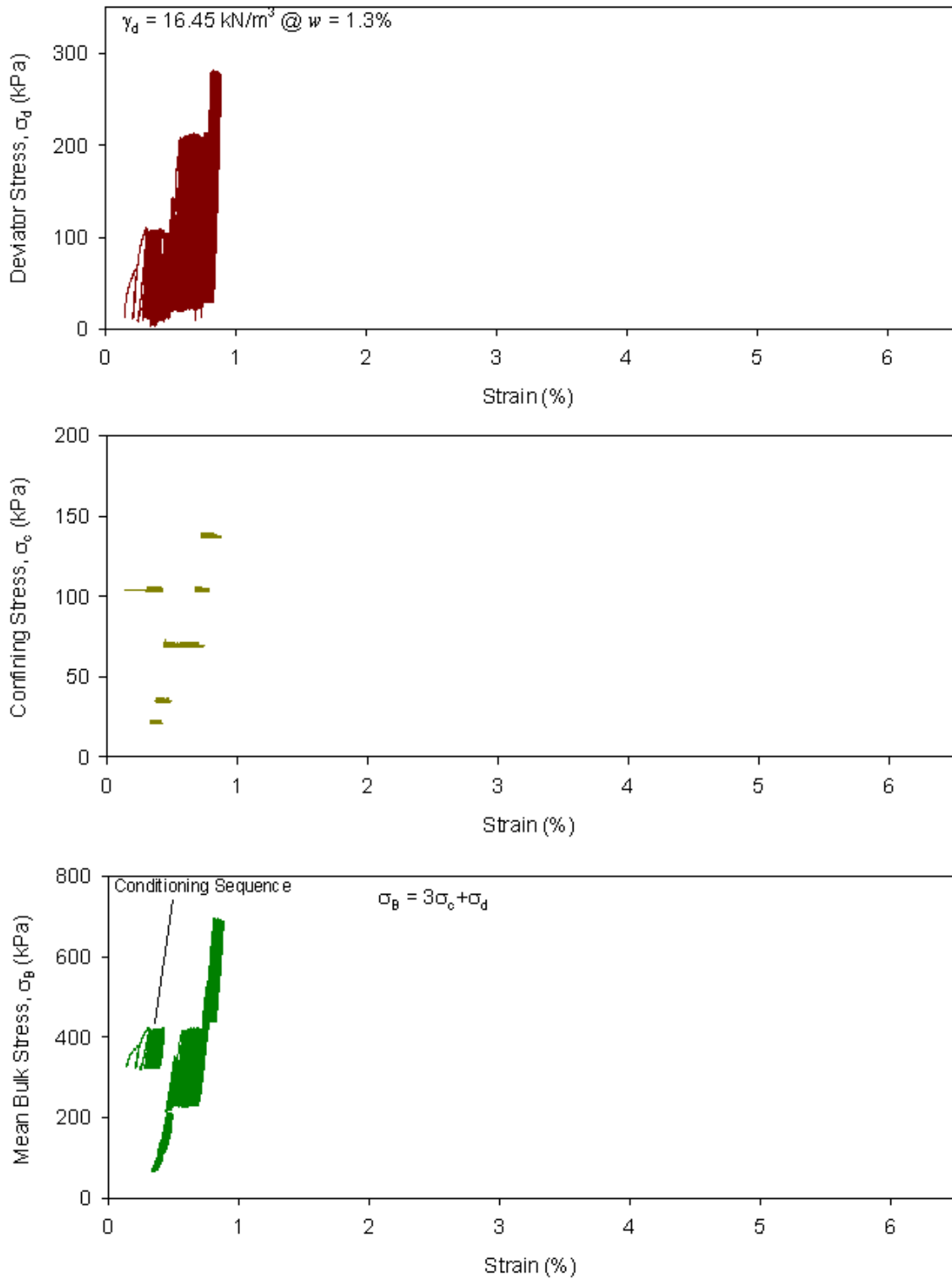


Figure 110. Cyclic stress-strain curves from M_r test for untrimmed base sample $16.45 \text{ kN/m}^3 @ 1.3\%$ moisture, scalp and replace method

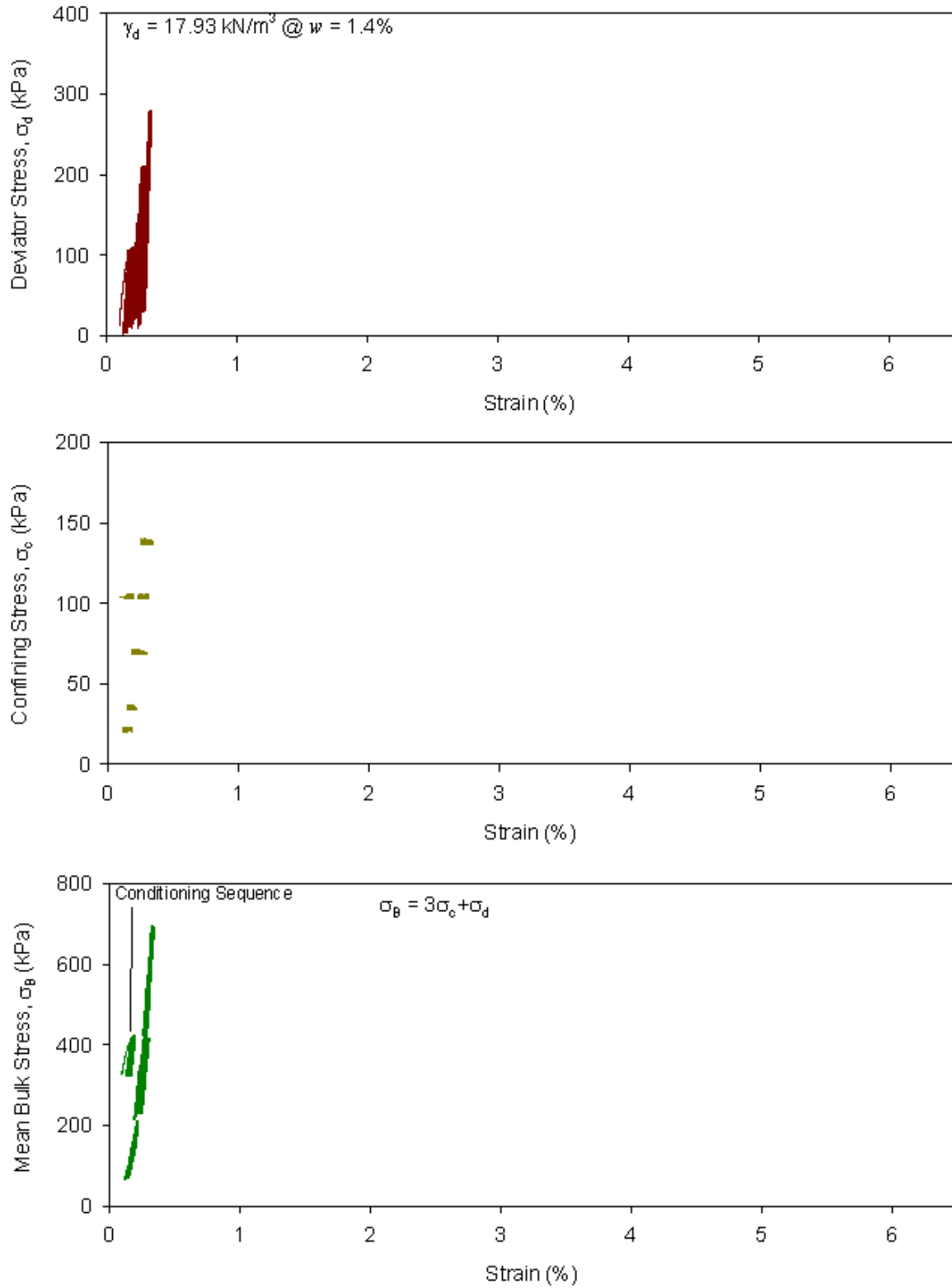


Figure 111. Cyclic stress-strain curves from M_r test for untrimmed base sample $17.93 \text{ kN/m}^3 @ 1.4\%$ moisture, scalp and replace method

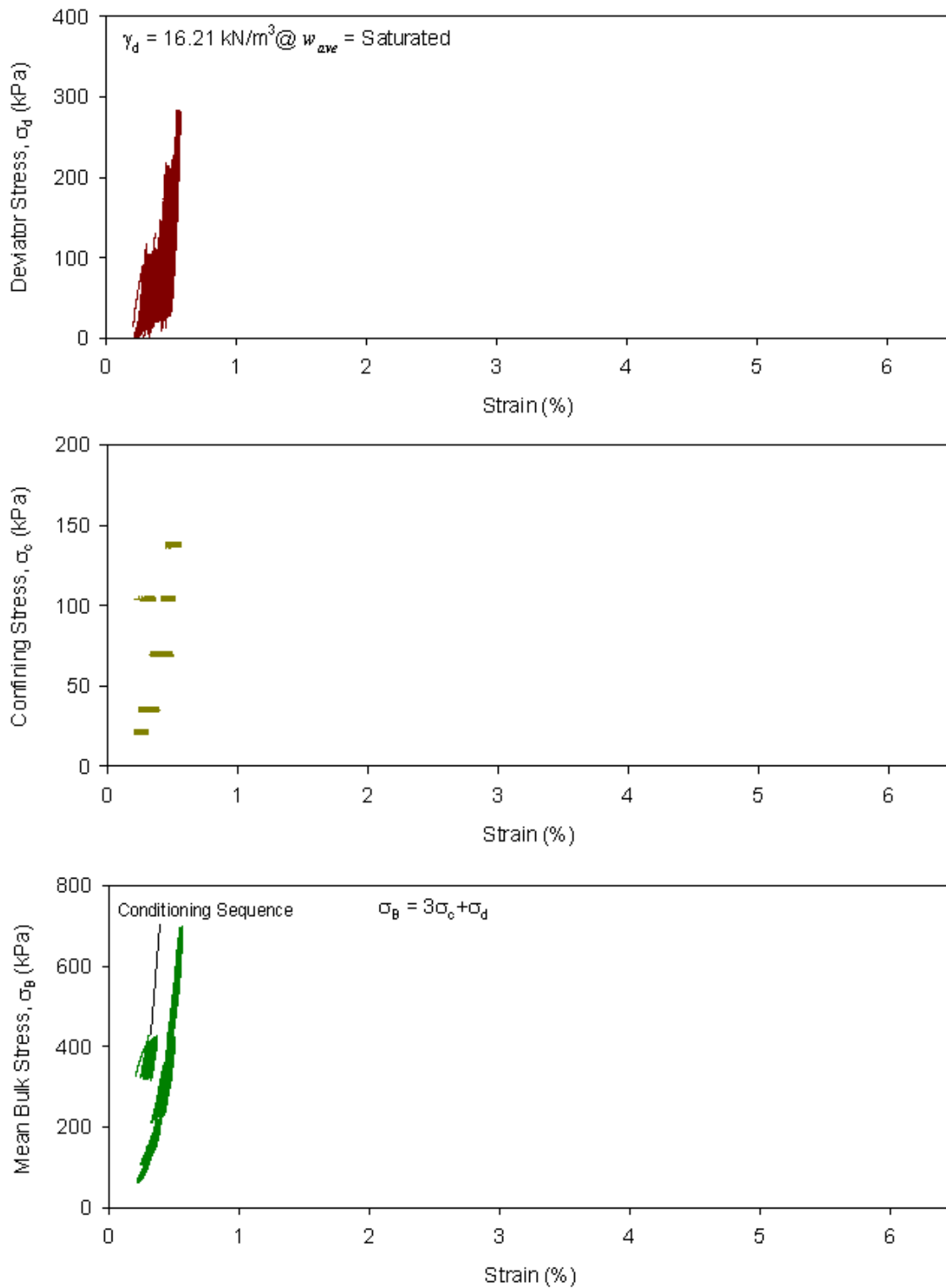


Figure 112. Cyclic stress-strain curves from M_r test for untrimmed base sample 16.21 kN/m³ back saturated, scalp and replace method

**APPENDIX E: SEM IMAGES AND ELEMENTAL ANALYSIS RESULTS FOR OGDC
BASE MATERIAL**

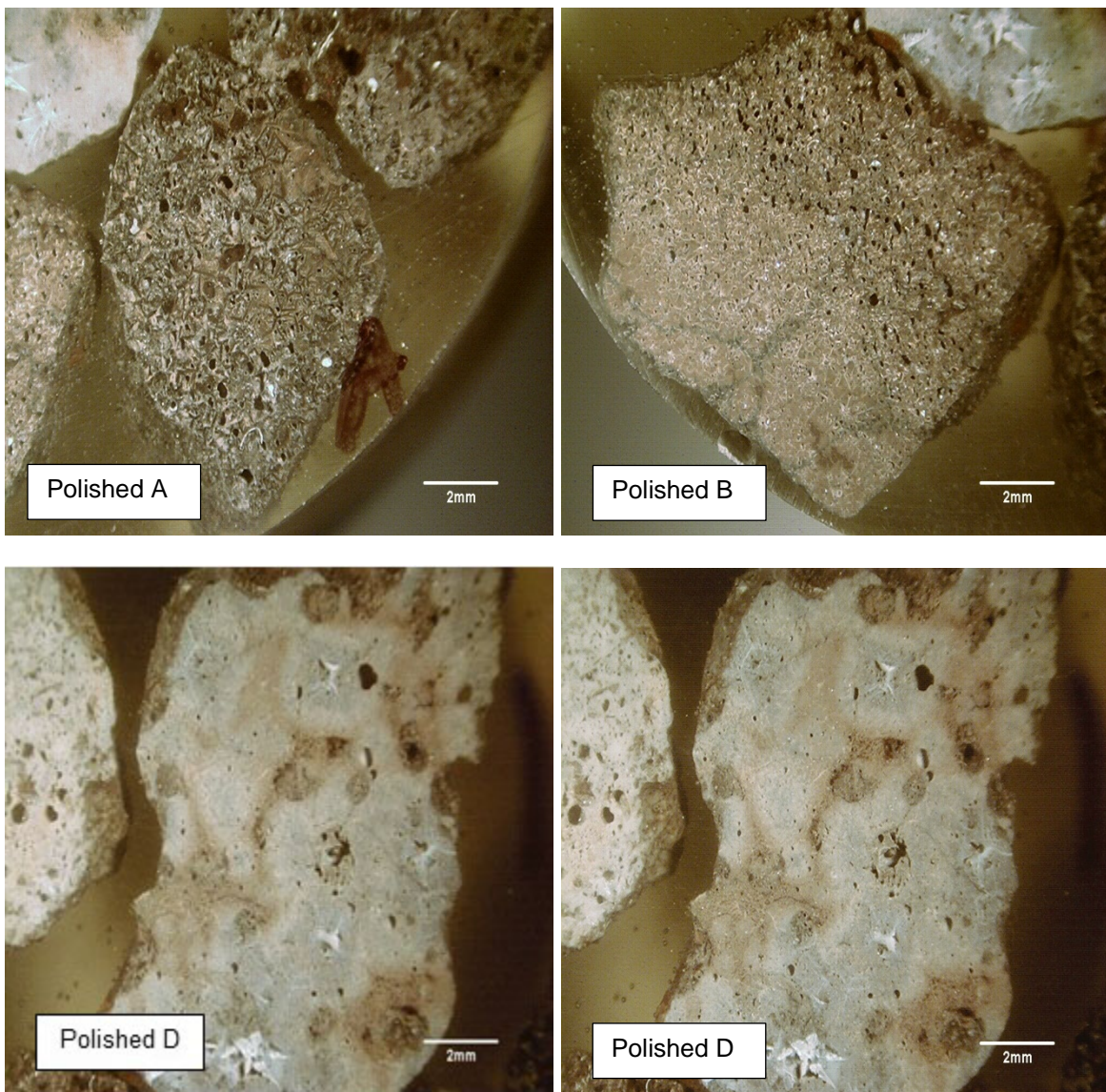


Figure 113. Color stereo microscope images of polished surfaces A, B, C, and D at 2 mm magnification

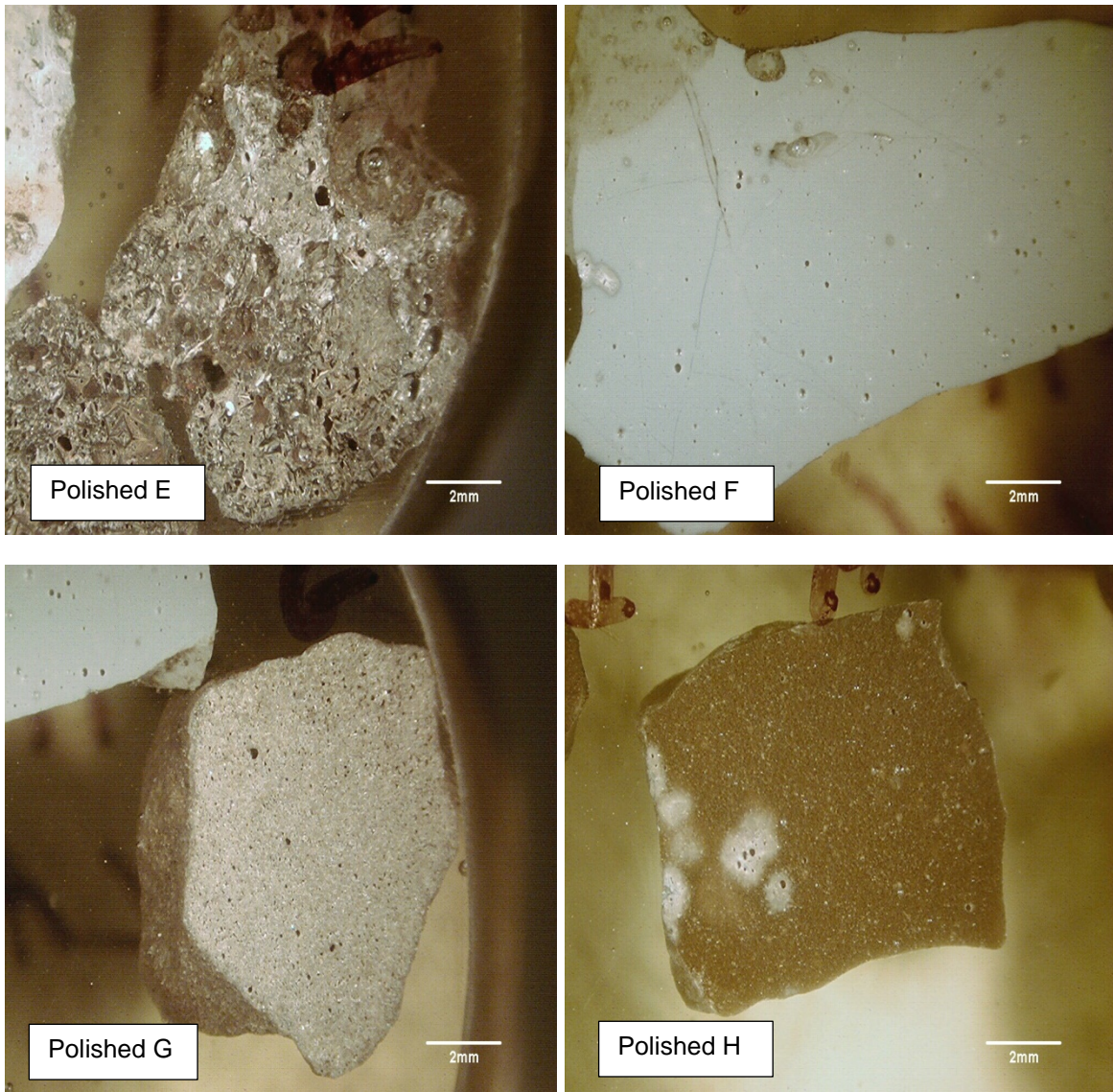


Figure 114. Color stereo microscope images of polished surfaces E, F, G, and H at 2 mm magnification

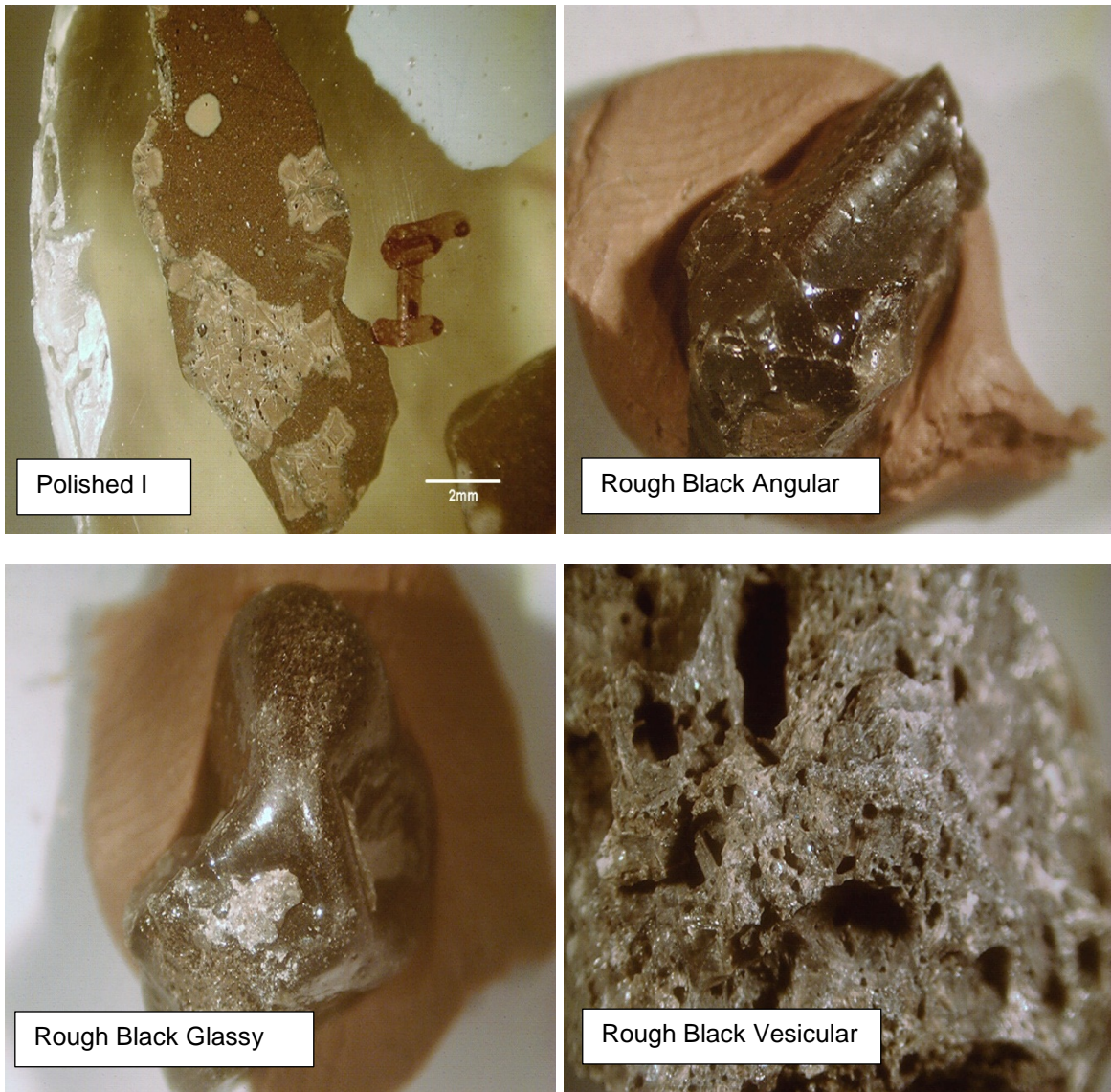


Figure 115. Color stereo microscope images of polished surface I, rough black angular, rough black glassy, and rough black vesicular surfaces at 2 mm magnification

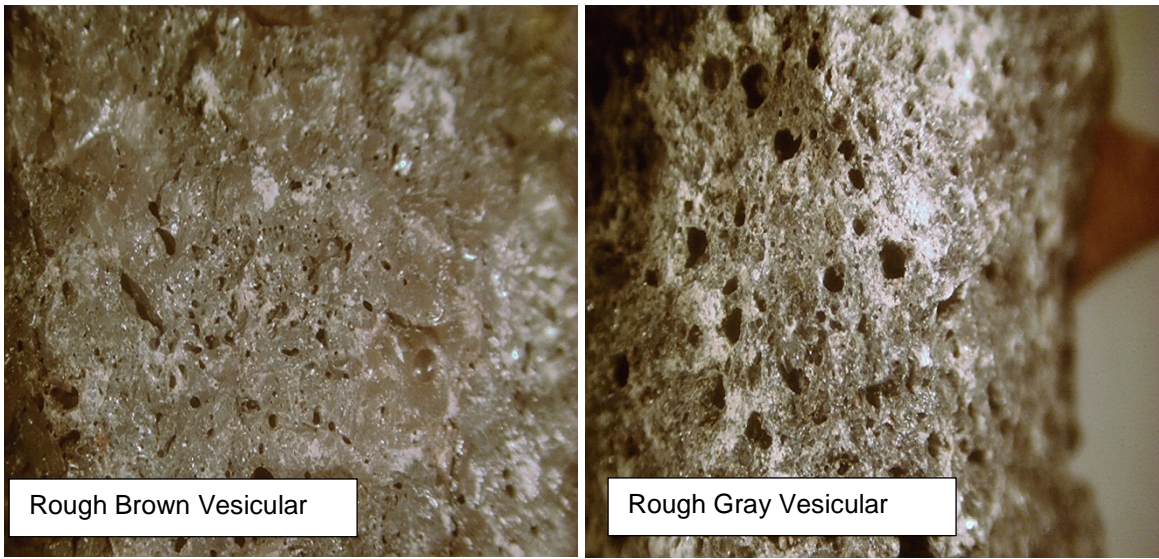


Figure 116. Color stereo microscope images of rough brown and gray vesicular surfaces at 2 mm magnification

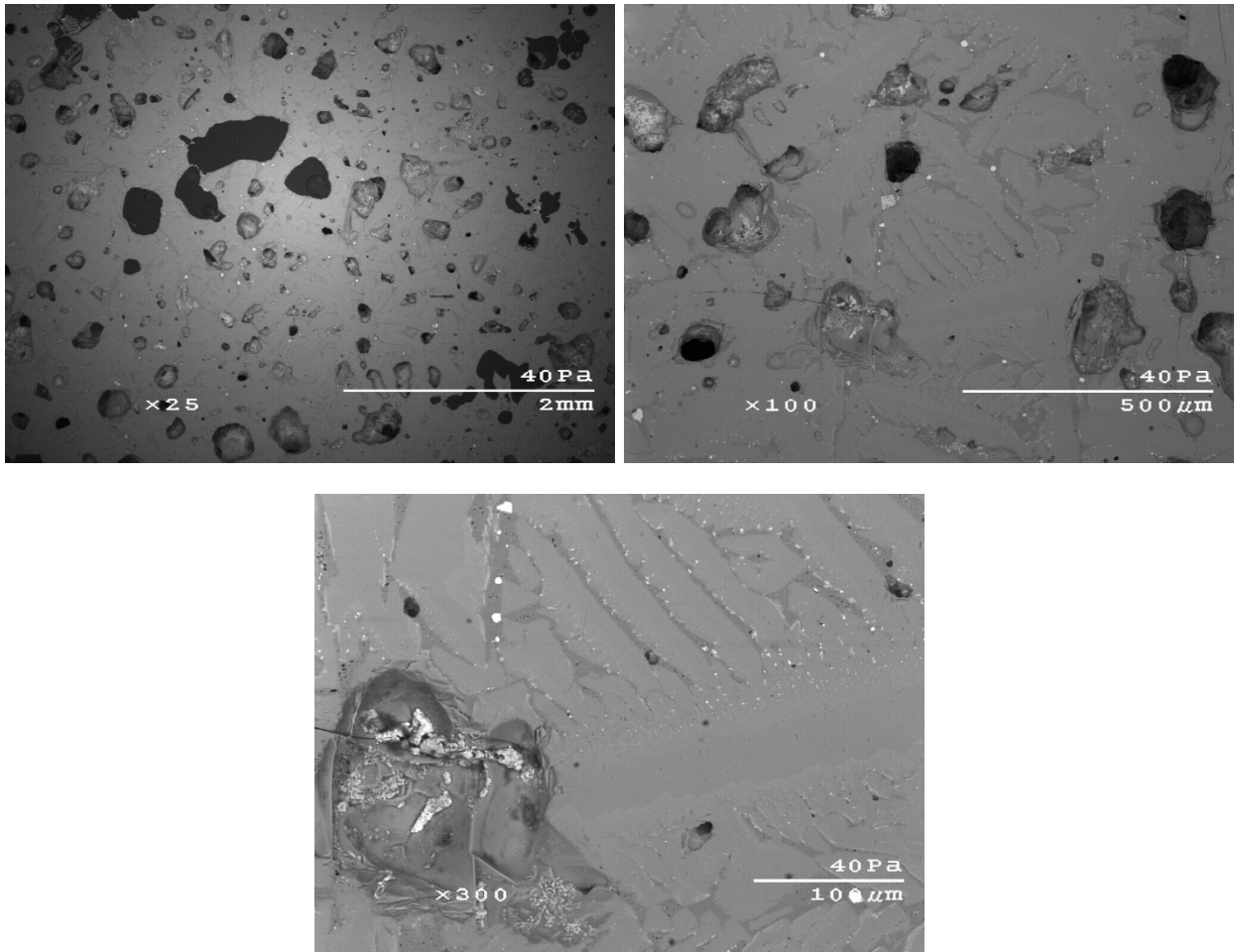


Figure 117. SEM images of polished surface A at 25x, 100x, and 300x magnification

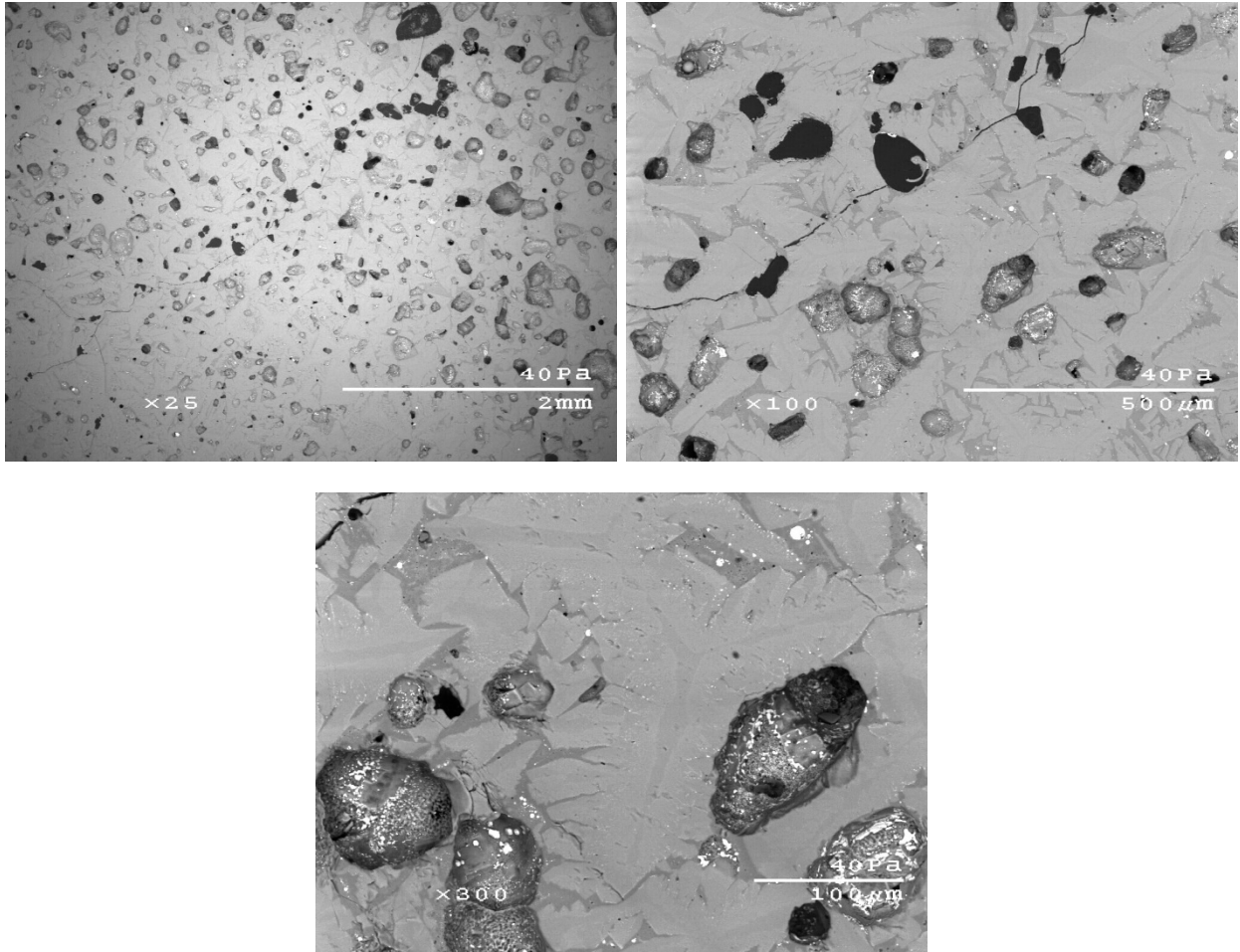


Figure 118. SEM images of polished surface B at 25x, 100x, and 300x magnification

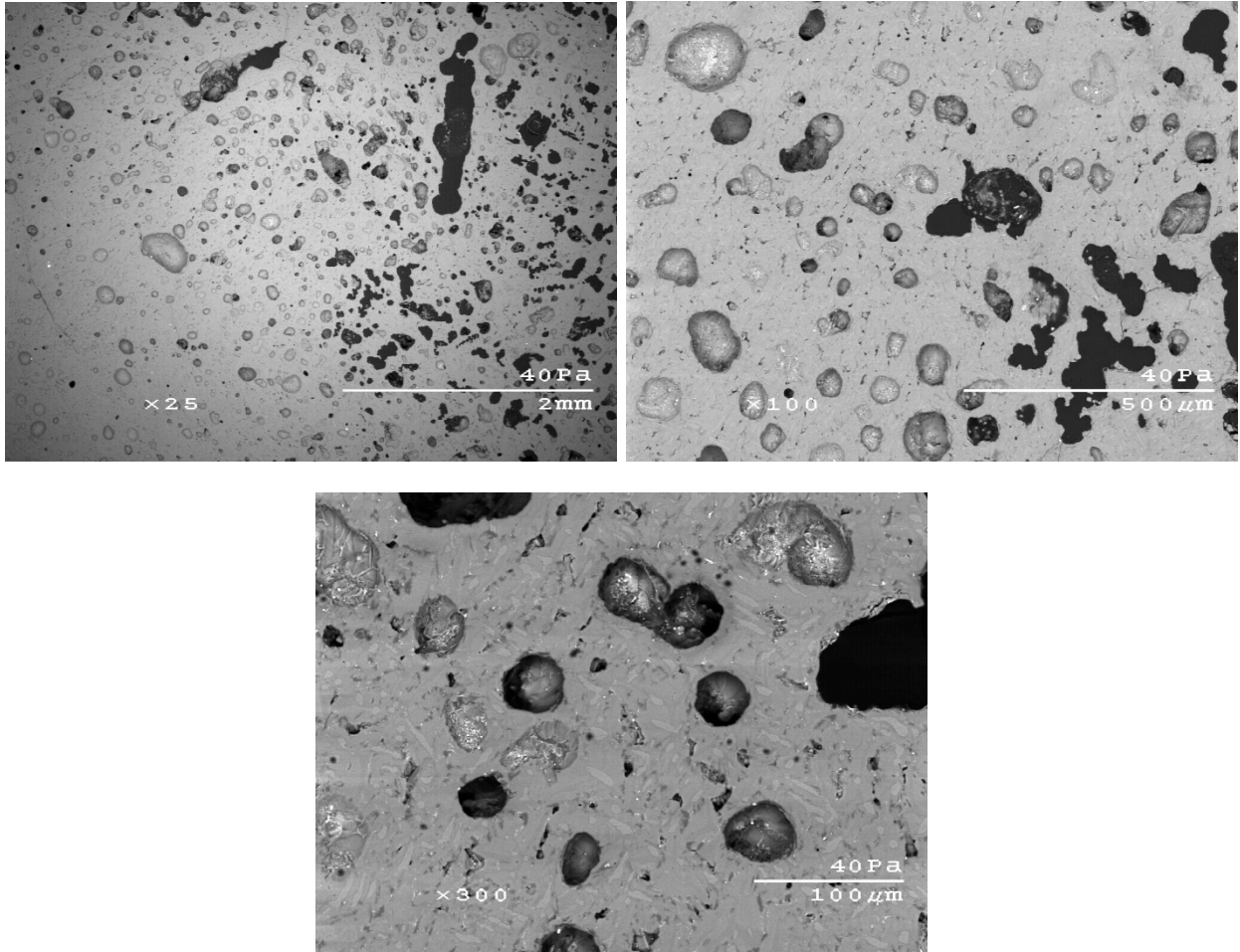


Figure 119. SEM images of polished surface C at 25x, 100x, and 300x magnification

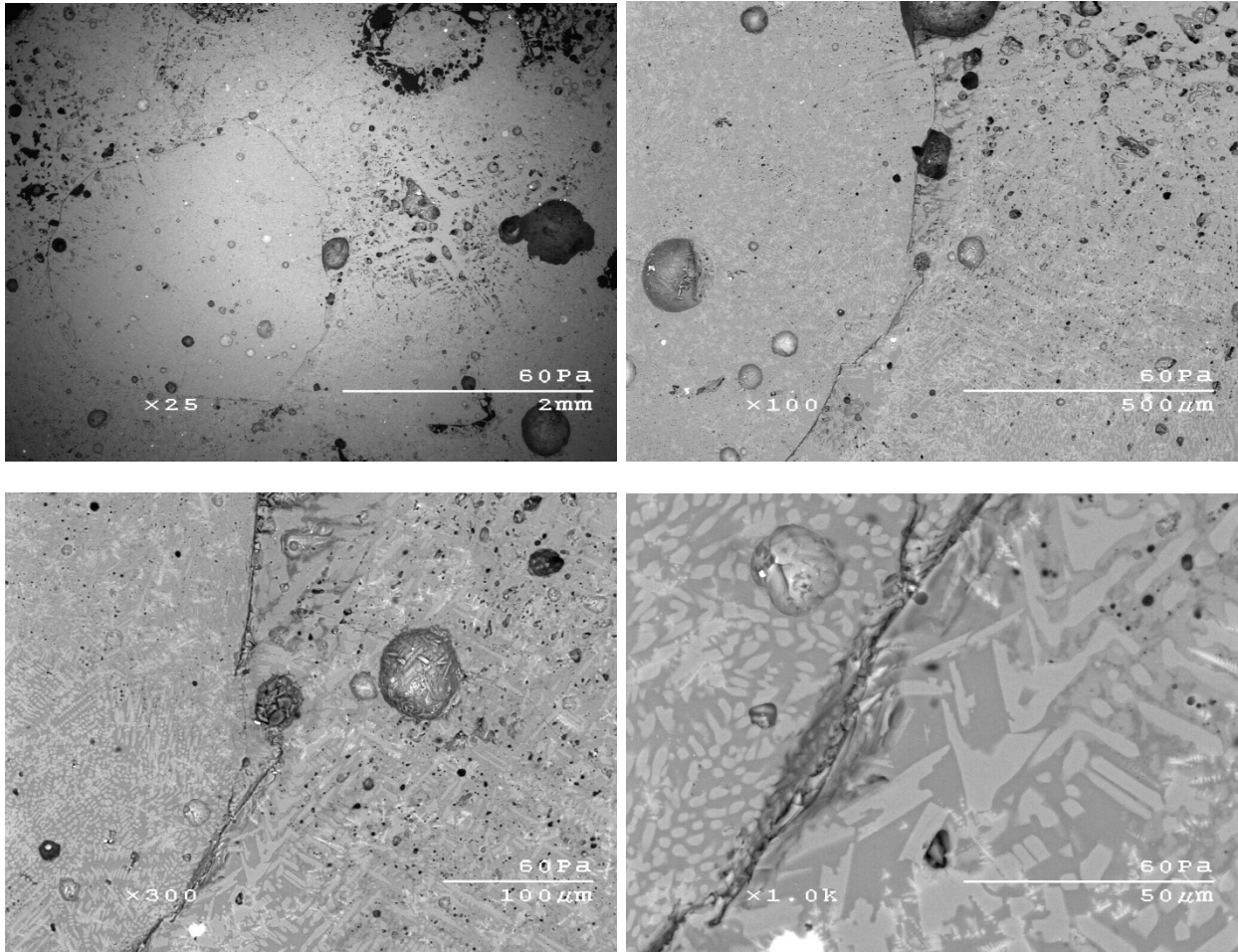


Figure 120. SEM images of polished surface D at 25x, 100x, 300x, and 1000x magnification

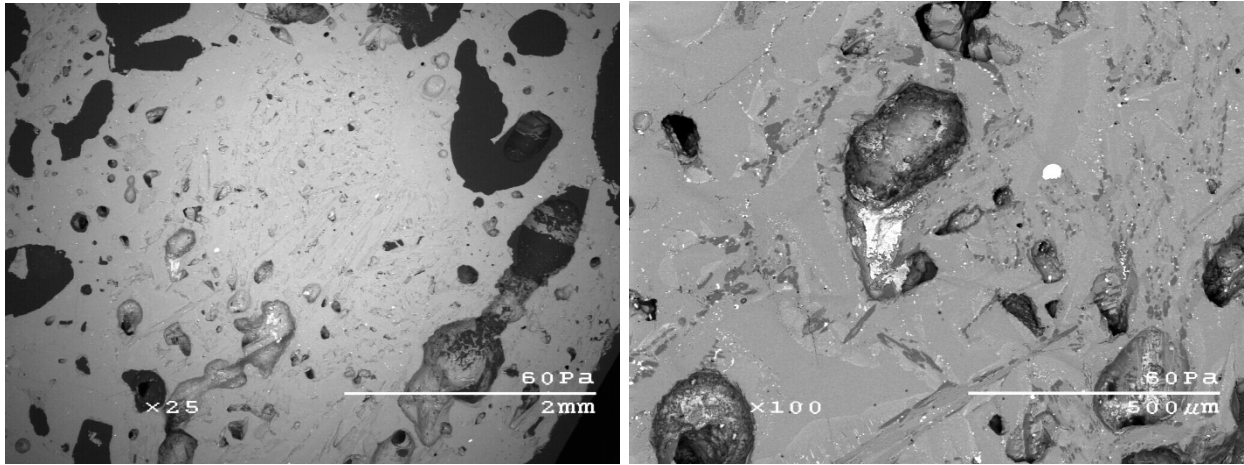


Figure 121. SEM images of polished surface E at 25x and 100x magnification

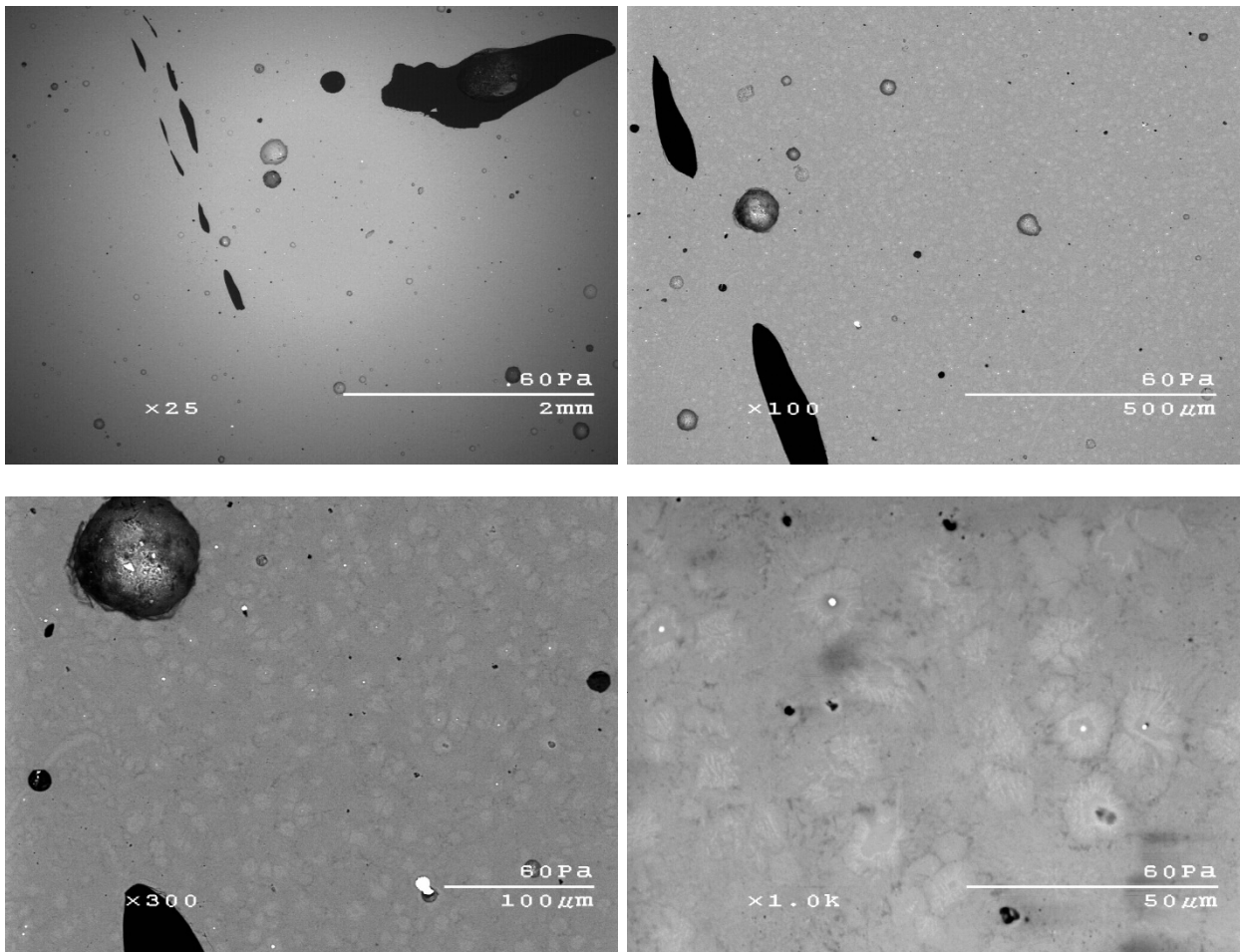


Figure 122. SEM images of polished surface F at 25x, 100x, 300x, and 1000x magnification

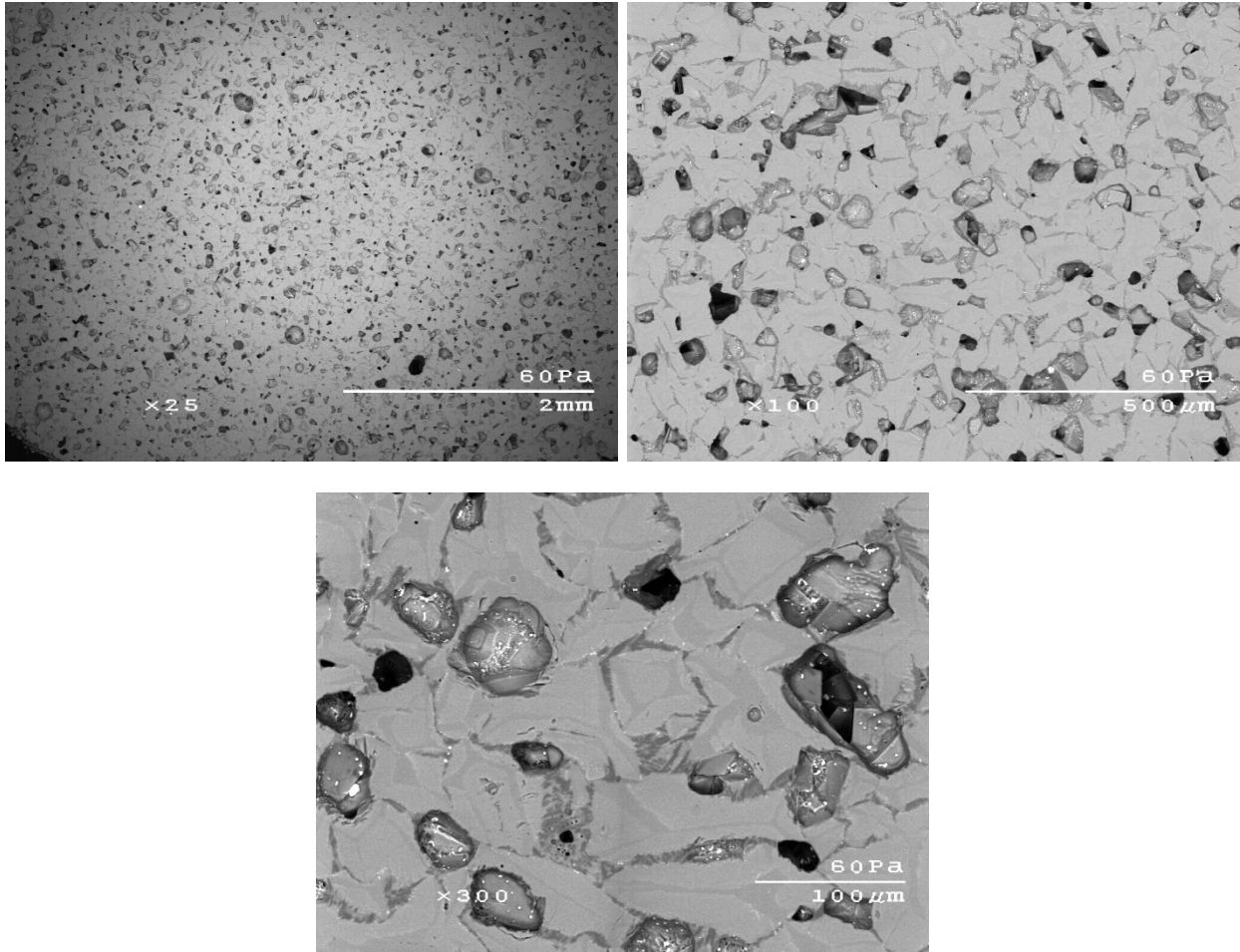


Figure 123. SEM images of polished surface G at 25x, 100x, and 300x magnification

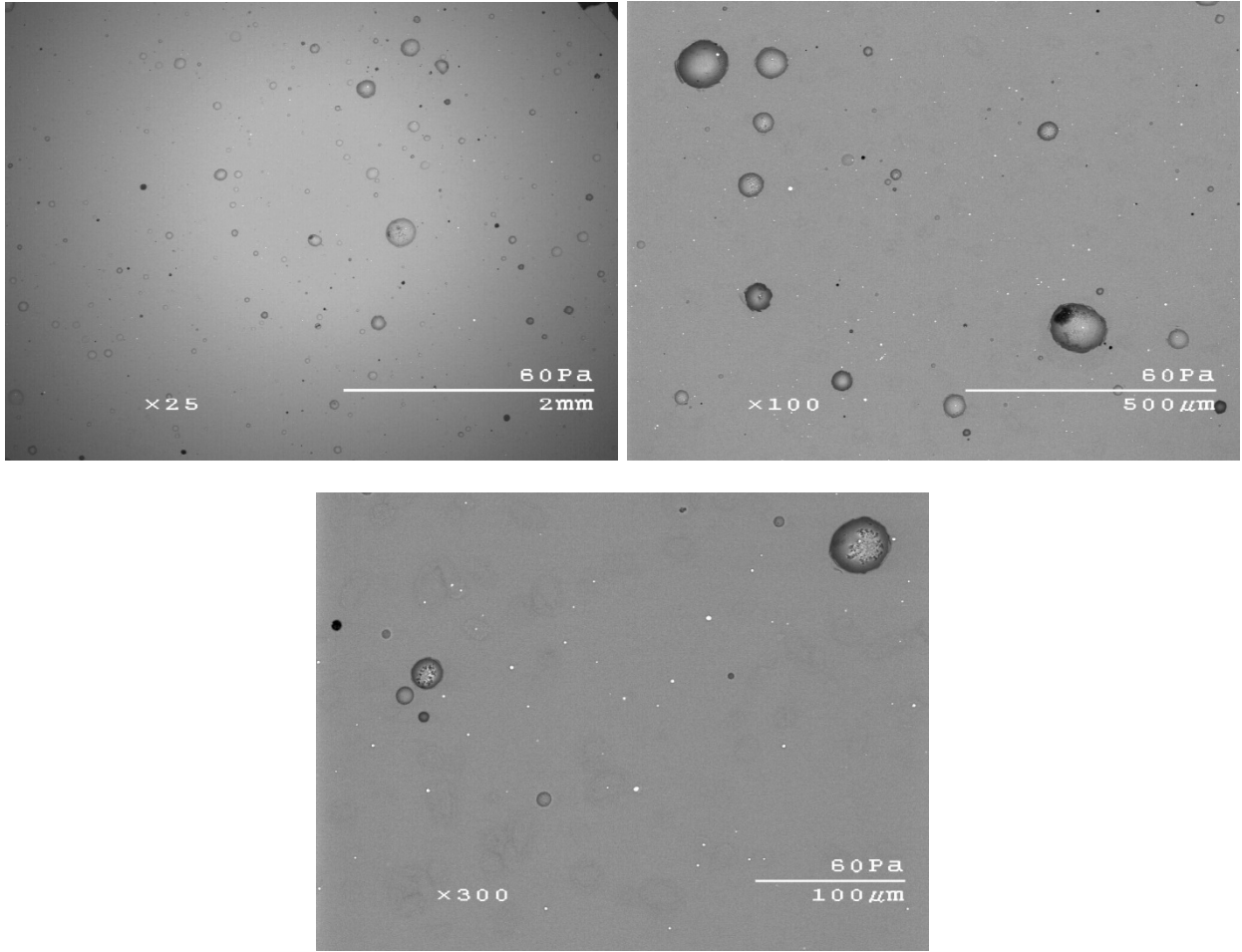


Figure 124. SEM images of polished surface H at 25x, 100x, and 300x magnification

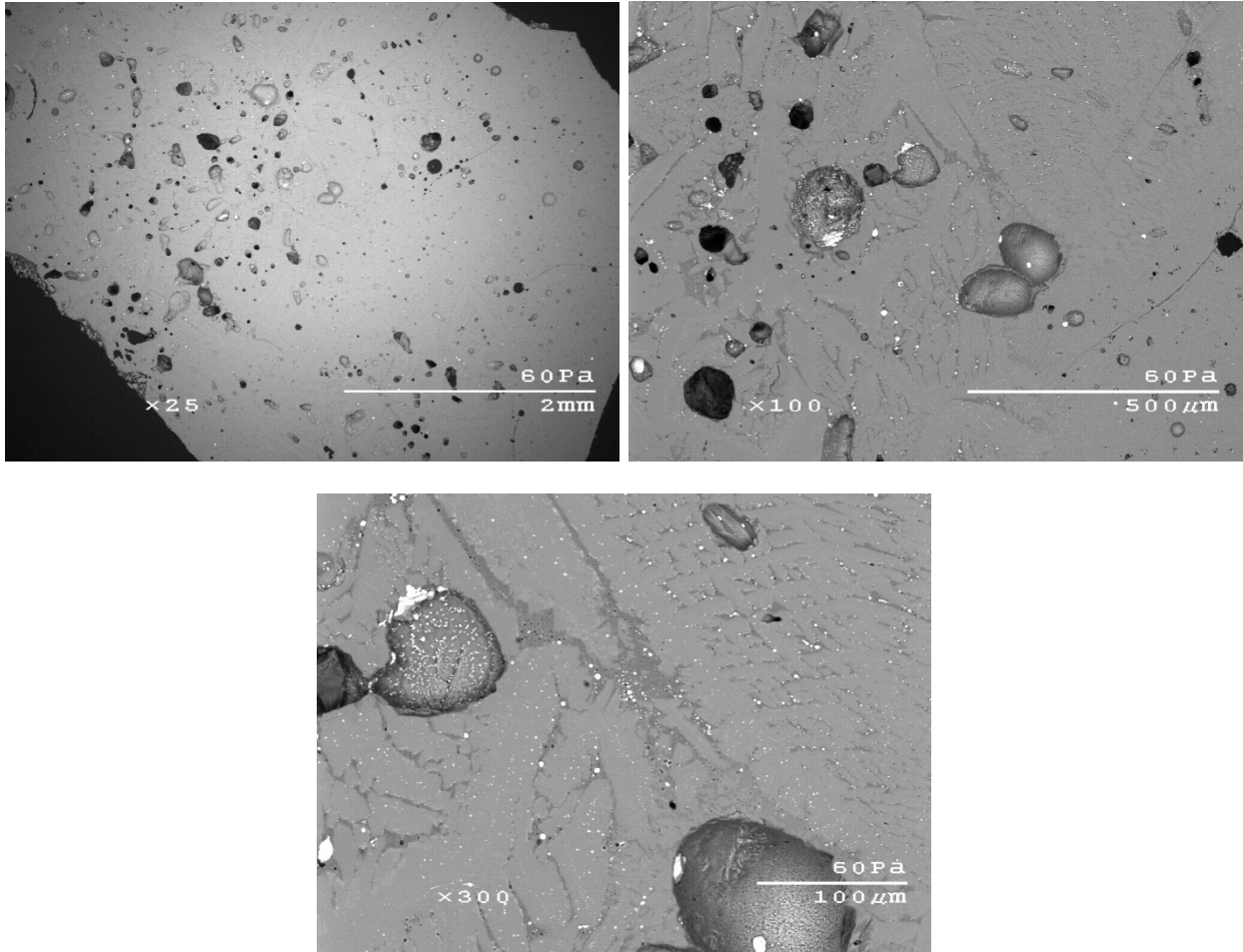


Figure 125. SEM images of polished surface I at 25x, 100x, and 300x magnification

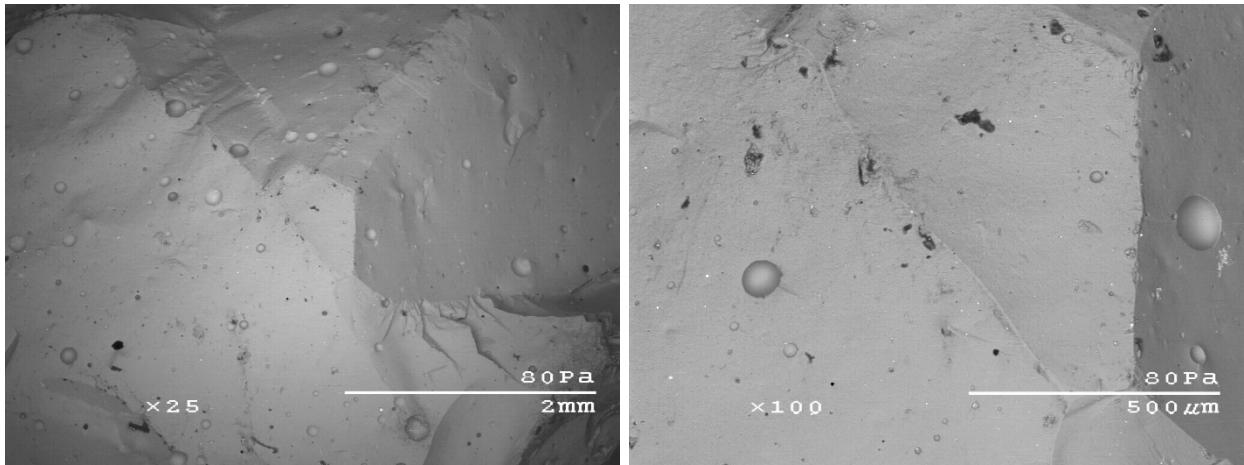


Figure 126. SEM images of black angular surface at 25x and 100x magnification

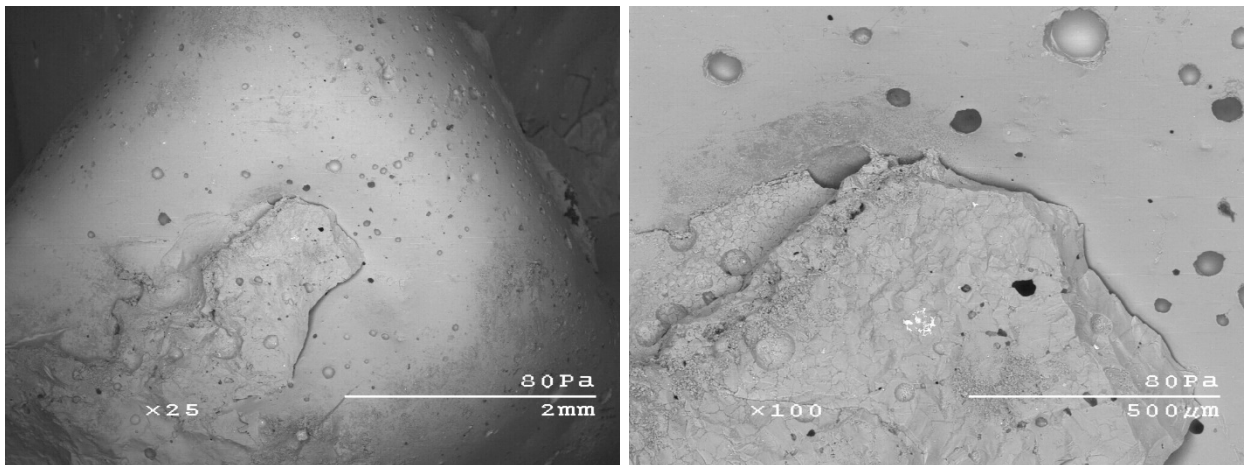


Figure 127. SEM images of black glassy surface at 25x and 100x magnification

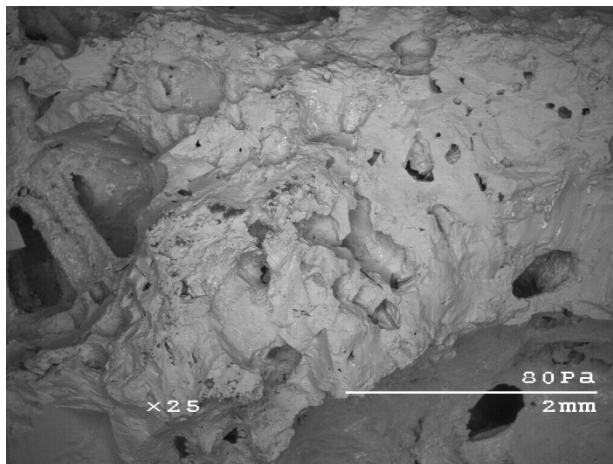


Figure 128. SEM image of black vesicular surface at 25x magnification

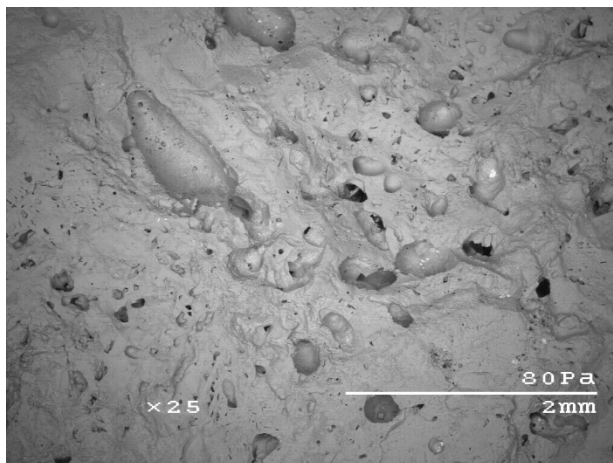


Figure 129. SEM image of brown vesicular surface at 25x magnification

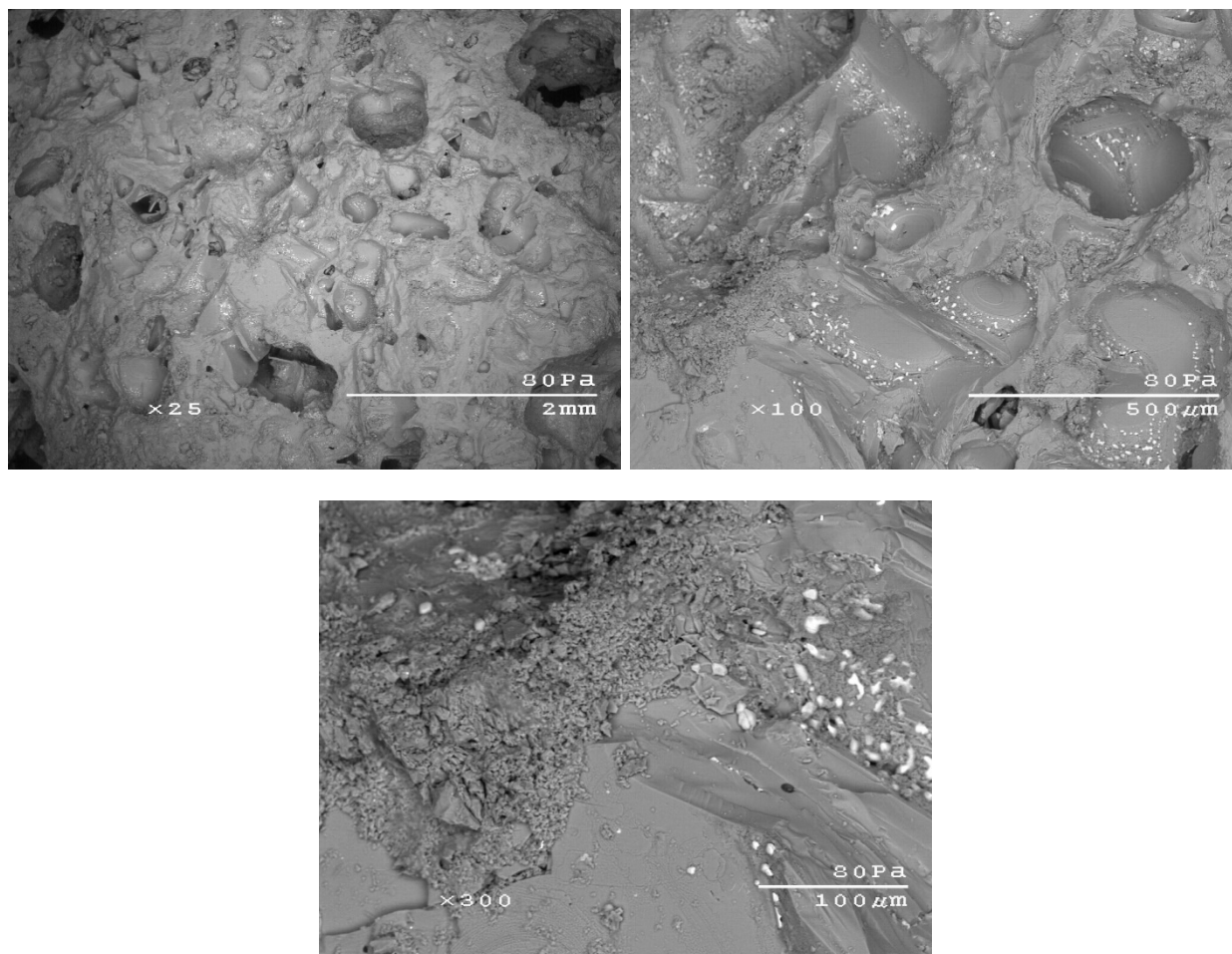


Figure 130. SEM images of gray vesicular surface at 25x, 100x, and 300x magnification

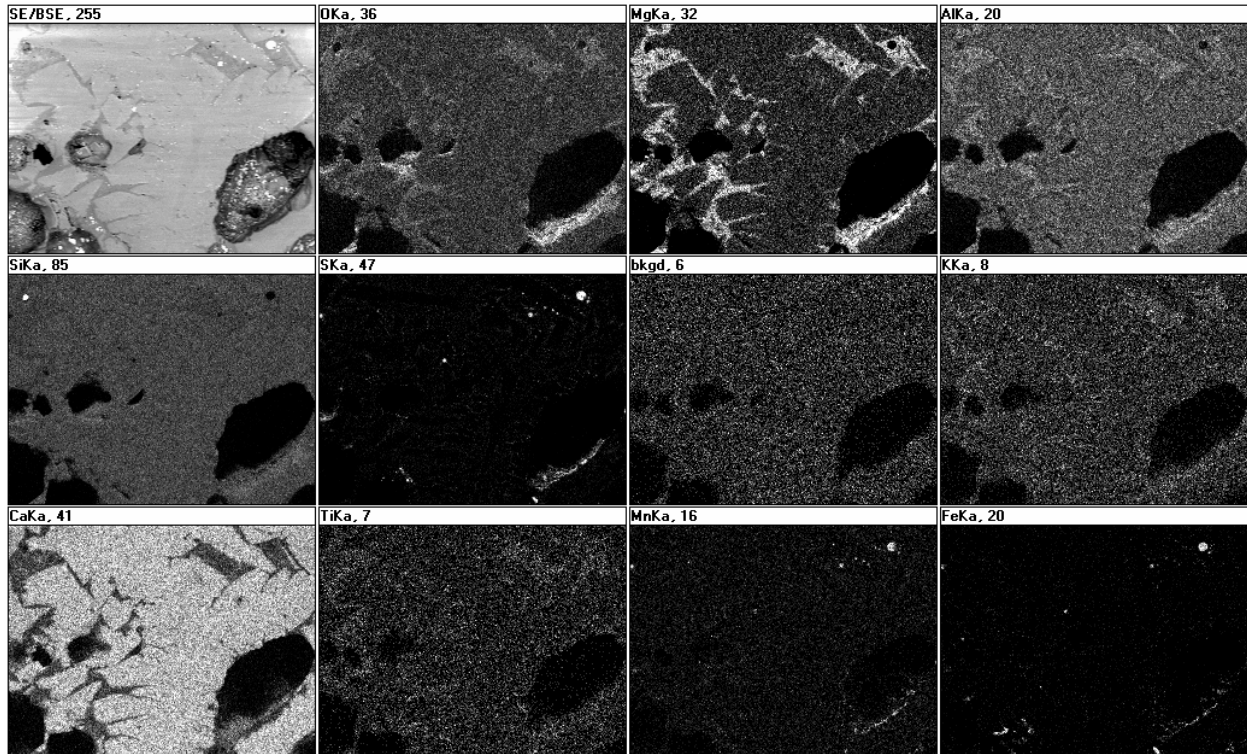


Figure 131. Elemental maps of polished surface B at 400x magnification

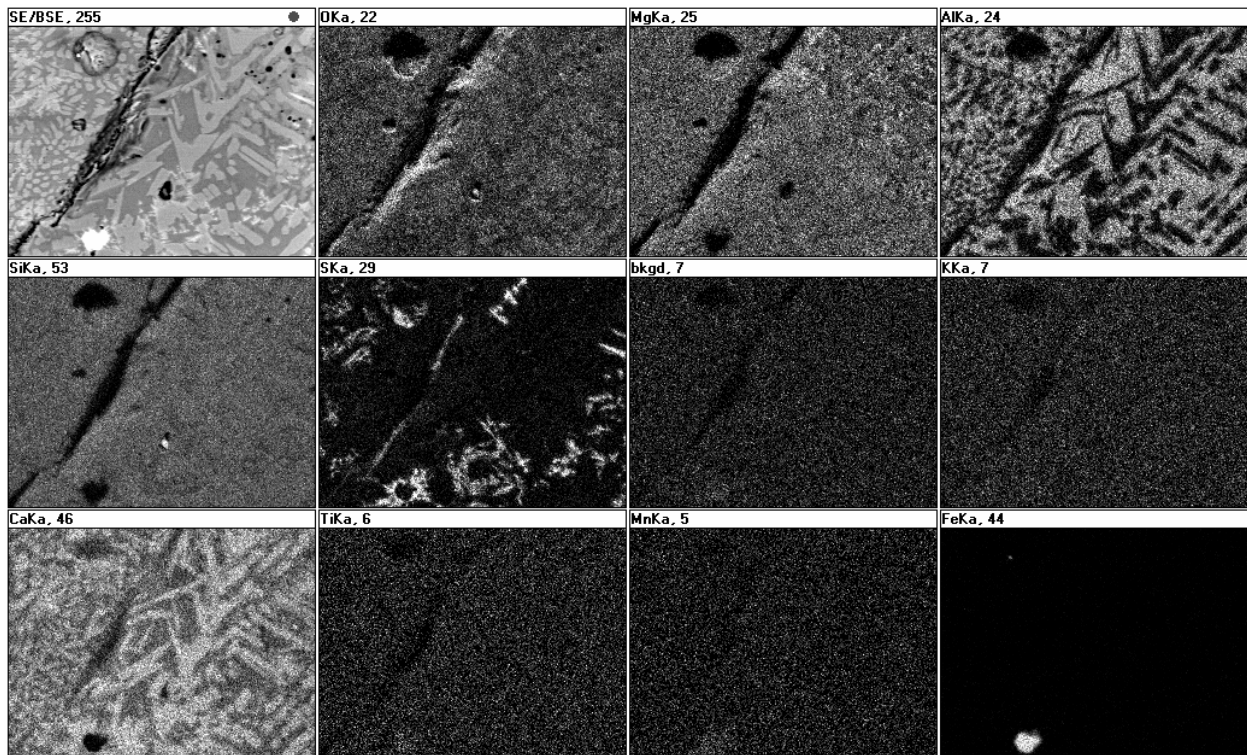


Figure 132. Elemental maps of polished surface D at 1000x magnification

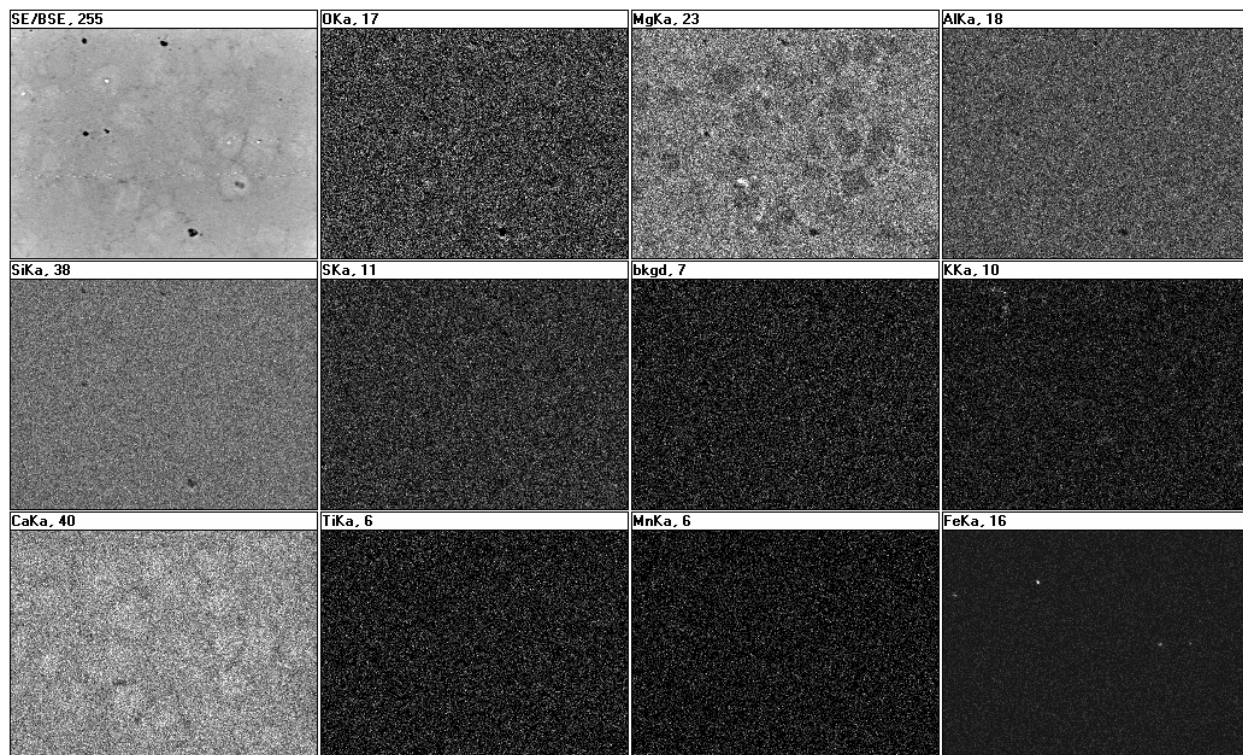


Figure 133. Elemental maps of polished surface F at 1000x magnification

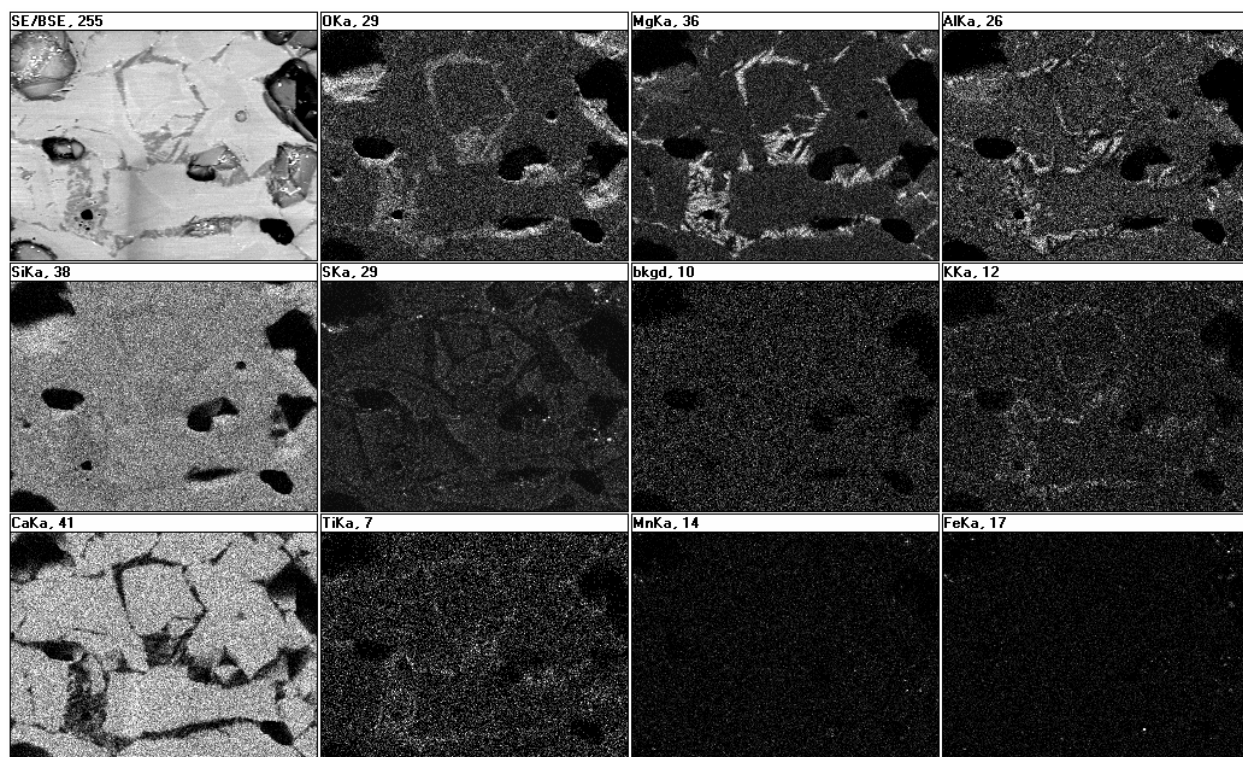


Figure 134. Elemental maps of polished surface G at 500x magnification

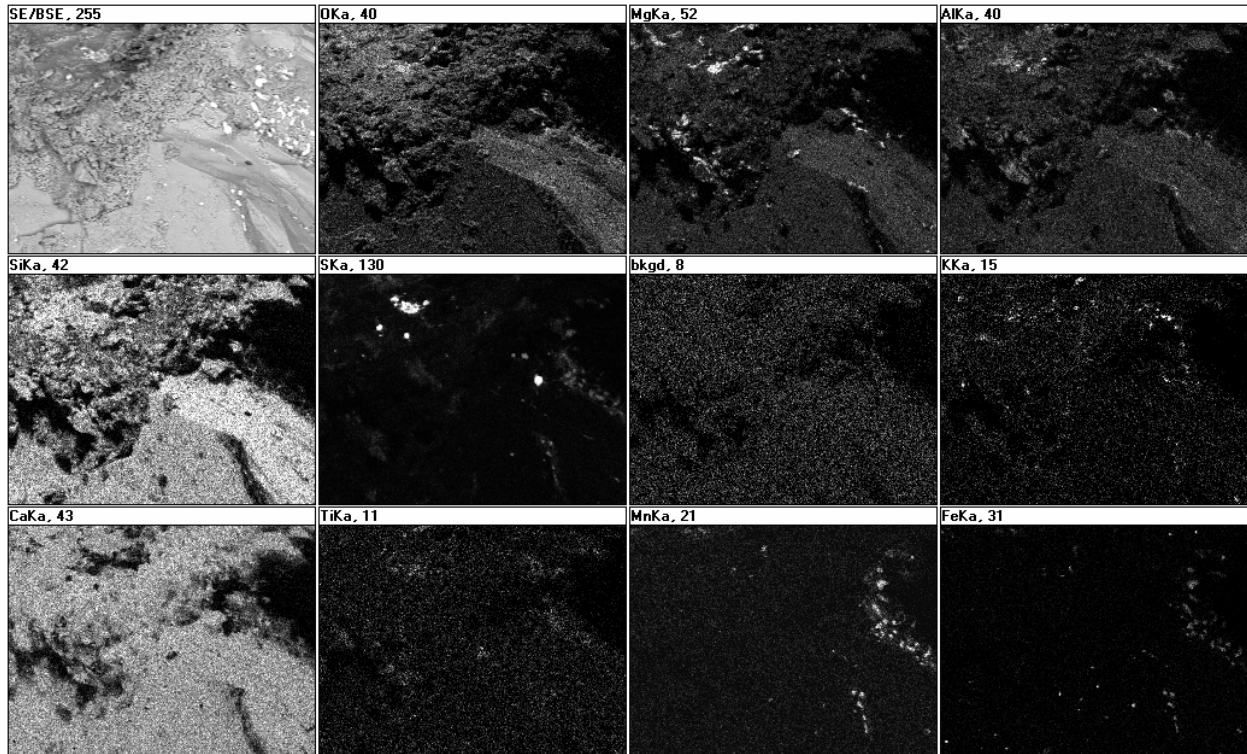


Figure 135. Elemental maps of gray vesicular surface at 300x magnification

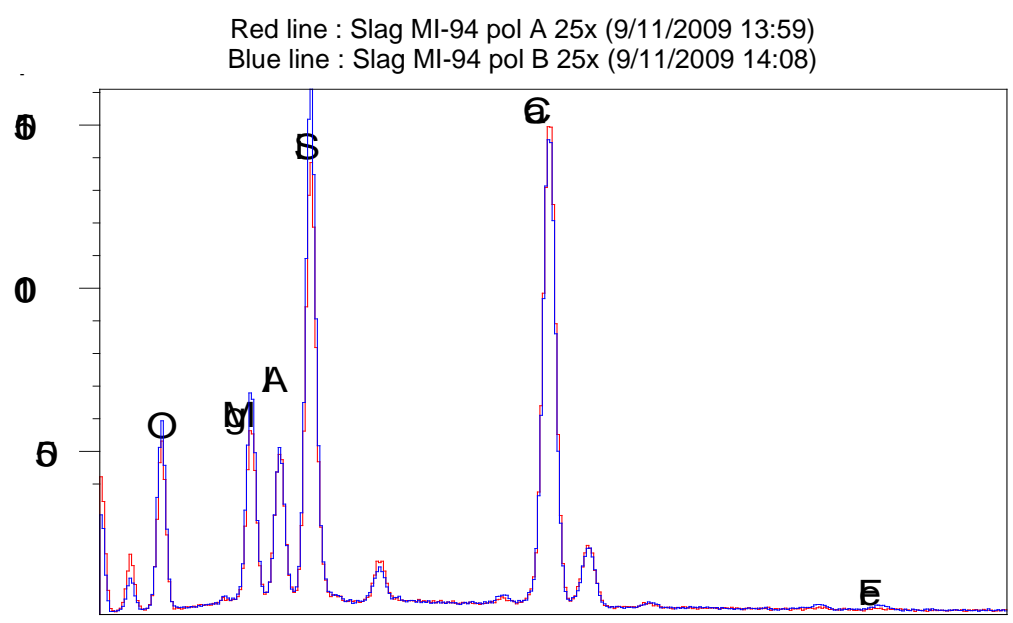


Figure 136. Elemental analysis of polished surfaces A and B at 25x magnification

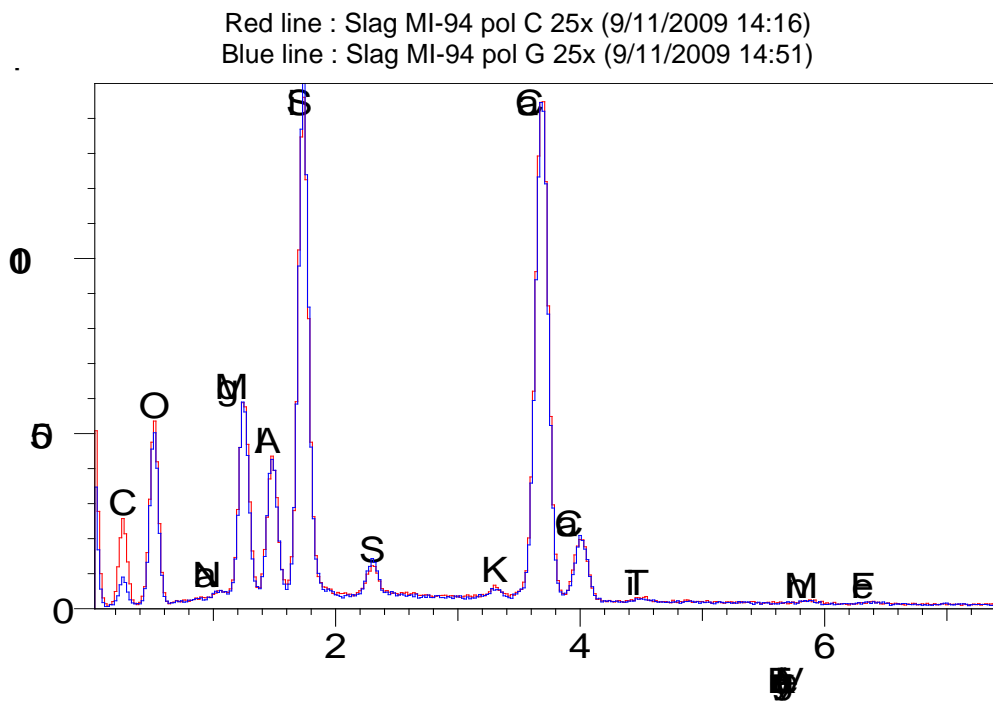


Figure 137. Elemental analysis of polished surfaces C and G at 25x magnification

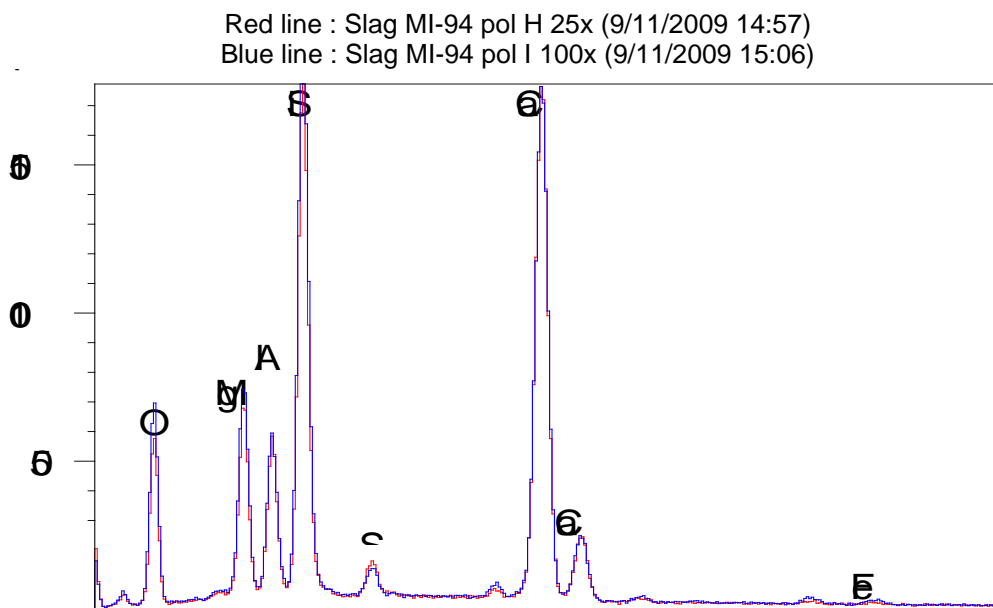


Figure 138. Elemental analysis of polished surfaces H and I at 25x magnification